

Toward the Upgrading of Hydrocarbons:
Synthesis, Characterization, and
Reactivity of Platinum and Palladium
Complexes

Thesis by

Paul Frederick Oblad

In Partial Fulfillment of the Requirements for the degree of

Doctor of Philosophy

CALIFORNIA INSTITUTE OF TECHNOLOGY

Pasadena, California

2012

(Defended August 26, 2011)

© 2012

Paul Frederick Oblad

All Rights Reserved

Acknowledgements

I have so many people to thank for their role in my education. First and foremost, I have all of my advisors to mention. John Bercaw and Harry Gray have been very generous in letting me join their groups as a refugee from Jonas Peters' group. John has been a great advisor, as he provided both direction and supervision when I needed it and freedom to pursue my interests when I was so inclined. Harry has been an eternal optimist and always providing me much needed direction and support. He taught me to laugh at my mistakes and, more importantly, how to correct them. I feel that I would not have been able to learn as much as I have from John and Harry if I had worked for any other advisor. I am also tremendously grateful to Jay Labinger. Though he was not officially responsible for me, he gave his time like he was. Jay was always available when I had questions and was able to answer those questions in a way that even I could understand. Jay Winkler was also an unofficial advisor that generously gave his time. His door was always open to me and he would patiently answer all of my questions. Also, even though he was only my advisor for a short time, I am very grateful to Jonas Peters for his role in my education. He even got me a fellowship for my first year. I am grateful for the opportunities he has given me and the time I spent in his lab. I would also like to thank other members of my committee, Nate Lewis and Mitchio Okumura for valuable guidance and for bearing with me while I tried to coordinate the busy schedules of all six of those on my panel. I am very grateful to Bruce Brunschwig and Jack Richards for coming to my group meetings and giving me valuable advice. Additionally, Tom Richmond, my advisor at the University of Utah, originally got me excited about chemistry and is why I ended up in graduate school.

Secondly, I would like to thank all the students and postdocs with whom I worked closely. Travis Williams taught me many of the laboratory techniques that I use most. I thoroughly enjoyed working with him, learning from him and listening to his puns. I have always strived not to “cross the streams” for fear of “total protonic reversal” (Ghostbusters). Unfortunately, most of my reactions resulted in what he termed a “diversity oriented synthesis” (DOS) or “the phonebook.” Nilay Hazari really taught me to think critically about chemistry. He always praised my work and made me feel that my contributions were valuable. I am a more confident and a harder worker because of him. Ted Weintrob has been a great friend during graduate school. We both were initially in the Peters group and subsequently moved to the Bercaw group. In the office our desks were always in the same section and for a while we shared the south half of 213 Noyes. We also had every class together. Though we never actually worked on the same project, Ted always talked to me about my project and made many valuable intellectual contributions. I also would take all the questions I was too embarrassed to ask anyone else to him first. More recently, Matt Winston has joined me on a few projects and impressed me with how motivated and smart he is. Matt’s work was instrumental in making these projects really take off and become interesting. These projects would not be anywhere near where they are without him. Jillian Dempsey taught me how to use the laser and very generously gave me more Ru(bipy)₃²⁺ and methyl viologen than she probably wanted to. Alec Durrell was very helpful with the laser and with photophysics. Though I tried to reciprocate and help him with some synthesis, he was much more helpful to me than I was to him. I not only

benefited from working very closely with all of these people, I benefitted tremendously from their friendship. Thank you all for everything.

There are a tremendous number of people with whom I was not fortunate enough to work closely with but to whom I am still very grateful. They either helped me with chemistry or otherwise supported me with their friendship. Alex Miller (a fellow Peters group refugee) was generous with his time when I had chemistry questions and is someone I look up to. I also really enjoyed dinners, camping and wine tasting with him and Jillian. Matt and Charlotte Whited were great sources of chemical expertise and fun to hang out with in our spare time. As our closest neighbors, they were always willing to join us for dinner or wine, babysit or carpool with us to the beach or movie night at the Durrell's. I have already mentioned Alec but I spent many hours watching Star Trek, Battlestar Galactica, and Breaking Bad with him. Additionally, he and his wife, Cristina Durrell, often invited us to the beach or their pool. I am so grateful that Christian and Charlotte were very good friends with my wife, Stephanie. Ian Tonks always had great stories and included me in sporting events. Aaron Wilson was a great rock climbing buddy and was kind to try to help me get a job. Steve Baldwin was also very helpful with chemistry and was very kind to my family. He was always excited to play with my son, Liam, and spent the entirety of several social events doing just that. Nathan West was happy to kill aliens with me on Xbox 360 while his wife, Erin, and my wife did things that they found more interesting. Paul Elowe was very kind to help me get an interview with his company. Jeffrey Warren, Nicole Bouley Ford, and Bert Lai were very kind to look over my out-of-field proposals. Valerie Scott, Jeffery A. Byers, Theodor Agapie, George Chen, Suzanne

Golisz, Bolin Lin, David Weinberg, Ross Fu, Rachel C. Klet, Yan Choi Lam, Taylor Lenton, Emannuelle Despagnet-Ayoub, Amaruka Hazari, Carl Laskowski, Sze-Man Yu, Peter Agbo, Matthew Bierman, Paul Bracher, Maraia Ener, Gretchen Keller, Judith Lattimer, James McKone, Qixi Mi, Astrid Mueller, Josh Palmer, Mike Rose, Bryan Stubbert, Heather Williamson, Keiko Yokoyama, Morgan Cable, Lionel Cheruzel, Matthew Hartings, Tetsunari Kimura, Kyle Lancaster, Don Walker, and Melanie Yen all helped me at some point during my graduate career, for which I am very grateful.

There are also a few Caltech staff member that were incredibly helpful. Larry Henling spent hours with me at the console of the X-ray diffractometer and became a very good friend of mine. Mike Day was always willing to work up even the worst data. Tom Dunn was very helpful for all my random electronics needs. David Vander Velde and Scott Ross taught me a great deal about NMR. Pat Anderson was always very friendly and willing to help with anything. Catherine May, Rick Jackson, Anne Penny, and Agnes Tong were very helpful with odds and ends.

Finally, I want to thank my family. Stephanie has stuck with me through it all. She has supported me though the highs and lows. I really would have not made it through graduate school without her. Thank you, Steph. Liam has brought new meaning to life. He never ceases to amaze me. I am so fortunate to have such a great kid. My parents, Nan and Bruce, are amazing. My Dad taught me to think like a scientist and my Mom taught me what mattered in life. I don't know how I can thank them enough. All my siblings, Rachel, Hayward, Mark, Stephen, John, Richard, and Bryant, and my mother-in-law, Gayle Hunt, have always been supportive and willing to do anything for me. There are so many

people I should thank, I have inevitably left someone out and for that I apologize. Thank you all.

Abstract

Herein, hydroxyl-dimers of platinum and palladium supported by diimine ligands have been prepared and studied. It was found that they are capable of activating allylic, benzylic, and aromatic carbon-hydrogen bonds. The kinetics of the C-H activation of cyclohexene with the platinum system and of indene with the palladium system were studied. In each case the rate-limiting step was found to be associative substitution. The catalytic dehydrogenation of cyclohexene to benzene with the palladium hydroxyl-dimer was investigated. The chemical oxidation of the η^3 -organometallic products synthesized via C-H activation of cyclohexene and indene with platinum and palladium, respectively, was explored. Treatment of these products with strong halogenating oxidants resulted in the liberation of halogenated substrates and bridging halide metal complexes. Uncharged platinum and palladium polypyrazoleborate complexes were synthesized and characterized. The kinetics of the degenerative ligand exchange of DMSO with palladium methyl DMSO complexes ligated with a polypyrazoleborate or a diimine ligand were studied and it was found that the associative substitution mechanism through which the diimine ligated complexes proceeds was unavailable to the polypyrazoleborate palladium complex. In the polypyrazoleborate system ligand exchange proceeded through a dissociative mechanism. The C-H activation substrate scope of the platinum and palladium hydroxyl-dimers was further explored. The diimine platinum hydroxyl-dimer was found to activate an allylic C-H bond in cyclopentene and form an η^3 -cyclopentenyl complex when heated with acid and dilute stoichiometric amounts of cyclopentene. Conversely, dehydrogenation of cyclopentene to a platinum-bound η^5 -cyclopentadiene resulted from the treatment of the

platinum hydroxyl-dimer with super-stoichiometric amounts of cyclopentene at room temperature. This difference in reactivity with the same substrate may be due to the relative reactivities of allylic versus homoallylic C-H bonds. Further evidence of a homoallylic C-H activation mechanism was demonstrated by treating the diimine platinum hydroxyl-dimer with *neo*-hexene to form a cyclometalated *neo*-hexenyl platinum complex. The diimine palladium hydroxyl-dimer was also found to catalytically oligomerize and isomerize olefins. Furthermore, the catalytic activity was supported by the presence of oxygen and stable in the presence of water. Most likely the oligomerization proceeded through a palladium hydride that can decompose to palladium(0) complex, which can be reoxidized by oxygen. The photochemical oxidation of platinum complexes with $\text{Ru}(\text{bipy})_3^{2+}$ was also investigated. Finally, the coordination chemistry of the tris(triphenylphosphino)silyl ligand was explored with cobalt, ruthenium, nickel, and platinum.

Table of Contents

List of Figures	xii
List of Tables	xiv
Chapter 1: General Introduction	1
References	4
Chapter 2: The Reactivity of Platinum and Palladium Hydroxyl-Bridged Dimers	7
Introduction	8
Results and Discussion	8
Conclusions	17
Experimental Section	17
References	32
Chapter 3: Comparing the Mechanism of C-H Bond Activation Between [(diimine)M ^{II} (μ_2 -OH)] ₂ ²⁺ Dimers (M = Pd, Pt) and Related [(diimine)M ^{II} (OH ₂) ₂] ²⁺ Monomers	33
Introduction	34
Results and Discussion	34
Conclusions	40
Experimental Section	41
References	48
Chapter 4: Oxidation of Organometallic Platinum and Palladium Complexes Obtained from C-H Activation	51
Introduction	52
Results and Discussion	53
Conclusions	62
Experimental Section	62
References	70
Chapter 5: Uncharged Platinum and Palladium Complexes Ligated With Polypyrazole Borates	72
Introduction	73
Results and Discussion	74
Conclusions	85
Experimental Section	86
References	92

Chapter 6: Homoallylic C-H Activation and Oligomerization	94
Introduction	95
Results and Discussion.....	95
Conclusions	104
Experimental Section	105
References	110
Appendix A: Oxidation of Diimine Platinum Complexes by Flash Quench.....	111
Introduction	112
Results and Discussion.....	113
Conclusions	117
Experimental Section	118
References	119
Appendix B: Coordination Chemistry of the Tris(triphenylphosphino)silyl Ligand	121
Introduction	122
Results and Discussion.....	123
Conclusions	131
Experimental Section	132
References	143
Appendix C: Crystallographic Section	145
[SiP ₃]CoCl.....	146
[SiP ₃]RuCl.....	151
[SiP ₃]NiCl	156
[(diimine)Pt(oxime)][BF ₄] (Ar = 3,5- ^t Bu ₂ C ₆ H ₃)	161
[(diimine)Pd(THF) ₂][BF ₄] ₂ (Ar = 3,5- ^t Bu ₂ C ₆ H ₃).....	167
[(diimine)PtBr] ₂ [BF ₄] ₂ (Ar = 3,5- ^t Bu ₂ C ₆ H ₃)	173
[(diimine)Pt(OH ₂) ₂][BF ₄] ₂ (Ar = 2,4,6-Me ₃ C ₆ H ₂).....	178
Polypyrazoleborate Pd ^I -Pd ^I decomposition product.....	183
Ph ₂ B(pz) ₂ PtCl(DMSO).....	188
Tp ^{Me} PtCl(DMSO)	192
Ph ₂ B(pz) ₂ PdMe ₂ K.....	196
[Ph ₂ Bpz ₂ Pd(μ-pz) ₂] ₂	201
(Ph ₂ Bpz ₂) ₂ Pd.....	206
Ph ₂ B(pz) ₂ PdMe ₂ (DMSO)	210
[(diimine)PtCl] ₂ [BF ₄] ₂	214
References	219

List of Figures

Chapter 2

Figure 2.1. Crystal structure of [(diimine)Pt(OH ₂) ₂] ²⁺ (Ar = 2,4,6-Me ₃ C ₆ H ₂)	9
Figure 2.2. Crystal structure of (diimine)Pt(oxime) ⁺	11
Figure 2.3. The device that will both heat and tumble a J. Young tube	14
Figure 2.4. Crystal structure of (diimine)Pd(THF) ₂ ²⁺	16
Figure 2.5. Crystal structure of [(diimine)Pt(μ-enolate)] ₂ ²⁺	17

Chapter 3

Figure 3.1. Graph of [(diimine)Pd(indenyl)] ⁺ _{end} – [(diimine)Pd(indenyl)] ⁺ ^{0.5} against time during reaction between [(diimine)Pd(OH)] ₂ ²⁺ and 40 equivalents of indene in a 5.5:1 mixture of CH ₂ Cl ₂ :TFE (675 equivalents of TFE)	39
---	----

Chapter 4

Figure 4.1. The structure of [(diimine)Pd(indenyl)] ⁺	59
Figure 4.2. The structures of [(diimine)Pt(μ-Br)] ₂ ²⁺ (a), [(diimine)Pd(μ-Br)] ₂ ²⁺ (b), and [(diimine)Pd(μ-Cl)] ₂ ²⁺ (c)	60–61

Chapter 5

Figure 5.1. Crystal structure of Pd ^I -Pd ^I decomposition product	75
Figure 5.2. Crystal structure of Tp ^{Me} PtCl(DMS)	77
Figure 5.3. Crystal structure of Ph ₂ Bpz ₂ PtCl(DMS)	77
Figure 5.4. Crystal structure of KPh ₂ Bpz ₂ PdMe ₂	79
Figure 5.5. Crystal structure of Ph ₂ Bpz ₂ PdMe(DMSO)	80
Figure 5.6. Crystal structure of [Ph ₂ Bpz ₂ Pd(μ-pz)] ₂	81
Figure 5.7. Crystal structure of (Ph ₂ Bpz ₂) ₂ Pd	81
Figure 5.8. NMR spectra of [(diimine)PdMe(DMSO)][BF ₄] at 10 °C (blue) and -45 °C (red)	83
Figure 5.9. Eyring plot for Ph ₂ Bpz ₂ PdMe(DMSO)	84
Figure 5.10. The exchange rate dependence of the concentration of DMSO for Ph ₂ Bpz ₂ PdMe(DMSO)	85

Chapter 6

Figure 6.1. Isotropic crystal structure of [(diimine)Pt(η ⁵ -cyclopentadienyl)] ⁺	97
Figure 6.2. GC trace for ethylene oligomerization	103

Appendix A

Figure A.1. Transient absorption of MV^+ (in red) and MV^+ in the presence of (diimine)PtMe(indole) ⁺ (in blue)	115
Figure A.2. Transient absorption of the bleach of Ru^{2+} (in red) and then in the presence of (diimine)PtMe(Indole) ⁺ (in blue)	116
Figure A.3. Transient absorption of the bleach of Ru^{2+} followed by a new absorption when in the presence of (diimine)PtMe(indole) ⁺ (in blue)	116
Figure A.4. Transient absorption of the bleach of Ru^{2+} followed immediately by a new absorption when in the presence of indole (in red) or (diimine)PtMe(indole) ⁺ (in blue).....	117

Appendix B

Figure B.1. Tris(phosphino)silyl ligand $H[SiP^R_3]$	122
Figure B.2. Crystal structure of $[SiP^{Ph}_3]CoCl$	124
Figure B.3. Cyclic voltammogram of $[SiP^{Ph}_3]CoCl$	125
Figure B.4. Crystal structure of $[SiP^{Ph}_3]RuCl$	127
Figure B.5. Cyclic voltammogram of $[SiP^{Ph}_3]RuCl$	127
Figure B.6. Crystals of $[SiP^{Ph}_3]NiCl$	129
Figure B.7. Crystal structure of $[SiP^{Ph}_3]NiCl$	129
Figure B.8. Crystal structure of $[SiP^{Ph}_3]PtCl$	131
Figure B.9. Crude proton NMR of $[SiP^{Ph}_3]RuCl$	136
Figure B.10. Crude phosphorus NMR of $[SiP^{Ph}_3]RuCl$	137
Figure B.11. Crude proton NMR of $[SiP^{Ph}_3]NiCl$	138
Figure B.12. Phosphorous NMR of $[SiP^{Ph}_3]NiCl$	139
Figure B.13. Crude phosphorus NMR of $[SiP^{Ph}_3]PtCl$	140
Figure B.14. Crude phosphorus NMR of $[SiP^{Ph}_3]PtMe$	141
Figure B.15. Crude proton NMR of $[SiP^{Ph}_3]PtMe$	142
Figure B.16. Crude Phosphorus NMR of the reaction of $H[SiP^{Ph}_3]$ and (COD)PtClMe ..	143

List of Tables

Chapter 2

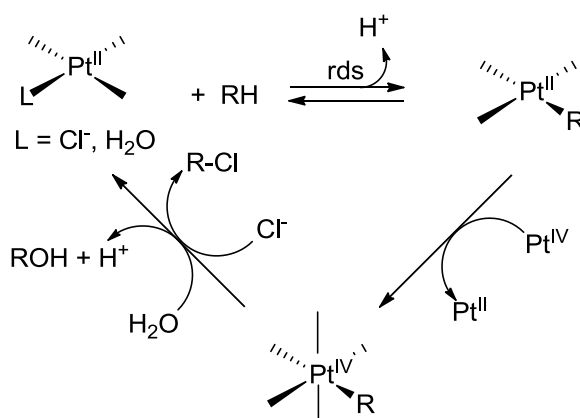
Table 2.1. K_{eq} calculations and van't Hoff plot	24
Table 2.2. Dependence of equilibrium position on $[HBF_4]$	25
Table 2.3. Rate dependence on [cyclohexene].....	26
Table 2.3. Rate dependence on $[HBF_4]$	28

Chapter 4

Table 4.1. Crystal and refinement data for complex $[(diimine)Pd(indenyl)]^+$, $[(diimine)Pt(\mu Br)]_2^{2+}$, $[(diimine)Pd(\mu-Br)]_2^{2+}$, and $[(diimine)Pd(\mu-Cl)]_2^{2+}$	63
---	----

Chapter 1
General Introduction

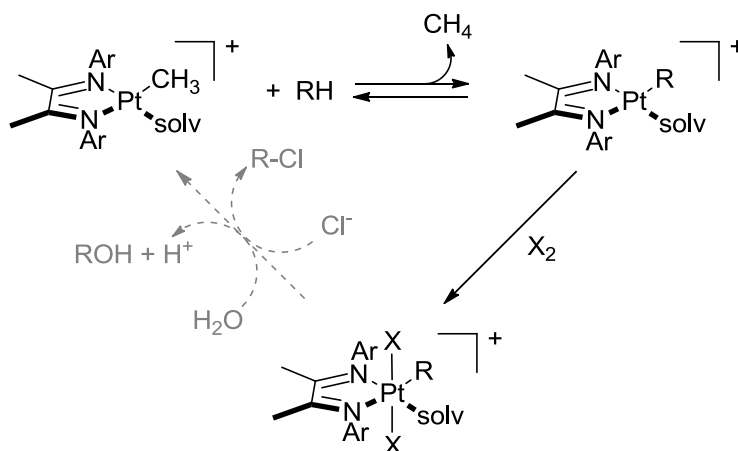
Carbon-hydrogen bond activation/functionalization has been a very active area of research.¹ These transformations are important for chemical synthesis as well as in the development and use of fuels. The partial oxidation of methane is of particular interest since methane, the principle component of natural gas, is used to fulfill 23% of our energy demand.^{1e,2} Natural gas is found mostly in remote locations and is expensive to transport because it must either be piped over long distances or compressed into a liquid.^{1a,1d} If methane can be partially oxidized to form methanol, a liquid at standard temperature and pressure, the cost of transportation could be greatly reduced. The way methanol is currently produced commercially is through an indirect method in which methane is steam reformed to produce synthesis gas and eventually methanol.^{1e} Unfortunately, this process is expensive and energy intensive. In 1972 Shilov and coworkers discovered a new method by which this conversion can be effected.³ They observed that tetrachloroplatinate could convert methane to methanol catalytically. The mechanism by which this is achieved is depicted in Scheme 1.1.⁴ Significantly, this system also has the desirable property of



Scheme 1.1. Shilov cycle

being able to function in air and water. However, in order to get catalytic turnover in this system, expensive reagents such as hexachloroplatinate must be used as a stoichiometric oxidant.⁵ Since this use of platinum is impractical, the Shilov cycle has only served as a basis for further development in this field. Much work has been done in order to understand and model this chemistry.^{1e,6}

Bercaw and co-workers have developed a system to model Shilov chemistry based around $[(\text{diimine})\text{Pt}^{\text{II}}(\text{Me})(\text{solv})]^+$ complexes (diimine = $\text{ArN}=\text{C}(\text{Me})-\text{C}(\text{Me})=\text{NAr}$, solv = 2,2,2-trifluoroethanol (TFE), H_2O) (Scheme 1.2).⁷ Interestingly, this system can activate a



Scheme 1.2. Model Shilov system

variety of C-H bonds to produce complexes of the form $[(\text{diimine})\text{Pt}^{\text{II}}(\text{R})(\text{solv})]^+$.⁸ However, in order to activate C-H bonds, methane has to be liberated as a sacrificial leaving group. Moreover, appropriate conditions for oxidation were never found. Upon further investigation, it was discovered that protonolysis of $[(\text{diimine})\text{Pt}^{\text{II}}(\text{Me})(\text{TFE})]^+$ led to $[(\text{diimine})\text{Pt}^{\text{II}}(\text{TFE})_2]^{2+}$, which, interestingly, could also facilitate C-H activation, but had a limited substrate scope due to the corrosive conditions required for the complex.⁹ This

finding led to the hypothesis that C-H activation could be achieved by starting with complexes that did not contain a platinum carbon bond. Bercaw and coworkers began exploring other routes starting with non-organometallic complexes. Previously it had been observed that silver salt metathesis of [(diimine)MCl₂] (where M = Pt¹⁰, Pd¹¹) would form [(diimine)M(solvent)₂]²⁺ and, in the presence of water, bis(hydroxo) bridged complexes. Though these were not new compounds, originally they were thought to be thermodynamic sinks and the reactivity of the [(diimine)M^{II}(μ₂-OH)₂]²⁺ was never explored. Additionally, this system seemed particularly interesting since water is presumably involved in oxidative functionalization, and thus a water-tolerant system like this would be desired. Further investigation has revealed that these hydroxyl-dimers have rich reactivity.¹² The [(iimine)M^{II}(μ₂-OH)₂]²⁺ complexes have been shown not only to react stoichiometrically with a variety of substrates to activate C-H bonds, but in the case where the metal is palladium, it has been demonstrated that several valuable catalytic transformations can be achieved. The chapters that follow contain the details of the investigations of the synthesis, characterization, and reactivity of platinum and palladium hydroxyl-dimers and related systems.

References

1. (a) Arndtsen, B. A.; Bergman, R. G.; Mobley, T. A.; Peterson, T. H., *Acc. Chem. Res.* **1995**, 28, 154. (b) Erker, G., *Angew. Chem. Int. Ed.* **1999**, 38, 1699. (c) Davies, H. M. L.; Antoulinakis, E. G., *J. Organomet. Chem.* **2001**, 617–618, 47. (d) Crabtree, R. H., *J.*

- Chem. Soc. Dalton Trans.* **2001**, 17, 2437. (e) Labinger, J. A.; Bercaw, J. E., *Nature* **2002**, 417, 507. (f) Fekl, U.; Goldberg, K. I., *Adv. Inorg. Chem.* **2003**, 54, 259.
2. (a) Gradassi, M. J.; Green, N. W., *Fuel Proc. Technol.* **1995**, 42, 65. (b) *BP Statistical Review of World Energy June 2006*. (British Petroleum) **June 2006**.
3. Shilov, A. E. *Zh. Fiz. Khim.* (English Transl.) **1972**, 42, 785.
4. Luinstra, G. A.; Wang, L.; Stahl, S. S.; Labinger, J. A.; Bercaw, J. E. *J. Organomet. Chem.* **1995**, 504, 75.
5. Shilov, A. E. *Nouv. J. Chim.* **1983**, 7, 729.
6. Shilov, A. E.; Shul'pin, G. B. *Chem. Rev.* **1997**, 97, 2879.
7. (a) Johansson, L.; Ryan, O. B.; Tilset, M. *J. Am. Chem. Soc.* **1999**, 121, 1974. (b) Johansson, L.; Tilset, M. *J. Am. Chem. Soc.* **2001**, 123, 739.
8. (a) Johansson, L.; Tilset, M.; Labinger, J. A.; Bercaw, J. E. *J. Am. Chem. Soc.* **2000**, 122, 10846. (b) Zhong, A. H.; Labinger, J. A.; Bercaw, J. E. *J. Am. Chem. Soc.* **2002**, 124, 1378. (c) Heyduk, A. F.; Driver, T. G.; Labinger, J. A.; Bercaw, J. E. *J. Am. Chem. Soc.* **2004**, 126, 15034. (d) Driver, T. G.; Day, M. W.; Labinger, J. A.; Bercaw, J. E. *Organometallics* **2005**, 24, 3644. (e) Owen, J. S., Labinger, J. A.; Bercaw, J. E. *J. Am. Chem. Soc.* **2006**, 128, 2005.
9. Driver, T. G.; Williams, T. J. Labinger, J. A.; Bercaw, J. E. *Organometallics* **2007**, 26, 294.
10. Kannan, S.; James, A. J.; Sharp, P. R. *Polyhedron* **2000**, 19, 155.
11. Ackerman, L. J.; Sadighi, J. P.; Kurtz, D. M.; Labinger, J. A.; Bercaw, J. E. *Organometallics* **2003**, 22, 3884.

12. Much of the research herein has been published in: Williams, T. J.; Caffyn, A. J. M.; Hazari, N.; Oblad, P. F.; Labinger, J. A.; Bercaw, J. E. *J. Am. Chem. Soc.* **2008**, *130*, 2418.

Chapter 2

The Reactivity of Platinum and Palladium Hydroxyl-Bridged Dimers

Adapted in part from:

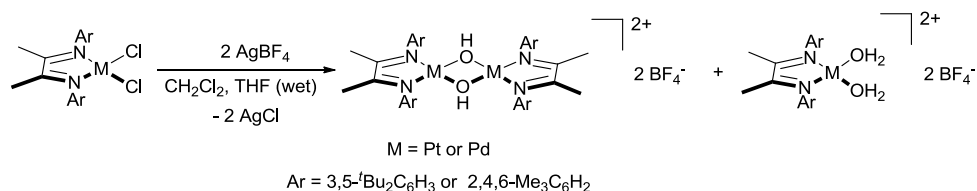
Williams, T. J.; Caffyn, A. J. M.; Hazari, N.; Oblad, P. F.; Labinger, J. A.; Bercaw, J. E. *J. Am. Chem. Soc.* **2008**, *130*, 2418.

Introduction

Platinum and palladium hydroxyl-dimers were previously thought to be thermodynamic resting states. However, it has been found that they have rich reactivity and are even capable of cleaving C-H bonds. Discussed in this chapter are the initial characterization, reactivity, and kinetics studies.

Results and Discussion

The treatment of (diimine) $M^{II}Cl_2$ with $AgBF_4$ in wet solvents results in the formation of a mixture of the dimer $[(diimine)M^{II}(\mu_2-OH)]_2^{2+} [BF_4^-]_2$ and the monomer $[(diimine)M^{II}(H_2O)]^{2+} [BF_4^-]_2$ (Scheme 2.1).¹ Cleanly isolating one of these complexes



Scheme 2.1. Synthesis of the hydroxyl-bridged dimers

proved difficult since there is an acid- and water-dependent equilibrium between the two species. Kinetics studies revealed an equilibrium constant (K_{eq}) of $1.33(14) \times 10^3 M^{-1}$ at 80 °C (for the 3,5-*t*butyl substitute platinum series). When prepared and isolated as in Scheme 2.1, the product was mostly the dimer $[(diimine)M^{II}(\mu_2-OH)]_2^{2+}$, and this mixture of products was typically then used for C-H activation studies. However, they have since been individually characterized. The 3,5-*t*butyl substitute platinum series had previously been prepared and characterized but the 2,4,6-Me₃C₆H₂ substituted platinum series had not. Fortunately, it was found that they could be prepared using the same methodology.

Crystals suitable for X-ray diffraction studies were grown for both the 2,4,6-Me₃C₆H₂ substituted platinum dimer and monomer. Poor crystal quality allowed only for verification of connectivity of the dimer, however, the structure quality for the monomer was very good (Figure 2.1). Additionally, this is the only structure of a diimine platinum bisquo complex we have been able to acquire.

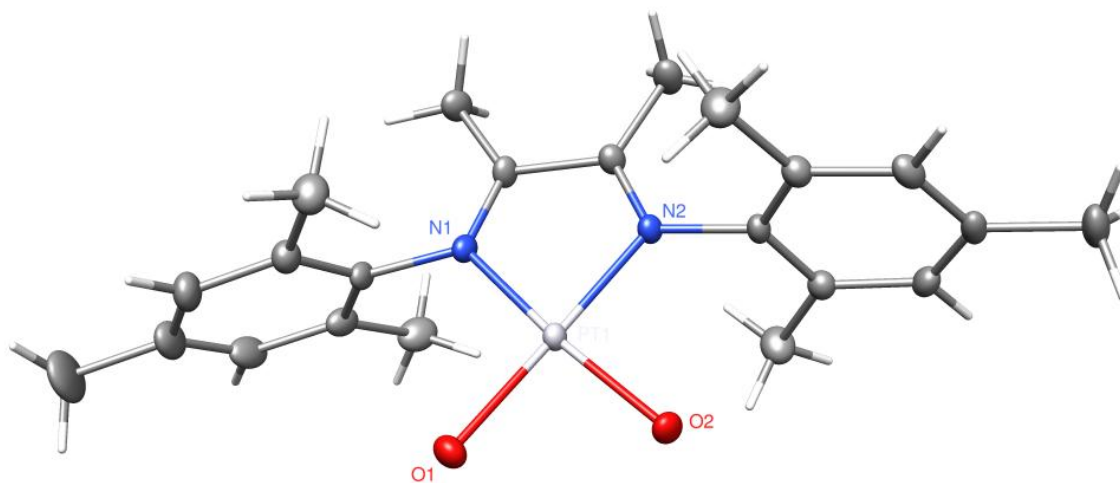
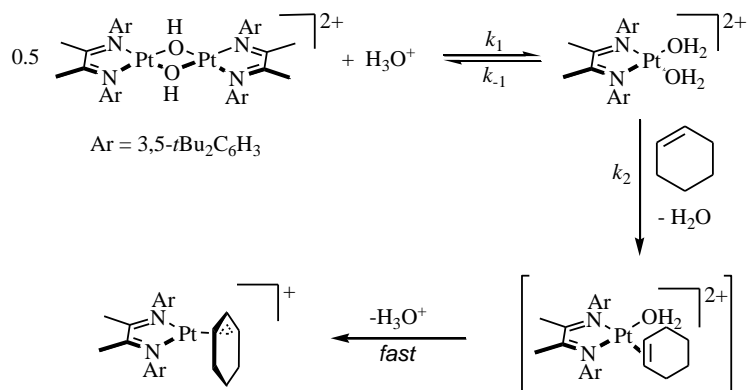


Figure 2.1. Crystal structure of [(diimine)Pt(OH₂)₂]²⁺ (Ar = 2,4,6-Me₃C₆H₂)
(50% ellipsoids)

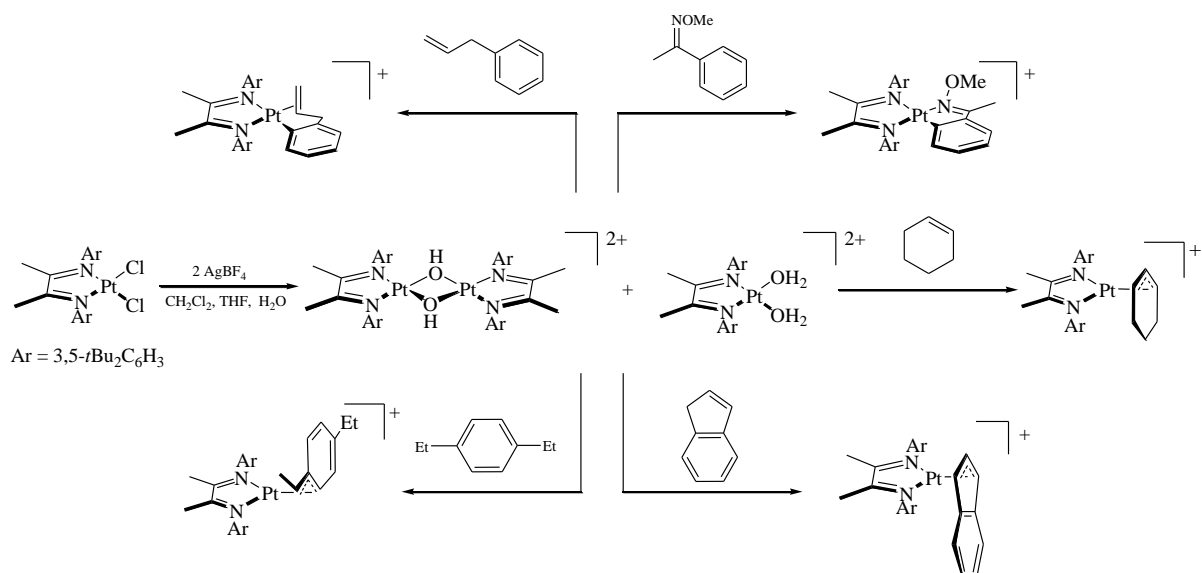
The reactivity of each series was explored and it was found that the platinum system, when treated with cyclohexene and acid, would form a η^3 -cyclohexenylplatinum(II) complex (Scheme 2.2). Kinetics studies were done to elucidate the mechanism by which



Scheme 2.2. Mechanism of formation

this occurs. NMR Analysis indicated that the platinum dimer was first converted to the monomer with a pseudo-first-order dependence on acid concentration. Cyclohexene then coordinated to the metal complex through the olefin. Surprisingly, the coordination of cyclohexene also exhibited acid dependence. We speculated that this may have been due to an acid-catalyzed dissociation of water. The olefin-bound cyclohexene adduct was not observed because the subsequent allylic C-H bond cleavage and the loss of H₃O⁺ was fast.

This platinum system showed activity toward a variety of C-H bonds (Scheme 2.3). Aside from the allylic C-H bond in cyclohexene, a benzylic C-H bond can be cleaved when the system is treated with 1,4-diethylbenzene. Similarly, a reaction was observed with the methylene C-H bond in indene. The platinum dimer however, showed no activity toward benzene and, not surprisingly, cyclohexane. Cyclometallated products are formed when the complex is treated with allylbenzene or an *O*-methyl oxime where an aromatic C-H bond is cleaved. The reaction with *O*-methyl oxime is unique, however, in that it proceeds without acid, probably because the oxime can cleave the hydroxyl-dimer. All complexes



Scheme 2.3. C-H activation products

were fully characterized by NMR (¹H and ¹³C), IR, high-resolution mass spectrometry, and in the case of the oxime cycloplatinatone complex, X-ray crystallography (Figure 2.2).

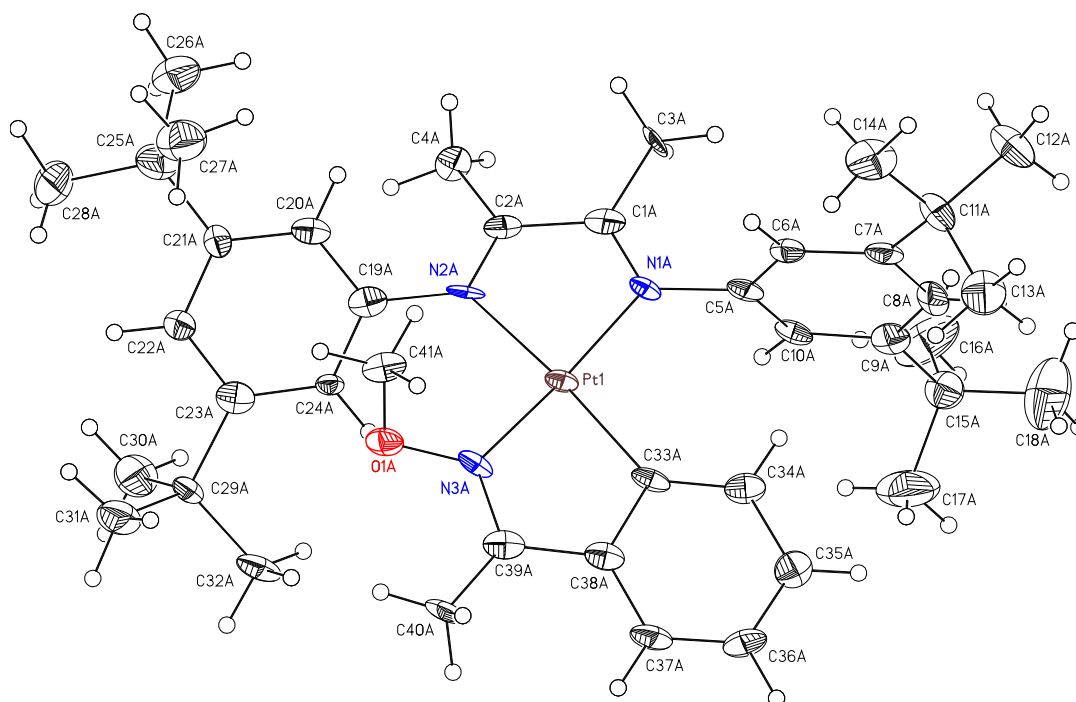
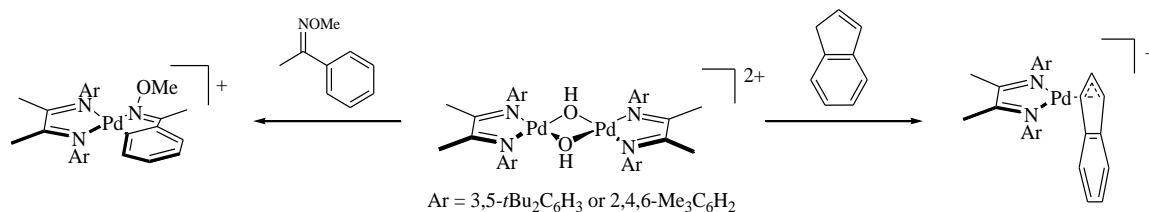


Figure 2.2. Crystal structure of (diimine)Pt(oxime)⁺ (50% ellipsoids)

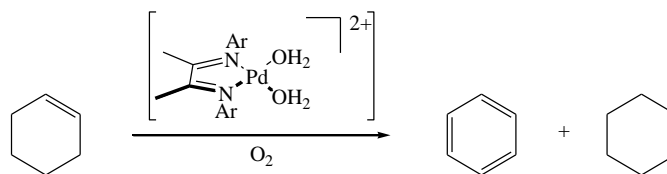
Only the reactivity of the platinum complex with the 3,5-*t*-butyl substituted ligand has been discussed above. However, varying the substitution of the aryl rings could potentially tune the reactivity of the complex. As such the 2,4,6-trimethylphenyl substituted $[(\text{diimine})\text{Pt}(\mu_2\text{-OH})_2]^{2+}$ complex was prepared and characterized crystallographically. Its reactivity is expected to be similar but as of yet has not been studied.

Related systems involving palladium were investigated and it has been shown that a mixture of the bridging hydroxypalladium dimer and bis-aquopalladium monomer behaves similarly to that of the homologous platinum system. In our lab oxime cyclopalladate and the η^3 -indenylpalladium complexes have been isolated and characterized (Scheme 2.4).



Scheme 2.4. Palladium homology

Initial attempts to make an η^3 -cyclohexenylpalladium similar to that formed with platinum led to surprising results. Hazari and Caffyn observed that treating the palladium dimer with cyclohexene resulted in the formation of benzene and cyclohexane (Scheme 2.5). Though



Scheme 2.5. Catalysis with palladium

the products themselves are not particularly interesting, they discovered that this reaction proceeded catalytically. Further investigation showed that the oxidation was potentially coupled with dioxygen, since the results varied in its absence. Specifically, the ratio of the formation of benzene to cyclohexane was 1:2 when the reaction was carried out under an inert atmosphere. In the presence of O₂, Hazari observed a decrease in the relative amount of cyclohexane formed as well as an increase in the amount of water present. It was hypothesized that there were two pathways involved, the first being that in the presence of O₂, cyclohexene reacted to produce benzene and water, and the second being a disproportionation reaction in which hydrogens from one molecule of cyclohexene would combine with two other molecules of cyclohexene to produce 1 equivalent of benzene and 2 equivalents of cyclohexane. In order to differentiate between pathways, attempts were made to shunt the disproportionation pathway. It was thought that disproportionation would only proceed if O₂ was unavailable and since the reaction was carried out in a very narrow J. Young tube, the amount of surface area exposed to the headspace was too small to allow dioxygen to efficiently diffuse throughout the solution. Stirring the solution could be sufficient to keep the concentration of dissolved dioxygen high enough to shunt the competing pathway but since the reaction also required multiple days of heating in a sealed J. Young tube, simply adding a magnetic stir bar would make it impossible to monitor the reaction by NMR. Periodically removing the stir bar would also terminate the experiment since the system must remain closed to be able to quantify the amount of oxygen consumed. An alternative to stirring the solution was to tumble the reaction vessel. This would allow for even more efficient diffusion of the headspace gases into the solution due to an

increased in the surface area of the solvent exposed to the gases in the head space, but tumbling would make it more difficult to heat. An apparatus in which an NMR tube could be tumbled and heated was therefore designed and constructed (Figure 2.3). Through this tumbling and heating technique, it was shown that the disproportionation reaction could be completely shut down resulting in only the formation of benzene.



Figure 2.3. The device that will both heat and tumble a J. Young tube

In order to verify the consumption of O_2 in the oxidation pathway, a Toepler pump was used to carefully quantify the amount of oxygen put into the reaction vessel. Upon

completion of the reaction, the remaining O₂ was measured and the volume of gas consumed was determined by difference. The amount of oxygen consumed was in good agreement with the quantity of benzene formed, as determined by NMR integration and GC analysis.

As complete characterization is essential in the development of a new catalyst, a reliable procedure for preparing the palladium starting material was needed. Surprisingly, in this effort a reliable methodology was developed for the preparation of the pure (diimine)Pd(H₂O)₂²⁺ monomer and not the dimer. Attempts to crystallize 3,5-^tbutyl substituted diimine complex were unsuccessful but vapor diffusion of hexanes or diethyl ether into a tetrahydrofuran (THF) solution of the bis aquo-monomer yielded high quality crystals of a similar compound, (diimine)Pd(THF)₂ (Figure 2.4). Interestingly, the bis-THF adduct has the same structural properties that made the bis-aquo adduct our target catalyst. Specifically, it is a non-organometallic compound without a sacrificial organic group. Initial attempts to prepare this compound for study have been unsuccessful but a reliable procedure was later developed by Matt Winston, as discussed in Chapter 6.

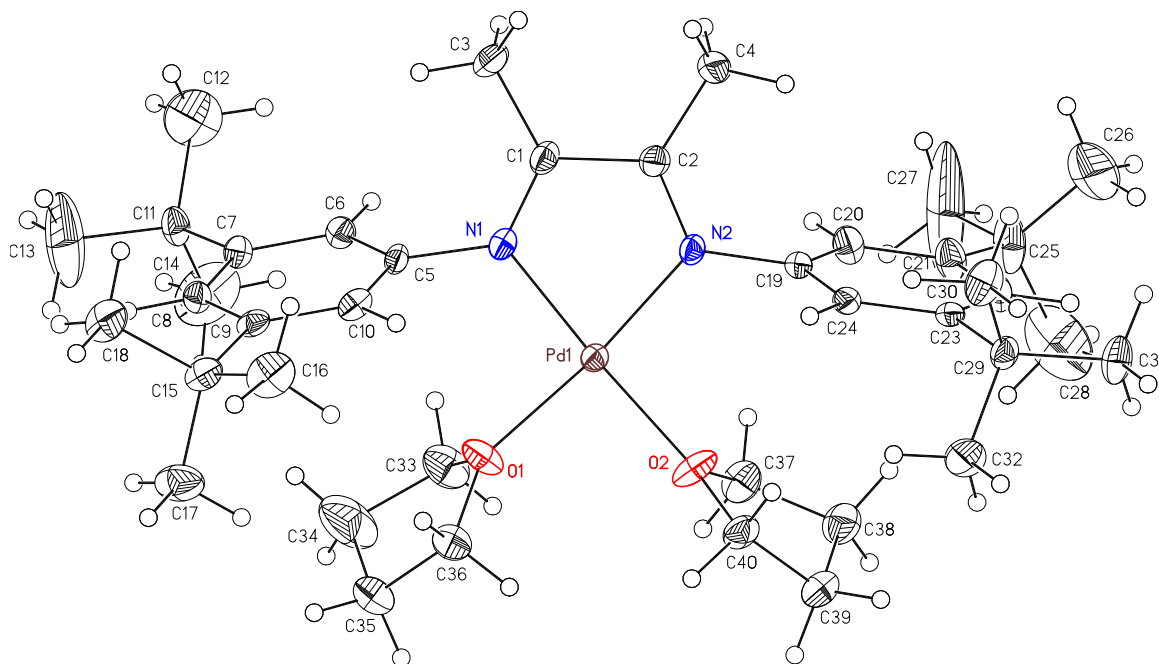


Figure 2.4. Crystal structure of (diimine)Pd(THF)₂²⁺ (50% ellipsoids)

An additional effort to produce crystals of the bis-aquo adduct resulted in the crystallographic characterization of another interesting complex. Vapor diffusion of hexanes or diethyl ether into an acetone solution of (diimine)Pd(H₂O)₂²⁺ again did yield crystals but not of the desired compound. Surprisingly, the compound that was characterized was a product of the C-H activation of acetone. The resulting organometallic compound was that of an enolate where two enolates bridged two palladium centers (Figure 2.5). C-H activation of acetone was highly unexpected, however, it represents a step toward Shilov chemistry since it is the activation of a primary carbon, albeit a much more easily activated one.

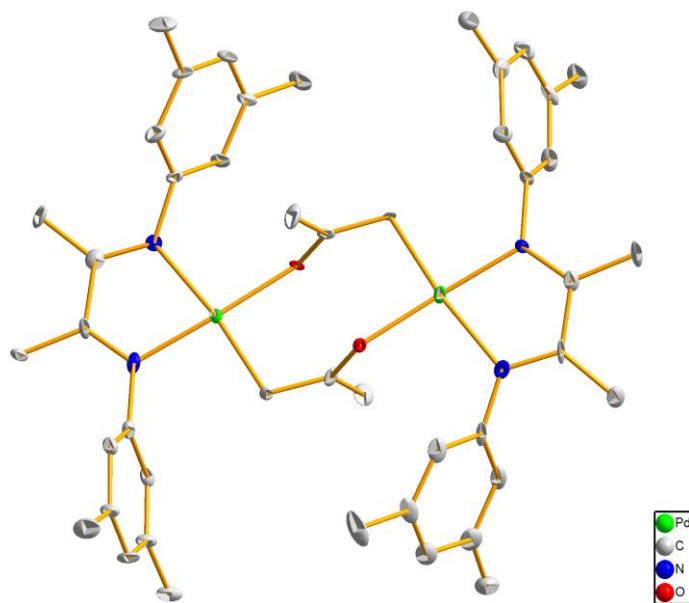


Figure 2.5. Crystal structure of $[(\text{diimine})\text{Pt}(\mu\text{-enolate})]_2^{2+}$ (50% ellipsoids). Solvent, hydrogens, *t*-butylmethyls and counter ions omitted for clarity.

Conclusions

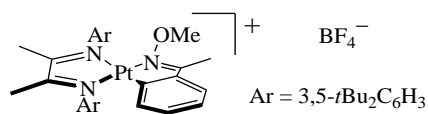
Platinum and palladium hydroxyl-dimers were found to be able to activate a variety of C-H bonds including allylic, benzylic, and aromatic C-H bonds. The kinetics of the C-H activation of cyclohexene by the platinum hydroxyl dimer were investigated. The reaction was found to proceed through an associative substitution mechanism with the rate-limiting step being the association of the substrate. It was also discovered that the palladium system could catalytically dehydrogenate cyclohexene to benzene.

Experimental Section

^1H NMR and ^{13}C NMR spectra were recorded at ambient temperature using a Varian Inova 500 or Mercury 300 MHz spectrometer. The data are reported by chemical shift (ppm) from tetramethylsilane, multiplicity (s, singlet; d, doublet; t, triplet; m, multiplet; dd,

double doublet; dt, double triplet), coupling constants (Hz), and integration. All ^{13}C NMR data were collected proton-decoupled, except where specified. Mass spectra were acquired on a Finnigan LCQ ion trap or Agilent 5973 Network mass selective detector and were obtained by peak matching. All reactions were carried out under an atmosphere of nitrogen (drybox) or argon (standard Schlenk techniques) in glassware that had been oven-dried. Unless otherwise noted, all reagents were commercially obtained and, where appropriate, purified prior to use. Tris(pentafluorophenyl)borane $[\text{B}(\text{C}_6\text{F}_5)_3]$ was purified by sublimation ($90\text{ }^\circ\text{C}$, 0.5 Torr). 2,2,2-Trifluoroethanol- d_3 (TFE- d_3) was dried over 3 \AA molecular sieves for at least 5 days and then vacuum distilled onto $\text{B}(\text{C}_6\text{F}_5)_3$. After 6 h, the TFE- d_3 was vacuum distilled and stored in a Teflon needle-valved vessel. When used in anhydrous conditions, dichloromethane- d_2 (DCM- d_2) and dichloroethane- d_4 (DCE- d_4) were prepared by vacuum transfer from a suspension of CaH_2 and filtration through a syringe filter to remove particulate residue. Anhydrous dichloromethane was prepared by sparging rigorously with nitrogen and passing it through a column of activated alumina. The diimine ligated platinum dichloride,² bridging platinum hydroxyl-dimer,³ platinum-allylbenzene³ adduct, and benzylplatinum complex³ were prepared by Travis Williams as described in the literature (diimine = $\text{ArN}=\text{C}(\text{Me})-\text{C}(\text{Me})=\text{NAr}$, $\text{Ar} = 3,5\text{-}t\text{Bu}_2\text{C}_6\text{H}_3$). TFE- d_3 , DCM- d_2 , DCE- d_4 , $\text{B}(\text{C}_6\text{F}_5)_3$, and platinum and palladium complexes were stored in a Vacuum Atmospheres nitrogen atmosphere drybox.

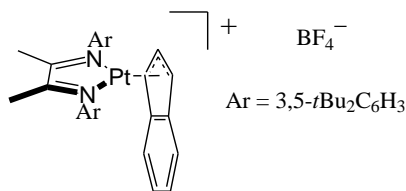
Oxime cycloplatinate



$[(\text{diimine})\text{Pt}(\mu_2\text{-OH})_2[\text{BF}_4]_2$ (diimine = $\text{ArN}=\text{C}(\text{Me})\text{-C}(\text{Me})=\text{NAr}$, Ar = 3,5-*t*Bu₂C₆H₃) (8.2 mg, 5.4 μmol) was weighed out in a standard NMR tube on the benchtop. Dichloromethane-*d*₂ (700 μL) and acetophenone-*O*-methyloxime (1.2 mg, 15 μmol)⁴ were added. The resulting suspension was sonicated until homogeneous and submerged (the tube was submerged up to but not including the Teflon cap) in a 80 °C oil bath for 4 days. Since the reaction was incomplete by ¹H NMR, another portion of oxime (4.7 mg, 56 μmol) was added. The tube was resubmerged in the 80 °C oil bath for an additional 6 days, at which point ¹H NMR indicated that the reaction was complete (> 95% yield). Concentration of the solution, followed by precipitation with hexane, gave the product as a burnt orange powder, which was collected over a Büchner funnel (5.0 mg, 62%).

¹H NMR (500 MHz, dichloromethane-*d*₂, 21 °C) δ = 7.57 (t, ⁴*J*(H,H) = 1.5 Hz, 1H), 7.48 (t, ⁴*J*(H,H) = 1.5 Hz, 1H), 7.17 (d, ³*J*(H,H) = 7.7 Hz, 1H), 7.16 (d, ⁴*J*(H,H) = 1.8 Hz, 2H), 7.08 (d, ⁴*J*(H,H) = 1.8 Hz, 2H), 6.95 (t, ³*J*(H,H) = 7.5 Hz, 1H), 6.68 (t, ⁴*J*(H,H) = 7.7 Hz, 1H), 5.14 (d, ³*J*(H,H) = 8.1 Hz, 1H), 3.04 (s, 3H), 2.31 (s, 3H), 2.31 (s, 3H), 2.27 (s, 3H), 1.36 (s, 9H), 1.36 (s, 9H), 1.33 (s, 9H), 1.33 (s, 9H). ¹³C{¹H} NMR (125 MHz, dichloromethane-*d*₂, 21 °C) δ = 183.8, 181.8, 177.5, 154.0 (2C), 152.7 (2C), 147.1, 145.9, 142.4, 141.4, 133.0, 130.5, 127.6, 125.5, 123.1, 122.4, 117.9 (2C), 117.4 (2C), 62.3, 35.7 (2C), 35.6 (2C), 31.6 (6C), 31.5 (6C), 22.2, 21.1, 12.6. FTIR (KBr) ν = 2960.7 (s), 2869.0 (m), 1600.9 (m), 1587.6 (m), 1475.5 (m), 1458.9 (m), 1437.6 (m), 1364.2 (m), 1248.3 (w), 1156.4 (m), 1083.7 (s), 1059.1 (s), 899.8 (m), 881.8 (m), 760.0 (w), 711.1 (w), 557.9 (w) cm⁻¹. HRMS for [C₄₁H₅₈N₃OPt]⁺: calc'd 803.4228 g/mol, found 803.4223 g/mol.

Indenylplatinum complex

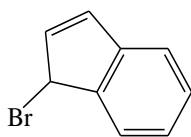


$[(\text{diimine})\text{Pt}(\mu_2\text{-OH})_2][\text{BF}_4]_2$ (diimine = ArN=C(Me)-C(Me)=NAr, Ar = 3,5-*t*Bu₂C₆H₃) (21.0 mg, 13.8 μmol) was weighed out in a J. Young NMR tube in the drybox. Dichloromethane-*d*₂ (700 μL), boron trifluoride (0.44 M in 2,2,2-trifluoroethanol-*d*₃, 62.8 mL, 27.6 μmol) and indene (4.9 μL , 4.8 mg, 42 μmol) were added, and the tube was taken out of the box and submerged (the tube was submerged up to but not including the Teflon cap) in a 40 °C oil bath for 19 hours. Whereas the reaction was incomplete by ¹H NMR, the tube was taken back into the drybox and another portion of indene (4.9 μL , 4.8 mg, 42 μmol) was added. The tube was taken back out of the box and resubmerged in the 40 °C oil bath for an additional 22 hours, at which point ¹H NMR indicated that the reaction was complete (> 95% yield). Concentration of the solution, followed by precipitation with pentane, gave the product as a red powder, which was collected over a Büchner funnel (20.0 mg, 84%).

¹H NMR (300 MHz, dichloromethane-*d*₂, 21 °C) δ = 7.51 (t, ⁴*J*(H,H) = 1.7 Hz, 2H), 7.09 (dd, ³*J*(H,H) = 5.6 Hz, ⁴*J*(H,H) = 3.0 Hz, 2H), 6.91-6.83 (m, 7H), 5.02 (d, ³*J*(H,H) = 2.8 Hz, ¹*J*(Pt,H) = 24 Hz, 2H), 5.02 (d, ³*J*(H,H) = 2.8 Hz, 2H), 2.33 (s, 6H), 1.41 (s, 36H).
¹H NMR (500 MHz, 2,2,2-trifluoroethanol-*d*₃, 21 °C) δ = 7.63 (t, ⁴*J*(H,H) = 1.7 Hz, 2H), 7.09 (dd, ³*J*(H,H) = 5.6 Hz, ⁴*J*(H,H) = 2.9 Hz, 2H), 6.90 (b, s, 4H), 6.82 (dd, ³*J*(H,H) = 5.6 Hz, ⁴*J*(H,H) = 3.2 Hz, 2H), 6.77 (t, ³*J*(H,H) = 2.8 Hz, 1H), 5.02 (d, ³*J*(H,H) = 2.8 Hz, 2H),

2.22 (s, 6H), 1.41 (s, 36H). $^{13}\text{C}\{^1\text{H}\}$ NMR (125 MHz, 2,2,2-trifluoroethanol- d_3 , 21 °C) δ = 172.6 (s, 2C), 155.5 (s, 4C), 151.9 (s, 2C), 135.4 (s, 2C), 129.6 (dd, $^1J(\text{C,H}) = 160$ Hz, $^2J(\text{C,H}) = 6$ Hz, 2C), 124.6 (t, $^2J(\text{C,H}) = 6$ Hz, 2C), 119.4 (d, $^1J(\text{C,H}) = 161$ Hz, 2C), 116.4 (d, $^1J(\text{C,H}) = 160$ Hz, 4C), 105.4 (d, $^1J(\text{C,H}) = 181$ Hz, 1C), 71.80 (d, $^1J(\text{C,H}) = 177$ Hz, $^1J(\text{C,Pt}) = 126$ Hz, 2C), 36.63 (s, 4C), 31.91 (q, $^1J(\text{C,H}) = 130$ Hz, 12C), 18.93 (q, $^1J(\text{C,H}) = 130$ Hz, 2C); J data from a separate non-decoupled experiment. FTIR (neat) ν = 2954.7 (m), 2903.7 (w), 2866.2 (w), 1601.0 (w), 1584.1 (w), 1423.5 (w), 1384.7 (w), 1300.7 (w), 1246.5 (w), 1051.2 (s), 707.5 (w) cm^{-1} . HRMS for $[\text{C}_{41}\text{H}_{55}\text{N}_2\text{Pt}]^+$: calc'd 770.4008 g/mol, found 770.4012 g/mol.

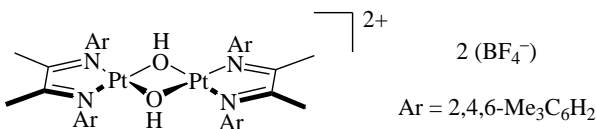
1-Bromoindene



To a dichloromethane solution of the indenylplatinum complex (16.2 mg, 19 μmol) was added 1.0 μL of Br_2 (19 μmol) by micro-syringe. The red solution immediately turned yellow. NMR revealed the formation of 1-bromoindene; and this product was confirmed by mass spectrometry.

^1H NMR (300 MHz, dichloromethane- d_2 , 21 °C) δ = 5.53 (s, broad, 1H), 6.47 (dd, 1H), 6.84 (d, 1H), 7.2-7.6 (4H).

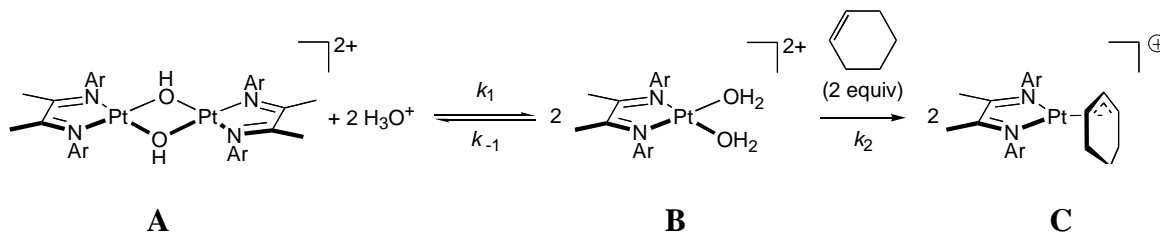
Platinum hydroxide dimer



In the drybox, [(diimine)PtCl₂] (diimine = ArN=C(Me)-C(Me)=NAr, Ar = 2,4,6-Me₃C₆H₂)³ (117 mg, 199 μmol) and silver tetrafluoroborate (80 mg, 408 μmol) were weighed out in an oven-dried 50 mL round bottom flask with a stir bar. To these solids were added ethanol and dichloromethane (each 5 mL) under positive argon pressure, and the suspension was stirred for 2 hours at room temperature. The resulting suspension was filtered through a glass frit to give a translucent orange-brown solution, which was concentrated to dryness under reduced pressure. The resulting residue was dissolved in a solution of ~ 70 mL of ~ 10:1 dichloromethane: tetrahydrofuran and the solution was cooled to 0 °C for 7 days. Product crystallized out of solution but dissolved as the solution warmed to room temperature. The solvent was removed under reduced pressure and the solids were dissolved in dichloromethane. The resulting solution was filtered through a glass micro-filter paper and concentrated down to ~ 2 mL. To this solution ~ 15 mL of hexanes were added and the resulting precipitate was collected over a Büchner funnel. The solids were washed with hexanes and solvent was removed under reduced pressure to give the product as a yellow solid, 101 mg, 82%.

¹H NMR (300 MHz, dichloromethane-*d*₂, 21 °C) δ = 6.94 (s, 8H), 2.34 (s, 24H), 2.21 (s, 12H), 1.98 (s, 12H), -1.02 (s, 2H). ¹³C{¹H} NMR (75 MHz, dichloromethane-*d*₂, 21 °C) δ = 182.3 (4C), 140.3 (8C), 138.9 (4C), 130.1 (4C), 130.1 (8C), 21.5 (4C), 18.8 (4C), 17.7 (8C). HRMS for [C₄₄H₅₈N₄O₂Pt₂]²⁺: calc'd 1064.386 g/mol, found 1064.383 g/mol.

Kinetic studies of the formation of cyclohexenyl platinum complex



Preparation of samples

A (19.3 mg, 12.7 μmol) was weighed out in a 5 mL volumetric flask in the drybox, and the volume was made up with 1,2-dichloroethane- d_4 . 500 μL of this solution was distributed into a screw-capped NMR tube, and each was further diluted with 200 μL DCE- d_4 . Appropriate amounts of cyclohexene and/or borofluoric acid (48%, 7.65 M aqueous, at the temperatures at which these experiments were conducted all the borofluoric acid appeared to be dissolved in the organic layer, so that the solution only contained one phase) were added to give the samples described in tables below. Travis Williams used these for van't Hoff analysis and [cyclohexene] dependence experiments.

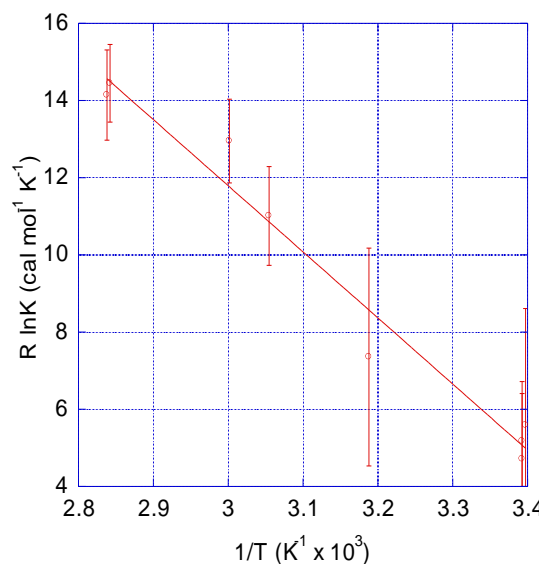
K_{eq} measurement and van't Hoff analysis

A sample of **A** and HBF_4 prepared as above was heated in a 300 MHz Varian (Mercury) NMR. K_{eq} was determined from integrations of *t*Bu peaks at the indicated temperatures (Table 1.1). Each sample was allowed to equilibrate at the indicated temperature until no further change was observed; this typically involved between 15 min (80 $^{\circ}\text{C}$) and 24 hr (20 $^{\circ}\text{C}$). The temperature was cycled twice from room temperature to 80 $^{\circ}\text{C}$. Equilibrium constants at each temperature were calculated from the formula $K_{\text{eq}} = [\text{B}]^2/([\text{A}] \cdot [\text{HBF}_4]^2) \text{ M}^{-1}$. Thermodynamic parameters obtained from the van't Hoff plot are $\Delta H = 17(1) \text{ kcal/mol}$ and $\Delta S = 63(4) \text{ eu}$, $R^2 = 0.971$.

Table 2.1. K_{eq} calculations and van't Hoff plot^a

Trials	Temp	HBF ₄ (aq)	K_{eq}
1	21.2 °C	5 equiv. to Pt	$1.7(25) \times 10^1 \text{ M}^{-1}$
2	40.5 °C	5 equiv. to Pt	$4.1(58) \times 10^1 \text{ M}^{-1}$
3	60.0 °C	5 equiv. to Pt	$6.8(37) \times 10^2 \text{ M}^{-1}$
4	79.2 °C	5 equiv. to Pt	$1.2(7) \times 10^3 \text{ M}^{-1}$
5	21.6 °C	5 equiv. to Pt	$1.1(9) \times 10^1 \text{ M}^{-1}$
6	21.6 °C	5 equiv. to Pt	$1.4(11) \times 10^1 \text{ M}^{-1}$
7	54.2 °C	5 equiv. to Pt	$2.6(61) \times 10^2 \text{ M}^{-1}$
8	78.7 °C	5 equiv. to Pt	$1.4(7) \times 10^3 \text{ M}^{-1}$

^a $R^2 = 0.971$



Dependence of equilibrium position on [HBF₄]

A (9.5 mg, 6.3 μmol) was weighed out in a 2 mL volumetric flask in the drybox, and the volume was made up with 1,2-dichloroethane-*d*₄. 600 μL of this solution was distributed into each of 3 screw-capped NMR tubes, and each was further diluted with 100 mL of DCE-*d*₄. The tubes were removed from the drybox and 0.25 μL , 0.62 μL , and 1.23 μL borofluoric acid (48%, 7.65 M aqueous) solutions were added to each (respectively). Each tube was equilibrated (~ 15 min) in the NMR probe (300 MHz) at 80(1) °C, and ¹H NMR spectra were recorded.

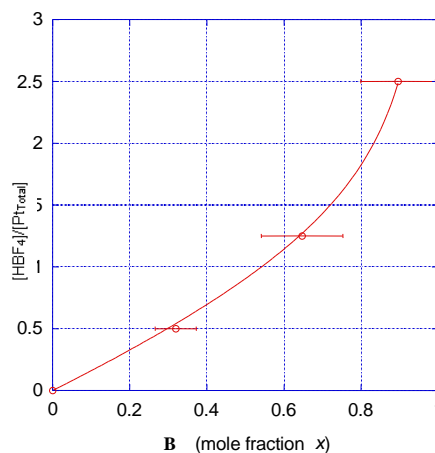
Defining $[\text{Pt}] = 2[\mathbf{A}] + [\mathbf{B}]$, $x = [\mathbf{A}]/[\text{Pt}]$, and $\mu = [\text{HBF}_4]/[\text{Pt}]$, we get the following relationships:

$$K_{\text{eq}} = \frac{[\mathbf{B}]^2}{[\mathbf{A}][\text{HBF}_4]^2} = \frac{2x^2}{[\text{Pt}](1-x)(\mu-x)^2} \quad \mu = x + \sqrt{\left(\frac{2}{K_{\text{eq}}[\text{Pt}]\right) \frac{x^2}{(1-x)}}$$

Data for μ vs. x are shown, along with a non-linear fit, in Table 2.2. The error bars arise from NMR integration over multiple peaks. The value of $K_{\text{eq}} = 1.2(1) \times 10^3 \text{ M}^{-1}$ ($R^2 = 0.999$) agrees well with that determined above at that temperature.

Table 2.2. Dependence of equilibrium position on $[\text{HBF}_4]$

Tria		
1	HBF_4 (μ)	Mole fraction \mathbf{B} (x)
1	1.0 equiv. to \mathbf{A}	31.9(53)%
2	2.5 equiv. to \mathbf{A}	66.5(79)%
3	5.0 equiv. to \mathbf{A}	92.1(87)%



Rate dependence on cyclohexene

NMR sample tubes were prepared as described above, incubated for several hours (3–10) at room temperature, and placed in the NMR probe heated to 80 °C. By the time thermal equilibration was reached, **A** was completely converted to **B**. The conversion of **A** to **C** was monitored by averaging NMR intensities for each aryl C-H signal. k_{obs} was determined for each trial; the plot of k_{obs} vs. [cyclohexene] is shown in Table 2.3.

Table 2.3. Rate dependence on [cyclohexene]^a

Tria	[cyclohexene]	HBF ₄ (aq)	$k_{2\text{ obs}}$
1	5 equiv. to Pt	5 equiv. To Pt	$6.14(90) \times 10^{-4} \text{ s}^{-1}$
2	10 equiv. to Pt	5 equiv. To Pt	$1.07(24) \times 10^{-3} \text{ s}^{-1}$
3	15 equiv. to Pt	5 equiv. To Pt	$1.37(16) \times 10^{-3} \text{ s}^{-1}$
4	20 equiv. to Pt	5 equiv. To Pt	$1.70(17) \times 10^{-3} \text{ s}^{-1}$

a. $R^2 = 0.991$.

Rate dependence on [HBF₄]

A (11.6 mg, 7.64 μmol) and cyclohexene (6.27 mg, 76.4 μmol, 7.72 μL) were mixed in a 2 mL volumetric flask in the drybox, and the volume was made up with 1,2-dichloroethane-*d*₄. 480 μL of this solution was distributed into each of 3 screw-capped NMR tubes, and each was further diluted with 220 μL of DCE-*d*₄. The tubes were removed from the drybox and individually incubated in the NMR probe at 80 °C. To initiate reaction, borofluoric acid (48%, 7.65 M aqueous, as indicated) and a makeup volume of

water (to make $\text{vol}(\text{HBF}_4 \text{ (aq)}) + \text{vol}(\text{H}_2\text{O}) = 2.6 \mu\text{L} = 3.7\%$) were injected, and kinetics data acquisition commenced immediately. Because of the timing of acid injection and excess water, all three species (**A**, **B**, and **C**) were observed. The ^1H NMR integration data was fit by Travis Williams to the general form of the equations for the concentrations of species involved in a series of first-order reactions⁵ (shown in Scheme 2.1), to generate values of $k_{1 \text{ obs}}$ and $k_{2 \text{ obs}}$ as shown in Table 2.4. The large error bars are a consequence of interference by signals due to exchangeable protons (from H_2O and HBF_4) in the NMR spectra; these obscure certain spectral markers. Since the position of the interfering peaks is concentration- and temperature-dependent, different marker peaks are masked at various points in the various runs. Concentrations were determined by averaging ^1H integrations of usable signals for each species, and k_{obs} values calculated by averaging rate constants obtained from the fits to the two appropriate equations.

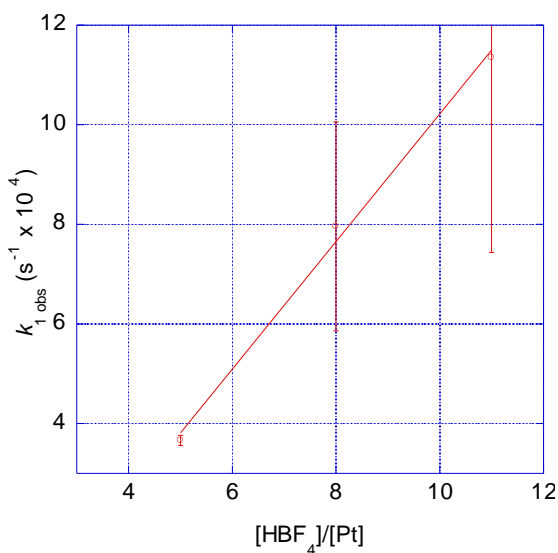
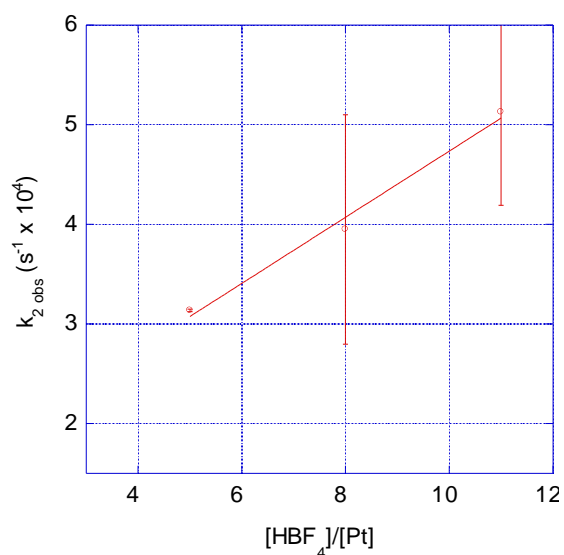
$$[\mathbf{A}] = [\mathbf{A}]_0 e^{(-k_{1 \text{ obs}} t)}$$

$$[\mathbf{B}] = \frac{k_{1 \text{ obs}}}{k_{2 \text{ obs}} - k_{1 \text{ obs}}} [\mathbf{A}]_0 (e^{(-k_{1 \text{ obs}} t)} - e^{(-k_{2 \text{ obs}} t)})$$

$$[\mathbf{C}] = [\mathbf{A}]_0 \left(1 + \frac{k_{2 \text{ obs}}}{k_{1 \text{ obs}} - k_{2 \text{ obs}}} e^{(-k_{1 \text{ obs}} t)} + \frac{k_{1 \text{ obs}}}{k_{2 \text{ obs}} - k_{1 \text{ obs}}} e^{(-k_{2 \text{ obs}} t)} \right)$$

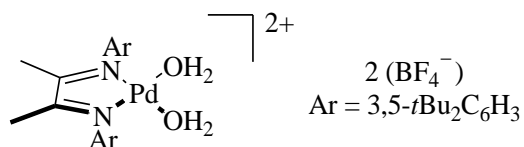
Table 2.4. Rate dependence on $[\text{HBF}_4]^a$

Tria					
1	[cyclohexene]	HBF_4 (aq)	$k_{1\text{ obs}}$	$k_{2\text{ obs}}$	n^a
1	10 equiv. to Pt	5 equiv. to Pt	$3.66(10) \times 10^{-4} \text{ s}^{-1}$	$3.13(1) \times 10^{-4} \text{ s}^{-1}$	2
2	10 equiv. to Pt	8 equiv. to Pt	$8.0(21) \times 10^{-4} \text{ s}^{-1}$	$3.9(12) \times 10^{-4} \text{ s}^{-1}$	2
3	10 equiv. to Pt	11 equiv. to Pt	$1.13(39) \times 10^{-3} \text{ s}^{-1}$	$5.1(9) \times 10^{-4} \text{ s}^{-1}$	4

Acid Dependence of $k_{1\text{ obs}}^b$ Acid Dependence of $k_{2\text{ obs}}^c$ 

^a n = number of measurements of each k . ^b $R^2 = 0.995$. ^c $R^2 = 0.989$.

Bisquo palladium monomer



$[(\text{diimine})\text{PdCl}_2]$ (diimine = $\text{ArN}=\text{C}(\text{Me})-\text{C}(\text{Me})=\text{NAr}$, $\text{Ar} = 3,5\text{-}t\text{Bu}_2\text{C}_6\text{H}_3$) (103

mg, 207 μmol) and 7 mL of dichloromethane (OmnisolvTM) were added to an oven-dried

100 mL round bottom flask with a stir bar. Silver tetrafluoroborate (86 mg, 439 μmol) was weighed out and dissolved in 7 mL of THF. The silver tetrafluoroborate solution was added to the palladium solution and the suspension was stirred for 3 hours at room temperature under positive argon pressure. The resulting suspension of an off-white solid in a yellow-orange solution was filtered through filter paper and washed with excess CH_2Cl_2 . The resulting yellow solution was concentrated to dryness by rotary evaporation. The resulting residue was dissolved in a minimal amount of dichloromethane (~ 2 mL). Addition of 30 mL of petroleum ether resulted in the formation of a light yellow precipitate which was collected over a Büchner funnel. The solid was collected and residual solvent was removed under reduced pressure to give a yellow solid, 94.4 mg, 69%.

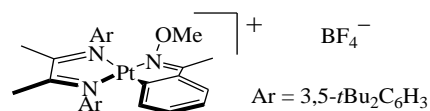
^1H NMR (300 MHz, dichloroethane- d_2 , 21 $^\circ\text{C}$) δ = 7.62 (s, 2H), 7.16 (s, 4H), 2.27 (s, 6H), 7.34 (s, 36H). A drop of trifluoroethanol was added to fully solubilize the product.

The diimine ligated palladium dichloride,² bridging palladium hydroxyl-dimer,³ indenylpalladium complex³, and oxime cyclopalladate³ were prepared by Andy Caffyn and Nilay Hazari as described in the literature (where diimine = $\text{ArN}=\text{C}(\text{Me})-\text{C}(\text{Me})=\text{NAr}$ and $\text{Ar} = 3,5\text{-}t\text{bu}_2\text{C}_6\text{H}_3$ and $2,4,6\text{-Me}_3\text{C}_6\text{H}_2$).

Crystal Structures

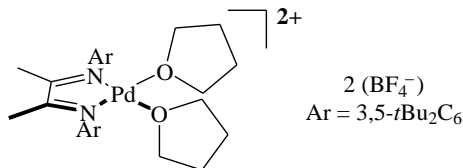
Crystals suitable for X-ray diffraction were grown as described for each compound. Each crystal was mounted on a glass fiber using Paratone-N oil. The structures were solved using direct methods with standard Fourier techniques.

Oxime cycloplatinate



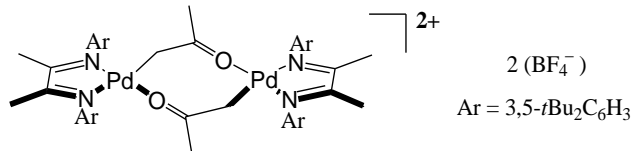
The diffusion of hexane into a methylene chloride solution of oxime cycloplatinate yielded crystals suitable for X-ray diffraction. The crystal data are summarized as follows: formula, $2[\text{C}_{41}\text{H}_{58}\text{N}_3\text{OPt}]^+ 2[\text{BF}_4]^- \cdot 3(\text{CH}_2\text{Cl}_2)$; formula weight, 2036.39; lattice system, triclinic; space group P-1; temperature 100 K; lattice parameters $a = 13.5252(11) \text{ \AA}$, $b = 18.0782(15) \text{ \AA}$, $c = 21.8802(19) \text{ \AA}$, $\alpha = 69.468(2)^\circ$, $\beta = 89.940(2)^\circ$, $\gamma = 71.002(2)^\circ$; unit cell volume $V = 4698.4(7) \text{ \AA}^3$; calculated density $D_{\text{calc}} = 1.439 \text{ Mg/m}^3$; number of molecule in the unit cell $Z = 2$; linear absorption coefficient $\mu = 3.207 \text{ mm}^{-1}$; empirical absorption correction; None; MoK α rays recorded on a Bruker SMART 1000 diffractometer; 73170 reflections collected, 11020 reflections used with $I > 2\sigma(I)$; $\theta_{\text{max}} = 25.33^\circ$; 1000 parameter; no restraints; H atoms were placed in calculated positions; all other atoms were refined anisotropically, full matrix least-squares on F^2 refinement method; reliability factor $R = 0.0601$, weighted reliability factor $R_w = 0.1224$; goodness-of-fit on F^2 2.230. Crystallographic data have been deposited at the CCDC, 12 Union Road, Cambridge CB2 1EZ, UK, and copies can be obtained on request, free of charge, by quoting the publication citation and the deposition number 655348.

Bistetrahydrofuran palladium complex



In an effort to crystallize the bis(aquo) palladium complex, hexane was diffused into a tetrahydrofuran (THF) solution of the bis(aquo) complex. In the process the THF displaced the coordinated water resulting in the crystallization of the bis(THF) palladium complex. The crystal data are summarized as follows: formula, $[\text{C}_{40}\text{H}_{64}\text{N}_2\text{O}_2\text{Pd}]^+ 2[\text{BF}_4]^- \cdot 2(\text{C}_4\text{H}_5\text{O})$; formula weight, 1029.16; lattice system, monoclinic; space group C2/c; temperature 100 K; lattice parameters $a = 21.1511(7) \text{ \AA}$, $b = 16.9881(5) \text{ \AA}$, $c = 28.7218(9) \text{ \AA}$, $\beta = 95.508(2)^\circ$; unit cell volume $V = 10272.6(6) \text{ \AA}^3$; calculated density $D_{\text{calc}} = 1.331 \text{ Mg/m}^3$; number of molecule in the unit cell $Z = 8$; linear absorption coefficient $\mu = 0.433 \text{ mm}^{-1}$; no empirical absorption correction; MoK α rays recorded on a Bruker KAPPA APEX II diffractometer; 200912 reflections collected, 13990 reflections used with $I > 2\sigma(I)$; $\theta_{\text{max}} = 34.18^\circ$; 600 parameter; 25 restraints; H atoms were placed in calculated positions; all other atoms were refined anisotropically, full matrix least-squares on F^2 refinement method; reliability factor $R = 0.0542$, weighted reliability factor $R_w = 0.0768$; goodness-of-fit on F^2 , 1.946. Crystallographic data have been deposited at the CCDC, 12 Union Road, Cambridge CB2 1EZ, UK, and copies can be obtained on request, free of charge, by quoting the publication citation and the deposition number 679914.

Palladium enolate complex



Vapor diffusion of hexanes into an acetone solution of the bis(aryl-imino)acetylacetonate palladium complex yielded X-ray quality crystals of a palladium enolate complex. The poor quality of the data allowed for only the connectivity to be extracted.

References

1. (a) Kannan, S.; James, A. J.; Sharp, P. R. *Polyhedron* **2000**, *19*, 155. (b) Ackerman, L. J.; Sadighi, J. P.; Kurtz, D. M.; Labinger, J. A.; Bercaw, J. E. *Organometallics* **2003**, *22*, 3884.
2. Wong-Foy, A. G.; Henling, L. M.; Day, M.; Labinger, J. A.; Bercaw, J. E. *J. Mol. Catal. A: Chem.* **2002**, *189*, 3.
3. Williams, T. J.; Caffyn, A. J. M.; Hazari, N.; Oblad, P. F.; Labinger, J. A.; Bercaw, J. E. *J. Am. Chem. Soc.* **2008**, *130*, 2418.
4. Beak, O.; Basha, A.; Kokko, B.; Loo, D. *J. Am. Chem. Soc.* **1986**, *108*, 6016.
5. See: Laidler, K. J. *Chemical Kinetics*, 3rd ed.; Harper & Row: New York, 1987.

Chapter 3

Comparing the Mechanism of C-H Bond Activation Between [(diimine)M^{II}(μ₂-OH)]₂²⁺
Dimers (M = Pd, Pt) and Related [(diimine)M^{II}(OH₂)₂]²⁺ Monomers

Adapted in part from:
Bercaw, J. E.; Hazari, N.; Labinger, J. A.; Oblad, P. F., *Angewandte Chemie International Edition* **2008**, 47 (51), 9941–9943.

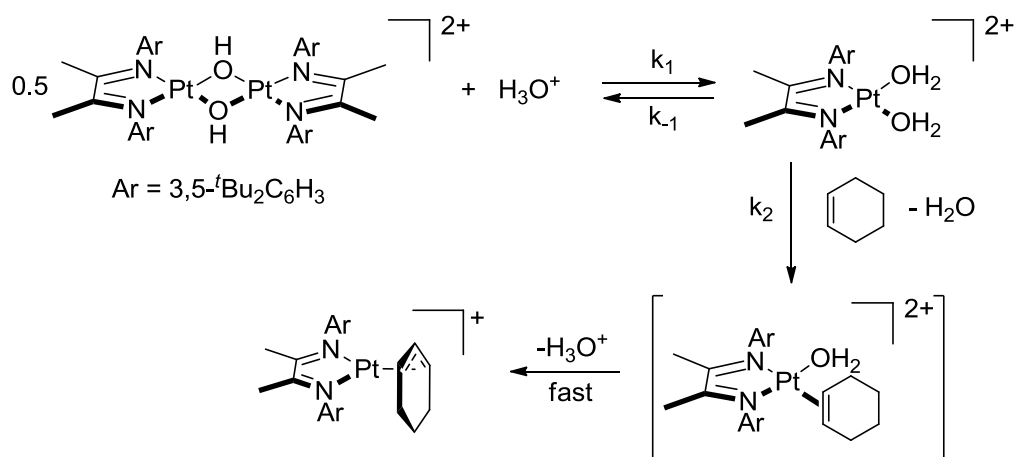
Introduction

Practical methods for the selective functionalization of C-H bonds could have a significant environmental and economic impact in areas ranging from fuels and commodity chemicals to pharmaceuticals.¹ Although there are now many transition metal complexes that can activate C-H bonds, most of these compounds are unstable or inactive in the presence of water or potential functionalized products such as alcohols. As water will usually be a byproduct of oxidative functionalization (especially using O₂) and alcohols are often desirable products, this incompatibility represents a large barrier to the development of catalysts for the transformation of C-H bonds. In order to address this problem, several groups have reported C-H bond activation reactions using metal alkoxide and hydroxyl complexes, which occur even in the presence of free alcohols and, in some cases, water.²

Results and Discussion

We recently reported that the air- and water-tolerant dimeric hydroxyl-bridged dimers [(diimine)M(OH)]₂²⁺ (M = Pt, Pd), can effect not only stoichiometric activation of a variety of C-H bonds (subject to the requirement that a multidentate ligand can be produced), but also catalytic conversion of cyclohexene to benzene, using dioxygen as the terminal oxidant, when the metal is Pd.³ The proposed mechanism for C-H bond activation of cyclohexene by Pt involves initial acid-mediated conversion of dimeric [(diimine)Pt(OH)]₂²⁺ to monomeric [(diimine)Pt(OH₂)]²⁺, followed by displacement of water by cyclohexene at a comparable rate, and then fast conversion of the cyclohexene adduct to an η³-cyclohexenyl species, with concomitant loss of H₃O⁺ (Scheme 3.1). The

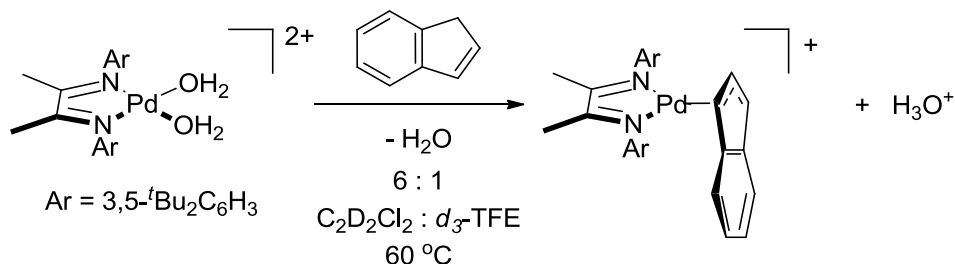
dimeric complex $[(\text{diimine})\text{Pt}(\text{OH})_2]_2^{2+}$ reacts extremely slowly (or not at all) with C-H bonds in the absence of acid, and kinetic data is consistent with consecutive (pseudo-) first-order reactions, with the first step being first-order in $[\text{HBF}_4]$ and the second in [cyclohexene]. Surprisingly, the second step is also first-order in $[\text{HBF}_4]$. We expected that the palladium analog would follow a similar pathway for C-H bond activation, but results presented in this communication demonstrate significant differences between the mechanisms of reactions involving $[(\text{diimine})\text{Pd}(\text{OH})_2]_2^{2+}$ and $[(\text{diimine})\text{Pt}(\text{OH})_2]_2^{2+}$.



Scheme 3.1. C-H activation mechanism

While compound 3,5-*t*-butyl substituted $[(\text{diimine})\text{Pt}(\text{OH}_2)_2]^{2+}$, the proposed active species for C-H activation starting with dimeric $[(\text{diimine})\text{Pt}(\text{OH})_2]_2^{2+}$, has not been isolated but only characterized using ^1H NMR spectroscopy,³ we have previously isolated monomeric $[(\text{diimine})\text{Pd}(\text{OH}_2)_2]^{2+}$.⁴ Although stoichiometric reactions of $[(\text{diimine})\text{Pd}(\text{OH}_2)_2]^{2+}$ with cyclohexene do not yield clean products, stoichiometric

reactions with indene were shown to cleanly yield the η^3 -indenyl species (Scheme 3.2).³
 This reaction was used for detailed mechanistic studies.⁶



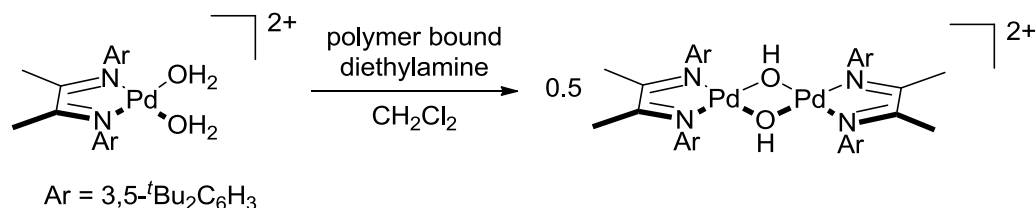
Scheme 3.2. Synthesis of η^3 -indenyl palladium species

Nilay Hazari followed the kinetics by ^1H NMR spectroscopy under the conditions shown in Scheme 3.2, with varying [indene]; acid concentration was also varied by adding BF_3 (which reacts with co-solvent trifluoroethanol (TFE) to generate H^+). The results show that the reaction is first-order in [Pd], [indene], and $[\text{BF}_3]$.⁷ The acid dependence is analogous to that observed for the reaction of $[(\text{diimine})\text{Pt}(\text{OH}_2)_2]^{2+}$ with cyclohexene,³ and suggests that general-acid catalysis assists in the displacement of coordinated water by indene as a result of weakening the Pd-OH₂ or Pt-OH₂ bond; a similar effect has been observed in related systems.⁸ Under acidic conditions, then, both $[(\text{diimine})\text{Pt}(\text{OH}_2)_2]^{2+}$ and $[(\text{diimine})\text{Pd}(\text{OH}_2)_2]^{2+}$ effect C-H activation by the same pathway: rate-limiting coordination of substrate followed by rapid C-H activation.

The reaction of $[(\text{diimine})\text{Pd}(\text{OH}_2)_2]^{2+}$ with indene is not inhibited by water, indicating that substitution of coordinated water by indene is associative. On the other hand, addition of greater than 50 equivalents of water causes an *increase* in the rate.⁷ Analysis of the ^1H NMR spectrum (in the absence of indene) reveals that as the quantity of free water is

increased, resonances corresponding to the hydroxyl-bridged dimer $[(\text{diimine})\text{Pd}(\text{OH})]_2^{2+}$ appear along with those of $[(\text{diimine})\text{Pd}(\text{OH}_2)_2]^{2+}$. Thus, at high concentrations, it appears that water is a sufficiently strong base to deprotonate monomer and establish an equilibrium between $[(\text{diimine})\text{Pd}(\text{OH})]_2^{2+}$ and $[(\text{diimine})\text{Pd}(\text{OH}_2)_2]^{2+}$. When such a solution is treated with indene, the resonances for $[(\text{diimine})\text{Pd}(\text{OH})]_2^{2+}$ disappear significantly *faster* than those for $[(\text{diimine})\text{Pd}(\text{OH}_2)_2]^{2+}$, while the indenyl species grows in. These observations imply that there is a direct pathway for C-H activation with $[(\text{diimine})\text{Pd}(\text{OH})]_2^{2+}$ that does *not* involve $[(\text{diimine})\text{Pd}(\text{OH}_2)_2]^{2+}$ as an intermediate, in contrast to the behavior of platinum analog $[(\text{diimine})\text{Pt}(\text{OH})]_2^{2+}$.

Addition of stronger bases such as 2,6-lutidine, triethylamine, or proton sponge to solutions of $[(\text{diimine})\text{Pd}(\text{OH}_2)_2]^{2+}$ results in rapid and complete deprotonation to $[(\text{diimine})\text{Pd}(\text{OH})]_2^{2+}$.⁷ When these deprotonation reactions were attempted on a preparative scale, the protonated amine could not be cleanly separated from the product; however, the use of a solid supported base, polystyrene-bound diethylamine, allowed the isolation of pure $[(\text{diimine})\text{Pd}(\text{OH})]_2^{2+}$ in 85% yield (Scheme 3.3).⁷ This synthesis represents a significant improvement on the previous method but was further improved upon by Matt Winston, as discussed in Chapter 6.^{3,4}



Scheme 3.3. Synthesis of palladium hydroxyl-bridged dimer

A solution of $[(\text{diimine})\text{Pd}(\text{OH})_2]^{2+}$ in CH_2Cl_2 reacts with indene to form the indenyl species even at room temperature, although very slowly ($t_{1/2} \sim 3$ days). Addition of a small amount of TFE or MeOH (typically a 6:1 ratio of CH_2Cl_2 to alcohol) results in a dramatic increase in rate ($t_{1/2} \sim 5$ minutes). A smaller increase in rate is obtained by adding THF, pentafluoropyridine, or even water ($t_{1/2} \sim 1$ day), but those reactions are not as clean. In contrast, none of $[(\text{diimine})\text{Pt}(\text{OH})_2]^{2+}$, $[(\text{diimine})\text{Pt}(\text{OH}_2)_2]^{2+}$, or $[(\text{diimine})\text{Pd}(\text{OH}_2)_2]^{2+}$ reacts with indene at any appreciable rate at room temperature.

The kinetics for the reaction of $[(\text{diimine})\text{Pd}(\text{OH})_2]^{2+}$ with varying concentrations of indene and TFE (or MeOH, when it was used as an additive) were determined using both ^1H NMR and UV/Vis spectroscopy by Nilay Hazari. The results reveal half-order dependence on $[\text{Pd}]$ (Figure 3.1) and first-order dependence on both $[\text{indene}]$ and $[\text{TFE}]$ (or $[\text{MeOH}]$).⁷ These findings are consistent with the mechanism shown in Scheme 3.4, consisting of a fast equilibrium involving the solvent-assisted separation of $[(\text{diimine})\text{Pd}(\text{OH})_2]^{2+}$ into two monocationic monomers⁹ (which explains both the half-order $[\text{Pd}]$ dependence and the substantial increase in rate when TFE or MeOH is added), followed by rate-determining displacement of coordinated solvent by indene, followed by fast C-H activation. The choice of rate-determining step, indicated by the observed first-order $[\text{indene}]$ dependence, may also explain why the reaction is faster for $[(\text{diimine})\text{Pd}(\text{OH})_2]^{2+}$ than for dicationic monomers $[(\text{diimine})\text{Pt}(\text{OH}_2)_2]^{2+}$ and $[(\text{diimine})\text{Pd}(\text{OH}_2)_2]^{2+}$: water is probably more tightly bound to the dicationic center in the latter, thus slowing displacement; TFE or methanol bound to monocationic monomers generated from $[(\text{diimine})\text{Pd}(\text{OH})_2]^{2+}$ are expected to be more readily displaced.¹⁰

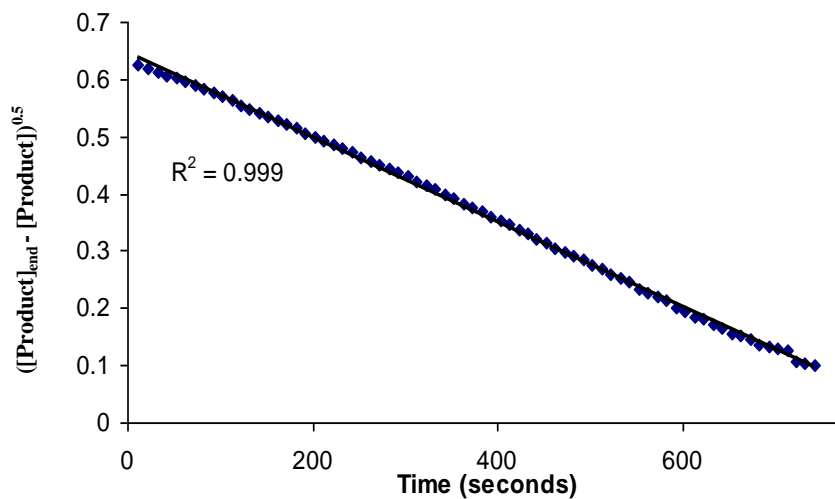
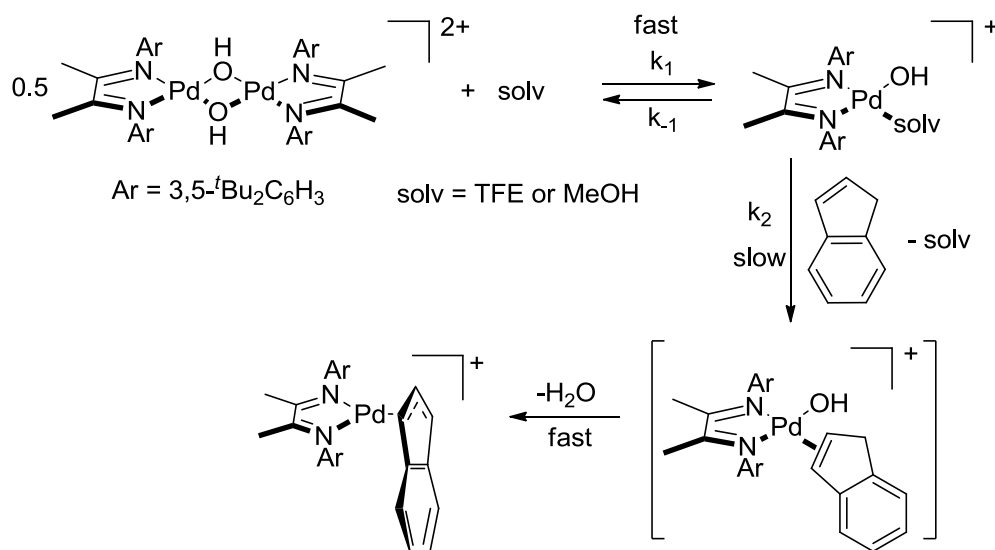


Figure 3.1. Graph of $([(\text{diimine})\text{Pd}(\text{indenyl})]^+_{\text{end}} - [(\text{diimine})\text{Pd}(\text{indenyl})]^+)^{0.5}$ against time during reaction between $([\text{diimine})\text{Pd}(\text{OH})]_2^{2+}$ and 40 equivalents of indene in a 5.5:1 mixture of CH_2Cl_2 :TFE (675 equivalents of TFE)⁷



Scheme 3.4. C-H activation mechanism

The kinetic isotope effect (KIE) for the conversion of 1,1,3-trideuteroindene¹¹ to the deuterated indenyl complex was determined by comparing rate constants for parallel reactions, which reveals a value of $k_H/k_D = 1.6(1)$. This result is consistent with the KIE observed for similar C-H activation reactions with other Pd(diimine) systems, where coordination of the substrate was proposed to be rate limiting.¹²

At this stage the exact reasons for the mechanistic differences between $[(\text{diimine})\text{Pt}(\text{OH})]_2^{2+}$ and $[(\text{diimine})\text{Pd}(\text{OH})]_2^{2+}$ are unclear. The proposed mechanism implies that the hydroxyl bridges are more readily broken by solvent for $[(\text{diimine})\text{Pd}(\text{OH})]_2^{2+}$ than $[(\text{diimine})\text{Pt}(\text{OH})]_2^{2+}$, although $[(\text{diimine})\text{Pd}(\text{OH})]_2^{2+}$ appears to be less basic than $[(\text{diimine})\text{Pt}(\text{OH})]_2^{2+}$ (K_{eq} for the reaction of $[(\text{diimine})\text{Pd}(\text{OH})]_2^{2+}$ with 3.62 eq. of HBF_4 to form $[(\text{diimine})\text{Pd}(\text{OH}_2)_2]^{2+}$ is around 1000 M^{-1} at room temperature, whereas the corresponding reaction with $[(\text{diimine})\text{Pt}(\text{OH})]_2^{2+}$ results in complete conversion to $[(\text{diimine})\text{Pt}(\text{OH}_2)_2]^{2+}$).⁷ On the other hand, the reaction between acid and $[(\text{diimine})\text{Pt}(\text{OH})]_2^{2+}$ takes almost 3 days to go to completion, while the corresponding reaction with $[(\text{diimine})\text{Pd}(\text{OH})]_2^{2+}$ equilibrates in 10 minutes, suggesting that the kinetic barrier to breaking apart $[(\text{diimine})\text{Pt}(\text{OH})]_2^{2+}$ is considerably greater.

Conclusions

The performance of solutions of pure $[(\text{diimine})\text{Pd}(\text{OH})]_2^{2+}$ in TFE in the catalytic conversion of cyclohexene to benzene under 1 atm of O_2 is substantially better than our previous results (which involved $[(\text{diimine})\text{Pd}(\text{OH}_2)_2]^{2+}$ or mixtures of $[(\text{diimine})\text{Pd}(\text{OH})]_2^{2+}$ and $[(\text{diimine})\text{Pd}(\text{OH}_2)_2]^{2+}$ in dichloroethane).³ the rate is sharply increased, there is no initiation period, and there is no competing disproportionation of

cyclohexene to benzene and cyclohexane (a major side reaction using $[(\text{diimine})\text{Pd}(\text{OH}_2)_2]^{2+}$).⁷ Such optimization by means of mechanistic understanding is a major goal of fundamental research in homogeneous catalysis, which we hope to continue to exploit in our further studies aimed at utilizing $[(\text{diimine})\text{Pd}(\text{OH})]_2^{2+}$ and related species for catalytic C-H activation.

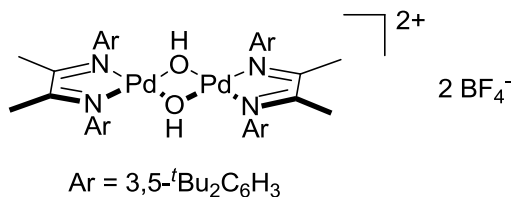
Experimental Section

Unless otherwise noted all reagents were commercially obtained and used without further purification. The Pt hydroxyl-bridged dimer $[(\text{diimine})\text{Pt}(\mu\text{-OH})_2][\text{BF}_4]_2$,³ Pd bis(aquo) dication $[(\text{diimine})\text{Pd}(\text{OH}_2)_2][\text{BF}_4]_2$,⁴ and solutions of BF_3 in TFE¹⁰ were synthesized using literature procedures. All reactions described were conducted under an atmosphere of air, and solvents were not dried prior to use unless otherwise noted. When used in anhydrous conditions, dichloromethane- d_2 (DCM- d_2) and dichloroethane- d_4 (DCE- d_4) were prepared by vacuum transfer from a suspension of CaH_2 and filtration through a syringe filter to remove particulate residue. ^1H NMR spectra were recorded at ambient temperature using a Varian Mercury 300 MHz spectrometer, unless otherwise noted. The data are reported by chemical shift (ppm) from tetramethylsilane, multiplicity (s, singlet; d, doublet; t, triplet; m, multiplet; dd, double doublet; dt, double triplet), coupling constants (Hz), and integration. Mass spectra were acquired on a Finnigan LCQ ion trap or Agilent 5973 Network mass selective detector and were obtained by peak matching. UV/Vis absorbance spectra were recorded on an Agilent 8453 UV/Vis Spectrometer equipped with an HP 89090A Peltier temperature control. Kinetics for the reaction between $[(\text{diimine})\text{Pt}(\mu\text{-OH})_2]^{2+}$, indene, and acid (either aqueous HBF_4 or BF_3 in TFE) were

performed using an analogous procedure to that described previously for the reaction between $[(\text{diimine})\text{Pt}(\text{OH})_2]^{2+}$, cyclohexene, and acid.³ These experiments indicated that these reactions appeared to follow the same pathway.

In the course of this work crystals of $[(\text{diimine})\text{Pd}(\text{OH})_2]^{2+}$ suitable for X-ray diffraction were grown from a saturated solution of CD_2Cl_2 .

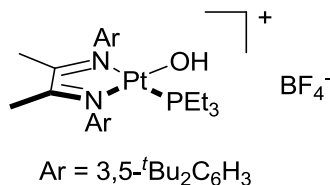
Improved synthesis of palladium hydroxyl-bridged dimer $[(\text{diimine})\text{Pd}(\text{OH})_2]^{2+}$



$[(\text{Diimine})\text{Pd}(\text{OH})_2]^{2+}$ (75 mg, 0.10 mmol) and polymer-bound diethylamine, 1 % cross linked with divinylbenzene (1.5 mmol per g, 140 mg) were weighed out in an 20 mL vial with a stir bar. To these solids was added dichloromethane (15 mL) and the suspension was stirred for 45 minutes at room temperature. The resulting suspension, consisting of a brown solid in a yellow solution, was filtered to give a yellow solution. The filtrate was collected and the solvent removed *in vacuo*. The resulting residue was dissolved in 10 mL of dichloromethane and filtered to remove any residual solid supported base. The filtrate was collected and the solvent removed *in vacuo* to give $[(\text{diimine})\text{Pd}(\text{OH})_2]^{2+}$ as a yellow solid, 37 mg, 85%. Crystals of $[(\text{diimine})\text{Pd}(\text{OH})_2]^{2+}$ suitable for X-ray diffraction were grown from a saturated solution of CD_2Cl_2 .

The ^1H NMR data was consistent with that previously reported for $[(\text{diimine})\text{Pd}(\text{OH})_2]^{2+}$.^{3,4}

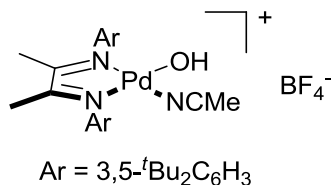
Synthesis of platinum(hydroxyl)triethylphosphine cation, [(diimine)Pt(OH)(PEt₃)]⁺



In a nitrogen-filled glove box, triethylphosphine (1.9 μ L, 12.9 μ mol) was added via a microliter syringe to a J. Young NMR tube containing a dichloromethane-*d*₂ (~ 600 μ L, anhydrous) solution of [(diimine)Pt(μ -OH)]₂²⁺ (10 mg, 6.6 μ mol). The solution immediately changed from turbid yellow to a clear orange-red. The resulting solution contained ¹H NMR signals consistent with [(diimine)Pt(OH)(PEt₃)]⁺; mass spectrometry also confirmed that a species consistent with this formula was present. Attempts to isolate this compound resulted in decomposition to multiple unknown products.

¹H NMR (300 MHz, dichloromethane-*d*₂, 21 °C) δ = 7.53 (t, ⁴*J*(H,H) = 1.2 Hz, 1H), 7.49 (t, ⁴*J*(H,H) = 1.2 Hz, 1H), 7.07 (d, ⁴*J*(H,H) = 1.8 Hz, 2H) 6.90 (d, ⁴*J*(H,H) = 1.8 Hz, 2H) 2.57 (s, 3H), 1.7 (s, 3H), 1.37 (s, 18H), 1.36 (s, 18H) 1.09–1.33 (m, 6H), 0.90–1.05 (m, 9H). ³¹P NMR (121.368 MHz, dichloromethane-*d*₂, 21 °C) δ = 8.82 (t, *J*(P,Pt) = 1918). HRMS for [C₃₈H₄₈PON₂Pt]⁺: calc'd 790.4430 g/mol, found 790.4404 g/mol.

Synthesis of palladium(hydroxyl)acetonitrile cation, [(diimine)Pd(OH)(MeCN)]⁺



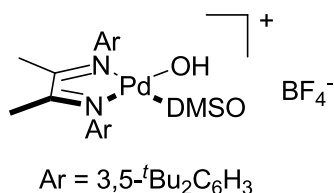
Acetonitrile (6.6 μ L, 0.12 mmol) was added via a microliter syringe to an NMR tube containing a dichloromethane- d_2 (~ 600 μ L, anhydrous) solution of [(diimine)Pd(μ -OH)]₂²⁺ (6.9 mg, 4.40 μ mol). After 30 minutes the turbid yellow solution homogenized. After 24 hours the solution had turned a yellow-orange, and ¹H NMR revealed the presence of new resonances consistent with [(diimine)Pd(OH)(MeCN)]⁺; mass spectrometry also confirmed that a species consistent with this formula was present. Attempts to isolate this compound resulted in decomposition to multiple unknown products.

¹H NMR (300 MHz, dichloromethane- d_2 , 21 °C) δ = 7.29 (t, ⁴ J (H,H) = 1.7 Hz, 1H), 7.15 (t, ⁴ J (H,H) = 1.7 Hz, 1H), 6.90 (d, ⁴ J (H,H) = 1.7 Hz, 2H), 6.64 (d, ⁴ J (H,H) = 1.2 Hz, 2H), 1.24 (s, 18H), 1.17 (s, 18H), 6H from the methyl backbone of the ligand and 3H from acetonitrile obscured by solvent and impurities. MS (FAB⁺) for [C₄₀H₅₁ON₃Pd]⁺: [M]⁺ = 625.2 m/z.

The solvent was removed under reduced pressure and the solids were dissolved in CD₂Cl₂. Indene (3.0 μ L, 26 μ mol) was added via syringe and the solution was heated for 24 hours at 40 °C. No change was observed so the solution was allowed to sit at room

temperature. After 5 days the solution was darker and analysis by ^1H NMR revealed conversion to the indenyl species.

Synthesis of palladium(hydroxyl)dimethylsulfoxide cation, $[(\text{diimine})\text{Pd}(\text{OH})(\text{DMSO})]^+$



Dimethylsulfoxide (12.0 μL , 0.160 mmol) was added via a microliter syringe to a J. Young NMR tube containing a dichloromethane- d_2 (~ 600 μL) solution of $[(\text{diimine})\text{Pd}(\text{OH}_2)_2]^{2+}$ (5.3 mg, 3.94 μmol). After several hours the turbid yellow solution homogenized. After 24 hours the solution had turned a yellow-orange and ^1H NMR revealed the presence of new resonances consistent with $[(\text{diimine})\text{Pd}(\text{OH})(\text{DMSO})]^+$; mass spectrometry also confirmed that a species consistent with this formula was present. Attempts to isolate this compound resulted in decomposition to multiple unknown products.

^1H NMR (300 MHz, dichloromethane- d_2 , 21 $^\circ\text{C}$) $\delta = 7.29$ (t, $^4J(\text{H,H}) = 1.5$ Hz, 1H), 7.15 (t, $^4J(\text{H,H}) = 1.5$ Hz, 1H), 6.90 (d, $^4J(\text{H,H}) = 1.5$ Hz, 2H), 6.58 (d, $^4J(\text{H,H}) = 1.5$ Hz, 2H), 1.23 (s, 18H), 1.17 (s, 18H), 6H from methyl backbone of the ligand and 6H from DMSO were obscured by solvent and impurities. MS (FAB $^+$) for $[\text{C}_{41}\text{H}_{54}\text{SO}_2\text{N}_2\text{Pd}]^+$: $[\text{M}]^+ = 661.4$ m/z.

Indene (5.0 μL , 43 μmol) was added via syringe to the J. Young NMR tube and the solution was heated at 60 $^{\circ}\text{C}$ for 4 days. The solution darkened and analysis by ^1H NMR revealed complete conversion to indenyl species.

Reactions between $[(\text{diimine})\text{Pt}(\mu\text{-OH})]_2^{2+}$, $[(\text{diimine})\text{Pd}(\mu\text{-OH})]_2^{2+}$, and HBF_4

We previously showed $[(\text{diimine})\text{Pt}(\mu\text{-OH})]_2^{2+}$ and $[(\text{diimine})\text{Pt}(\text{OH}_2)_2]^{2+}$ equilibrate slowly in the presence of added aqueous HBF_4 .¹³ These reactions were carried out using CD_2Cl_2 as the solvent. When $[(\text{diimine})\text{Pd}(\mu\text{-OH})]_2^{2+}$ was treated with 3 equivalents of aqueous HBF_4 in CD_2Cl_2 , a yellow solid precipitated out of solution. Addition of 50 μL of d_3 -TFE led to the dissolution of the yellow solid and ^1H NMR indicated that only $[(\text{diimine})\text{Pd}(\text{OH}_2)_2]^{2+}$ was present in solution. The insolubility of $[(\text{diimine})\text{Pd}(\text{OH}_2)_2]^{2+}$ in CD_2Cl_2 presumably drives the reaction to completion and therefore this reaction cannot be used to estimate K_{eq} .

In order to obtain an estimate for the value of K_{eq} for the reaction between $[(\text{diimine})\text{Pd}(\mu\text{-OH})]_2^{2+}$ and added aqueous HBF_4 , the solvent was changed to a 6:1 mixture of $\text{CD}_2\text{Cl}_2:d_3$ -TFE. In this solvent mixture both $[(\text{diimine})\text{Pd}(\text{OH})]_2^{2+}$ and $[(\text{diimine})\text{Pd}(\text{OH}_2)_2]^{2+}$ are fully soluble. K_{eq} was determined from integrations of the aromatic peaks at room temperature using the formula $K_{\text{eq}} = \frac{[(\text{diimine})\text{Pd}(\text{OH}_2)_2]^{2+}}{[(\text{diimine})\text{Pd}(\text{OH})]_2^{2+} \cdot [\text{HBF}_4]^2} \text{ M}^{-1}$. When 3.62 equivalents of aqueous HBF_4 were added to $[(\text{diimine})\text{Pd}(\text{OH})]_2^{2+}$, equilibration between $[(\text{diimine})\text{Pd}(\text{OH})]_2^{2+}$ and $[(\text{diimine})\text{Pd}(\text{OH}_2)_2]^{2+}$ appeared to occur in minutes at room temperature and K_{eq} was 1217 M^{-1} . A comparison experiment was performed between

$[(\text{diimine})\text{Pt}(\mu\text{-OH})_2]^{2+}$ and added aqueous HBF_4 in a 6:1 mixture of $\text{CD}_2\text{Cl}_2:d_3\text{-TFE}$. In this case the reaction was extremely slow, but after 72 hours only $[(\text{diimine})\text{Pt}(\text{OH}_2)_2]^{2+}$ was observed in solution by ^1H NMR spectroscopy, so complete conversion of $[(\text{diimine})\text{Pt}(\text{OH})_2]^{2+}$ had occurred.

Catalytic conversion of cyclohexene to benzene

Representative procedure for cyclohexene oxidation with $[(\text{diimine})\text{Pd}(\text{OH})_2]^{2+}$

$[(\text{diimine})\text{Pd}(\text{OH})_2]^{2+}$ (3.0 mg, 2.2 μmol) was weighed out in a J. Young NMR tube. $\text{TFE-}d_4$ (600 μL) and cyclohexene (16.2 mg, 197 μmol) were added, and the tube was degassed using three consecutive freeze-pump-thaw cycles. The reaction mixture was then placed under 1 atmosphere of O_2 and submerged in a 60 $^\circ\text{C}$ oil bath. The reaction was monitored at regular time intervals using ^1H NMR spectroscopy.

We have previously observed in the reaction of $[(\text{diimine})\text{Pd}(\text{OH}_2)_2]^{2+}$ with cyclohexene under 1 atmosphere of O_2 that even after twelve hours no benzene (or cyclohexane) had formed and that the oxidation/disproportionation reactions did not appear to commence until after the mixture had been heated for approximately fifteen hours.¹⁰ In the reactions of $[(\text{diimine})\text{Pd}(\text{OH})_2]^{2+}$ with cyclohexene, benzene was observed after two hours. After 24 hours using 1 mol % $[(\text{diimine})\text{Pd}(\text{OH})_2]^{2+}$ as the catalyst, 25 % of the cyclohexene had been converted to benzene, whereas the corresponding number using 5 mol % of $[(\text{diimine})\text{Pd}(\text{OH}_2)_2]^{2+}$ was only 8 %. Conversion continued to occur after this time, but in the case of catalysis using $[(\text{diimine})\text{Pd}(\text{OH}_2)_2]^{2+}$ after 24 hours the

disproportionation of cyclohexene to benzene and cyclohexane also started to occur, which makes direct comparison difficult. A maximum conversion of 60% after 3 days was reached using $[(\text{diimine})\text{Pd}(\text{OH})_2]^{2+}$ as a catalyst without the observation of any cyclohexane. Also, once conversion had stopped, presumably because of the complete consumption of O_2 which was the limiting reagent, a palladium mirror was coated on the walls of the NMR tube during catalysis with $[(\text{diimine})\text{Pd}(\text{OH}_2)_2]^{2+}$, while this was not the case for catalysis using $[(\text{diimine})\text{Pd}(\text{OH})_2]^{2+}$ and ^1H NMR spectroscopy indicated that at least some of $[(\text{diimine})\text{Pd}(\text{OH})_2]^{2+}$ catalyst was still intact. Taken together these results demonstrate that $[(\text{diimine})\text{Pd}(\text{OH})_2]^{2+}$ is a considerably more active and stable catalyst.

References

1. (a) Crabtree, R. H. *J. Chem. Soc. Dalton Trans.* **2001**, 17, 2437. (b) Labinger, J. A.; Bercaw, J. E. *Nature* **2002**, 417, 507. (c) Fekl, U.; Goldberg, K. I. *Adv. Inorg. Chem.* **2003**, 54, 259.
2. (a) Tenn, W. J. I.; Young, K. J. H.; Bhalla, G.; Oxgaard, J.; Goddard, W. A.; Periana, R. A. *J. Am. Chem. Soc.* **2005**, 127, 14172. (b) Feng, Y.; Lail, M.; Barakat, K. A.; Cundari, T. R.; Gunnoe, T. B.; Petersen, J. L. *J. Am. Chem. Soc.* **2005**, 127, 14174. (c) Hanson, S. K.; Heinekey, D. M.; Goldberg, K. I. *Organometallics* **2008**, 27, 1454.
3. Williams, T. J.; Caffyn, A. J. M.; Hazari, N.; Oblad, P. F.; Labinger, J. A.; Bercaw, J. E. *J. Am. Chem. Soc.* **2008**, 130, 2418.
4. Ackerman, L. J.; Sadighi, J. P.; Kurtz, D. M.; Labinger, J. A.; Bercaw, J. E. *Organometallics* **2003**, 22, 3884.

5. Previous studies³ have shown that $[(\text{diimine})\text{Pd}(\text{OH}_2)_2]^{2+}$ is able to catalytically convert cyclohexene to benzene under an atmosphere of O_2 . We believe that in stoichiometric reactions an η^3 -cyclohexenyl species is initially formed, but is unstable and decomposes to give palladium(0) and organic byproducts such as 1,3-cyclohexadiene.
6. In order to exclude the possibility that the difference in behavior is due to changing the organic substrate rather than the metal, some kinetic studies were carried out for the reaction of $[(\text{diimine})\text{Pt}(\mu\text{-OH})_2]^{2+}$ and indene in the presence of acid.⁷ The mechanism of C-H activation appears to be completely the same as that for reactions between $[(\text{diimine})\text{Pt}(\text{OH})_2]^{2+}$ and cyclohexene.³
7. Experimental details and more extensive discussion are provided in the experimental section.
8. (a) Annibale, G.; Bergamini, P.; Bertolasi, V.; Bortoluzzi, M.; Cattabriga, M.; Pitteri, B. *Eur. J. Inorg. Chem.* **2007**, 5743. (b) Bortoluzzi, M.; Annibale, G.; Paolucci, G.; Pitteri, B. *Polyhedron* **2008**, 27, 1497.
9. Consistent with this proposal we find that reaction of $[(\text{diimine})\text{Pt}(\text{OH})_2]^{2+}$ with PEt_3 results in the formation of $[(\text{diimine})\text{Pt}(\text{OH})(\text{PEt}_3)]^+$. Similarly, reaction of $[(\text{diimine})\text{Pd}(\text{OH})_2]^{2+}$ with MeCN or DMSO results in the formation of new complexes which contain resonances in the ^1H NMR spectrum consistent with species of the type $[(\text{diimine})\text{Pd}(\text{OH})(\text{MeCN})]^+$ or $[(\text{diimine})\text{Pd}(\text{OH})(\text{DMSO})]^+$, respectively. Both these Pd species activate indene to form indenyl species. See experimental section for more details.
10. Driver, T. G.; Williams, T. J.; Labinger, J. A.; Bercaw, J. E. *Organometallics* **2007**, 26, 294.

11. For the synthesis of 1,1,3-trideuteroindene see Yasuda, M.; Pak, C.; Sakurai, H. *Bull. Chem. Soc. Jpn.* **1980**, *53*, 502.
12. (a) Zhong, H. A.; Labinger, J. A.; Bercaw, J. E. *J. Am. Chem. Soc.* **2002**, *124*, 1378. (b) Heyduk, A. F.; Driver, T. G.; Labinger, J. A.; Bercaw, J. E. *J. Am. Chem. Soc.* **2004**, *126*, 15034.

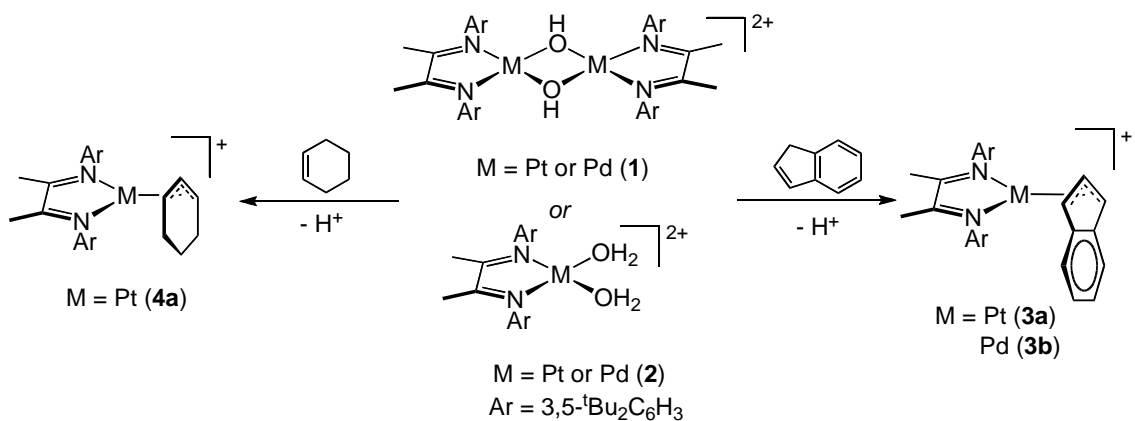
Chapter 4

Oxidation of Organometallic Platinum and Palladium Complexes Obtained from C-H Activation

Adapted in part from:
Oblad, P. F.; Bercaw, J. E.; Hazari, N.; Labinger, J. A., *Organometallics* **2010**, *29* (4),
789–794.

Introduction

The development of practical methods for C-H bond functionalization could have important applications in areas ranging from fuel and commodity chemicals to pharmaceuticals.¹ While many transition metal complexes can activate C-H bonds, controlled transformation of the resulting organometallic species into value-added organic products has been harder to achieve, especially with simple substrates.¹ Complexes $[(\text{diimine})\text{M}(\mu\text{-OH})_2]^{2+}$ and $[(\text{diimine})\text{M}(\text{H}_2\text{O})_2]^{2+}$, where $\text{M} = \text{Pt}$ or Pd and diimine = 1,3-bis(3,5-di-*tert*-butylphenyl)-2,3-dimethyl-1,3-diaza-1,3-butadiene, activate a variety of allylic, benzylic, and aromatic C-H bonds, leading to products including η^3 -indenyl platinum and palladium, and η^3 -cyclohexenyl platinum complexes (Scheme 4.1).^{2,3} One approach to catalytic functionalization based on this chemistry could involve liberation of an organic product by oxidation, as in the Shilov system⁴ (for which these air- and water-stable hydroxo and aquo complexes serve as models). We report here that selective oxidation of the η^3 -complexes platinum and palladium affords halogenated organic products along with well-defined Pd(II) and Pt(II) complexes.

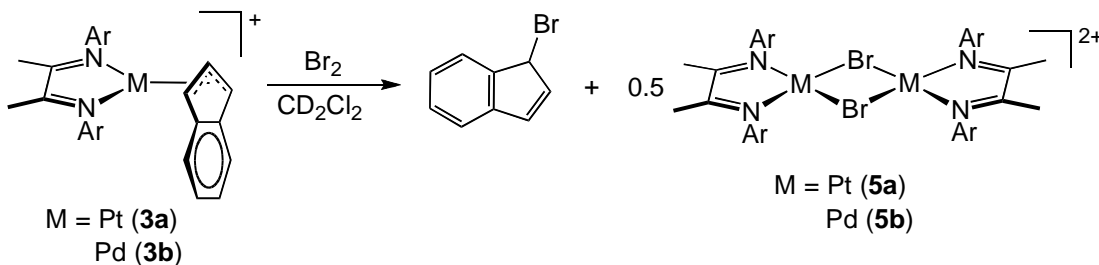


Scheme 4.1. Formation of η^3 -indenyl and cyclohexenyl complexes

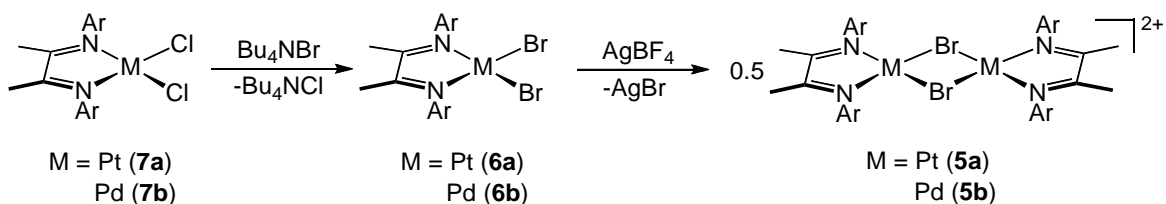
Results and Discussion

Oxidation of indenyl and cyclohexenyl complexes

Addition of one equivalent of Br₂ to a CD₂Cl₂ solution of indenyl complexes of platinum or palladium at room temperature resulted in the rapid and quantitative (by ¹H NMR spectroscopy) formation of 1-bromoindene and dimeric [(diimine)M(μ-Br)]₂²⁺ (M = Pt, Pd) (Scheme 4.2). Both were fully characterized by ¹H and ¹³C NMR spectroscopy, high resolution mass spectrometry (HRMS), and X-ray crystallography, and their formation further confirmed by independent synthesis from [(diimine)MBr₂] (M = Pt, Pd) and AgBF₄ (Scheme 4.3). The formation of 1-bromoindene⁵ was established by ¹H NMR spectroscopy and confirmed by HRMS and independent synthesis from published procedures; its instability to the reaction conditions precluded isolation.

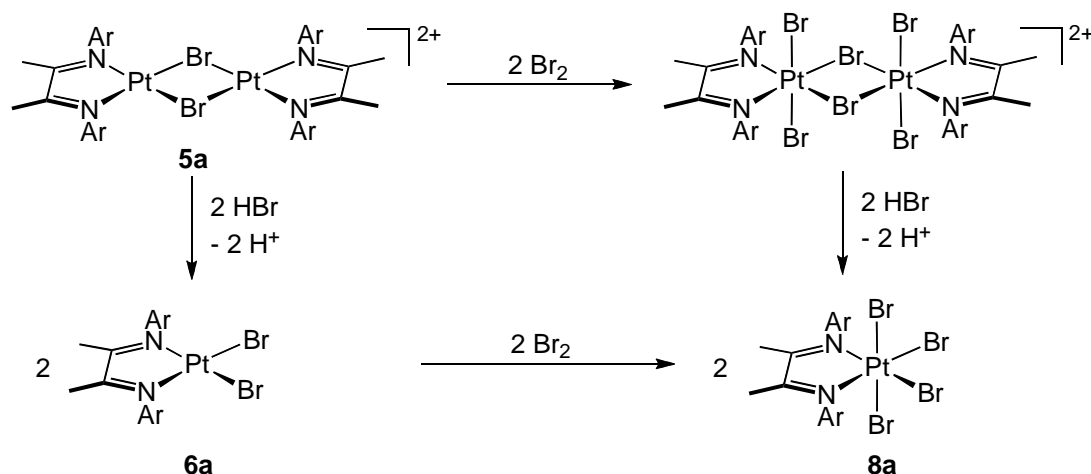


Scheme 4.2. Oxidation of η^3 -indenyl complexes



Scheme 4.3. Independent synthesis of bromo-bridged dimers

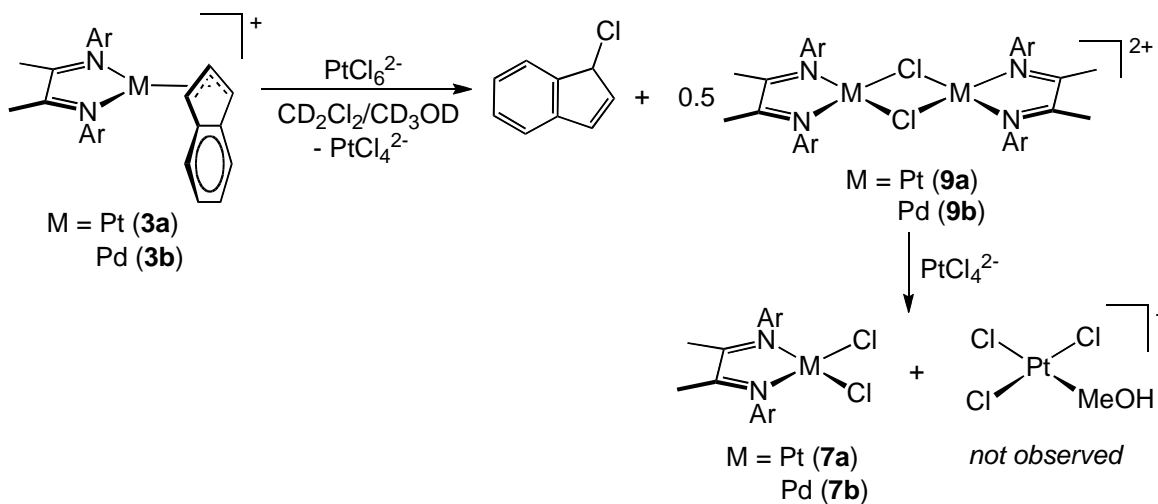
Upon the addition of one equivalent of Br₂, the formation of 1-bromoindene and 5 is observed with only trace amounts of polyhalogenated indane. When excess Br₂ was used, the two indenyl complexes exhibited somewhat different behavior: with indenyl Pd complex, ¹H NMR spectroscopy indicated the partial conversion of 1-bromoindene into a complex mixture of the *trans,trans*- *trans,cis*- and *cis,cis*-isomers of 1,2,3-tribromoindane,⁷ whereas with the η³-indenyl platinum complex, in addition to the conversion of 1-bromoindene to polyhalogenated indanes, the excess Br₂ caused the conversion of [(diimine)Pt(μ-Br)]₂²⁺ into the Pt(IV) species [(diimine)PtBr₄], whose identity was confirmed by independent synthesis through the reaction of [(diimine)PtBr₂] with Br₂. Direct reaction of [(diimine)Pt(μ-Br)]₂²⁺ with Br₂ would not lead to [(diimine)PtBr₄]; most probably adventitious water present reacted with Br₂ to generate HOBr and HBr,⁸ with the latter adding to [(diimine)Pt(μ-Br)]₂²⁺, followed by another equivalent of Br₂ (or the reverse sequence) to form [(diimine)PtBr₄] and H⁺ (Scheme 4.4). The overall process requires three equivalents of Br₂ (excluding the Br₂ consumed in reactions with indene); with fewer than three (but more than one) equivalents of Br₂, mixtures of [(diimine)Pt(μ-Br)]₂²⁺ and [(diimine)PtBr₄] are obtained.



Scheme 4.4. Pathways to platinum tetrabromide complex

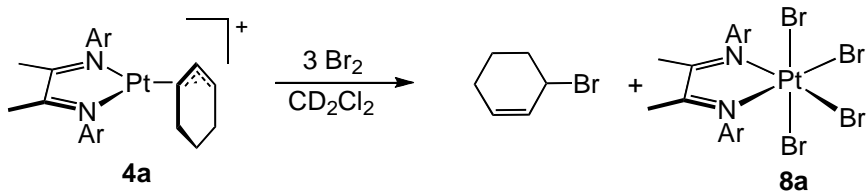
Reaction of **3** with the milder oxidant K_2PtCl_6 in the presence of methanol (to solubilize the oxidant) resulted in quantitative formation (by ^1H NMR spectroscopy) of 1-chloroindene⁹ and $[(\text{diimine})\text{MCl}_2]$ (**7**); the reaction was somewhat cleaner for Pd than for Pt. **7** most likely results from reaction of $[(\text{diimine})\text{M}(\mu\text{-Cl})_2]^{2+}$ ($\text{M} = \text{Pt}, \text{Pd}$), the initial product expected by analogy to the Br_2 chemistry, with the $[\text{PtCl}_4]^{2-}$ that would be generated by reduction of $[\text{PtCl}_6]^{2-}$ (Scheme 4.5). Indeed, $[(\text{diimine})\text{Pd}(\mu\text{-Cl})_2]^{2+}$ (synthesized from $[(\text{diimine})\text{PdCl}_2]$ by abstraction of Cl^- with AgBF_4) reacted with K_2PtCl_4 in methanol to give $[(\text{diimine})\text{PdCl}_2]$ (and, presumably, $\text{PtCl}_x(\text{MeOH})_{4-x}$); furthermore, oxidation of the indenyl palladium complex with two equivalents of CuCl_2 (which would not provide excess Cl^-) gave $[(\text{diimine})\text{Pd}(\mu\text{-Cl})_2]^{2+}$, along with 1-chloroindene. Neither the η^3 -indenyl platinum nor η^3 -indenyl palladium complexes reacted with O_2 or H_2O_2 , even at elevated temperatures. Attempts to catalyze oxidation by O_2 with CuCl_2 , as in the Wacker process,¹⁰ resulted in only stoichiometric (relative to

CuCl_2) conversion of the indenyl palladium complex to $[(\text{diimine})\text{Pd}(\mu\text{-Cl})_2]^{2+}$ and 1-chloroindene.



Scheme 4.5. Oxidation with hexachloroplatinate

Similarly, addition of one equivalent of Br_2 to a CD_2Cl_2 solution of the cyclohexenyl complex gave some 3-bromocyclohexene (identified by comparison with an authentic commercial sample) and $[(\text{diimine})\text{PtBr}_4]$, but a significant amount of the cyclohexenyl complex remained unreacted; the reaction did not go to completion until three equivalents of Br_2 were added (Scheme 4.6). As in the reaction of Br_2 with the indenyl complexes, small amounts of polyhalogenated cyclohexanes were formed. 3-bromocyclohexene was produced in approximately 60% yield from this reaction as quantified by integration from ^1H NMR.

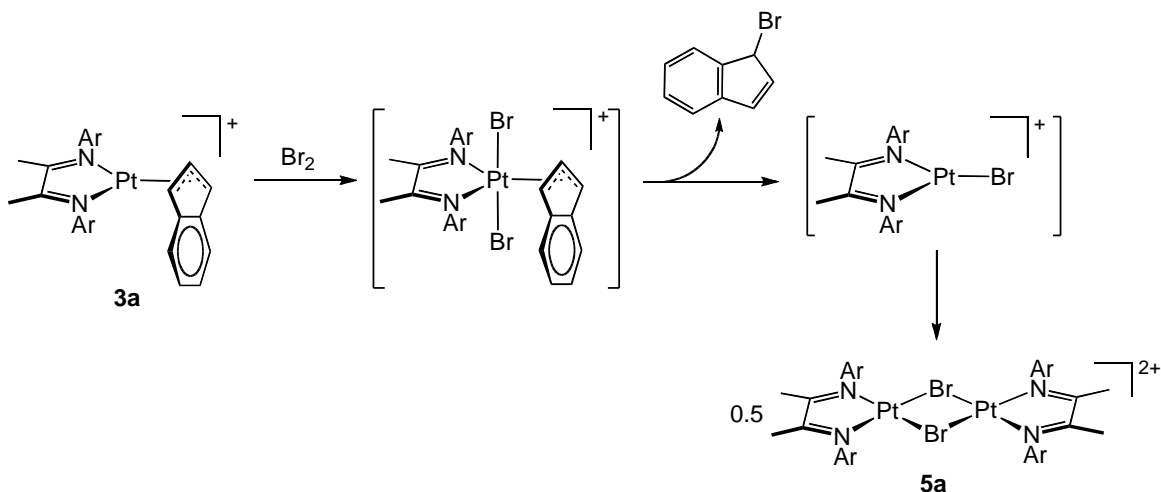


Scheme 4.6. Oxidation with bromine

These observations—that [(diimine)PtBr₄] is the only complex observed, and that excess Br₂ is required for complete conversion of the cyclohexenyl complex—suggest that Br₂ oxidizes the cyclohexenyl platinum complex considerably more slowly than the η³-indenyl platinum complex, and also more slowly than it subsequently oxidizes the (presumed) initial product [(diimine)Pt(μ-Br)]₂²⁺, so that the latter is never observed. Other oxidations of the cyclohexenyl platinum complex were similarly slower than the corresponding reactions of the η³-indenyl platinum complex. The reaction of the cyclohexenyl platinum complex with K₂PtCl₆ to generate 3-chlorocyclohexene (identified by comparison with an authentic commercial sample) and [(diimine)PdCl₂] took place at a reasonable rate only upon heating to 40 °C, while the reaction of the cyclohexenyl platinum complex with CuCl₂ was only 50% complete after three days at room temperature. This comparison suggests that the η³-indenyl ligand is a better donor than η³-cyclohexenyl, making the metal center in the indenyl complex effectively more electron-rich.

The detailed mechanism (or mechanisms: it is quite possible that they are not all the same) of these oxidative cleavages remains unclear at this stage. The Shilov system proceeds via two-electron oxidation of an alkyl Pt(II) intermediate by [PtCl₆]²⁻,¹¹ followed by reductive elimination (via nucleophilic attack).¹² The analogous pathway for

these reactions (Scheme 4.7) appears reasonable, at least for the Pt complexes; for the case of (neutral) [(diimine)PtBr₂], Br₂ is a sufficiently strong oxidant to convert Pt(II) to Pt(IV). Oxidation of Pd(II) to Pd(IV) is likely less favorable, although not unprecedented;¹³ alternative pathways could involve direct attack of either X⁻ or X⁺ on the η³-coordinated ligand or M(0) intermediates.



Scheme 4.7. Possible oxidation mechanism

Molecular structures

X-ray diffraction quality crystals of the indenyl palladium complex were obtained from a saturated solution in 1:1 hexane and CH₂Cl₂. The structure is shown in Figure 4.1, along with selected bond distances and angles. The binding of the diimine ligand to palladium is unexceptional and the bulky aryl substituents are oriented perpendicular to the Pd-N-C-C-N plane. The coordination of the indenyl ligand to palladium is more interesting; the data suggest a hapticity intermediate between η³ and η⁵. Three parameters are typically used to measure the extent of indenyl “ring slippage” in transition metal complexes: ΔM-C (here equal to 0.5{(M-C(33) + M-C(38))} - 0.5{(M-C(39) + M-C(41))}),

the hinge angle (between the {C(39)-C(40)-C(41)} and {C(39)-C(41)-C(33)-C(38)} planes), and the fold angle (between the {C(39)-C(40)-C(41)} plane and the six-membered ring plane).¹⁴ In the indenyl palladium complex, these values are $\Delta M-C = 0.3$ Å, hinge angle = 15.5°, and fold angle = 9.82°. Similar values have been reported for Ni(indenyl)₂,¹⁵ which is considered to be the stereotypical example of an intermediate hapticity indenyl complex.

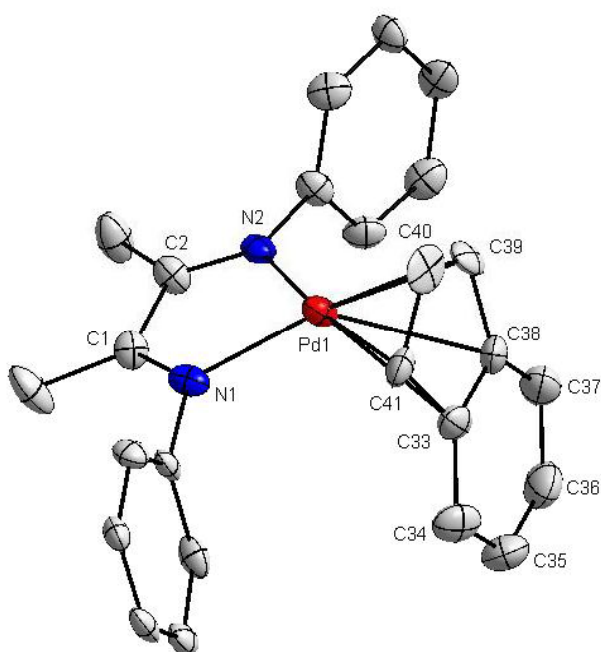
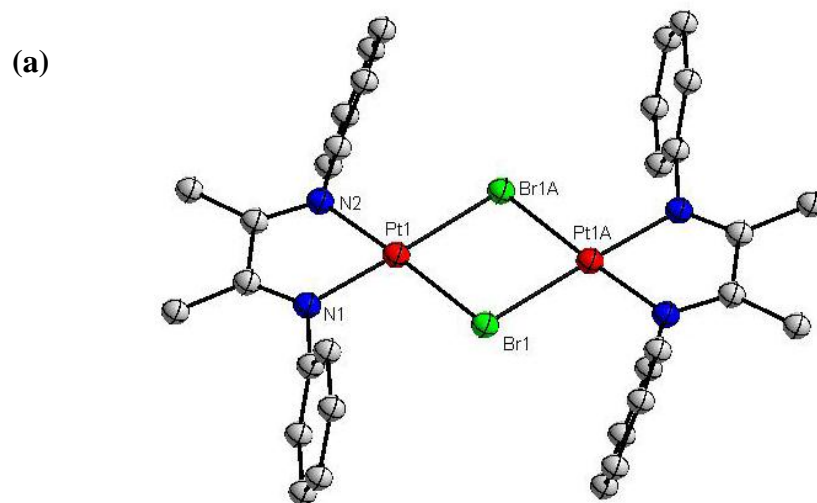


Figure 4.1. The structure of [(diimine)Pd(indenyl)]⁺. All H atoms, the C atoms of the *tert*-butyl substituents on the aryl rings, and the BF₄⁻ counter ion were omitted for clarity. Selected bond distances (Å) and angles (°): Pd(1)-N(1) 2.035(5), Pd(1)-N(2) 2.039(4), Pd(1)-C(41) 2.157(5), Pd(1)-C(39) 2.171(6), Pd(1)-C(40) 2.193(5), Pd(1)-C(33) 2.479(5), Pd(1)-C(38) 2.479(6), N(1)-Pd(1)-N(2) 77.77(19), C(41)-Pd(1)-C(39) 62.9(2), C(41)-Pd(1)-C(40) 37.56(19)

Structures of the related compounds $[(\text{diimine})\text{Pt}(\mu\text{-Br})_2]^{2+}$, $[(\text{diimine})\text{Pd}(\mu\text{-Br})_2]^{2+}$, and $[(\text{diimine})\text{Pd}(\mu\text{-Cl})_2]^{2+}$ are shown in Figure 4.2, along with selected bond distances and angles. Although these complexes all have normal coordination geometries and bond lengths and distances, some general trends may be observed. The differences between platinum and palladium bromo-dimers are small and consistent with the ionic radius of Pt(II) being slightly smaller than that of Pd(II):¹⁶ Pd-N = 2.010(3), 2.015(3) Å; Pt-N = 1.992(2), 2.001(2) Å, while the Pd-Br and Pt-Br distances are identical within error. Both the N-Pt-N (78.56(8)°) and the Br-Pt-Br (83.916(10)°) bond angles are slightly contracted, compared with N-Pd-N (79.61(14)°) and Br-Pd-Br (84.337(19)°), respectively. Compounds $[(\text{diimine})\text{Pd}(\mu\text{-Br})_2]^{2+}$ and $[(\text{diimine})\text{Pd}(\mu\text{-Cl})_2]^{2+}$ are isostructural and have essentially identical Pd-N bond lengths. The Pd-Cl bonds in $[(\text{diimine})\text{Pd}(\mu\text{-Cl})_2]^{2+}$ are shorter than the Pd-Br bonds in $[(\text{diimine})\text{Pd}(\mu\text{-Br})_2]^{2+}$, which is consistent with the differences in size between the halogen atoms. Finally subsequent to the completion of this study a crystal structure of $[(\text{diimine})\text{Pd}(\mu\text{-Cl})_2]^{2+}$ was obtained and found also to be isostructural. Details of which can be found in Appendix C (PFO56).



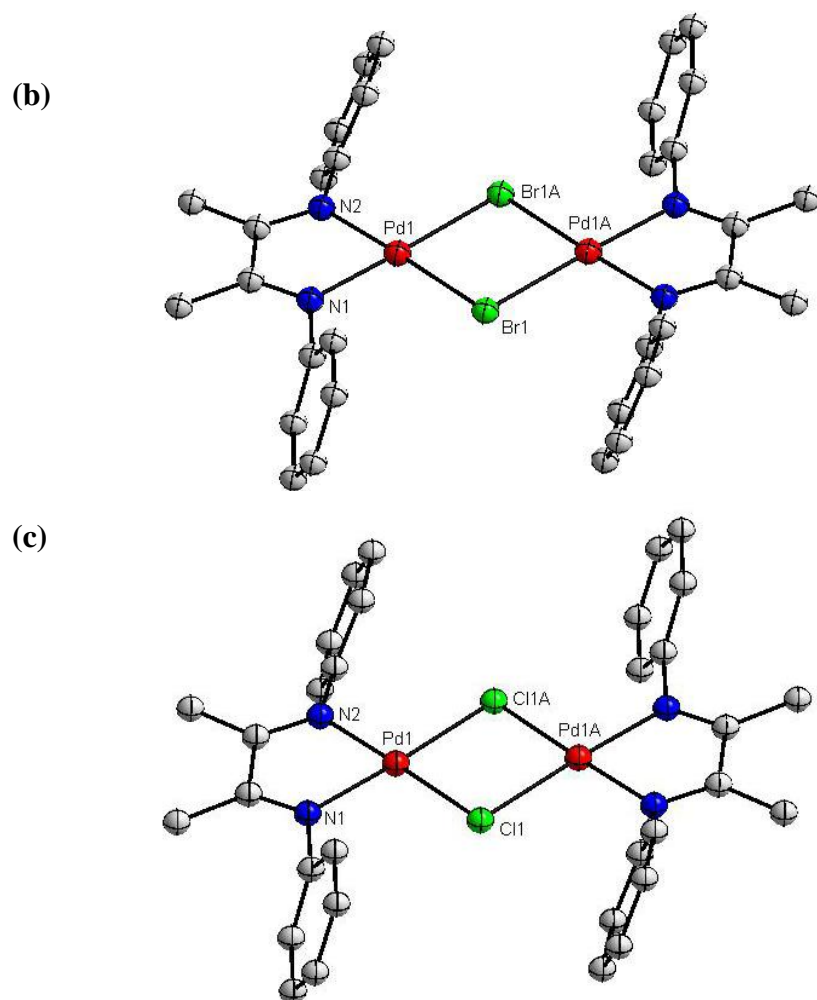


Figure 4.2. The structures of $[(\text{diimine})\text{Pt}(\mu\text{-Br})_2]^{2+}$ (a), $[(\text{diimine})\text{Pd}(\mu\text{-Br})_2]^{2+}$ (b), and $[(\text{diimine})\text{Pd}(\mu\text{-Cl})_2]^{2+}$ (c). All H atoms, the C atoms of the *tert*-butyl substituents on the aryl rings, and the BF_4^- counter ion were omitted for clarity. Selected bond distances (Å) and angles ($^\circ$) of $[(\text{diimine})\text{Pt}(\mu\text{-Br})_2]^{2+}$: Pt(1)-N(2) 1.992(2), Pt(1)-N(1) 2.001(2), Pt(1)-Br(1) 2.4386(3), Pt(1)-Br(1A) 2.4415(3), N(2)-Pt(1)-N(1) 78.56(8), N(2)-Pt(1)-Br(1) 177.36(6), N(1)-Pt(1)-Br(1) 98.85(6), N(2)-Pt(1)-Br(1A) 98.66(6), N(1)-Pt(1)-Br(1A) 177.09(6), Br(1)-Pt(1)-Br(1A) 83.916(10); of $[(\text{diimine})\text{Pd}(\mu\text{-Br})_2]^{2+}$: Pd(1)-N(1) 2.010(3), Pd(1)-N(2) 2.015(3), Pd(1)-Br(1) 2.4447(6), Pd(1)-Br(1A) 2.4401(6), N(1)-Pd(1)-N(2) 79.61(14), N(1)-Pd(1)-Br(1A) 177.40(10), N(2)-Pd(1)-Br(1A) 97.82(10), N(1)-Pd(1)-Br(1) 98.23(10), N(2)-Pd(1)-Br(1) 177.84(10), Br(1A)-Pd(1)-Br(1) 84.337(19); of $[(\text{diimine})\text{Pd}(\mu\text{-Cl})_2]^{2+}$: Pd(1)-N(2) 2.004(2), Pd(1)-N(1) 2.029(2), Pd(1)-Cl(1) 2.3512(7), Pd(1)-Cl(1A) 2.3330(7), N(2)-Pd(1)-N(1) 79.10(9), N(2)-Pd(1)-Cl(1A) 177.81(7), N(1)-Pd(1)-Cl(1A) 98.81(7), N(2)-Pd(1)-Cl(1) 98.10(7), N(1)-Pd(1)-Cl(1) 177.11(7), Cl(1A)-Pd(1)-Cl(1) 83.98(3)

Conclusions

We have shown that several strong oxidants are able to liberate functionalized organic products from organoplatinum and -palladium species obtained by C-H activation. In most cases the process regenerates well-defined platinum(II) and palladium(II) halide complexes, which in principle could be reconverted to hydroxyl-dimers by salt metathesis, in effect closing a catalytic cycle for the conversion of cyclohexene and indenes into halogenated products. Practical catalytic hydrocarbon functionalization will require a system that works with oxidants such as hydrogen peroxide or O₂, leading to direct regeneration of the hydroxo or aquo complexes (and, perhaps, formation of alcohols or other oxygenates instead of organic halides), as well as extension of the range of C-H bonds that can be activated, ultimately to include simple alkanes.

Experimental Section

Unless otherwise stated all reactions were performed under an atmosphere of air. The η^3 -cyclohexenyl platinum, η^3 -indenyl platinum and palladium, and the dichloride platinum and palladium complexes were synthesized according to previously reported literature procedures.² All reagents were commercially obtained and used without further purification. Dichloromethane-*d*₂ and methanol-*d*₄ were purchased from Cambridge Isotope Laboratories and used as received. ¹H and ¹³C NMR spectra were recorded at ambient temperature using a Varian Mercury 300 MHz or Varian Inova 500 MHz spectrometer, equipped with the VNMRJ software program, version 2.2d. The data are reported by chemical shift (ppm) from tetramethylsilane, multiplicity (s, singlet; d, doublet; t, triplet; m, multiplet; dd, double doublet; dt, double triplet), coupling constants (Hz), and integration.

All ^{13}C NMR data were collected proton-decoupled ($^{13}\text{C}\{^1\text{H}\}$), except where specified. Mass spectra were acquired on a Finnigan LCQ ion trap or Agilent 5973 Network mass selective detector and were obtained by peak matching. X-ray crystallographic data were collected on a Bruker KAPPA APEX II instrument, with the crystals mounted on a glass fiber with Paratone-N oil. Structures were determined using direct methods as implemented in the Bruker AXS software package, and crystal and refinement data for $[(\text{diimine})\text{Pd}(\text{indenyl})]^+$, $[(\text{diimine})\text{Pt}(\mu\text{-Br})_2]^{2+}$, $[(\text{diimine})\text{Pd}(\mu\text{-Br})_2]^{2+}$, and $[(\text{diimine})\text{Pd}(\mu\text{-Cl})_2]^{2+}$ are given in Table 4.1.

Table 4.1. Crystal and refinement data for complex $[(\text{diimine})\text{Pd}(\text{indenyl})]^+$, $[(\text{diimine})\text{Pt}(\mu\text{-Br})_2]^{2+}$, $[(\text{diimine})\text{Pd}(\mu\text{-Br})_2]^{2+}$ and $[(\text{diimine})\text{Pd}(\mu\text{-Cl})_2]^{2+}$

	$[(\text{diimine})\text{Pd}(\text{indenyl})]^+$	$[(\text{diimine})\text{Pt}(\mu\text{-Br})_2]^{2+}$	$[(\text{diimine})\text{Pd}(\mu\text{-Br})_2]^{2+}$	$[(\text{diimine})\text{Pd}(\mu\text{-Cl})_2]^{2+}$
Empirical formula	$[\text{C}_{41}\text{H}_{55}\text{N}_2\text{Pd}]^{2+}$ $[\text{BF}_4]^-$	$[\text{C}_{64}\text{H}_{96}\text{N}_4\text{Br}_2\text{Pt}_2]^{2+}$ $2[\text{BF}_4]^- \cdot 2(\text{CH}_2\text{Cl}_2)$	$[\text{C}_{64}\text{H}_{96}\text{N}_4\text{Br}_2\text{Pd}_2]^{2+}$ $2[\text{BF}_4]^- \cdot 6(\text{CH}_2\text{Cl}_2)$	$[\text{C}_{64}\text{H}_{96}\text{N}_4\text{Cl}_2\text{Pd}_2]^{2+}$ $2[\text{BF}_4]^- \cdot 6(\text{CH}_2\text{Cl}_2)$
Formula weight	769.08	1814.92	1977.24	1888.32
Temperature (K)	100(2)	100(2)	100(2)	100(2)
a (Å)	15.5924(9)	31.4961(15)	10.8238(8)	10.8151(9)
b (Å)	10.1874(5)	12.4942(6)	14.2654(10)	14.1838(12)
c (Å)	25.7509(13)	19.3944(10)	16.1568(10)	16.1254(13)
α (deg)	90	90	70.601(3)	71.201(2)
β (deg)	99.400(3)	92.389(2)	74.007(3)	74.183(2)
γ (deg)	90	90	73.310(3)	73.886(2)
Volume (Å ³)	4035.5(4)	7625.4(6)	2208.7(3)	2203.6(3)
Z	4	4	1	1
Crystal system	Monoclinic	Monoclinic	Triclinic	Triclinic
Space group	$\text{P}2_1/n$	$\text{C}2/c$	$\text{P}-1$	$\text{P}-1$
d_{calc} (Mg/m ³)	1.266	1.581	1.487	1.423
θ range (deg)	2.15 to 26.37	1.75 to 29.36	2.00 to 26.78	1.55 to 33.73
μ (mm ⁻¹)	0.507	4.912	1.731	0.889
Abs. correction	None	None	None	None
GOF	1.105	1.371	1.648	1.539
$R_1,^a wR_2^b [I > 2\sigma(I)]$	0.0610, 0.0618	0.0261, 0.0479	0.0451, 0.0841	0.0553, 0.1029

$$^a R_1 = \frac{\sum ||F_o| - |F_c||}{\sum |F_o|}, \quad ^b wR_2 = \frac{[\sum [w(F_o^2 - F_c^2)^2]]}{\sum [w(F_o^2)^2]}^{1/2}.$$

General procedure for oxidation reactions

The following procedures are representative examples of oxidation reactions on both small and large scales. Analogous procedures were used for reactions with Pd starting materials and other oxidants.

Small-scale reactions of $[(\text{diimine})\text{Pt}(\text{cyclohexenyl})]^+$ and $[(\text{diimine})\text{Pt}(\text{indenyl})]^+$ with Br_2

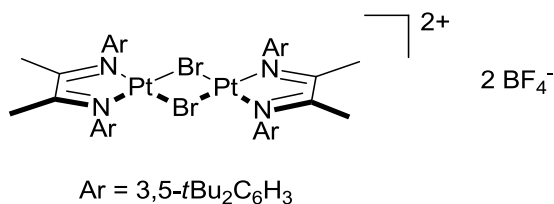
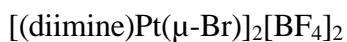
$[(\text{diimine})\text{Pt}(\text{cyclohexenyl})]^+$ (13 mg, 16 μmol) was weighed out and dissolved in 600 μL of CD_2Cl_2 in an NMR tube. Br_2 (1.6 μL , 32 μmol) was added via microliter syringe and tetramethylsilane (5.0 μL , 37 μmol) was also added as an internal standard. The reaction was monitored by ^1H NMR spectroscopy; at the end of the reaction, $[(\text{diimine})\text{Pt}(\text{cyclohexenyl})]^+$, $[(\text{diimine})\text{PtBr}_4]$ and 3-bromocyclohexene were present. When another equivalent of Br_2 was added only $[(\text{diimine})\text{PtBr}_4]$ and 3-bromocyclohexene were present.

$[(\text{diimine})\text{Pt}(\text{indenyl})]^+$ (13.9 mg, 16.2 μmol) was weighed out and dissolved in 600 μL of CD_2Cl_2 in an NMR tube. Br_2 was added via microliter syringe in 0.5 equivalent (0.4 μL , 7.8 μmol) increments. After one equivalent was added ^1H NMR spectroscopy revealed the major product to be $[(\text{diimine})\text{Pt}(\mu\text{-Br})_2]$, and mass spectroscopy revealed the presence of 1-bromoindene. After three equivalents of Br_2 were added the only Pd-containing product present was $[(\text{diimine})\text{PtBr}_4]$.

Large-scale reaction of $[(\text{diimine})\text{Pt}(\text{cyclohexenyl})]^+$ with Br_2

$[(\text{diimine})\text{Pt}(\text{cyclohexenyl})]^+$ (102 mg, 124 μmol) was weighed out and dissolved in 5 mL of CD_2Cl_2 in a 20 mL scintillation vial. Br_2 (13 μL , 248 μmol) was added via microliter syringe. ^1H NMR spectroscopy indicated that the ratio of product to starting

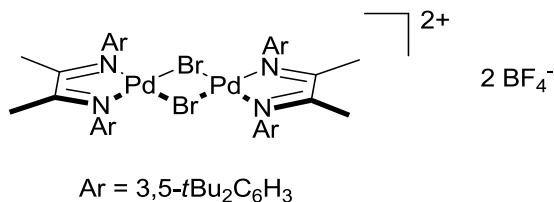
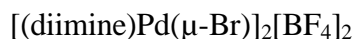
material was 3:1. The solution was filtered through glass filter paper and concentrated to approximately 0.5 mL under reduced pressure. Hexanes were added to the solution until a precipitate formed. The brown solid was collected by filtration over a Büchner funnel to give 101 mg of a 3:1 mixture of [(diimine)PtBr₄] and [(diimine)PtBr₂]. 3-bromocyclohexene was observed by ¹H NMR in 60 ± 10% yield by integration against an internal standard; a more accurate determination of yield was precluded by the instability of 3-bromocyclohexene.



[(diimine)PdBr₂] (21 mg, 26 μmol; preparation below) and silver tetrafluoroborate (5 mg, 26 μmol) were weighed out and transferred to a 20 mL vial equipped with a stir bar. To these solids were added CH₂Cl₂ and THF (each 5 mL) and the suspension was stirred for 1 hour at room temperature. The solution was filtered to remove AgBr and the volatiles were removed under reduced pressure. The remaining solid was dissolved in methanol, the solution was filtered, and the solvent removed under reduced pressure. The resulting yellow solid was dissolved in the minimum amount of CH₂Cl₂ and hexane was added until a precipitate formed. The precipitate was collected by filtration, washed with hexane and dried *in vacuo* to give [(diimine)Pt(μ-Br)]₂[BF₄]₂ as a yellow powder (Yield: 14 mg, 65%).

¹H NMR (300 MHz, dichloromethane-*d*₂, 21 °C) δ = 7.33 (t, ⁴*J*(H,H) = 1.7 Hz, 4H), 7.00 (d, ⁴*J*(H,H) = 1.7 Hz, 8H), 2.02 (s, 12H), 1.23 (s, 72H). ¹³C{¹H} NMR (126 MHz,

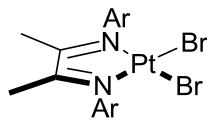
dichloromethane- d_2 , 21 °C) δ = 183.8 (4C), 153.4 (8C), 143.7 (4C), 123.8 (4C), 117.7 (8C), 35.7 (8C), 31.6 (24C), 21.1 (4C). HRMS for $[\text{C}_{64}\text{H}_{96}\text{Br}_2\text{N}_4\text{Pt}_2]^+$: calc'd 1470.528 g/mol, found 1470.525 g/mol. Anal. Calcd ($\text{C}_{64}\text{H}_{96}\text{B}_2\text{Br}_2\text{F}_8\text{N}_4\text{Pt}_2$) (%) C, 46.73; H, 5.88; N, 3.41. Found C, 46.87; H, 5.69; N, 3.36.



$[(\text{diimine})\text{PdBr}_2]$ (30 mg, 41 μmol ; preparation below) and silver tetrafluoroborate (8 mg, 41 μmol) were weighed out in a 20 mL vial equipped with a stir bar. To these solids were added CH_2Cl_2 and THF (each 5 mL, OmnisolvTM) and the suspension was stirred for 2 hours at room temperature. The solution was filtered and the solvent removed from the filtrate under reduced pressure. The resulting yellow solid was dissolved in the minimum amount of CH_2Cl_2 and hexane was added until a precipitate formed. The precipitate was collected by filtration, washed with hexane and then dried *in vacuo* to give $[(\text{diimine})\text{Pd}(\mu\text{-Br})_2][\text{BF}_4]_2$ as a yellow powder (Yield: 7 mg, 26%).

^1H NMR (300 MHz, dichloromethane- d_2 , 21 °C) δ = 7.30 (4H), 6.93 (8H), 2.15 (s, 12H), 1.21 (s, 72H). $^{13}\text{C}\{^1\text{H}\}$ NMR (75 MHz, dichloromethane- d_2 , 21 °C) δ = 184.6 (4C), 153.1 (8C), 144.8 (4C), 123.5 (4C), 117.1 (8C), 35.6 (8C), 31.5 (24C), 21.4 (4C). HRMS for $[\text{C}_{64}\text{H}_{96}\text{Br}_2\text{N}_4\text{Pd}_2]^+$: calc'd 1294.407 g/mol, found 1294.409 g/mol. Anal. Calcd ($\text{C}_{64}\text{H}_{96}\text{B}_2\text{Br}_2\text{F}_8\text{N}_4\text{Pd}_2$) (%) C, 52.37; H, 6.59; N, 3.82. Found C, 52.18; H, 6.53; N, 3.70.

[(diimine)PtBr₂]

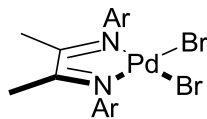


Ar = 3,5-*t*Bu₂C₆H₃

[(diimine)PtCl₂] (119 mg, 0.16 mmol) and tetrabutylammonium bromide (1.01 g, 3.1 mmol) were weighed out and combined in a 100 mL round bottom flask equipped with a stir bar. To these solids was added CH₂Cl₂ (30 mL) and the suspension was stirred for 12 hours at room temperature. The solvent was removed under reduced pressure and the remaining solid suspended in methanol (20 mL) and filtered. ¹H NMR spectroscopy showed the precipitate to be a mixture of [(diimine)PtCl₂] and [(diimine)PtBr₂]. The above procedure was repeated seven times, until only the product remained. [(diimine)PtBr₂] was isolated as a yellow powder (Yield: 100 mg, 80%).

¹H NMR (300 MHz, dichloromethane-*d*₂, 21 °C) δ = 7.41 (t, ⁴*J*(H,H) = 1.7 Hz, 2H), 6.95 (d, ⁴*J*(H,H) = 1.7 Hz, 4H), 1.70 (s, 6H), 1.37 (s, 36H). ¹³C{¹H} NMR (126 MHz, dichloromethane-*d*₂, 21 °C) δ = 177.2 (2C), 151.8 (4C), 146.3 (2C), 122.4 (2C), 118.3 (4C), 35.6 (4C), 31.6 (12C), 21.5 (2C). HRMS for [C₃₂H₄₈Br₂N₂Pt]⁺: calc'd 816.1890 g/mol, found 816.1851 g/mol. Anal. Calcd (C₃₂H₄₈Br₂N₂Pt) (%) C, 47.12; H, 5.93; N, 3.43. Found C, 47.21; H, 6.10; N, 3.36.

[(diimine)PdBr₂]

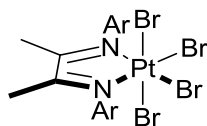


Ar = 3,5-*t*Bu₂C₆H₃

[(diimine)PdCl₂] (250 mg, 0.39 mmol) and tetrabutylammonium bromide (1.26 mg, 3.9 mmol) were weighed out in a 100 mL round bottom flask equipped with a stir bar. To these solids was added CH₂Cl₂ (30 mL) and the suspension was stirred for 12 hours at room temperature. The solvent was removed under reduced pressure and the remaining solid suspended in methanol (20 mL) and filtered. ¹H NMR spectroscopy showed the precipitate to be a mixture of [(diimine)PdCl₂] and [(diimine)PdBr₂]. The above procedure was repeated seven times, until only the product remained.. [(diimine)PdBr₂] was isolated as a yellow powder (Yield: 100 mg, 35%).

¹H NMR (300 MHz, dichloromethane-*d*₂, 21 °C) δ = 7.38 (2H), 6.88 (4H), 2.11 (s, 6H), 1.36 (s, 36H). ¹³C{¹H} NMR (75 MHz, dichloromethane-*d*₂, 21 °C) δ = 177.9 (2C), 151.8 (4C), 146.2 (2C), 122.1 (2C), 117.5 (4C), 35.5 (4C), 31.6 (12C), 21.5 (2C). HRMS for [C₃₂H₄₈Br₂N₂Pd]⁺: calc'd 726.1227 g/mol, found 726.1199 g/mol. Anal. Calcd (C₃₂H₄₈Br₂N₂Pd) (%) C, 52.87; H, 6.66; N, 3.85. Found C, 53.15; H, 6.86; N, 3.88.

[(diimine)PtBr₄]



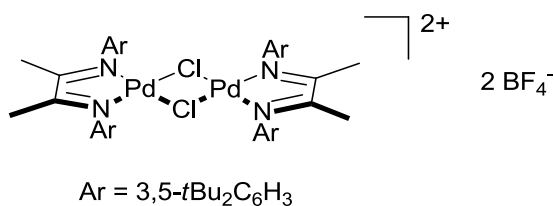
Ar = 3,5-*t*Bu₂C₆H₃

[(diimine)PtBr₂] (22.4 mg, 27.5 μmol) was placed in a vial with 10 mL of CH₂Cl₂ and a stir bar. A solution of bromine (1.6 μL, 31.2 μmol) in approximately 0.5 mL of CH₂Cl₂ was added while stirring; the color immediately changed from dark brown-orange to golden yellow. The solvent was removed under reduced pressure, the resulting yellow solid dissolved in the minimum amount of CH₂Cl₂, and hexane was added until a

precipitate formed. The precipitate was collected by filtration, washed with hexane and then dried to give [(diimine)PtBr₄] as a yellow powder (Yield: 22.4 mg, 83%).

¹H NMR (300 MHz, dichloromethane-*d*₂, 21 °C) δ = 7.38 (t, ⁴J(H,H) = 1.6 Hz, 2H), 6.88 (d, ⁴J(H,H) = 1.6 Hz, 4H), 2.11 (s, with Pt satellites ⁴J(Pt,H) = 9.0 Hz, 6H), 1.36 (s, 36H). ¹³C{¹H} NMR (75 MHz, dichloromethane-*d*₂, 25 °C) δ = 182.0 (2C), 152.7 (4C), 143.5 (2C), 124.0 (2C), 117.9 (4C), 35.6 (4C), 31.5 (12C), 24.1 (2C). HRMS for [C₃₂H₄₈Br₄N₂Pt]⁺: calc'd 976.0158 g/mol, found 976.0152 g/mol. Anal. Calcd (C₃₂H₄₈Br₄N₂Pt) (%) C, 39.40; H, 4.96; N, 2.87. Found C, 39.96; H, 4.32; N, 2.90.

[(diimine)Pd(μ-Cl)]₂[BF₄]₂:



[(diimine)PdCl₂] (40 mg, 63 μmol) and silver tetrafluoroborate (12 mg, 63 μmol) were weighed out in a 20 mL vial equipped with a stir bar. To these solids were added CH₂Cl₂ and THF (each 5 mL) and the suspension was stirred for 2 hours at room temperature, filtered, and the solvent removed under reduced pressure. The resulting yellow solid was dissolved in the minimum amount of CH₂Cl₂ and hexane was added until a precipitate formed. The precipitate was collected by filtration, washed with hexane and dried *in vacuo* to give [(diimine)Pd(μ-Cl)]₂²⁺ as a yellow powder (Yield: 6 mg, 16 %).

¹H NMR (300 MHz, dichloromethane-*d*₂, 21 °C) δ = 7.32 (4H), 6.95 (8H), 2.14 (s, 12H), 1.20 (s, 72H). ¹³C{¹H} NMR (75 MHz, dichloromethane-*d*₂, 21 °C) δ = 185.0 (4C), 153.1 (8C), 143.8 (4C), 123.7 (4C), 117.4 (8C), 35.5 (8C), 31.5 (24C), 21.3 (4C). HRMS

for $[\text{C}_{64}\text{H}_{96}\text{Cl}_2\text{N}_4\text{Pd}_2]^+$: calc'd 1204.503 g/mol, found 1204.509 g/mol. Anal. Calcd ($\text{C}_{64}\text{H}_{96}\text{B}_2\text{Br}_2\text{F}_8\text{N}_4\text{Pd}_2$) (%) C, 55.75; H, 7.02; N, 4.06. Found C, 55.48; H, 6.99; N, 4.08.

References

1. For recent reviews on C-H activation and functionalization, see: (a) Arndtsen, B. A.; Bergman, R. G.; Mobley, T. A.; Peterson, T. H. *Acc. Chem. Res.* **1995**, *28*, 154–162. (b) Erker, G. *Angew. Chem. Int. Ed.* **1999**, *38*, 1699–1712. (c) Davies, H. M. L.; Antoulinakis, E. G. *J. Organomet. Chem.* **2001**, *617–618*, 47–55. (d) Crabtree, R. H. *J. Chem. Soc. Dalton Trans.* **2001**, *17*, 2437–2450. (e) Labinger, J. A.; Bercaw, J. E. *Nature* **2002**, *417*, 507–514. (f) Fekl, U.; Goldberg, K. I. *Adv. Inorg. Chem.* **2003**, *54*, 259–320. (g) Vedernikov, A. N. *Current Organic Chemistry* **2007**, *11*, 1401.
2. (a) Williams, T. J.; Caffyn, A. J. M.; Hazari, N.; Oblad, P. F.; Labinger, J. A.; Bercaw, J. E. *J. Am. Chem. Soc.* **2008**, *130*, 2418–2419. (b) Bercaw, J. E.; Hazari, N.; Labinger, J. A. *J. Org. Chem.* **2008**, *73*, 8654–8657. (c) Bercaw, J. E.; Hazari, N.; Labinger, J. A.; Oblad, P. F. *Angew. Chem., Int. Ed.* **2008**, *47*, 9941–9943. (d) Ackerman, L. J.; Sadighi, J. P.; Kurtz, D. K.; Labinger, J. A.; Bercaw, J. E. *Organometallics* **2003**, *22*, 3884.
3. The palladium analogue of cyclohexenyl complex is unstable: under inert atmosphere the palladium system causes cyclohexene to disproportionate into cyclohexane and benzene, while under oxygen they catalyze dehydrogenation to benzene.²
4. Gol'dshleger, N. F.; Es'kova, V. V.; Shilov, A. E.; Shteinman, A. A. *Zh. Fiz. Khim.* **1972**, *46*, 1353.

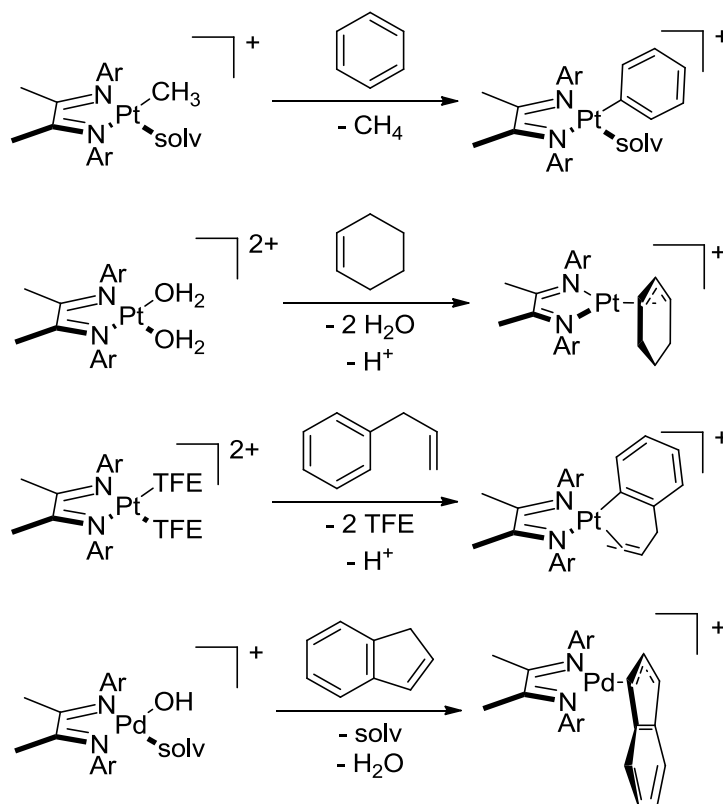
5. Woell, J. B.; Boudjouk, P. *J. Org. Chem.* **1980**, *45*, 5213.
6. Bunnett, J. F.; Creary, X.; Sundberg, J. E. *J. Org. Chem.* **1976**, *41*, 1707.
7. Tutar, A.; Cakmak, O.; Balci, M. *J. Chem. Res., Synop.* **2006**, *8*, 507.
8. Cotton, F. A.; Wilkinson, G. *Advanced Inorganic Chemistry*, 4th ed.; John Wiley & Sons: New York, 1980, pp. 556–557.
9. Friedrich, E. C.; Taggart, D. B. *J. Org. Chem.* **1975**, *40*, 720.
10. Henry, Patrick M. In *Handbook of Organopalladium Chemistry for Organic Synthesis*, Negishi, E., Ed.; Wiley & Sons: New York, **2002**; p. 2119.
11. (a) Kushch, L. A.; Lavrushko, V. V.; Misharin, Y. S.; Moravskii, A. P.; Shilov, A. *E. Nouv. J. Chim.* **1983**, *7*, 729. (b) Luinstra, G. A.; Wang, L.; Stahl, S. S.; Labinger, J. A.; Bercaw, J. E. *J. Organomet. Chem.* **1995**, *504*, 75. (c) Scollard, J. D.; Day, M.; Labinger, J. A.; Bercaw, J. E. *Helv. Chim. Acta.* **2001**, *84*, 3247.
12. Eisenstein, O.; Crabtree, R. H. *New J. Chem.* **2001**, *25*, 665.
13. Dick, A. R.; Kampf, J. W.; Sanford, M. S. *J. Am. Chem. Soc.* **2005**, *127*, 12790.
14. Zargarian, D. *Coord. Chem. Rev.* **2002**, *233–234*, 157.
15. Westcott, S. A.; Kakkar, A. K.; Stringer, G.; Taylor, N. J.; Marder, T. B. *J. Organomet. Chem.* **1990**, *394*, 777.
16. Shannon, R. D. *Acta Crystallogr., Sect. A: Found. Crystallogr.* **1976**, *A32*, 751.

Chapter 5

Uncharged Platinum and Palladium Complexes Ligated With Polypyrazole Borates

Introduction

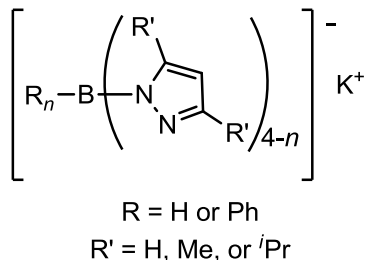
Previous platinum and palladium model systems studied in our laboratory have been based around diimine ligated cationic complexes.¹ Each of these systems facilitated the activation of a variety of C-H bonds (Scheme 5.1) and, as discussed in Chapters 2–3,



Scheme 5.1. C-H activation with cationically charged metal complexes

the rate-limiting step was observed to be associative substitution of the substrate.^{1c, d} The nonpolar nature of the target substrates stood out in contrast to the cationic complexes and led us to question the role the formal charge of the molecule plays in the chemistry. To investigate this we began studying new complexes supported with anionically charged polypyrazolylborate ligands that could yield an uncharged metal complex (Scheme 5.2).

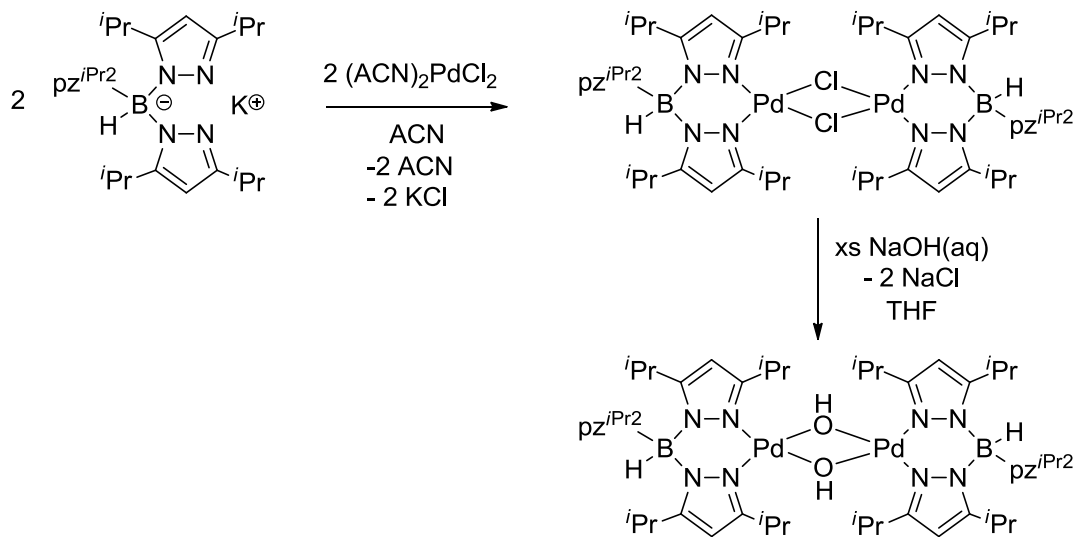
We hypothesize that an uncharged complex could make activation of nonpolar substrates more facile.



Scheme 5.2. Polypyrazolyborate ligands

Results and Discussion

Akita demonstrated that $[Tp^{iPr}Pd-\mu-OH]_2$ (where Tp^{iPr} = hydrotris(3,5-diisopropylpyrazol-1-yl)borate) could be synthesized by treating the dichloro precursor with an aqueous solution of NaOH (Scheme 5.3).² This complex seemed like a reasonable starting



Scheme 5.3. Synthesis of $[Tp^{iPr2}PdOH]_2$

point since we had found the diimine hydroxyl-dimers to be so reactive. Unfortunately, the $[\text{Tp}^{i\text{Pr}}\text{Pd}-\mu\text{-OH}]_2$ was unreactive toward C-H bonds at room temperature even in the presence of acid or a coordinating solvent. At elevated temperature the reaction mixture turned from light yellow to red. Efforts to purify the red product in this solution yielded red crystals suitable for X-ray diffraction studies. Surprisingly the palladium starting material did not react with the substrate but decomposed to form an asymmetric bimetallic palladium complex in which there was a Pd-Pd bond and a bridging pyrazole (Figure 5.1). Interestingly, both palladium centers had been reduced to the +1 oxidation state, two boron-

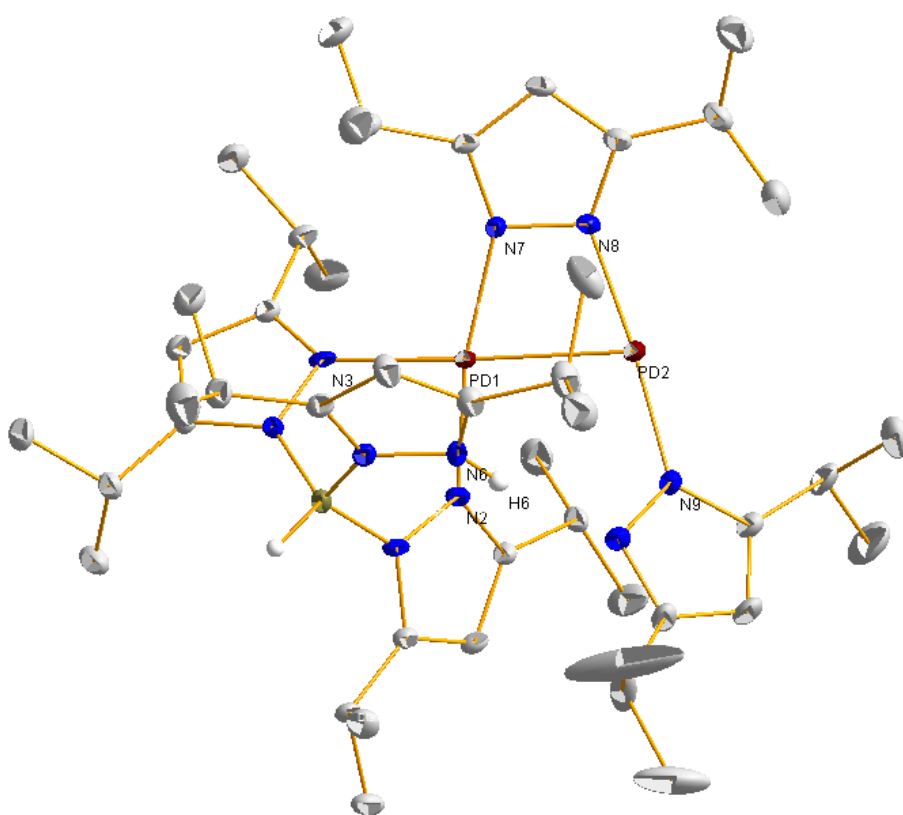


Figure 5.1. Crystal structure of $\text{Pd}^{\text{I}}\text{-Pd}^{\text{I}}$ decomposition product (50% ellipsoids). Hydrogens and counter ion omitted for clarity.

nitrogen bonds had been cleaved, and the pendant pyrazol on the remaining intact ligand had been protonated. We initially thought that the instability of this complex could be due to either the bulky isopropyl substituents or the pendant pyrazol. We, therefore, explored the possibility of forming similar compounds utilizing the less bulky hydrotris(3,5-dimethylpyrazol-1-yl)borate (Tp^{Me}) and diphenylbispyrazol-1-ylborate (Ph_2Bpz_2). Metallation of Tp^{Me} proved to be more difficult than Tp^{iPr} . Treatment with bisacetonitrile palladium dichloride to form the chloro-bridged dimer yielded multiple products by NMR and the speciation increased over time. Due to the instability of the chlorinated products, isolation was not attempted and the solution was treated immediately with a solution of aqueous NaOH. This procedure resulted in trace amounts of the product, as observed by the diagnostic hydroxyl proton peaks in the NMR spectrum, but this product was also unstable and could not be isolated. Finally, treatment of bisacetonitrile palladium dichloride with $\text{Ph}_2\text{Bpz}_2\text{K}$ resulted in no stable isolable products.

Platinum metallation of this series of polypyrazoleborates was also investigated. It was found that treatment of $(\text{DMS})_2\text{PtCl}_2$ in THF with these ligands yielded three new complexes: $\text{Tp}^{\text{iPr}}\text{PtCl}(\text{DMS})$, $\text{Tp}^{\text{Me}}\text{PtCl}(\text{DMS})$, and $\text{Ph}_2\text{Bpz}_2\text{PtCl}(\text{DMS})$. These complexes have been fully characterized including crystal structures for the latter two (Figures 5.2 and 5.3, respectively). We explored the possibility of displacing DMS or chloride. Unfortunately, treatment with silver salts, NaOH, or alkyllithium reagents only resulted in decomposition products. It is anticipated that these complexes may have interesting reactivity, however, due to lack of time, they were not fully explored.

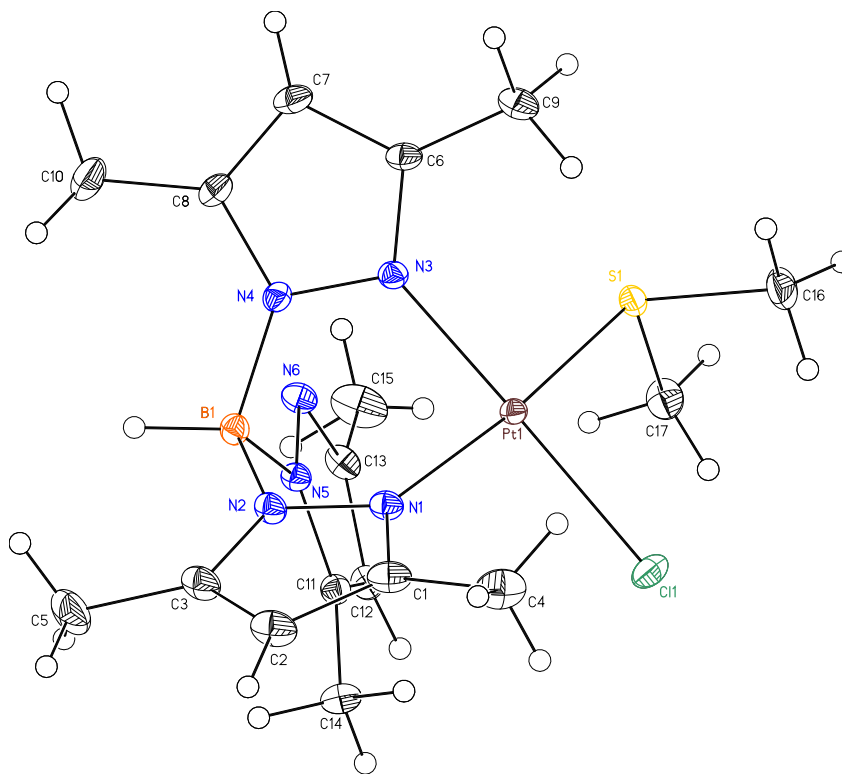


Figure 5.2. Crystal structure of $\text{Tp}^{\text{Me}}\text{PtCl}(\text{DMS})$ (50% ellipsoids)

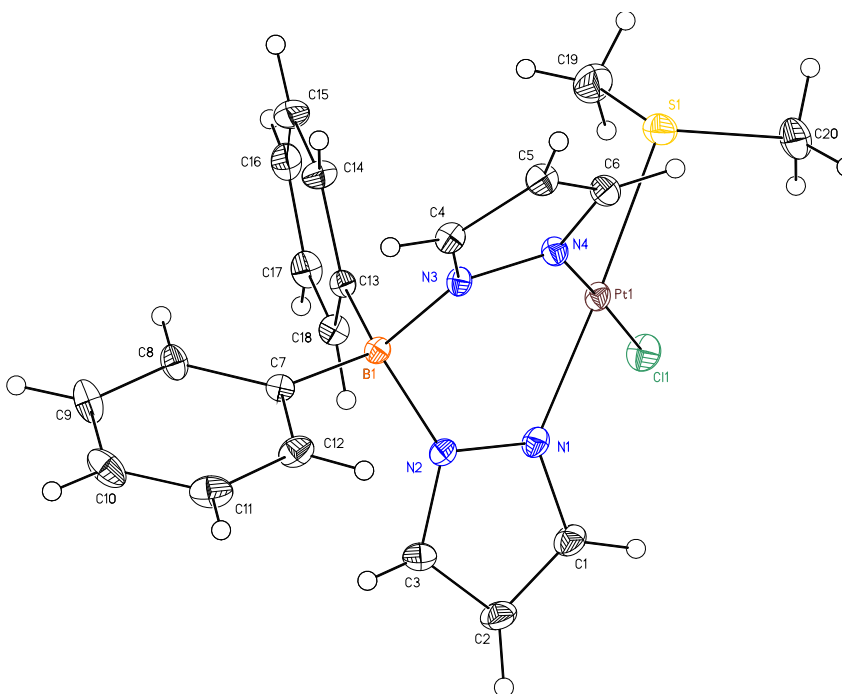
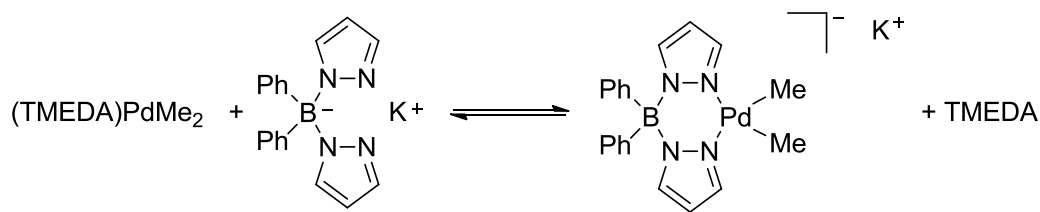


Figure 5.3. Crystal structure of $\text{Ph}_2\text{Bpz}_2\text{PtCl}(\text{DMS})$ (50% ellipsoids)

The inability of the polypyrazoleborate palladium hydroxyl-dimers to facilitate C-H activation led to an exploration of other possible palladium complexes. We found that treating (TMEDA)PdMe₂ (TMEDA = tetramethylethylenediamine) with diphenyl bispyrazol-1-ylborate (Ph₂Bpz₂) resulted in an equilibrium between the starting materials, free TMEDA, and a new complex, KPh₂Bpz₂PdMe₂ (Figure 5.4). Unfortunately, the



Scheme 5.4. Synthesis of KPh₂Bpz₂PdMe₂

equilibrium favored the starting materials. The reaction could be advanced incrementally however, by intermittently pulling a vacuum on the mixture to remove the TMEDA. This methodology was slow since both the acetonitrile solvent and TMEDA have relatively high boiling points. Fortunately, we found a much more efficient synthesis. By making a biphasic mixture of acetonitrile and hexanes, the TMEDA could be drawn into the organic layer while the palladium product remained in the acetonitrile. Periodically pipetting off the layer of hexanes and free TMEDA then adding clean hexanes allowed the reaction to be driven to greater than 95% completion in less than 3 hours. Reaction times longer than 3 hours would lead to formation of small amounts of palladium(0) decomposition. The resulting KPh₂Bpz₂PdMe₂ complex was also characterized crystallographically. Interestingly, in the solid state, the complex formed a structure in which there were chains of complexes linked by a potassium ion that was coordinated to the palladium methyl

center and phenyl group of one complex and the pyrazols of a neighboring complex (Figure 5.4). Our studies have shown that this compound has interesting reactivity.

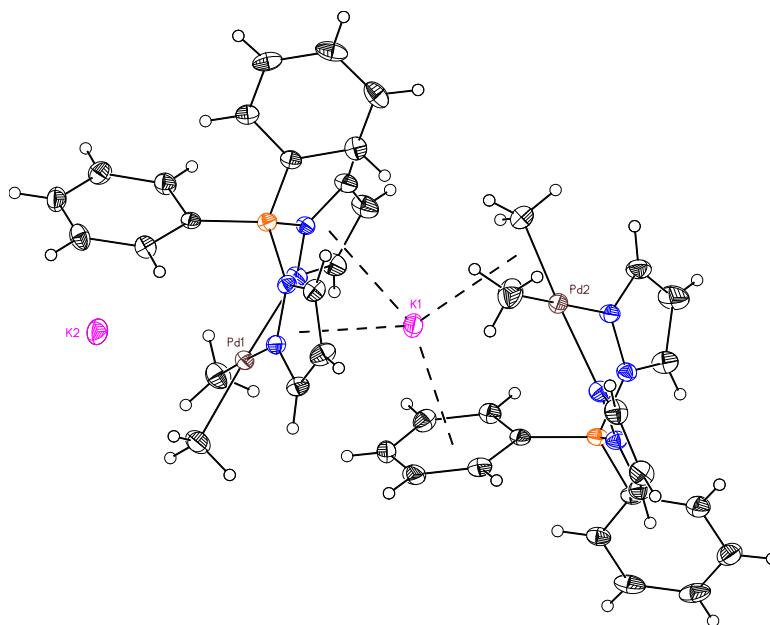
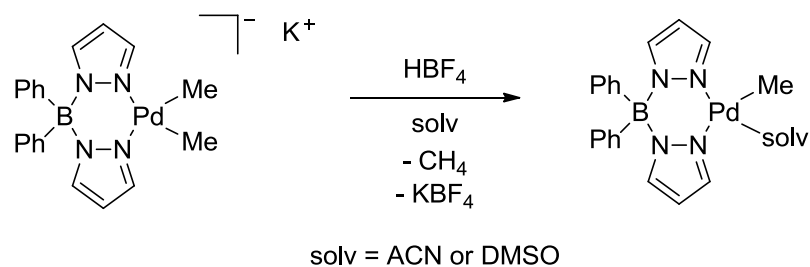


Figure 5.4. Crystal structure of $\text{KPh}_2\text{Bpz}_2\text{PdMe}_2$ demonstrating the potassium coordination (50% ellipsoids)

$\text{KPh}_2\text{Bpz}_2\text{PdMe}_2$ reacted with halogenated alkyls (R-X) to liberate ethane and presumably form $\text{Ph}_2\text{Bpz}_2\text{Pd(R)(X)}$, though this complex could not be cleanly isolated. Additionally, treating this complex with an acid-liberated methane and formed $\text{Ph}_2\text{Bpz}_2\text{PdMe(solvent)}$ in coordinating solvents like acetonitrile (ACN) and dimethylsulfoxide (DMSO) (Scheme 5.5). A crystal structure was obtained for the $\text{Ph}_2\text{Bpz}_2\text{PdMe(DMSO)}$ complex (Figure 5.5). The reactivity of the $\text{Ph}_2\text{Bpz}_2\text{PdMe(ACN)}$ complex was briefly



Scheme 5.5. Synthesis of uncharged palladium complexes

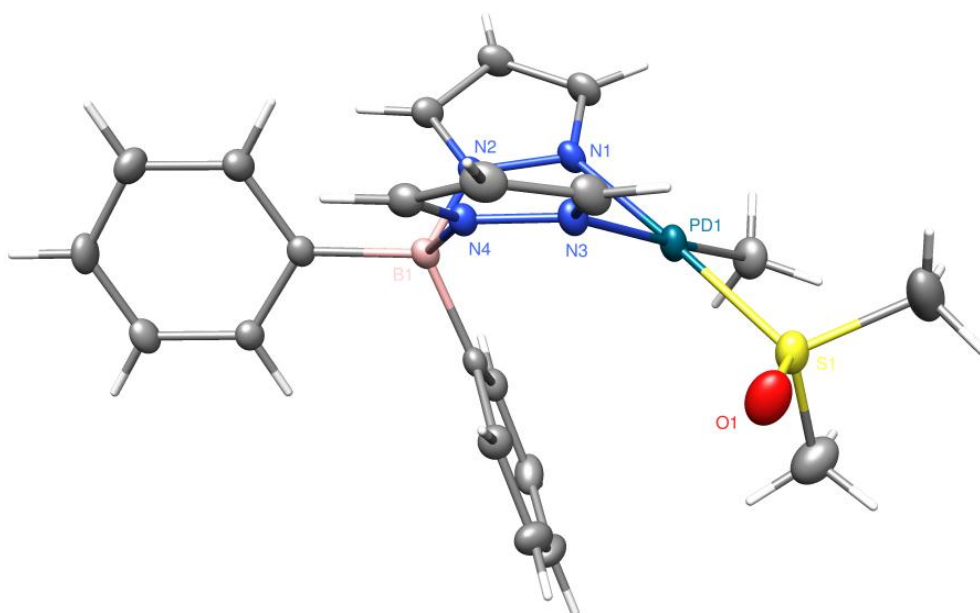


Figure 5.5. Crystal structure of $\text{Ph}_2\text{Bpz}_2\text{PdMe}(\text{DMSO})$ (50% ellipsoids)

explored but resulted mostly in decomposition. Two of the decomposition products that were formed when the $\text{Ph}_2\text{Bpz}_2\text{PdMe}(\text{ACN})$ complex was treated with CO, $[\text{Ph}_2\text{Bpz}_2\text{Pd}(\mu\text{-pz})]_2$ and $(\text{Ph}_2\text{Bpz}_2)_2\text{Pd}$, were also characterized crystallographically, (Figures 5.6 and 5.7, respectively). The reactivity of the $\text{Ph}_2\text{Bpz}_2\text{PdMe}(\text{solv})$ complexes remains to be fully explored, however, these solvento adducts are uncharged complexes that we hypothesized could aid in elucidating the role of the charge in C-H activation.

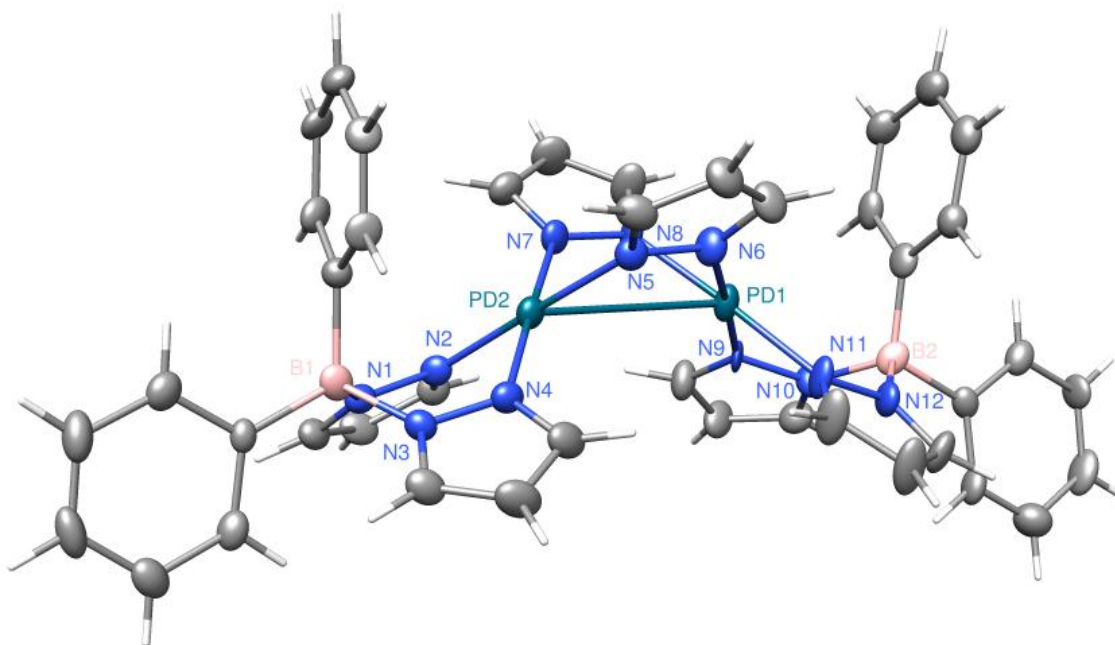


Figure 5.6. Crystal structure of $[\text{Ph}_2\text{Bpz}_2\text{Pd}(\mu\text{-pz})]_2$ (50% ellipsoids)

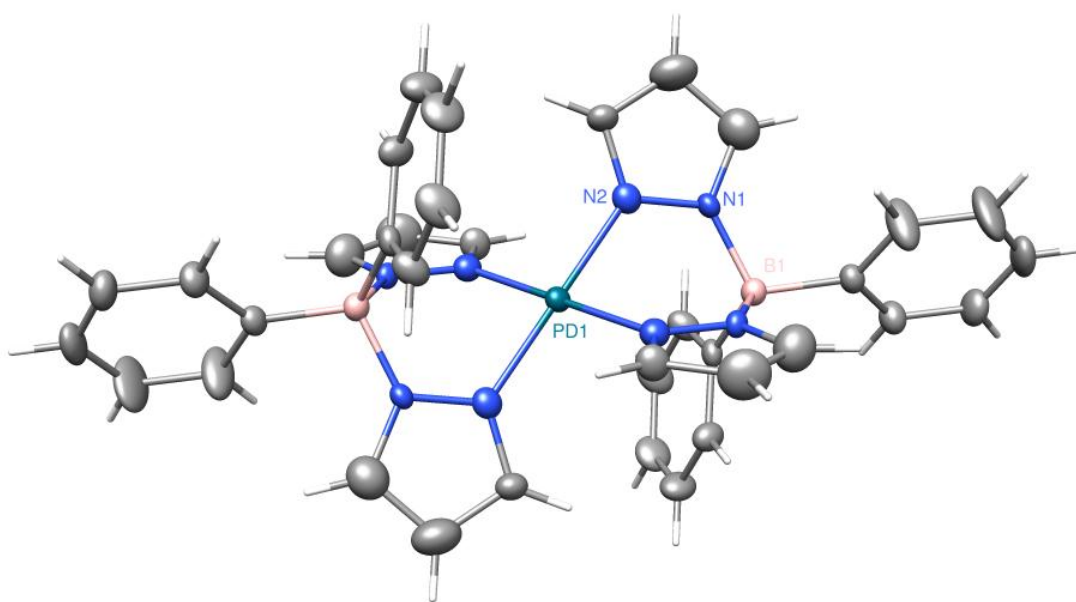
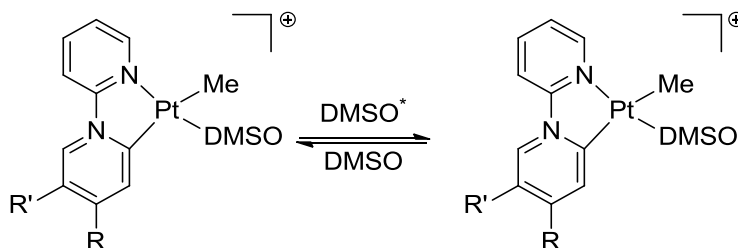


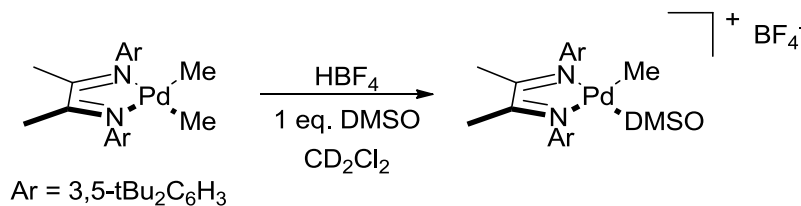
Figure 5.7. Crystal structure of $(\text{Ph}_2\text{Bpz}_2)_2\text{Pd}$ (50% ellipsoids)

Romeo et al. and Bercaw et al. have utilized ligand exchange kinetics to compare associative substitution rates of a variety of platinum methyl DMSO complexes (Scheme 5.6).³ In these studies degenerate DMSO exchange kinetics were analyzed to reveal how



Scheme 5.6. Owen studied the degenerate DMSO of a variety of platinum complexes.

varying the ligand would affect the rate. Similarly, we wanted to quantify the degenerate DMSO exchange rate of the $\text{Ph}_2\text{Bpz}_2\text{PdMe}(\text{DMSO})$ complex. Unfortunately, they only studied the platinum systems and no data existed for analogous palladium complexes. We, therefore, synthesized an analogous diimine palladium methyl DMSO cation. Treatment of a known diimine palladium dimethyl complex⁴ with an equivalent of HBF_4 and DMSO at low temperature yielded $[(\text{diimine})\text{PdMe}(\text{DMSO})][\text{BF}_4]$ (Scheme 5.7). The exchange kinetics of $[(\text{diimine})\text{PdMe}(\text{DMSO})][\text{BF}_4]$ can be directly compared to those of $\text{Ph}_2\text{Bpz}_2\text{PdMe}(\text{DMSO})$ to give insight into the role the ligand has on the rate.



Scheme 5.7. Synthesis of diiminePdMe(DMSO)⁺

Interestingly, NMR data of $[(\text{diimine})\text{PdMe}(\text{DMSO})][\text{BF}_4]$ collected near room temperature showed broad peaks that could have been mistaken for a symmetrical complex (Figure 5.8). Upon cooling however, the peaks sharpen and resolve as expected for an

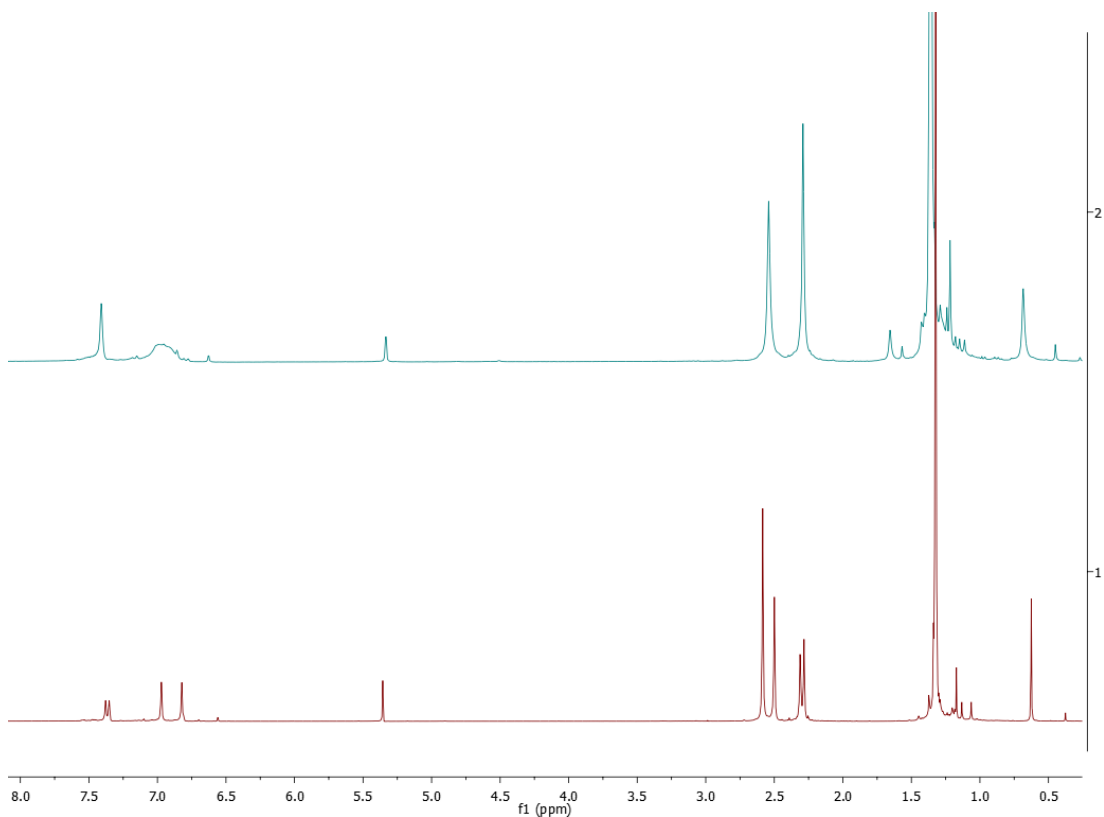


Figure 5.8. NMR spectra of $[(\text{diimine})\text{PdMe}(\text{DMSO})][\text{BF}_4]$ at 10 °C (blue) and -45 °C (red)

asymmetric species undergoing an exchange process. Variable temperature line shape analysis was done at several concentrations of DMSO. Unfortunately, the data was incomplete due to the freezing out of the exchange and formation of a precipitate at low temperature. More studies will be needed for a complete kinetics analysis. However,

qualitatively the rate of the reaction increased with temperature and DMSO concentration, indicating a probable associative substitution mechanism.

The $\text{Ph}_2\text{Bpz}_2\text{PdMe}(\text{DMSO})$ complex also had broad peaks in NMR data collected at room temperature, however, this turned out not to be because of DMSO exchange. The fluxionality was due the inversion of the boat conformation of the six-membered ring composed of the boron bispyrazole palladium moiety.⁴ In fact, DMSO exchange was too slow to be observed by line shape analysis even with 40 equivalents of DMSO at 80 °C. The exchange process could, however, be observed by magnetization transfer techniques. The observed rate constant (k_{obs}) increased with temperature (Figure 5.9) as expected but, interestingly, varying the DMSO concentration did not affect the exchange rate (Figure 5.10). That absence of a rate dependent on the concentration of DMSO indicated that a dissociative mechanism was most likely operative (Scheme 5.8).

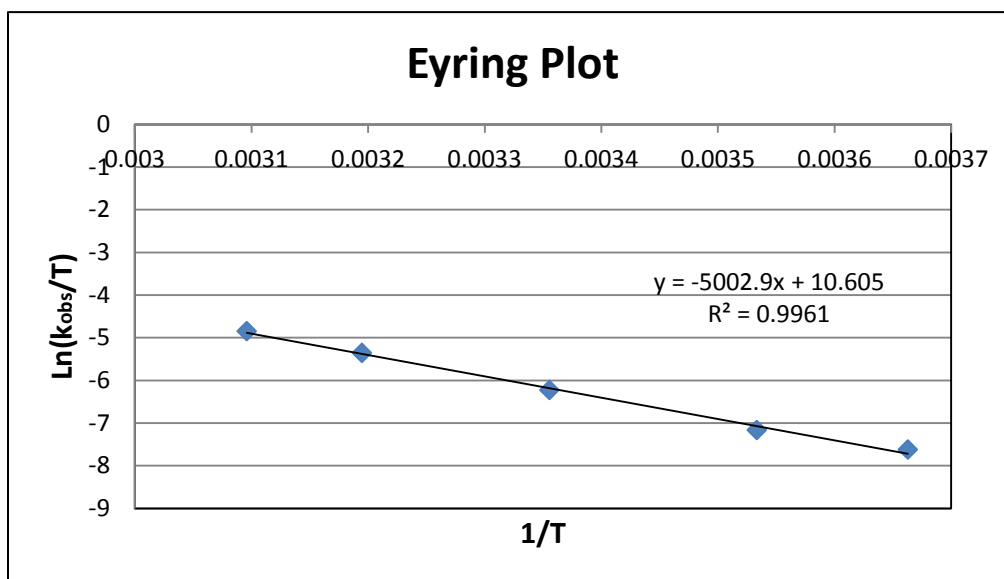


Figure 5.9. Eyring plot for $\text{Ph}_2\text{Bpz}_2\text{PdMe}(\text{DMSO})$

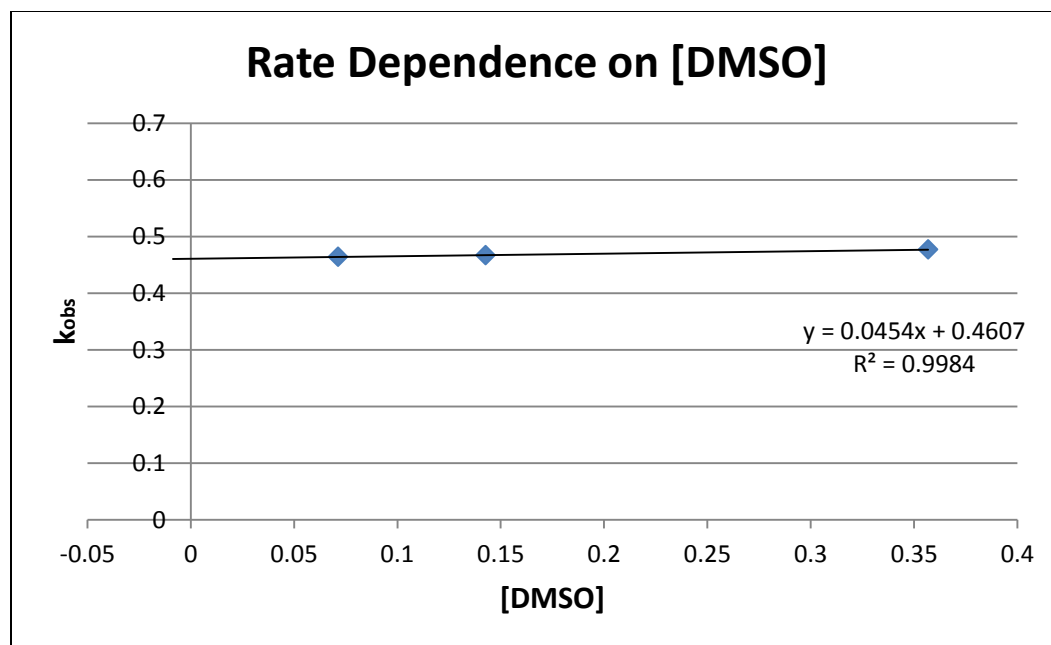
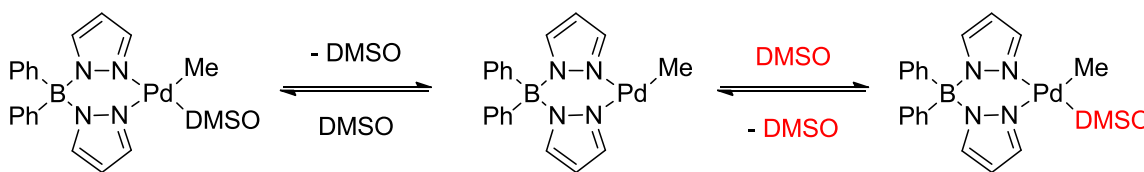


Figure 5.10. The exchange rate dependence of the concentration of DMSO for $\text{Ph}_2\text{Bpz}_2\text{PdMe}(\text{DMSO})$



Scheme 5.8. Dissociative substitution of DMSO on $\text{Ph}_2\text{Bpz}_2\text{PdMe}(\text{DMSO})$

Conclusions

Several uncharged polypyrazoleborate palladium and platinum complexes were synthesized including $[\text{Tp}^{i\text{Pr}}\text{PdOH}]_2$, $[\text{Tp}^{\text{Me}}\text{PdOH}]_2$, $\text{Tp}^{i\text{Pr}}\text{PtCl}(\text{DMS})$, $\text{Tp}^{\text{Me}}\text{PtCl}(\text{DMS})$, and $\text{Ph}_2\text{Bpz}_2\text{PtCl}(\text{DMS})$. The uncharged palladium hydroxyl-dimers were found to be inert to C-H bonds and thermally unstable. $\text{Ph}_2\text{Bpz}_2\text{PdMe}(\text{DMSO})$ and $[(\text{diimine})\text{PdMe}(\text{DMSO})][\text{BF}_4]$ were prepared by treating the corresponding palladium dimethyl complex with H^+ in the presence of DMSO. Degenerate DMSO exchange was

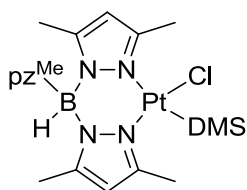
studied to elucidate the role of the charge on the complex. DMSO exchange with [(diimine)PdMe(DMSO)][BF₄] was found to increase with increased DMSO concentration and speculated to proceed via an associative substitution mechanism. Surprisingly, the associate substitution mechanism was shut down in the Ph₂Bpz₂PdMe(DMSO) complex and DMSO exchange proceeded via a dissociative substitution mechanism.

Experimental Section

Unless otherwise noted all reagents were commercially obtained and used without further purification. The (diimine)PdMe₂ complex was synthesized using literature procedures.⁵ All reactions described were conducted under an atmosphere of air, and solvents were not dried prior to use unless otherwise noted. When used in anhydrous conditions, dichloromethane-*d*₂ (DCM-*d*₂), tetrahydrofuran-*d*₈ (THF- *d*₈), and acetonitrile-*d*₃ (DCE-*d*₃) were dried by passing them through alumina and a syringe filter to remove particulate residue. ¹H NMR spectra were recorded at ambient temperature using a Varian Mercury 300 MHz spectrometer, unless otherwise noted. The data are reported by chemical shift (ppm) from tetramethylsilane, multiplicity (s, singlet; d, doublet; t, triplet; m, multiplet; dd, double doublet; dt, double triplet), coupling constants (Hz), and integration. Mass spectra were acquired on a Finnigan LCQ ion trap or Agilent 5973 Network mass selective detector and were obtained by peak matching. Kinetics for the reaction between PdMe(DMSO) complexes and DMSO were performed using an analogous procedure to that described previously for the exchange between PtMe(DMSO) complexes and DMSO using a Varian ^{UNITY}INOVA 500 (499.853 MHz for ¹H) spectrometer.^{3e}

In the course of this work, crystals of the Pd^I-Pd^I decomposition product, Tp^{Me}PtCl(DMS), and Ph₂Bpz₂PtCl(DMS), Ph₂Bpz₂PdMe₂K and [(diimine)PdMe(DMSO)][BF₄], suitable for X-ray diffraction were grown by procedures described in the experimental synthetic details for each and data tables have been provided in Appendix C.

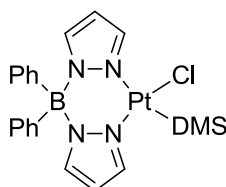
Tp^{Me}PtCl(DMS)



In a nitrogen-filled glove box, (DMS)₂PtCl₂ (145.0 mg, 371.6 μmol) and potassium hydrotris(3,5-dimethylpyrazol-1-yl)borate (136.5 mg, 405.9 μmol) were added to a 20 mL vial equipped with a stir bar. THF (8 mL) was added and the light yellow solution was stirred for 17 hours. The solvent removed under reduced pressure and the solids were dissolved in a minimal amount of CH₂Cl₂. Pentane was added until a light yellow solid precipitated which was removed by filtration and discarded. The solvent was removed from the remaining pentane solution and 150.0 mg of clean white product was collected (68.4% yield). X-ray quality crystals were formed by diffusion of pentane into a saturated CH₂Cl₂ solution. ¹H NMR (500 MHz, 25 °C, CD₂Cl₂) δ = 5.91 (s, 1H), 5.89 (s, 1H), 5.79 (s, 1H), 4.42 (vb q, 1H), 2.42 (s, 6H), 2.38 (s, 3H), 2.29 (s, 3H), 2.29 (s, *J*(Pt,H) = 17 Hz, 3H), 2.14 (s, 3H), 1.91 (s, *J*(Pt,H) = 17 Hz, 3H), 1.72 (d, *J* = 0.5 Hz, 3H). ¹³C NMR (126 MHz,

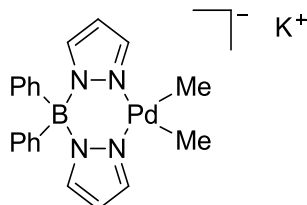
25°C, CD₂Cl₂) δ = 151.09, 148.93, 148.24, 147.25, 147.03, 144.44, 107.61, 106.90, 106.60, 22.02, 21.53, 14.67, 14.60, 14.11, 13.68, 13.62, 11.80.

Ph₂Bpz₂PtCl(DMS)



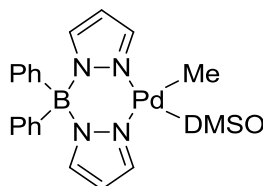
In a nitrogen-filled glove box, (DMS)₂PtCl₂ (117.1 mg, 300.1 μ mol) and potassium diphenylbispyrazol-1-ylborate (101.5 mg, 300.1 μ mol) were added to a 20 mL vial equipped with a stir bar. THF (8 mL) was added and the light yellow solution was stirred for 3 days. The solution was filtered to remove KCl and the solvent removed under reduced pressure. The remaining solid was collected (156.3 mg, 88.1% yield). X-ray quality crystals were formed by diffusion of pentane into a saturated THF solution. ¹H NMR (500 MHz, 25 °C, CD₂Cl₂) δ = 7.92 (dd, *J* = 2.2, 0.9 Hz, 1H), 7.62 (dd, *J* = 2.2, 0.8 Hz, 1H), 7.49 (dd, *J* = 2.6, 0.8 Hz, 1H), 7.39 (dd, *J* = 2.5, 0.9 Hz, 1H), 7.27 (dd, *J* = 5.2, 1.8 Hz, 6H), 7.16–6.66 (b s, 4H), 6.42–6.11 (m, 2H), 2.10 (b s, 6H). ¹³C NMR (126 MHz, 25°C, CD₂Cl₂) δ = 140.69, 140.21, 137.39, 137.27, 134.13, 127.24, 126.65, 105.04, 104.26, 21.98.

Ph₂Bpz₂PdMe₂K



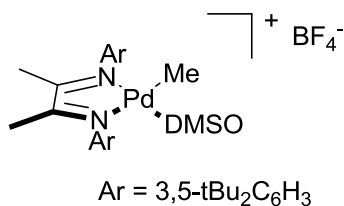
In a nitrogen-filled glove box, TMEDAPdMe₂ (156.2 mg, 618.1 μmol) and potassium diphenylbispyrazol-1-ylborate (218.6 mg, 646.2 μmol) were added to a 250 mL Schlenk bomb equipped with a stir bar. Acetonitrile (10 mL) and hexanes were added to form a biphasic solution, and the solution was heated to 40 °C and stirred for 2 hours. The solution was allowed to settle and the hexane layer was removed with a pipet. An additional 15 mL of hexanes was added and the solution was stirred for 5 minutes. The solution was allowed to settle and the acetonitrile layer removed and filtered. The solvent removed under reduced pressure and the remaining solid was collected (244 mg, 83.1% yield). X-ray quality crystals were formed by diffusion of pentane into a saturated Et₂O solution. ¹H NMR (300 MHz, 25 °C, cd₃cn) δ = 7.66 (dd, *J* = 1.9, 0.8 Hz, 2H), 7.24–7.15 (m, 8H), 6.85–6.76 (m, 4H), 6.15–6.13 (m, 2H), -0.27 (s, 6H).

Ph₂Bpz₂PdMe(DMSO)



In a liquid nitrogen cooled cold well in a nitrogen-filled glove box, $\text{Ph}_2\text{Bpz}_2\text{PdMe}_2\text{K}$ (77.1 mg, 162.4 μmol) was dissolved in cold CH_2Cl_2 (5 mL) in a 20 mL vial equipped with a stir bar. A solution of HBAr^{F} (164.4 mg, 162.3 μmol) and DMSO (38.1 mg 322.5 μmol) in cold CH_2Cl_2 (5 mL) was then added dropwise. The solution was then stirred and slowly allowed to warm to room temperature. The solvent was removed under reduced pressure and the remaining solid was dissolved in benzene and filtered. The solvent was again removed under reduced pressure. The remaining solid was dissolved in a minimal amount of benzene (~ 2 mL), and hexanes (~ 10 mL) were added to crash out the product. The product was collected and once again dissolved in benzene and then filtered. After the benzene was removed under reduced pressure, the solid was collected to give 56 mg of product (69% yield). The molecular connectivity was confirmed by X-ray analysis of crystals that were grown by diffusion of hexanes into a saturated benzene solution (pfo50). ^1H NMR (500 MHz, 25 $^\circ\text{C}$, CD_2Cl_2) δ = 7.78 (d, J = 2.0 Hz, 1H), 7.64 (d, J = 2.1 Hz, 1H), 7.58 (d, J = 2.4 Hz, 1H), 7.46 (d, J = 2.5 Hz, 1H), 7.39 (d, J = 0.7 Hz, 1H), 7.28 (b s, 7H), 6.83 (vb s, 2H), 6.29 (t, J = 2.3 Hz, 1H), 6.23 (t, J = 2.1 Hz, 1H), 2.67 (vb s, 6H), 0.41 (s, 3H).

$[(\text{diimine})\text{PdMe}(\text{DMSO})][\text{BF}_4]$



(diimine)PdMe₂ (9.4 mg, 15.7 μmol) was dissolved in 600μL of CD₂Cl₂ in an NMR tube. DMSO (1.1μL, 15.5 μmol) and HBF₄ (aq.) (1.9 μL of a 54% solution, 16.1 μmol) were added via a microliter syringe and the solution was shaken. NMR analysis reveal near complete conversion (> 95%) to the product, which was not isolated. ¹H NMR (300 MHz, 25 °C, CD₂Cl₂) δ = 7.40 (s, 2H), 6.95 (bs, 4H), 2.55 (bs, 6H), 2.28 (bs, 6H), 1.36 (s, 36H), 0.68 (s, 3H). ¹H NMR (500 MHz, -45°C, CD₂Cl₂) δ = 7.38 (t, *J* = 1.7 Hz, 1H), 7.36 (t, *J* = 1.6 Hz, 1H), 6.97 (d, *J* = 1.7 Hz, 2H), 6.82 (d, *J* = 1.7 Hz, 2H), 2.50 (s, 6H), 2.31 (s, 3H), 2.28 (s, 3H), 1.33 (s, 18H), 1.32 (s, 18H), 0.63 (s, 3H).

DMSO exchange kinetics for Ph₂Bpz₂PdMe(DMSO)

Ligand exchange kinetics were studied using magnetization transfer techniques at between 0 °C and 50 °C. The bound DMSO NMR signal was saturated using a presaturation pulse sequence and the signal frequency. The relaxation time (T₁) was measured before each run. The ligand exchange was observed by monitoring the decrease in the free DMSO signal as it equilibrated with the magnetically saturated DMSO. The observed rate (k_{obs}) constant was calculated from the relaxation time and the ratio of the intensity of the free DMSO signal before exchange (S_i) to the intensity of the free DMSO signal after an equilibrium has been reached (S_f) and the relaxation time.

$$k_{\text{obs}} = ((S_i / S_f) - 1) / T_1$$

References

1. (a) Johansson, L.; Ryan, O. B.; Tilset, M., *J. Am. Chem. Soc.* **1999**, *121* (9), 1974–1975; (b) Johansson, L.; Tilset, M., *J. Am. Chem. Soc.* **2001**, *123* (4), 739–740; (c) Williams, T. J.; Caffyn, A. J.; Hazari, N.; Oblad, P. F.; Labinger, J. A.; Bercaw, J. E., *J. Am. Chem. Soc.* **2008**, *130* (8), 2418–2419; (d) Bercaw, J. E.; Hazari, N.; Labinger, J. A.; Oblad, P. F., *Angew. Chem., Int. Ed.* **2008**, *47* (51), 9941–9943; (e) Johansson, L.; Tilset, M.; Labinger, J. A.; Bercaw, J. E., *J. Am. Chem. Soc.* **2000**, *122* (44), 10846–10855; (f) Zhong, H. A.; Labinger, J. A.; Bercaw, J. E., *J. Am. Chem. Soc.* **2002**, *124* (7), 1378–1399; (g) Heyduk, A. F.; Driver, T. G.; Labinger, J. A.; Bercaw, J. E., *J. Am. Chem. Soc.* **2004**, *126* (46), 15034–15035; (h) Driver, T. G.; Day, M. W.; Labinger, J. A.; Bercaw, J. E., *Organometallics* **2005**, *24* (15), 3644–3654; (i) Owen, J. S.; Labinger, J. A.; Bercaw, J. E., *J. Am. Chem. Soc.* **2006**, *128* (6), 2005–2016.
2. Akita, M.; Miyaji, T.; Muroga, N.; Mock-Knoblauch, C.; Adam, W.; Hikichi, S.; Moro-oka, Y., *Inorg. Chem.* **2000**, *39* (10), 2096–2102.
3. (a) Romeo, R.; Fenech, L.; Carnabuci, S.; Plutino, M. R.; Romeo, A., *Inorg. Chem.* **2002**, *41* (11), 2839–2847; (b) Romeo, R.; Fenech, L.; Scolaro, L. M.; Albinati, A.; Macchioni, A.; Zuccaccia, C., *Inorg. Chem.* **2001**, *40* (14), 3293–3302; (c) Romeo, R.; Monsù Scolaro, L.; Nastasi, N.; Arena, G., *Inorg. Chem.* **1996**, *35* (17), 5087–5096; (d) Romeo, R.; Nastasi, N.; Scolaro, L. M.; Plutino, M. R.; Albinati, A.; Macchioni, A., *Inorg. Chem.* **1998**, *37* (21), 5460–5466; (e) Owen, J. S.; Labinger, J. A.; Bercaw, J. E., *J. Am. Chem. Soc.* **2004**, *126* (26), 8247–8255.

4. Jalon, F. A.; Manzano, B. R.; Gomez-De, I. T. F.; Guerrero, A. M.; Rodriguez, A. M., *Targets Heterocycl. Syst.* **1999**, *3*, 399–438.
5. Ackerman, L. J.; Sadighi, J. P.; Kurtz, D. M.; Labinger, J. A.; Bercaw, J. E., *Organometallics* **2003**, *22*, 3884–3890.

Chapter 6

Homoallylic C-H Activation and Oligomerization

Adapted in part from:

Oblad, P. F.; Winston, M. S.; Labinger, J. A.; Bercaw, J. E., *Provisional patent filed on 5/3/2011. CIT file # CIT-5876-P.*

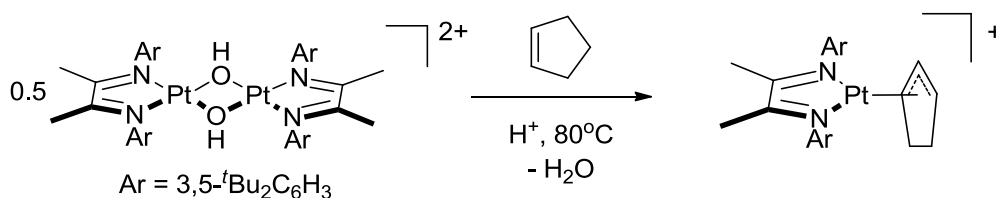
Introduction

Platinum and palladium hydroxyl-bridged dimers have been demonstrated to facilitate the activation of a variety of carbon-hydrogen bonds.¹ Additionally, it has been demonstrated that the palladium hydroxyl-dimer can be used to break the C-H bonds of cyclohexene catalytically using oxygen as a terminal oxidant.¹ However, all the substrates in which these complexes could cleave a C-H bond were specifically selected because they had a structure that would promote this reactivity. Namely, indene, cyclohexene, and 1,4-diethylbenzene each have an already activated allylic or benzylic C-H bond (or a C-H bond which is both in the case of indene) and an olefin that facilitates the reactivity by first coordinating to the metal center and then directing the bond cleavage. In the case of allylbenzene and acetophenone-*O*-methyloxime, an olefin or the lone pair on the nitrogen (respectively) coordinate and then direct the activation of an aromatic C-H bond. Since, ultimately, we would like to be able to cleave C-H bonds in simple, unactivated hydrocarbons; we further explored the potential substrate scope of these systems. Although we have not discovered conditions under which unactivated hydrocarbons will react with the platinum or palladium hydroxyl-dimers, we have observed reactivity with more interesting and less activated substrates. Specifically, we have found interesting reactivity with cyclopentene, *neo*-hexene, and linear olefins.

Results and Discussion

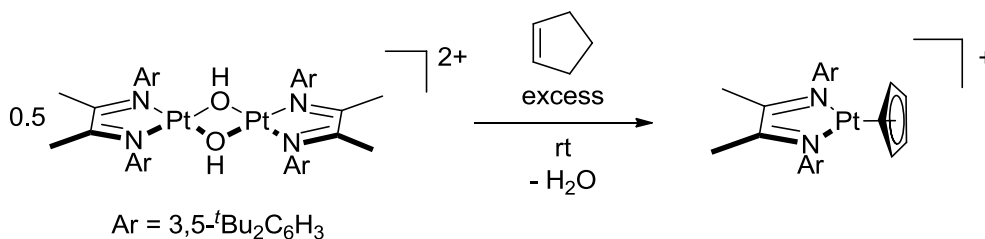
Cyclopentene was expected to react with the platinum hydroxyl-dimer in a similar fashion to cyclohexene to form an η^3 -cyclopentenyl complex. Additionally, it was thought that cyclopentene might be different enough from cyclohexene that, when combined with

palladium, we might see an η^3 -cyclopentenyl palladium complex rather than catalytic dehydrogenation. When the platinum hydroxyl-dimer was treated with cyclopentene what resulted was dependent on the substrate concentration, temperature, and the presence of acid. If the platinum complex was treated with 1 equivalent of dilute cyclopentene and heated, no reaction occurred. If the reaction was heated with HBF_4 , an η^3 -cyclopentenyl platinum complex formed (Scheme 6.1). Interestingly, when the platinum hydroxyl-dimer



Scheme 6.1. Formation of η^3 -cyclopentenyl platinum complex

was treated with a larger excess of cyclopentene, a [(diimine)Pt(η^5 -cyclopentadienyl)][BF₄] complex is formed (Scheme 6.2). Similarly to the catalytic dehydrogenation of



Scheme 6.2. Formation of η^5 -cyclopentadienyl platinum complex

cyclohexene to benzene with [(diimine)Pd(μ -OH)]₂[BF₄]₂, multiple hydrogens are cleaved from the cyclopentene to form cyclopentadiene (Cp) in this reaction. The transformation was evidenced by a single diagnostic cyclopentadienyl ¹H peak with platinum satellites in the NMR. Crystals suitable for X-ray diffraction studies were grown from a concentrated pentane solution at -30 °C (Figure 6.1). Unfortunately, the structure quality was low and

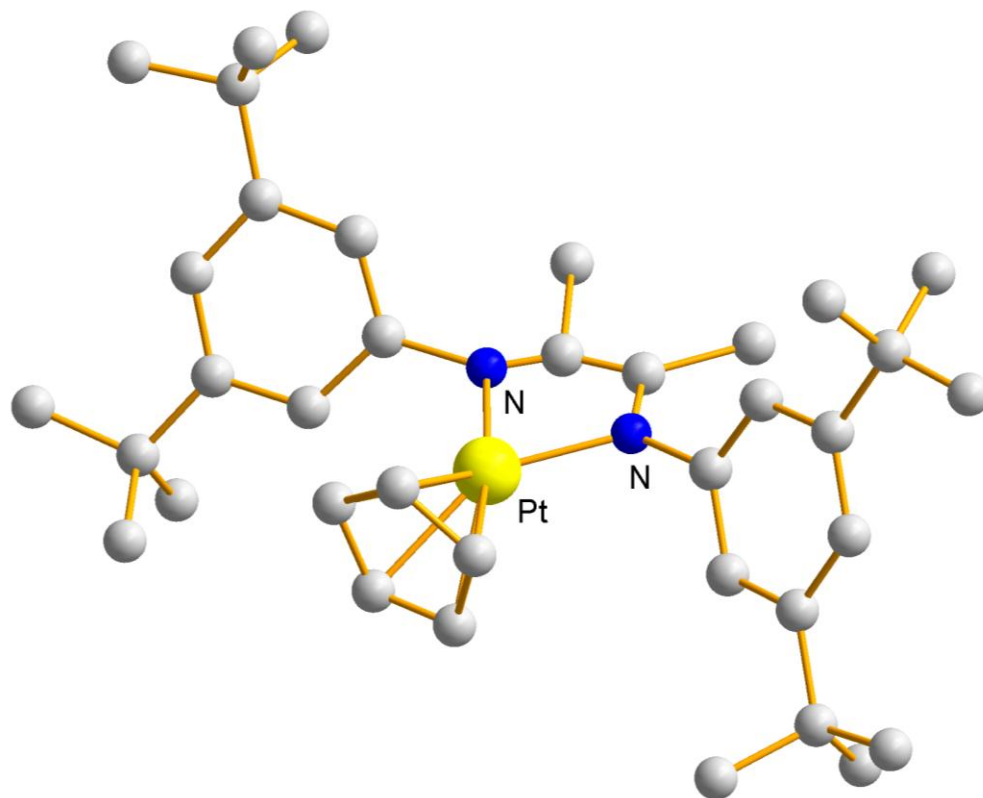
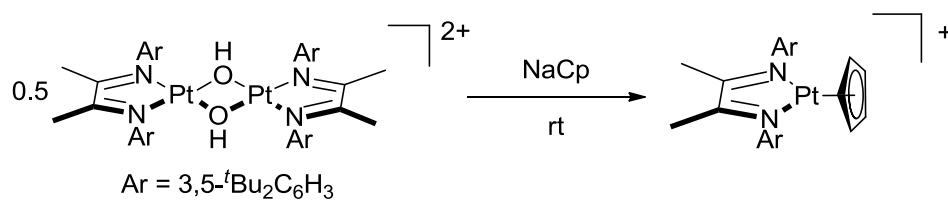


Figure 6.1. Isotropic crystal structure of $[(\text{diimine})\text{Pt}(\eta^5\text{-cyclopentadienyl})]^+$

only connectivity could be extracted. This product was verified with an independent synthesis of the cyclopentadienyl product from $[(\text{diimine})\text{Pt}(\mu\text{-OH})_2[\text{BF}_4]_2]$ and NaCp (Scheme 6.3). It is unclear whether the hydrogen atoms ultimately reduce O_2 to form water

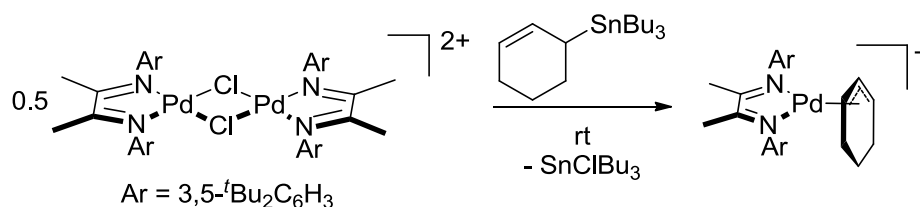


Scheme 6.3. Independent synthesis of η^5 -cyclopentadienyl platinum complex

or if there is a disproportionation reaction in which cyclopentane is formed. We favor the later pathway however, since the $\text{Pt}(\eta^3\text{-cyclopentenyl})^+$ complex is air stable and a peak potentially due to cyclopentane is observed in the NMR.

Why different platinum complexes are formed is unclear. We speculate that there are two separate mechanisms in operation. It seems that in the platinum system, since oxygen cannot be utilized as a terminal oxidant, the concentration of cyclopentene must be large enough for the disproportionation reaction to proceed at a reasonable rate at room temperature. Under our conditions if only one equivalent of cyclopentene was used, the disproportionation reaction was too slow to be able to observe appreciable amounts within a few hours. Heating the reaction with acid in conditions identical to the preparation of the $\eta^3\text{-cyclohexenyl}$ and $\eta^3\text{-indenyl}$ complex would result in the formation of the $\eta^3\text{-cyclopentenyl}$ complex. The $\eta^3\text{-cyclopentenyl}$ platinum complex also seemed inert to further dehydrogenation. This led us to hypothesize that the η^3 complexes formed in reactions with the platinum and palladium hydroxyl-dimers might be unreactive resting states and not intermediates as was invoked for the proposed mechanism of catalytic dehydrogenation of cyclohexene.¹ To test this idea, we reexamined the reactivity of the diimine platinum complexes with cyclohexene. Treatment of the $[(\text{diimine})\text{Pt}(\eta^3\text{-cyclohexenyl})][\text{BF}_4]$ complex with a large excess of cyclohexene resulted in no reaction. Conversely, treatment of the platinum hydroxyl-dimer with a large excess of cyclohexene resulted in a rapid color change (less than 5 minutes). Although the product of this reaction has not been fully characterized, it is speculated that dehydrogenation is likely occurring. We were more interested immediately in the implications for the palladium

dehydrogenation of cyclohexene. Initially, since the analogous [(diimine)Pd(η^3 -cyclohexenyl)]⁺ had never been observed, it was thought that this complex was just an intermediate on the pathway to benzene formation. Moreover, it was thought that it was only observed in the platinum system because platinum was not capable of further dehydrogenation. This new reactivity observed with platinum and cyclopentene led us to reexamine the palladium system's reactivity with cyclohexene. The efficiency of dehydrogenation with the palladium hydroxyl-dimer meant that the palladium η^3 -cyclohexenyl complex could not be formed under similar conditions. Fortunately, Matt Winston discovered an alternate route to the palladium η^3 -cyclohexenyl complex. Treatment of [(diimine)Pd(μ -Cl)]₂[BF₄]₂ with cyclohexenyl stannane resulted in the formation of [(diimine)Pd(η^3 -cyclohexenyl)][BF₄] (Scheme 6.4). Importantly, this new

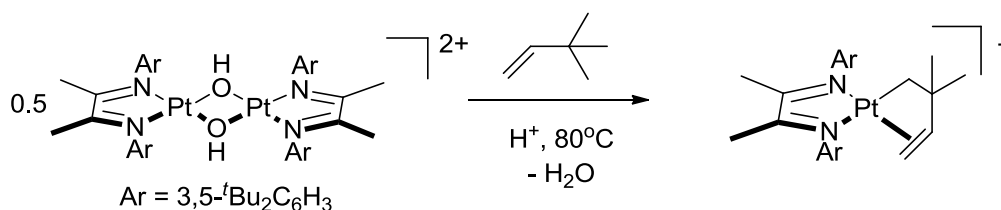


Scheme 6.4. Independent synthesis of η^3 -cyclohexadienyl platinum complex

complex was stable in the presence of oxygen and did not undergo dehydrogenation. Furthermore, treatment with a large excess of cyclohexene also did not result in dehydrogenation. These results are strong evidence that the η^3 -cyclohexenyl complex is not an intermediate as previously thought. We speculate that one possible explanation is that dehydrogenation proceeds through homoallylic C-H activation and not allylic

potentially due to the proximity of the homoallylic C-H bond to the metal while in the axial position of the cyclohexene chair conformation.

Further substrate exploration led to other interesting results. Heating $[(\text{diimine})\text{Pt}(\mu\text{-OH})_2][\text{BF}_4]_2$ in the presence of acid and *neo*-hexene resulted in the formation of a cyclometallated platinum(*neo*-hexenyl) complex (Scheme 6.5). This



Scheme 6.4. Synthesis of *neo*-hexenyl platinum complex

reaction was interesting to us for a few reasons. First, the C-H bond cleaved in *neo*-hexene is on a terminal sp^3 hybridized methyl group and is the strongest bond activated by the hydroxyl-dimer systems so far. Secondly, it is the first unambiguous example of homoallylic C-H activation with these systems which is relevant to the discussion above of the dehydrogenation mechanism.

The final class of substrates that we explored was also the most interesting. As we wanted to extend the reactivity of the hydroxyl-dimers to simple alkanes, a logical step in this direction was linear olefins. The reason being that the olefin could first coordinate the metal and potentially facilitate C-H activation further down the chain. We found that the platinum system did not react with linear olefins. However, when the palladium hydroxyl-dimer was treated with 1-butane, 1-pentene, 1-hexene, or 1-decene, NMR analysis revealed a fast conversion of the terminal olefins to internal olefins. Olefin isomerization

had previously been observed by Nilay Hazari but the reactivity was not explored further. In order to more fully characterize the reaction products, the solution was filtered through silica and injected into a GC/MS. GC/MS analysis revealed that, in addition to many isomerization products, there were oligomerization products. It was also discovered that this reaction proceeded catalytically. A range of linear olefins were evaluated and it was found that the turnover frequency and extent of oligomerization increased with shorter chain lengths. The most reactive substrates were ethylene and propylene.

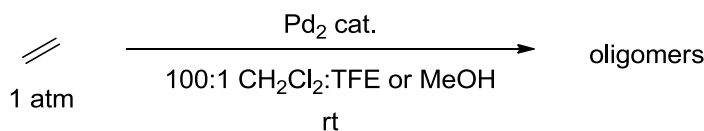
Ethylene and propylene oligomerization are important processes that convert these simple olefinic feedstocks into valuable products. A number of transition metal catalysts have been developed for these reactions, with a variety of structurally and electronically tunable ligands to vary product distribution.² These homogeneous catalysts usually require air- and moisture-sensitive activating agents, such as boranes or methylaluminoxane, to prepare the reaction-initiating organometallic complexes; the latter in most cases also have sensitive metal-carbon bonds.³ Consequently, olefin oligomerizations generally require rigorously air and moisture-free conditions that may be inconvenient to achieve on an industrial scale.

We found that the Pd hydroxyl-bridged dimer functions as precatalyst for olefin oligomerization and isomerization reactions. In contrast to most oligomerization catalysts, the dimer has no sensitive metal-carbon bonds and requires no activator, either stoichiometric or superstoichiometric, to initiate oligomerization. In addition, the dimer itself is tolerant to both air and water. Oligomerization/isomerization reactions also do not

need to be run under an inert atmosphere, and can be carried out in solvents that do not need to be rigorously degassed and dried.

To facilitate reactivity studies, Matt Winston optimized the large-scale synthesis of the starting material. He found that $[(\text{diimine})\text{Pd}(\mu\text{-OH})_2][\text{BF}_4]_2$ can be synthesized in moderate yield in three steps from cheap, easily-acquired precursors. The $(\text{diimine})^4$ ligand and $(\text{PhCN})_2\text{PdCl}_2$ were stirred for 1 hour at room temperature in dry, degassed CH_2Cl_2 to afford $(\text{diimine})\text{PdCl}_2$, which was then treated with AgBF_4 in $\text{CH}_2\text{Cl}_2:\text{THF}$ to afford the dicationic solvento-adduct $[(\text{diimine})\text{Pd}(\text{THF})_2][\text{BF}_4]_2$, which has been characterized crystallographically previously (see Chapter 1). This slightly moisture-sensitive solid is then treated with polymer-bound base in CH_2Cl_2 with several drops of water for 3 minutes at $0\text{ }^\circ\text{C}$ to afford the hydroxyl-dimer in 70% overall yield as an air and moisture-tolerant solid.

The dimer can be dissolved in either wet CH_2Cl_2 or 1,2-dichloroethane with the assistance of 1 vol% methanol or trifluoroethanol (Scheme 6.5). Addition of an excess of α -olefin to the solution, under air, results in olefin oligomerization. Ethylene is converted to a mixture of branched and linear oligomers, with a turnover frequency (TOF) of at least $5\text{ min}^{-1}\text{ mol dimer}^{-1}$ at $25\text{ }^\circ\text{C}$ and 1 atm (Figure 6.2).



Scheme 6.5. Ethylene oligomerization

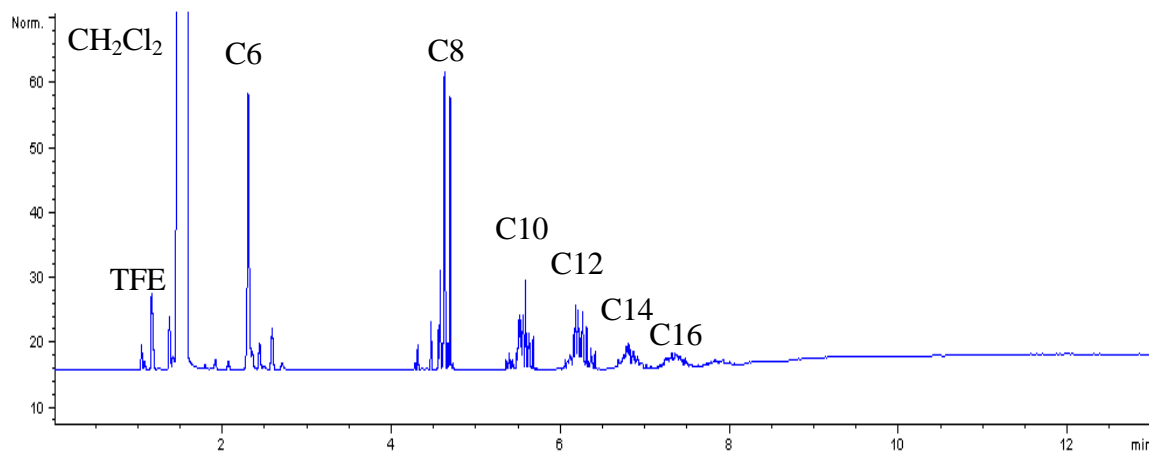
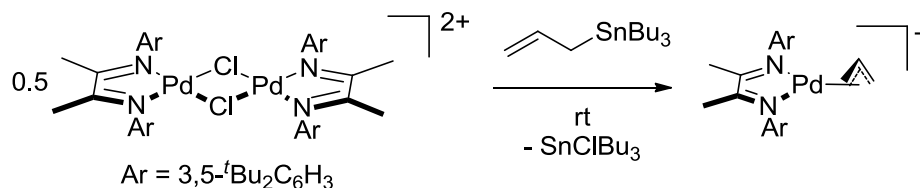


Figure 6.2. GC trace for ethylene oligomerization

Propylene (0.75 atmosphere) is oligomerized with a TOF of at least 2 min^{-1} at $25 \text{ }^\circ\text{C}$ and 0.75 atm; the product distribution indicates that 1,2- and 2,1-insertion are about equally favorable. Significantly, it was found that a partial atmosphere of O_2 is required to prevent deposition of reduced palladium.

For olefins longer than propene, isomerization is faster than oligomerization, and internal olefins undergo oligomerization more slowly than terminal olefins. Since internal olefins are favored thermodynamically, the overall rate of oligomerization is dramatically slowed due to the reduced concentration of terminal olefin.

Originally, we speculated that the oligomerization proceeded through an η^3 intermediate. However, a new understanding of the inactivity of the η^3 intermediates in dehydrogenation led to the reevaluation of the mechanistic proposal. Matt Winston demonstrated that the η^3 -complexes were not actually intermediates in oligomerization by independently synthesizing $[(\text{diimine})\text{Pd}(\eta^3\text{-allyl})][\text{BF}_4]$. Treatment of $[(\text{diimine})\text{Pd}(\mu\text{-Cl})_2][\text{BF}_4]_2$ with allyl stannane yielded this product which was subsequently treated with propylene and did not product any oligomers (Scheme 6.6).



Scheme 6.6. Synthesis of [(diimine)Pd(η^3 -allyl)]⁺

Closer examination of the products of the oligomerization reactions revealed the formation of ketones. We speculate that Wacker-type reactivity of olefins with the palladium starting material could lead to the formation of ketones and palladium hydride species. This palladium hydride complex could be the active oligomerization catalyst. Matt Winston is currently probing this hypothesis and evaluating the data. These results will be forthcoming. Interestingly, if this palladium hydride mechanism is operative, the role of oxygen could be in reoxidizing palladium(0) complexes that result from the decomposition of hydridic species, thus explaining why no palladium black is observed when the reaction is run under oxygen.

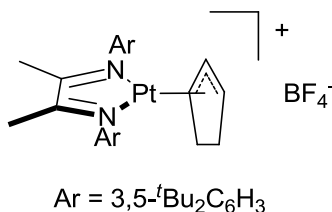
Conclusion

It has been demonstrated that the [(diimine)Pt(μ -OH)]₂[BF₄]₂ complex will form an η^3 -cyclopentenyl complex when heated with acid and cyclopentene. Conversely, treatment with a large excess of cyclopentene results in multiple dehydrogenation steps to form an η^5 -cyclopentadienyl complex. The differences in these reactions are likely due the differences in reactivity of allylic versus homoallylic C-H activation. Furthermore, homoallylic activation was demonstrated in the reaction between the platinum hydroxyl-dimer and *neo*-hexene in which a C-H bond in a terminal methyl group was cleaved forming a cyclometallated *neo*-hexenyl platinum complex. It was also demonstrated that the

palladium hydroxyl-dimer will isomerize and oligomerize linear olefins, likely via an oxygen-stabilized palladium hydride formation mechanism.

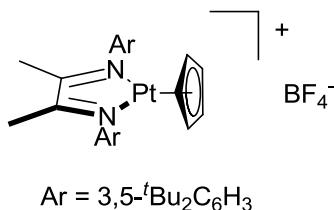
Experimental Section

Unless otherwise stated all reactions were performed under an atmosphere of air. All reagents were commercially obtained and used without further purification. Dichloromethane- d_2 and methanol- d_4 were purchased from Cambridge Isotope Laboratories and used as received. ^1H and ^{13}C NMR spectra were recorded at ambient temperature using a Varian Mercury 300 MHz or Varian Inova 500 MHz spectrometer, equipped with the VNMRJ software program, version 2.2d. The data are reported by chemical shift (ppm) from tetramethylsilane, multiplicity (s, singlet; d, doublet; t, triplet; m, multiplet; dd, double doublet; dt, double triplet), coupling constants (Hz), and integration. All ^{13}C NMR data were collected proton-decoupled ($^{13}\text{C}\{^1\text{H}\}$), except where specified. Mass spectra were acquired on a Finnigan LCQ ion trap or Agilent 5973 Network mass selective detector and were obtained by peak matching. X-ray crystallographic data were collected on a Bruker KAPPA APEX II instrument, with the crystals mounted on a glass fiber with Paratone-N oil. Structures were determined using direct methods as implemented in the Bruker AXS software package.



On the benchtop, [(diimine)Pt(μ -OH)]₂[BF₄]₂ (114.2 mg, 75.2 μ mol) was added to a 50 mL Schlenk bomb with a stirbar and dissolved in dichloroethane (10 mL). To this yellow solution was added cyclopentene (13.77 μ l, 150.4 μ mol) and HBF₄ (54% aqueous solution) (8.86 μ l, 75.2 μ mol). The yellow solution was stirred at 80 °C and the color gradually changed to red over 7 hours. The solution was filtered through glass filter paper and the solvent was removed under reduced pressure. NMR revealed the major product to be [(diimine)Pt(η^3 -cyclopentenyl)][BF₄] with a small amount of [(diimine)Pt(η^5 -cyclopentadienyl)][BF₄]. The product was purified by repeated crystallizations from pentane at -30 °C. ¹H NMR (300 MHz, CD₂Cl₂) δ 7.44 (t, 2H), 7.04 (d, 4H), 5.28 (t, *J*(Pt,H) = 28 Hz, 1H), 3.89 (m, *J*(Pt,H) = 18 Hz, 2H), 2.35 (s, 6H), 1.93 (m, 2H), 1.89 (m, 2H), 1.38 (s, 36H).

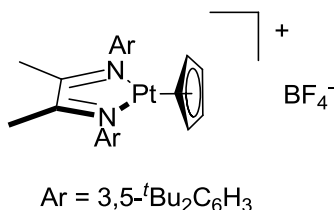
[(diimine)Pt(η^5 -cyclopentadienyl)][BF₄] from cyclopentene



On the benchtop, [(diimine)Pt(μ -OH)]₂[BF₄]₂ (49.9 mg, 32.9 μ mol) was added to a 20 mL vial with a stirbar and dissolved in CH₂Cl₂ (1 mL). To this yellow solution was added a large excess of cyclopentene (~ 1 ml). The yellow solution was stirred at room temperature and the color changed to red within 15 minutes. The reaction was stirred for another 24 hours. The solution was filtered through glass filter paper and the solvent was removed under reduced pressure. NMR revealed the major product to be [(diimine)Pt(η^5 -

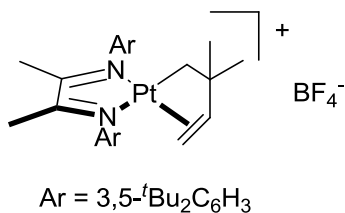
cyclopentadienyl)][BF₄]. ¹H NMR (300 MHz, CD₂Cl₂) δ 7.46 (s, 2H), 7.04 (d, *J* = 1.6 Hz, 4H), 5.51 (s, *J*(Pt,H) = 12 Hz, 5H), 2.39 (s, *J*(Pt,H) = 9 Hz, 6H), 1.39 (s, 36H).

[(diimine)Pt(η⁵-cyclopentadienyl)][BF₄] from sodium cyclopentadiene



In a glove box, [(diimine)Pt(μ-OH)]₂[BF₄]₂ (9.4 mg, 6.2 μmol) was added to a 20 mL vial with a stirbar and dissolved in CH₂Cl₂ (1 mL). To this yellow solution was added sodium cyclopentadiene (1.0 mg, 11.4 μmol). The yellow solution was stirred at room temperature for 1 hour during which the color gradually changed to red. The reaction was filtered through glass filter paper and the solvent was removed under reduced pressure. NMR revealed the conversion to [(diimine)Pt(η⁵-cyclopentadienyl)][BF₄] (58% yield by NMR integration). ¹H NMR (300 MHz, CD₂Cl₂) δ 7.46 (s, 2H), 7.04 (d, *J* = 1.6 Hz, 4H), 5.51 (s, *J*(Pt,H) = 12 Hz, 5H), 2.39 (s, *J*(Pt,H) = 9 Hz, 6H), 1.39 (s, 36H).

[(diimine)Pt(*neo*-hexenyl)][BF₄]



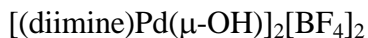
On the benchtop, [(diimine)Pt(μ-OH)]₂[BF₄]₂ (15.3 mg, 10.1 μmol) was dissolved in dichloroethane-*d*₄ (700 μL) and trifluoroethanol-*d*₃ (4 drops) and added to a J. Young tube. To this yellow solution was added *neo*-hexene (2.5 μl, 29.7 μmol). It was

determined by NMR that the starting material was 80% [(diimine)Pt(OH₂)₂]⁺ and thus HBF₄ (54% aqueous solution) (0.24 μl, 2.0 μmol) was added to convert the remaining dimer to monomer. The yellow solution was stirred at 60 °C and the color gradually darkened over 45 hours. The solution was filtered through glass filter paper and the solvent was removed under reduced pressure. NMR revealed the major product to be [(diimine)Pt(*neo*-hexenyl)][BF₄]. The product was purified by diffusion of pentane into a solution of DCE. ¹H NMR (300 MHz, CD₂Cl₂) δ 7.40 (s, 2H), 6.92 (broad s, 2H), 6.84 (broad s, 2H), 4.67 (dd, *J* = 14.9, 8.0 Hz, *J*(Pt,H) = 37 Hz, 1H), 4.11 (d, *J* = 14.9 Hz, *J*(Pt,H) = 37 Hz, 1H), 2.87 (d, *J* = 8.0 Hz, *J*(Pt,H) = 29 Hz, 1H), 2.36 (s, 3H), 2.19 (s, 3H), 1.37 (s, 36H), 1.11 (s, 3H), 0.75 (s, 3H), 0.67 (d, *J* = 8.6 Hz, *J*(Pt,H) = 45 Hz, 1H), -0.12 (d, *J* = 8.2 Hz, *J*(Pt,H) = 52 Hz, 1H).

Improved large-scale steps for the synthesis of [(diimine)Pd(μ-OH)]₂[BF₄]₂

[(diimine)Pd(THF)₂][BF₄]₂

To a flame-dried round bottom flask containing a stirbar and (diimine)PdCl₂ (588 mg, 0.922 mmol, 1.00 equiv) was added dry CH₂Cl₂ (8 mL) and THF (8 mL). A solution of AgBF₄ (360 mg, 1.85 mmol, 2.01 equiv) in THF (4 mL) was added dropwise under argon. Insoluble AgCl deposited immediately. The orange suspension was stirred for 3 hours and filtered through Celite in a dry box to afford an orange solution. Concentration *in vacuo* afforded [(diimine)Pd(THF)₂][BF₄]₂ (735 mg) as an orange powder in 90% yield.



To a round bottom flask containing a stirbar and $[(\text{diimine})\text{Pd}(\text{THF})_2][\text{BF}_4]_2$ (460 mg, 0.520 mmol, 1.00 equiv) was added CH_2Cl_2 (50 mL). The yellow solution was cooled to 0 °C in an ice-water bath for 10 minutes before several drops of water were added. The yellow suspension was stirred at 0 °C for 10 minutes. With the reaction stirring vigorously, polymer-bound diethylamine (856 mg, 1.07 mmol, 2.05 equiv) was added over 1 minute. The reaction was stirred for 3 minutes at 0 °C. Fast filtration through a bed of Celite afforded a yellow solution that was concentrated *in vacuo* to afford $[(\text{diimine})\text{Pd}(\mu\text{-OH})_2][\text{BF}_4]_2$ (558 mg) as a yellow powder in 80% yield.

Oligomerization procedures

Ethylene oligomerization

To a 48 ml round bottom flask equipped with a side-arm valve and a 180° joint was added **1** (8 mg, 6 μmol, 0.0030 equiv) and a large stirbar. The flask was evacuated and back-filled with 1.0 atm of ethylene. A rubber septum was affixed to the side-arm valve through which a premixed solution of d^2 -dichloromethane (4.0 mL) and d^3 -trifluoroethanol (4.0 μL) was syringed. The light yellow solution was stirred, and aliquots (500 μL) were taken via syringe for NMR analysis at 30 minute intervals.

Propylene oligomerization

To a 270 ml thick-walled flask equipped with a side-arm valve and a 180° joint was added **1** (16 mg, 12 μmol, 0.0015 equiv) and a stirbar. The flask was evacuated and back-

filled with 0.75 atm of propylene. The flask was then attached and very briefly (~ 1 s) opened to O₂ (1 atm). A rubber septum was affixed to the side-arm valve through which a premixed solution of d⁴-dichloroethane (12 mL) and d³-trifluoroethanol (12 μL) were added via syringe. The light yellow solution was stirred, and aliquots (500 μL) were taken via syringe for NMR analysis at 30 min intervals.

References

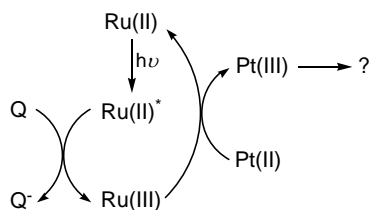
1. (a) Williams, T. J.; Caffyn, A. J.; Hazari, N.; Oblad, P. F.; Labinger, J. A.; Bercaw, J. E., *J. Am. Chem. Soc.* **2008**, *130* (8), 2418–2419; (b) Bercaw, J. E.; Hazari, N.; Labinger, J. A.; Oblad, P. F., *Angew. Chem., Int. Ed.* **2008**, *47* (51), 9941–9943.
2. Skupinska, J., *Chem. Rev.* **1991**, *91* (4), 613–648.
3. (a) Small, B. L.; Brookhart, M., *J. Am. Chem. Soc.* **1998**, *120* (28), 7143–7144; (b) Svejda, S. A.; Brookhart, M., *Organometallics* **1998**, *18* (1), 65–74.
4. Zhong, H. A.; Labinger, J. A.; Bercaw, J. E., *J. Am. Chem. Soc.* **2002**, *124* (7), 1378–1399.

Appendix A

Oxidation of Diimine Platinum Complexes by Flash Quench

Introduction

In a catalytic cycle similar to the Shilov system, the step following the formation of the metal-carbon bond involves the oxidation of the organometallic complex. With the Shilov cycle, this step seems to be the Achilles heel, since the only catalytically efficient oxidant, hexachloroplatinate, is economically impractical. Though there have been other oxidants that have been able to turn the system over, each has critical limitations.¹ Chemical oxidation of the organometallic products of C-H activation with diimine ligated platinum and palladium complexes was discussed in Chapter 4 but little is known about how these oxidations or those in the Shilov cycle proceed. To better understand the mechanism for the oxidation of methane to methanol by platinum, ultra-fast flash-quench studies using a Nd:YAG laser were undertaken. This spectroscopic technique has been used to successfully identify short-lived intermediates and was employed here to identify intermediates in systems that model Shilov chemistry.² The goal was to generate an oxidant *in situ*, and by using transient absorption spectroscopy, probe the subsequent electron transfer events (Scheme A.1). The knowledge gained in these studies would increase our



Scheme A.1. Photochemical reaction sequence

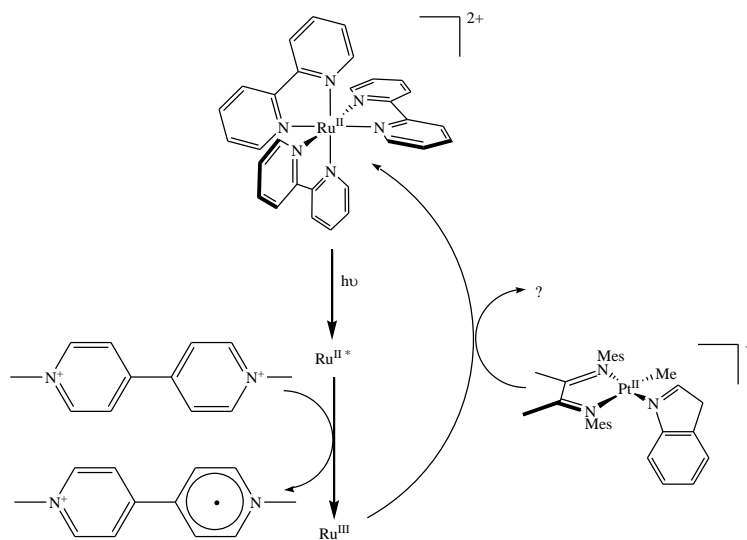
understanding of electron transfer in our catalytic cycle and potentially allow us to develop a system with an industrially relevant oxidant.

Results and Discussion

As finding an industrially relevant oxidant for the platinum system has proven to be an obstacle, we have begun studies into the fundamental nature of the platinum oxidation step in the Shilov cycle. There were two possible mechanisms by which this step could occur, the first being the transfer of the alkyl group from the organometallic platinum(II) complex to that of the oxidant, $\text{Na}_2[\text{Pt}^{\text{IV}}\text{Cl}_6]$, with the second being inner-sphere electron transfer from the organometallic complex to the oxidant. Luinstra et al. did an important study that helped to elucidate the mechanism of this step.³ To differentiate between the two, the reaction was studied with isotopically labeled hexachloroplatinate $\text{Na}_2[^{195}\text{Pt}^{\text{IV}}\text{Cl}_6]$. NMR analysis revealed that the organometallic product was not isotopically enriched, demonstrating that the reaction proceeded via electron transfer and not alkyl transfer. There were additional studies that confirmed these findings.⁴

It has also been shown for acetic acid oxidation that platinum(II) can be converted to platinum(IV) with oxidants other than hexachloroplatinate. Namely, it can be turned over with quinines, cupric and cuprous chlorides, and polyoxometallates.⁵ Since cupric chloride is a one-electron oxidant, it raises the question: could there be a platinum(III) intermediate? If there is such an intermediate, detection should be possible using ultra-fast spectroscopy with a Nd/YAG laser.² Samples were prepared and, though attempts were made to study intermediate products from direct oxidation of platinum compounds, either no reaction occurred or it was too fast to study.

Another approach involved using a flash-quench technique with which an oxidant could be generated *in situ*. In this system an electron on $\text{Ru}^{\text{II}}(\text{bpy})_3(\text{PF}_6)_2$ (where bpy = 2,2'-bipyridine) was excited by flashing into the MLCT band of the complex (Scheme B.2).⁶ Once in the excited state, the electron could be removed with the quencher, methyl viologen (MV^{2+}), to yield a Ru^{III} complex. The resulting compound potentially



Scheme A.2. Generation of an oxidant using flash quench

could oxidize platinum. Observation of short-lived intermediates generated in the reaction is possible with this transient absorption spectroscopic technique.

Acetonitrile solutions containing $(\text{Ru}(\text{bpy})_3)^{2+} 2(\text{PF}_6^-)$, MV^{2+} , and $(\text{diimine})\text{PtMe}(\text{indole})^+(\text{BF}_4^-)$ were prepared for studies of reactions after excitation of the MLCT transition at 480 nm in $(\text{Ru}(\text{bpy})_3)^{2+}$. To ensure there were no unexpected side reactions, emission lifetimes of the ruthenium excited state (Ru^*) were measured. When quenched by MV^{2+} , the lifetime was 250 ns, as measured at 610 nm. The presence of the

platinum complex did not affect the Ru* lifetime, indicating that the platinum complex did not interfere in the reactions involving the excitation of Ru and the quenching of Ru* by MV²⁺. The quenching event was further verified by the formation of MV⁺ as observed by transient absorption spectroscopy at 390 and 605 nm (Figure A.1).⁷ The formation of MV⁺ combined with the bleach of the Ru^{II} MLCT as observed at 440 nm indicated the formation

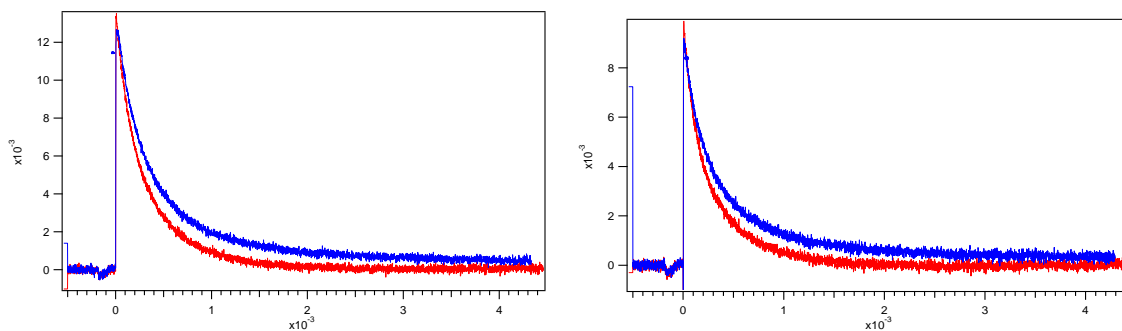


Figure A.1. Transient absorption of MV⁺ (in red) and MV⁺ in the presence of (diimine)PtMe(indole)⁺ (in blue). The solutions were excited at 480 nm and probed at 390 and 605 nm, respectively.

of Ru^{III}. Interestingly, when the platinum indole complex was present, the formation of an intermediate was observed (Figure A.2). The initial bleach of the Ru^{II} was briefly observed, immediately followed by the formation of a new species, which absorbed at 440 nm and was short lived (Figure A.3). Control experiments deficient in the platinum

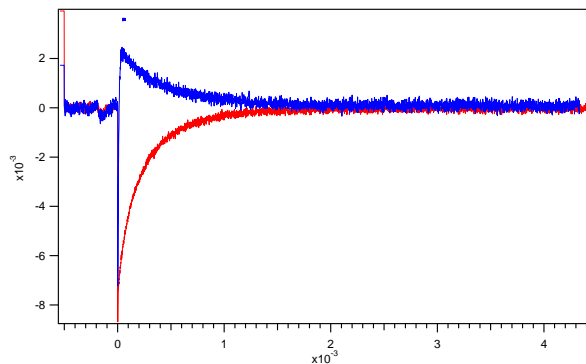


Figure A.2. Transient absorption of the bleach of Ru^{2+} (in red) and then in the presence of $(\text{diimine})\text{PtMe}(\text{Indole})^+$ (in blue). The solutions were excited at 480 nm and probed at 440 nm.

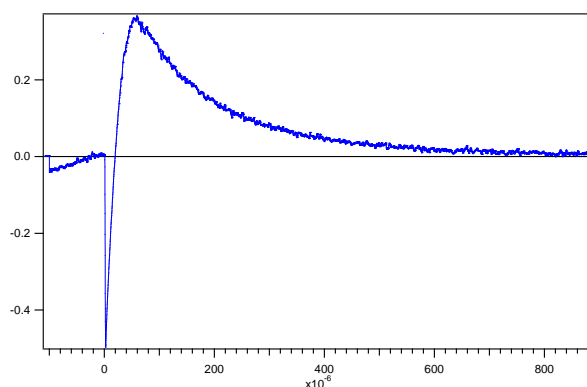


Figure A.3. Transient absorption of the bleach of Ru^{2+} followed by a new absorption when in the presence of $(\text{diimine})\text{PtMe}(\text{indole})^+$ (in blue). The solutions were excited at 480 nm and probed at 440 nm.

complex confirmed that this absorption only grew in when the platinum complex was present. Unfortunately, control experiments involving only $\text{Ru}(\text{bpy})_2^{2+}$, MV^{2+} , and unligated indole (no platinum) indicated that Ru^{III} could just be reacting with free indole to generate an indole radical (Figure A.4). NMR experiments confirmed the slow formation of $(\text{diimine})\text{PtMe}(\text{ACN})^+$ as the solvent coordinated to the platinum center with release of indole.

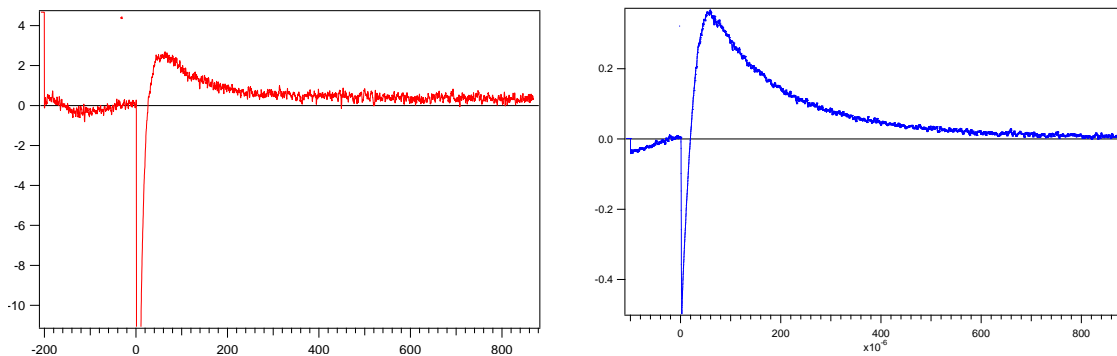


Figure A.4. Transient absorption of the bleach of Ru^{2+} followed immediately by a new absorption when in the presence of indole (in red) or (diimine)PtMe(indole)⁺ (in blue). The solutions were excited at 480 nm and probed at 440 nm.

Conclusions

Though the oxidation of indole was not the target reaction, it could potentially be harnessed and used to facilitate the oxidation of platinum. Gray and colleagues demonstrated that the oxidation of a ligand attached to platinum allowed for the ultimate oxidation of the metal center as assisted by the association of another ligand.⁸ If indole could be oxidized while it was still on the metal, coordination of a nucleophile could facilitate the oxidation of the metal. This would require the use of a solvent in which indole will remain coordinated to the metal. Initial attempts to identify an appropriate solvent replacement have been unsuccessful. Solubility issues preclude the use of nonpolar solvents. Attempts were made using acetone, however, it was found that unresolved speciation of the platinum complex occurred, as observed by NMR. Consequently, a suitable platinum complex for flash-quench oxidation studies was not found and work on this project was discontinued.

Experimental Section

Solutions were mixed in a 15 mL round bottom flask sealed with Kontes Teflon stoppers and custom fitted with a quartz cuvette side arm. Samples were degassed by freezing the solution and then evacuating the headspace. After the solution was thawed, this degassing technique was repeated two more times. The samples were flashed with a Nd:YAG laser directed through an OPO (Quanta Ray Pro, Spectra Physics) with a pulse length of 8 ns repeated at 10 Hz. The laser beam was aligned with probe light from a 75 watt PTI continuous wave arc lamp (model 1010). Data were collected by passing the light through an Instruments SA DH-10 monochromater and into a photomultiplier tube (Hamamatsu R928). A LeCroy 9354A transient digitizer recorded and amplified the current from the photomultiplier tube. The instruments were synchronized with the laser pulse with an EG & G digital delay generator (9650). The data collected from this set up were analyzed with Wavemetrics from Igor Pro 5.01 where the data were converted to ΔOD with the equation $\Delta OD = -\log(I/I_0)$.

Chemicals were purchased from Aldrich unless otherwise stated and used without further purification. $[\text{Ru}(\text{bpy})_3](\text{PF}_6)_2$ and methylviologen bis(hexfluorophosphate) were prepared by a salt exchange reaction in water with NH_4PF_6 and $[\text{Ru}(\text{bpy})_3]\text{Cl}_2$ (as purchased from Strem) and methylviologen dichloride, respectively. $[\text{Ru}(\text{bpy})_3](\text{PF}_6)_2$ was dried under reduced pressure and purified through crystallization by diffusing diethyl ether into a solution of acetonitrile. Crystals of $[\text{Ru}(\text{bpy})_3](\text{PF}_6)_2$ were collected, excess solvent was removed under reduced pressure, and then the crystals were used without further purification. Methylviologen bis(hexfluorophosphate) was dried under reduced pressure

and used without further purification. Tetra-*n*-butylammonium hexafluorophosphate was added to all solutions to a concentration of 0.1 M. The [(diimine)Pt^{II}Me(indole)][BF₄] was prepared according to literature procedures.⁹ Solutions were prepared such that the concentration of [Ru(bpy)₃](PF₆)₂ would be 50 μM, methylviologen bis(hexafluorophosphate) would be 2.0 mM, and [(diimine)Pt^{II}Me(indole)][BF₄] would be 100 μM when present.

References

1. (a) Goldschleger, N. F.; Lavrushko, V. V.; Khrushch, A. P.; Shteinman, A. A. *Izv. Akad. Nauk SSSR, Ser. Khim.* **1976**, *10*, 2174. (b) Geletii, Yu. V.; Shilov, A. E. *Kinet. Katal.* **1983**, *24*, 486. (c) Shilov, A. E.; Shteinman, A. A. *Coord. Chem.* **1977**, *24*, 97. (d) Weinberg, D. R.; Labinger, J. A.; Bercaw, J. E. *Organometallic*, **2007**, *26*, 167.
2. (a) Ogata, T.; Yanagida, S.; Brunschig, B. S.; Fujita, E. *J. Am. Chem. Soc.* **1995**, *117*, 6708. (b) Berglund, J.; Pasher, T.; Winkler, J. R.; Gray, H. B. *J. Am. Chem. Soc.* **1997**, *119*, 2464.
3. Luinstra, G. A.; Wang, L.; Stahl, S. S.; Labinger, J. A.; Bercaw, J. E. *J. Organomet. Chem.* **1995**, *504*, 75.
4. Wang, L.; Stahl, J. A.; Labinger, J. E.; Bercaw, J. E. *J. Mol. Catal. A* **1997**, *116*, 269.
5. (a) Goldschleger, N. F.; Lavrushko, V. V.; Khrushch, A. P.; Shteinman, A. A. *Izv. Akad. Nauk SSSR, Ser. Khim.* **1976**, *10*, 2174. (b) Geletii, Yu. V.; Shilov, A. E. *Kinet. Katal.* **1983**, *24*, 486. (c) Shilov, A. E.; Shteinman, A. A. *Coord. Chem.* **1977**, *24*, 97.6. Nazeeruddin, M. K.; Zakeeruddin, S. M.; Kalyanasundaram, K. *J. Phys. Chem.* **1993**, *97*, 9607.

7. Kosower, E. M.; Cotter, J. L. *J. Am. Chem. Soc.* **1964**, 86, 5524.
8. Che, C. M.; Cho, K. C.; Chan, W. S.; Gray, H. B. *Inorg. Chem.* **1986**, 25, 4906.9.
Williams, T. J.; Labinger, J. A.; Bercaw, J. E. *Organomet.* 2007, 26, 281.

Appendix B

Coordination Chemistry of the Tris(triphenylphosphino)silyl Ligand

Adapted in part from:

Whited, M. T.; Mankad, N. P.; Lee, Y.; Oblad, P. F.; Peters, J. C., *Inorganic Chemistry*
2009, 48 (6), 2507-2517.

Introduction

Dinitrogen fixation through Haber-Bosch process is an enormously important industrial method to produce ammonia for fertilizer and feed the world today. The demand for this process is so great that about 1% of the world's energy production goes to driving this reaction.¹ The necessity of fertilizer and the huge energy cost required for fixing N_2 have motivated scientific inquiry into improving this technology.² Much of these efforts have centered on inorganic nitrogenase enzymes that utilize transition-metal-based cofactors to fix nitrogen.² The iron and molybdenum cofactor in FeMo-nitrogenase inspired Schrock et al. to develop a trivalent triamidoamine $[NN_3]Mo-N_2$ species that can access four oxidation states to reduce N_2 .³ Similarly, the Peters group and others have developed low-coordinate iron sites that facilitate the reduction of small molecules.⁴ More recently, Peters et al. have utilized a tris(phosphino)silyl ligand $[SiP^R_3]$ on iron to facilitate N_2 chemistry (Figure B.1).⁵ This tetradentate-phosphine-rich ligand has a

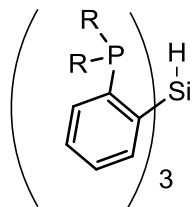


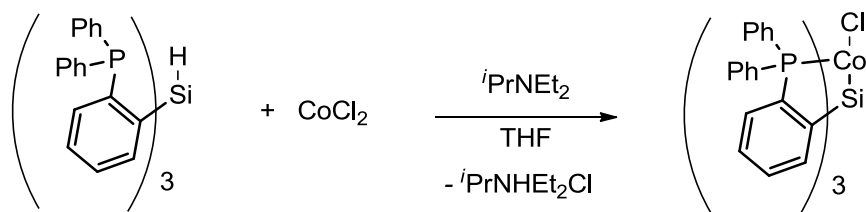
Figure B.1. Tris(phosphino)silyl ligand $H[SiP^R_3]$

single X-type silyl donor with a strong trans-influence designed to help labilize bound substrates and promote catalysis.⁶ In addition to being a competent scaffold for iron base N_2 chemistry, we have found that $[SiP^R_3]$ coordinates a variety of transition metals.

However, as I only spent a few months actually doing research in Jonas Peters' laboratories, I was unable to follow these projects to completion and as a result some of these complexes have not been fully characterized. The NMR and crystallographic data however, make the identification of these complexes unambiguous. In order to accurately represent my contributions, I have only included my procedures and data. The ruthenium, nickel, and platinum projects have since been picked up by other students in the Peters group and more fully developed. Some of their results have been published and I am thankful that my contributions were recognized in the acknowledgement section of these papers.⁷ Herein I describe the synthesis and characterization of $[\text{SiP}^{\text{Ph}}_3]$ cobalt, ruthenium, nickel, and platinum complexes.

Results and Discussion

As $[\text{SiP}^{\text{Ph}}_3]$ complexes were demonstrated to be an appropriate scaffold to facilitate the binding of N_2 on iron, an investigation of ligand coordination to similar late transition metals like cobalt and ruthenium was the logical next step. It was likewise demonstrated that treatment of CoCl_2 with $\text{H}[\text{SiP}^{\text{Ph}}_3]$ in THF resulted in the formation of $[\text{SiP}^{\text{Ph}}_3]\text{CoCl}$, as evidenced by the disappearance of the Si-H IR stretch and the observation of a paramagnetic species in the NMR (Scheme B.1). This complex was also characterized crystallographically by vapor diffusion of petroleum ether into a saturated methylene chloride solution (Figure B.2). $[\text{SiP}^{\text{Ph}}_3]\text{CoCl}$ was explored electrochemically



Scheme B.1. Synthesis of $[\text{SiP}^{\text{Ph}}_3]\text{CoCl}$

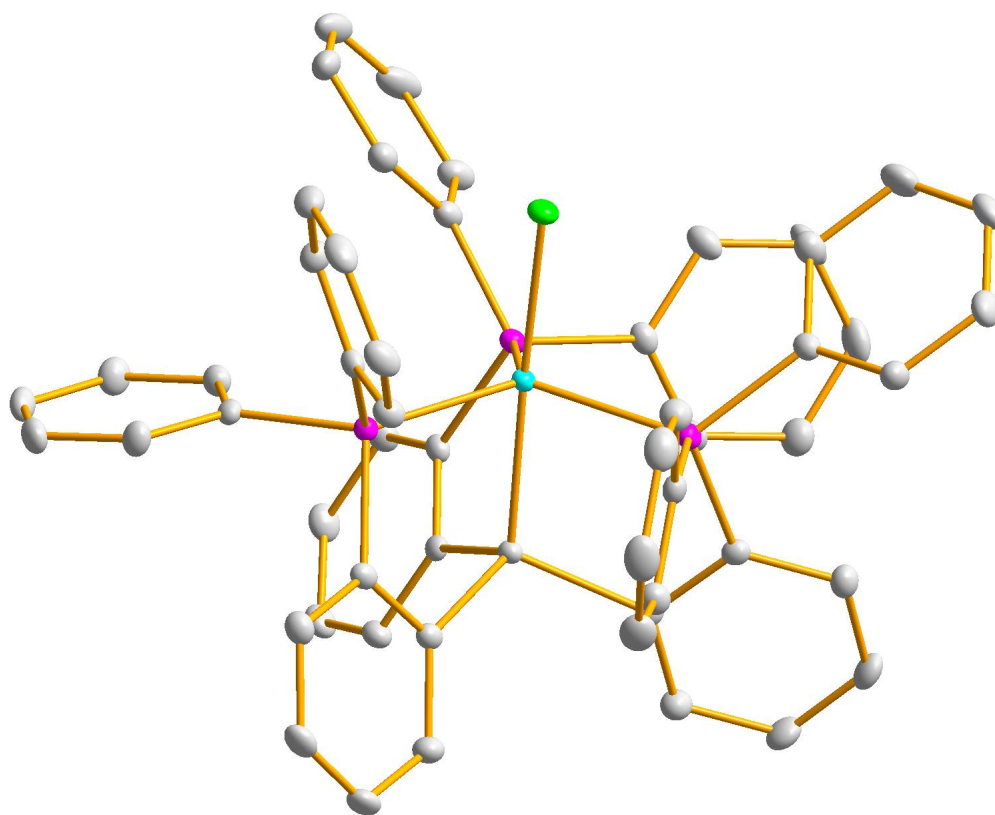


Figure B.2. Crystal structure of $[\text{SiP}^{\text{Ph}}_3]\text{CoCl}$

by cyclic voltammetry and found to have a reversible $\text{Co}^{\text{III/II}}$ couple at -0.4 V and a quasi-reversible $\text{Co}^{\text{II/I}}$ at -1.6 V (Figure B.3) Interestingly, there was also a half-wave potential

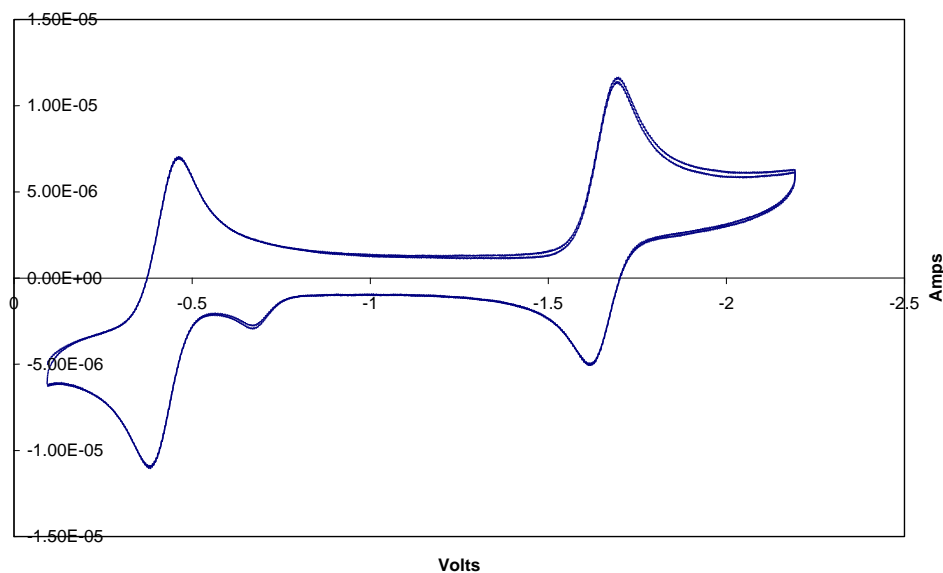
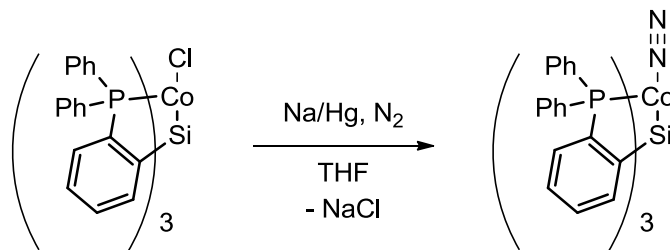


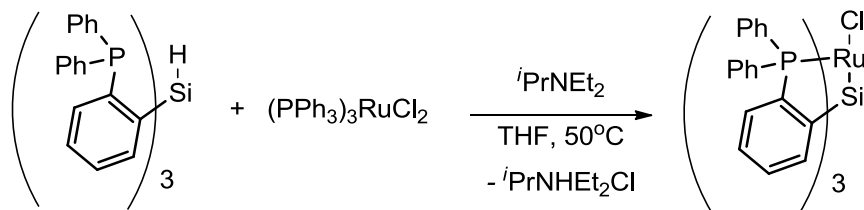
Figure B.3. Cyclic voltammogram of $[\text{SiP}^{\text{Ph}}_3]\text{CoCl}$ recorded at a scan rate of 100 mV/s in THF under an N_2 atmosphere. Potentials are referenced to Fc/Fc^+ .

event at -0.6 V which did not appear when the experiment was run under argon. This event was attributed to the electrochemical production of $[\text{SiP}^{\text{Ph}}_3]\text{CoN}_2$. It was also demonstrated that $[\text{SiP}^{\text{Ph}}_3]\text{CoCl}$ could be reduced chemically by Na/Hg amalgam under N_2 to produce the $[\text{SiP}^{\text{Ph}}_3]\text{CoN}_2$ complex (Scheme B.2). This conversion was evidenced by the formation of a diamagnetic species in the NMR that had an IR stretch diagnostic of a terminally bound N_2 adduct at 2095 cm^{-1} .



Scheme B.2. Synthesis of $[\text{SiP}^{\text{Ph}}_3]\text{CoN}_2$

Ruthenium behaved similarly to iron. Treatment of $(PPh_3)_3RuCl_2$ with $H[SiP^{Ph}_3]$ and base in THF resulted in the formation of a new complex, $[SiP^{Ph}_3]RuCl$ (Scheme B.3).



Scheme B.3. Synthesis of $[SiP^{Ph}_3]RuCl$

This Ru(II) complex was diamagnetic as expected and lacked the Si-H IR stretch visible in the unbound ligand. $[SiP^{Ph}_3]RuCl$ was also characterized crystallographically and by CV (Figures B.4 and B.5, respectively). Interestingly, the electrochemical reduction of $[SiP^{Ph}_3]RuCl$ showed an unidentified event that appeared when the CV was performed under N_2 but not under argon, similarly to the cobalt system. Chemical reduction with Na/Hg resulted in a paramagnetic species observed by NMR but no N_2 stretch was visible by IR. The reduced ruthenium complex was never fully characterized, however, it is speculated that an N_2 -bridged ruthenium dimer may have been formed. The reactivity of the $[SiP^{Ph}_3]RuCl$ was more thoroughly explored later by other Peters group members.^{7a}

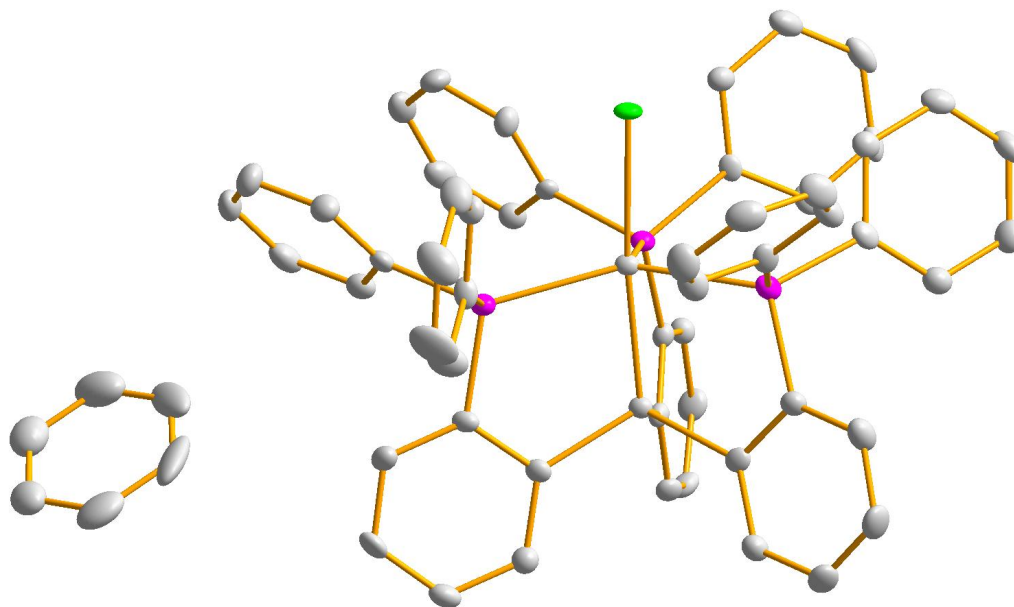


Figure B.4. Crystal structure of $[\text{SiP}^{\text{Ph}}_3]\text{RuCl}$

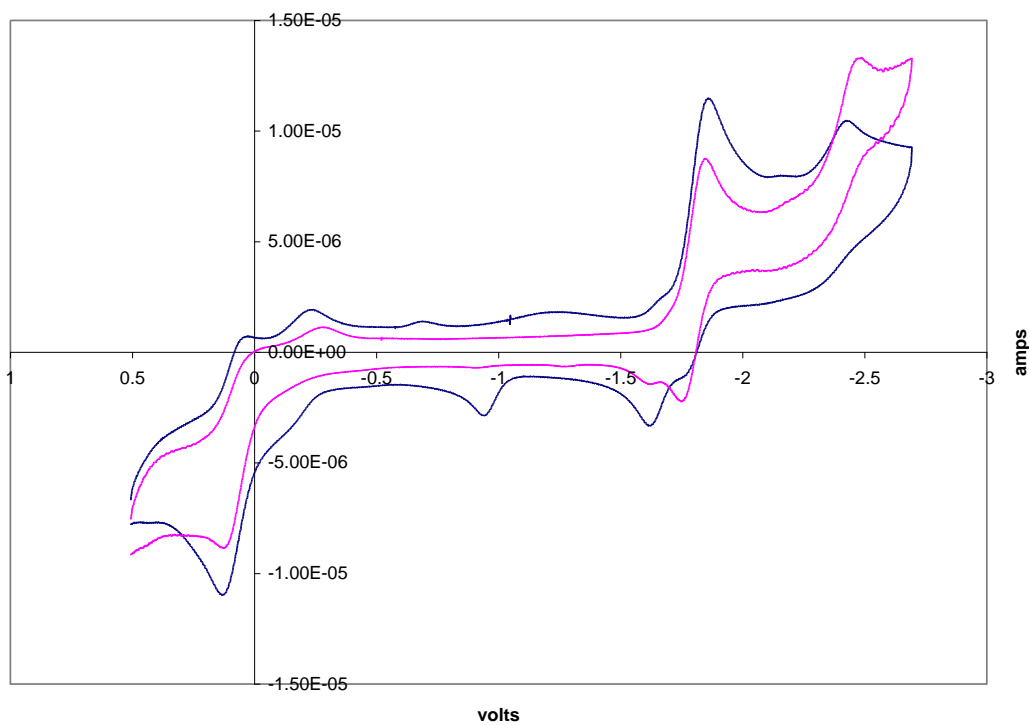
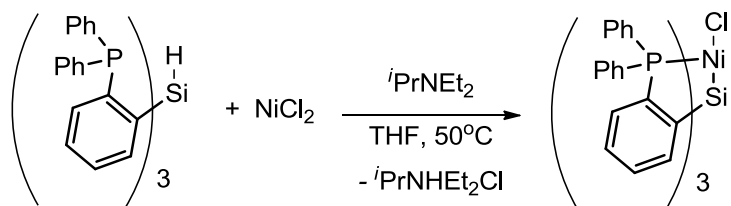


Figure B.5. Cyclic voltammogram of $[\text{SiP}^{\text{Ph}}_3]\text{RuCl}$ in THF under an N_2 atmosphere (blue) and argon (pink). Potentials are referenced to Fc/Fc^+ .

The final series of $\text{H}[\text{SiP}^{\text{Ph}}_3]$ coordination complexes explored were with group 10 transition metals nickel and platinum. Treatment of NiCl_2 with ligand and base at $50\text{ }^\circ\text{C}$ resulted in the formation of a diamagnetic $[\text{SiP}^{\text{Ph}}_3]\text{NiCl}$ complex (Scheme B.4). Well-



Scheme B.4. Synthesis of $[\text{SiP}^{\text{Ph}}_3]\text{NiCl}$.

formed red crystals were obtained by vapor diffusion of ether into a saturated solution of $[\text{SiP}^{\text{Ph}}_3]\text{NiCl}$ in CH_2Cl_2 (Figures B.6 and B.7). Reduction was attempted with Na/Hg and a color change from red to blue was observed, however the products of this reaction were never fully characterized.

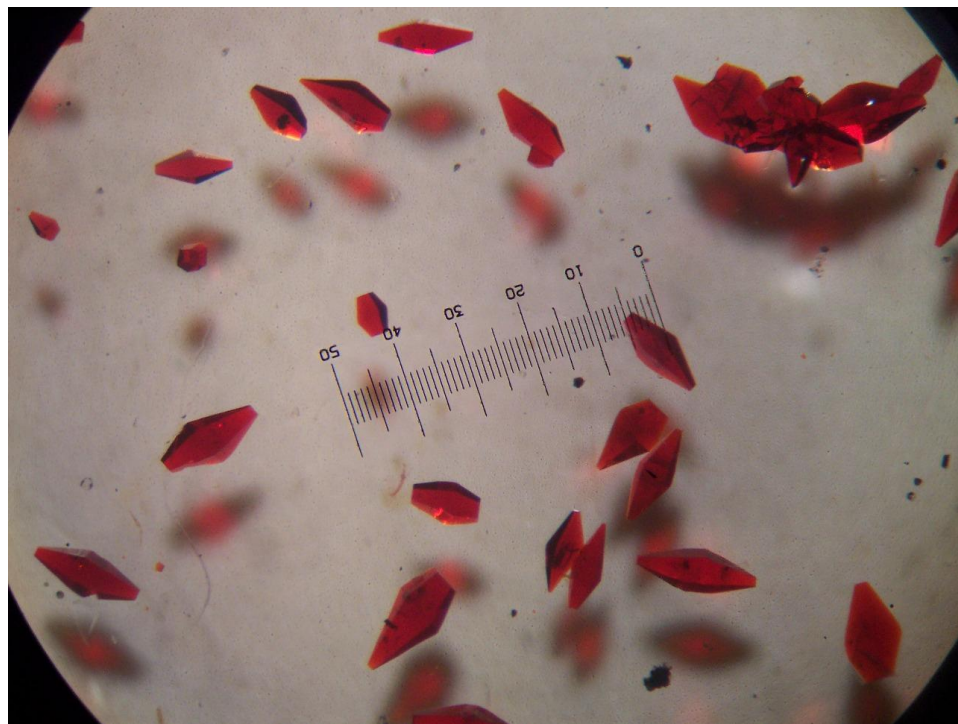


Figure B.6. Crystals of [SiP^{Ph}₃]NiCl

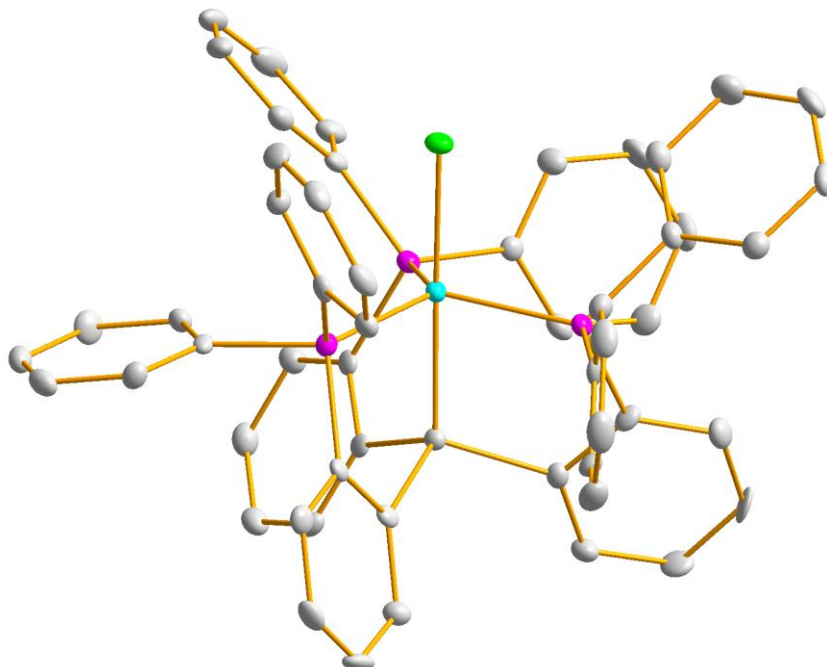
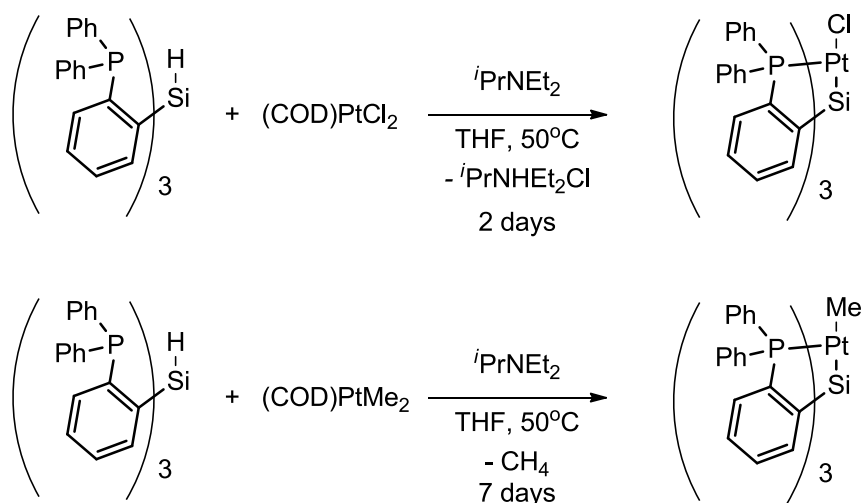


Figure B.7. Crystal structure of [SiP^{Ph}₃]NiCl

Of this series of $[\text{SiP}^{\text{Ph}}_3]$ coordination complexes, the platinum system is potentially the most surprising. Treatment of $(\text{COD})\text{PtCl}_2$ ($\text{COD} = 1,5\text{-cyclooctadiene}$) with $\text{H}[\text{SiP}^{\text{Ph}}_3]$ and base in THF led to the formation of an uncommon trigonal bipyrimidal platinum complex (Scheme B.5). Similarly, treatment of $(\text{COD})\text{PtMe}_2$ with



Scheme B.5. Synthesis of $[\text{SiP}^{\text{Ph}}_3]\text{PtCl}$

$\text{H}[\text{SiP}^{\text{Ph}}_3]$ slowly formed $[\text{SiP}^{\text{Ph}}_3]\text{PtMe}$. Methane was also likely released in this reaction. Additionally, a mixture of both the $[\text{SiP}^{\text{Ph}}_3]\text{PtCl}$ and $[\text{SiP}^{\text{Ph}}_3]\text{PtMe}$ could be formed in less than an hour if $(\text{COD})\text{PtClMe}$ was used as a starting material. Unfortunately, they co-crystallize and another methodology to separate each was not developed (Figure B.8). The reactivity of these platinum complexes was more thoroughly explored later by other Peters group members.^{7b}

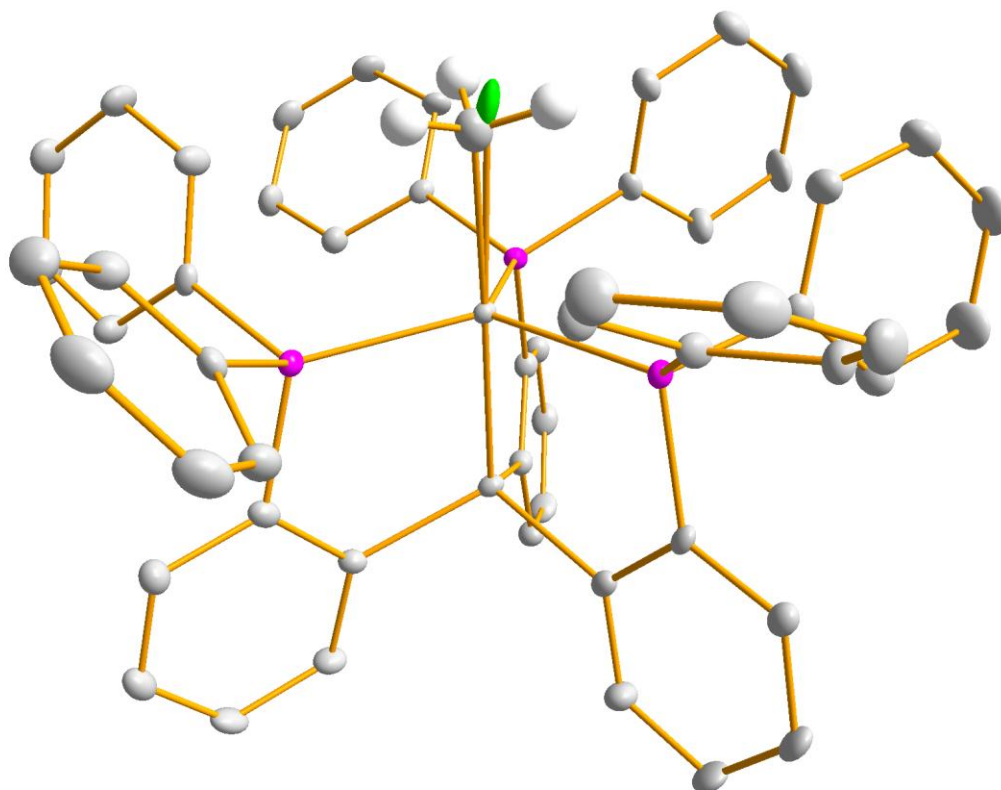


Figure B.8. Crystal structure of $[\text{SiP}^{\text{Ph}}_3]\text{PtCl}$ with partial occupancy by a methyl group in the Cl position

Conclusions

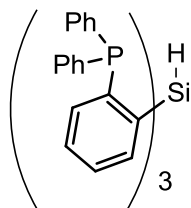
The $[\text{SiP}^{\text{Ph}}_3]$ anion has been demonstrated to be a versatile ligand that is capable of supporting a trigonal bipyramidal geometry on a variety of transition metals. Syntheses of $[\text{SiP}^{\text{Ph}}_3]\text{CoCl}$, $[\text{SiP}^{\text{Ph}}_3]\text{RuCl}$, $[\text{SiP}^{\text{Ph}}_3]\text{NiCl}$, and $[\text{SiP}^{\text{Ph}}_3]\text{PtCl}$ have herein been developed. The cobalt and ruthenium complexes have been shown to have rich redox chemistry. A cobalt complex was even isolated with an N_2 adduct in the Co(I) oxidation state. The $[\text{SiP}^{\text{Ph}}_3]\text{NiCl}$ complex potentially has interesting redox activity that has yet to be fully characterized. Finally, $[\text{SiP}^{\text{Ph}}_3]$ ligand will even support a trigonal bipyramidal geometry and an organometallic Pt-Me moiety with Pt(II).

Experimental Section

All manipulations were carried out using standard Schlenk or glovebox techniques under a dinitrogen atmosphere. Unless otherwise noted, solvents were deoxygenated and dried by thorough sparging with N₂ gas followed by passage through an activated alumina column. Non-halogenated solvents were typically tested with a standard purple solution of sodium benzophenone ketyl in tetrahydrofuran to confirm effective oxygen and moisture removal. (2-bromophenyl)diphenylphosphine was prepared according to literature procedures. All other reagents were purchased from commercial vendors and used without further purification unless otherwise noted. Deuterated solvents were purchased from Cambridge Isotopes Laboratories, Inc., and were degassed and stored over activated 3 Å molecular sieves prior to use.

Elemental analyses were performed by Desert Analytics, Tucson, AZ. A Varian Mercury-300 spectrometer was used to record ¹H, ³¹P{¹H}, and ¹³C{¹H} spectra at room temperature unless otherwise noted. ¹H and ¹³C{¹H} chemical shifts were referenced to residual solvent. ³¹P{¹H} NMR are reported relative to an external standard of 85% H₃PO₄ (0 ppm). Abbreviations for reported signal multiplicities are as follows: s, singlet; d, doublet; t, triplet; q, quartet; m, multiplet; br, broad. IR spectra were recorded on a Bio-Rad Excalibur FTS 3000 spectrometer controlled by Win-IR Pro software using a KBr solution cell. Solution magnetic moments were measured at 298 K following the Evans method. UV-vis measurements were recorded on a Varian Cary 50 Bio Spectrophotometer controlled by Cary WinUV Software. All measurements were recorded using a quartz cell fitted with a Teflon cap. XRD studies were carried out in the

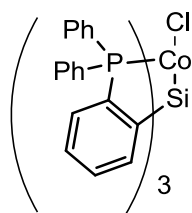
Beckman Institute Crystallographic Facility on a Bruker Smart 1000 CCD diffractometer. Electrochemical analysis was performed on a CHI 600B Potentiostat/Galvanostat using a glassy carbon working electrode, a platinum wire auxiliary electrode, and an Ag/AgNO₃ non-aqueous reference electrode filled with THF and Bu₄NPF₆.



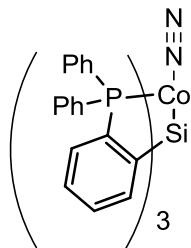
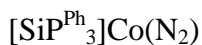
(2-Bromophenyl)diphenylphosphine (10.24 g, 30.0 mmol) was dissolved in diethyl ether (150 mL) and cooled to $-78\text{ }^{\circ}\text{C}$. *n*-Butyllithium (1.60 M in hexanes, 18.8 mL, 30.0 mmol) was added slowly, giving a light orange solution with a tan-colored precipitate. This mixture was allowed to warm gradually to room temperature and then stirred for 1 h, after which the volatiles were removed *in vacuo*. Toluene (150 mL) was added, and the cloudy orange solution was cooled back to $-78\text{ }^{\circ}\text{C}$. Trichlorosilane (1.01 mL, 10.0 mmol) was added in one portion, and the resulting mixture was warmed to room temperature gradually. After stirring for 30 min, the reaction was heated in a sealed reaction bomb to $110\text{ }^{\circ}\text{C}$ for 15 h. The resulting yellow solution and white precipitate were cooled to room temperature and filtered through Celite, and the filtrate was concentrated to white solids. Petroleum ether (100 mL) was added, and the resulting mixture was stirred vigorously for 20 min, at which point tan solids were collected on a sintered glass frit and washed with additional petroleum ether ($2 \times 30\text{ mL}$) to

afford $\text{H}[\text{SiP}^{\text{Ph}}_3]$ as a fine tan powder (6.15 g, 76%). ^1H NMR (C_6D_6): δ 7.63 (dm, $J = 1.5$ and 6.3 Hz, 3H), 7.34 (ddm, $J = 1.0, 3.9,$ and 7.8 Hz, 3H), 7.25–7.20 (m, 12H), 7.05 (td, $J = 1.5$ and 7.3 Hz, 6H), 7.02–6.95 (m, 19H). ^{13}C NMR (C_6D_6): δ 145.5 (d, $J = 11.4$ Hz), 144.3 (t, $J = 4.0$ Hz), 144.0 (t, $J = 4.0$ Hz), 138.8 (d, $J = 14.6$ Hz), 138.5 (d, $J = 12.8$ Hz), 134.7, 134.5 (d, $J = 19.2$ Hz), 130.4, 128.8, 128.6 (d, $J = 17.3$ Hz). ^{31}P NMR (C_6D_6): δ -10.4 (s). IR (KBr, cm^{-1}) $\nu(\text{Si-H})$: 2170. Anal. Calcd for $\text{C}_{54}\text{H}_{43}\text{P}_3\text{Si}$: C, 79.78; H, 5.33. Found: C, 79.39; H, 5.61.

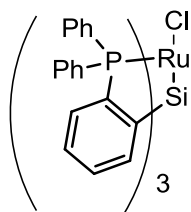
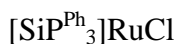
$[\text{SiP}^{\text{Ph}}_3]\text{CoCl}$



$\text{H}[\text{SiP}^{\text{Ph}}_3]$ (0.483 g, 0.595 mmol) and CoCl_2 (0.0830 g, 0.639 mmol) were combined in THF (30 mL) with $i\text{Pr}_2\text{NEt}$ (110 μL , 0.666 mmol). After several minutes, the blue solution adopted a red hue and was stirred for 16 h. Solvent was removed under reduced pressure, and the remaining solid was dissolved in benzene (30 mL). This solution was filtered through a glass microfilter and lyophilized to yield spectroscopically pure $[\text{SiP}^{\text{Ph}}_3]\text{CoCl}$ as a fluffy red powder (0.4686 g, 87%). Crystals suitable XRD were obtained by vapor diffusion of petroleum ether into a saturated solution of $[\text{SiP}^{\text{Ph}}_3]\text{CoCl}$ in methylene chloride. ^1H NMR (C_6D_6): δ 10.3, 8.1, 7.7, 5.6, 3.0, -1.2. UV-vis (C_6H_6) λ_{max} , nm (ϵ , $\text{M}^{-1} \text{cm}^{-1}$): 402 (5700), 506 (3800).



A red solution of [SiP^{Ph}₃]CoCl (0.035 g, 0.039 mmol) in THF (10 mL) was added onto a 0.5 weight % Na/Hg amalgam (0.0015 g, 0.066 mmol sodium dissolved in 0.3025 g of mercury) with stirring, causing a gradual color change to brown. After 12 h, the mixture was decanted from the amalgam and filtered through Celite to give an orange solution. Solvent was removed *in vacuo*, and the residues were extracted into benzene, filtered, and lyophilized to afford [SiP^{Ph}₃]Co(N₂) as an orange powder (0.014 g, 45%). ¹H NMR (C₆D₆): δ 8.1, 7.4, 7.2, 7.0, 6.9, 6.8. ³¹P NMR (C₆D₆): δ 63.5. UV-vis (C₆H₆) λ_{max}, nm (ε, M⁻¹ cm⁻¹): 378 (2000). IR (KBr, cm⁻¹) ν(N₂): 2095.



H[SiP^{Ph}₃] (0.0999 g, 0.123 mmol) and RuCl₂(PPh₃)₃ (0.1203 g, 0.125 mmol) were combined in THF with ⁱPr₂NEt (25 μL, 0.151 mmol) and heated at 50 °C. The golden yellow solution gradually became red over the course of 25 hrs. The solution was filtered, the solvent was removed under reduced pressure, and the remaining solid was washed

with benzene. Phosphorous NMR revealed spectroscopically pure $[\text{SiP}^{\text{Ph}}_3]\text{RuCl}$. Crystals suitable XRD were obtained by vapor diffusion of petroleum ether into a saturated solution of $[\text{SiP}^{\text{Ph}}_3]\text{RuCl}$ in benzene. NMR data was lost when the HgBI hard drive failed, therefore, scanned copies of crude proton and phosphorus NMRs have been included.

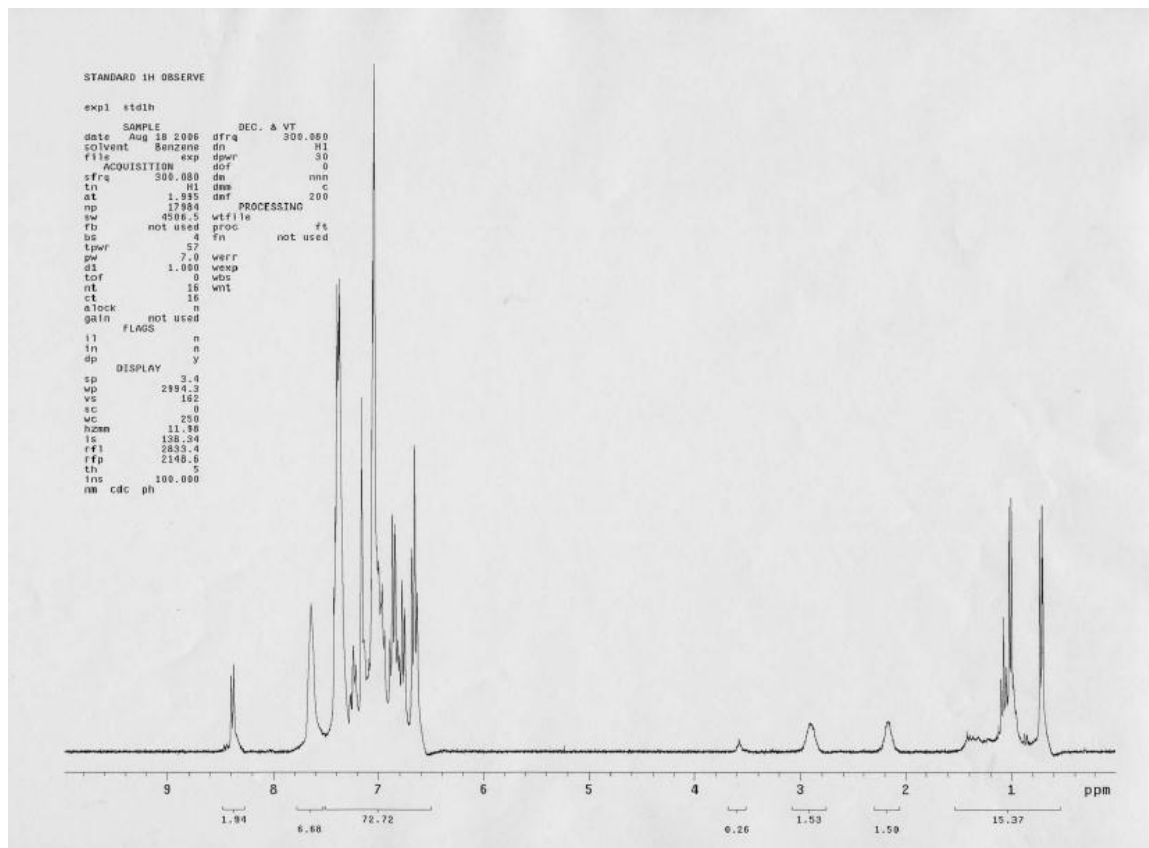


Figure B.9. Crude proton NMR of $[\text{SiP}^{\text{Ph}}_3]\text{RuCl}$

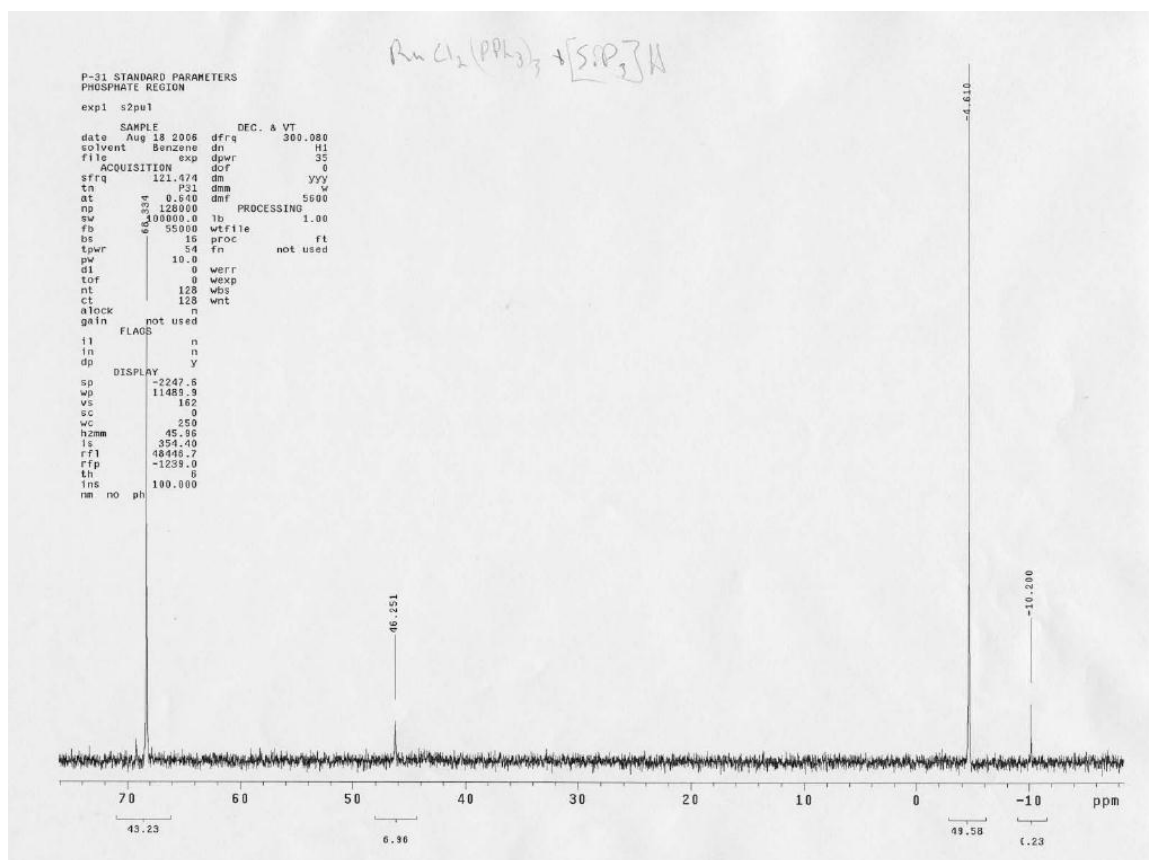
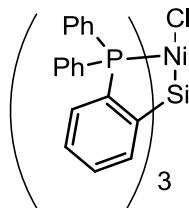


Figure B.10. Crude phosphorus NMR of $[\text{SiP}^{\text{Ph}}_3]\text{RuCl}$

$[\text{SiP}^{\text{Ph}}_3]\text{NiCl}$



$\text{H}[\text{SiP}^{\text{Ph}}_3]$ (0.0766 g, 0.942 mmol) and NiCl_2 (0.0161 g, 0.124 mmol) were combined in THF with $i\text{Pr}_2\text{NEt}$ and heated at 50 °C. The milky yellow solution gradually became red over the course of 5 hrs. The solution was filtered, the solvent was removed under reduced pressure, and the remaining solid was collected. Phosphorous NMR revealed spectroscopically pure $[\text{SiP}^{\text{Ph}}_3]\text{NiCl}$. Crystals suitable XRD were obtained by

vapor diffusion of ether into a saturated solution of $[\text{SiP}^{\text{Ph}}_3]\text{NiCl}$ in CH_2Cl_2 . NMR data was lost when the HgBI hard drive failed, therefore, scanned copies of crude proton and phosphorus NMRs have been included.

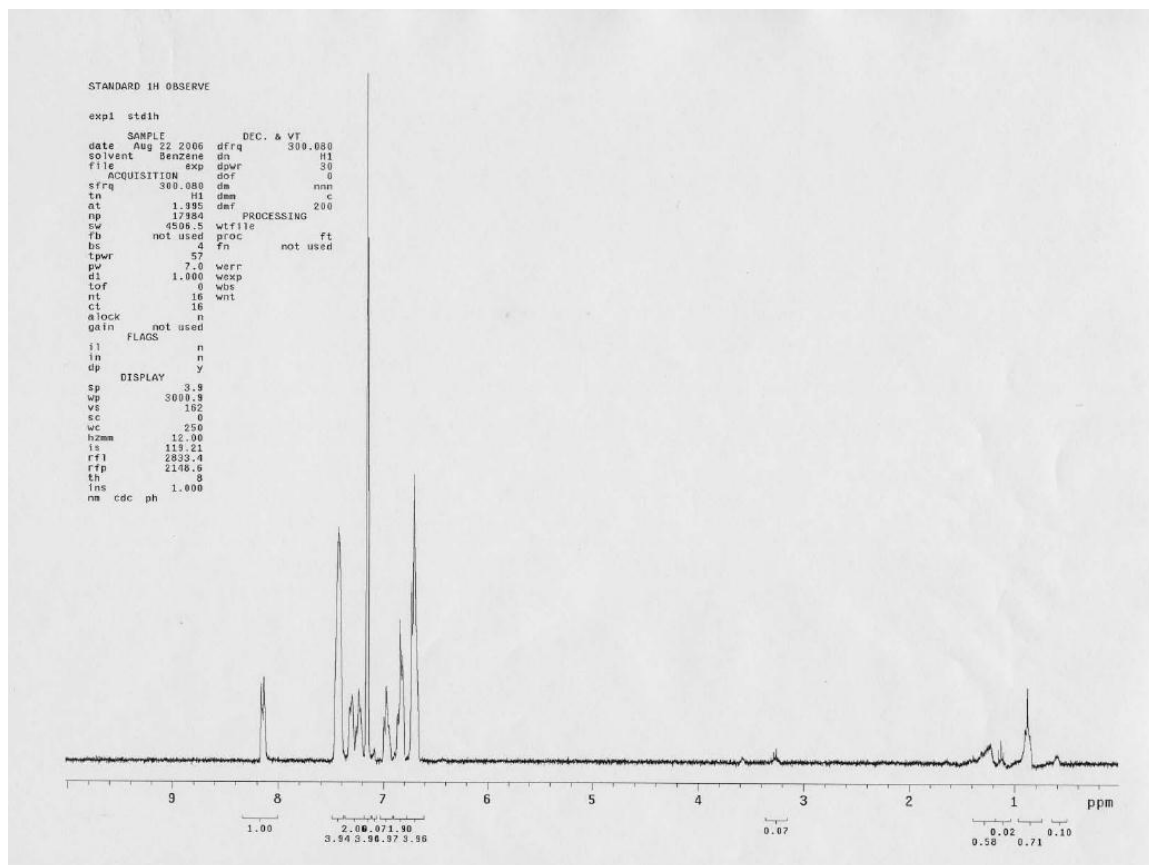


Figure B.11. Crude proton NMR of $[\text{SiP}^{\text{Ph}}_3]\text{NiCl}$

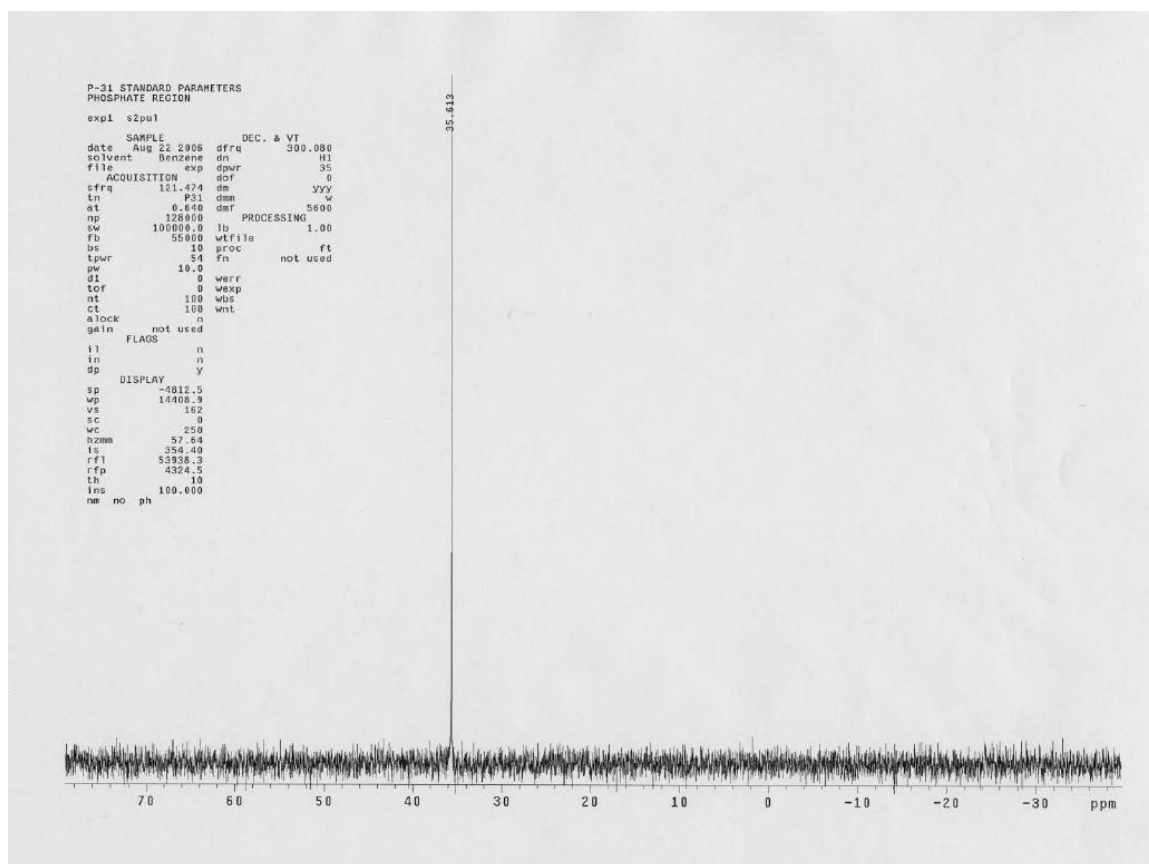
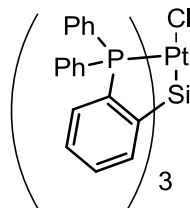
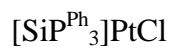


Figure B.12. Phosphorous NMR of $[\text{SiP}^{\text{Ph}}_3]\text{NiCl}$



$\text{H}[\text{SiP}^{\text{Ph}}_3]$ (.0150g, 0.184 μmol), $(\text{COD})\text{PtCl}_2$ (0.0069 g, 0.184 μmol), and $^i\text{Pr}_2\text{NEt}$ were combined in THF and stirred for 48 hours. NMR data was lost when the HgBI hard drive failed, therefore, scanned copies of a crude phosphorus NMR has been included.

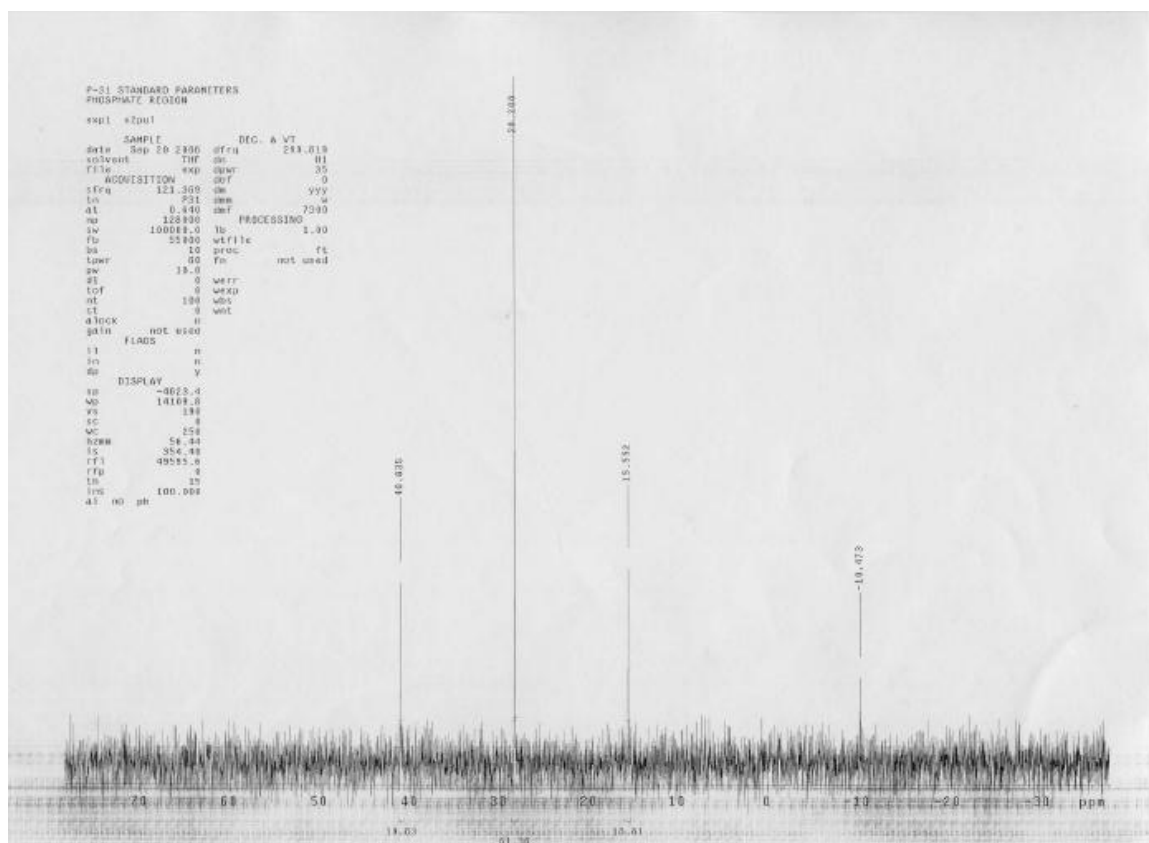
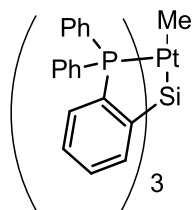
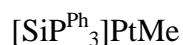


Figure B.13. Crude phosphorus NMR of $[\text{SiP}^{\text{Ph}}_3]\text{PtCl}$



$\text{H}[\text{SiP}^{\text{Ph}}_3]$ and $(\text{COD})\text{PtMe}_2$ were combined in THF and heated at 50 °C. After 1 day $i\text{Pr}_2\text{NEt}$ was added and the solution was heated for an additional 6 days. Crystals suitable for XRD were obtained by vapor diffusion of CH_2Cl_2 into a saturated solution of $[\text{SiP}^{\text{Ph}}_3]\text{RuCl}$ in THF. NMR data was lost when the HgBI hard drive failed, therefore, scanned copies of a crude phosphorus NMR has been included.

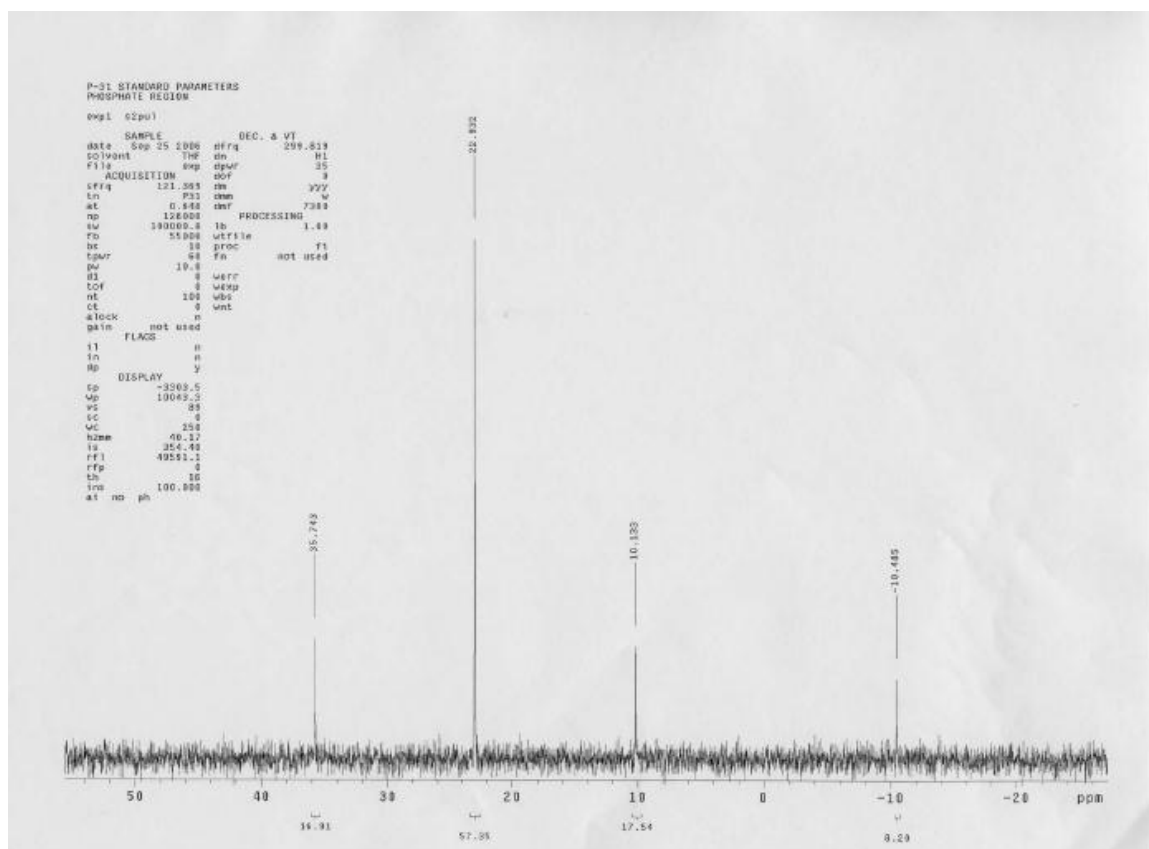


Figure B.14. Crude phosphorus NMR of $[\text{SiP}^{\text{Ph}}_3]\text{PtMe}$

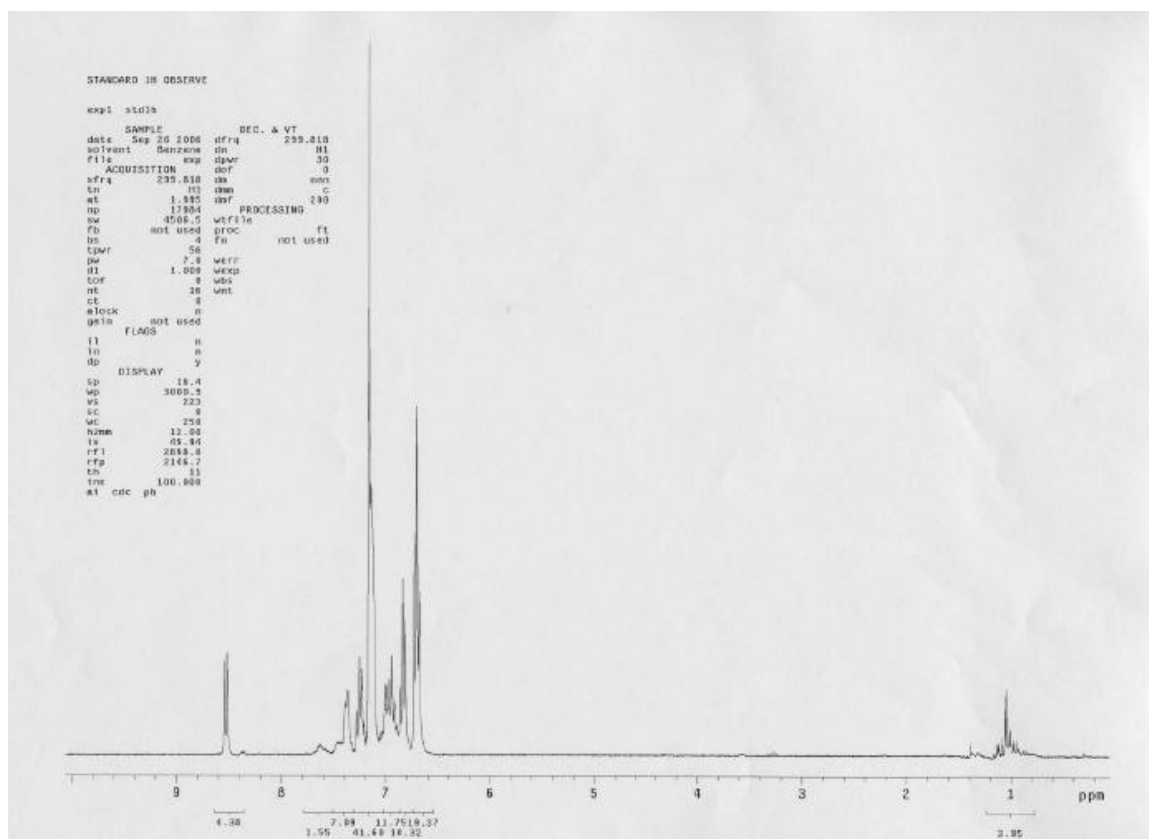


Figure B.15. Crude proton NMR of $[\text{SiP}^{\text{Ph}}_3]\text{PtMe}$

Reaction of $(\text{COD})\text{PtClMe}$ with $\text{H}[\text{SiP}^{\text{Ph}}_3]$

$\text{H}[\text{SiP}^{\text{Ph}}_3]$ (.0131g, 0.184 μmol), $(\text{COD})\text{PtClMe}$ (0.0060 g, 0.184 μmol), and $i\text{Pr}_2\text{NEt}$ (1 drop) were combined in THF and stirred. The solution turned yellow in less than 5 minutes. NMR data was lost when the HgBI hard drive failed, therefore, scanned copies of a crude phosphorus NMR has been included. Interestingly, phosphorus NMR reveals that both the $[\text{SiP}^{\text{Ph}}_3]\text{PtCl}$ and the $[\text{SiP}^{\text{Ph}}_3]\text{PtMe}$ complexes were formed with the dominate species being the $[\text{SiP}^{\text{Ph}}_3]\text{PtCl}$.

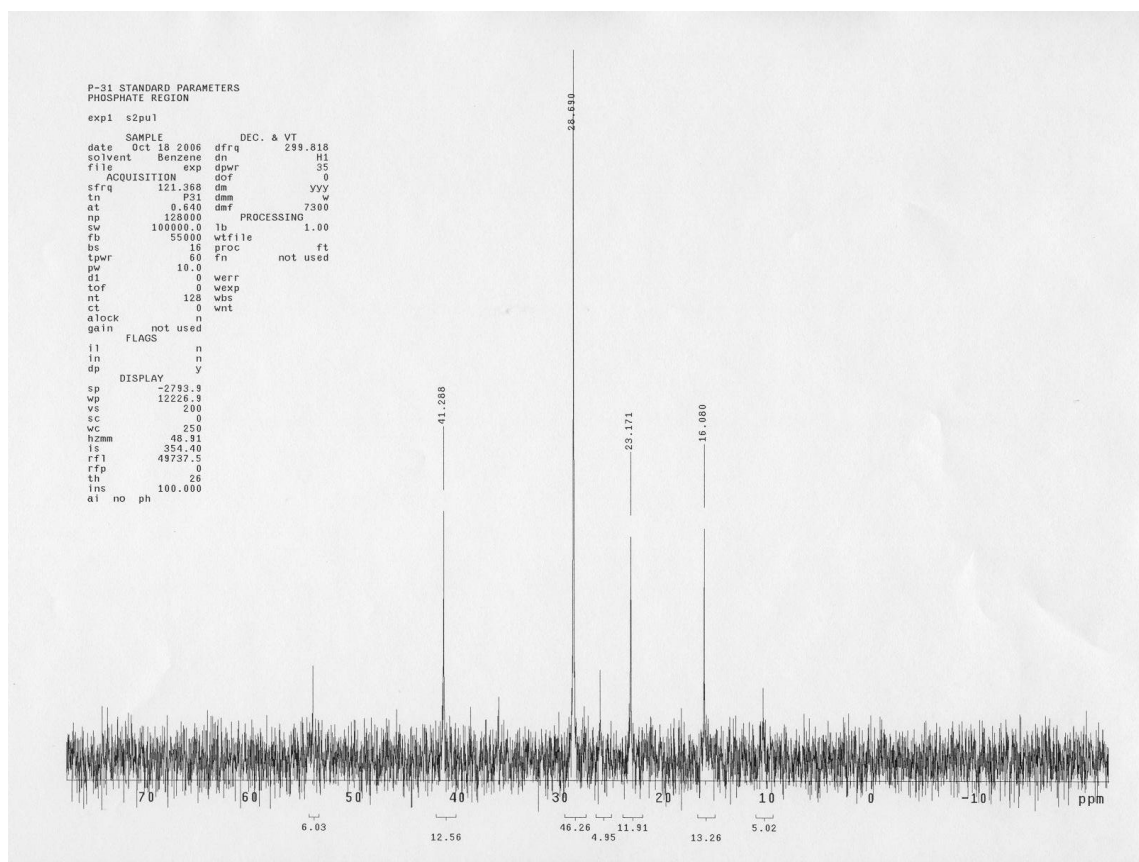


Figure B.16. Crude Phosphorus NMR of the reaction of $\text{H}[\text{SiP}^{\text{Ph}}_3]$ and $(\text{COD})\text{PtClMe}$

References

1. Smith, B. E., *Science* **2002**, 297 (5587), 1654–1655.
2. (a) Howard, J. B.; Rees, D. C., *Chem. Rev.* **1996**, 96, 2965–2982; (b) Peters, J. C.; Mehn, M. P. In *Bio-organometallic approaches to nitrogen fixation chemistry*, Wiley-VCH Verlag GmbH & Co., 2006; pp. 81–119; (c) Chatt, J.; Dilworth, J. R.; Richards, R. L., *Chem. Rev.* **1978**, 78, 589–625.

3. (a) Yandulov, D. V.; Schrock, R. R., *Science* **2003**, *301*, 76–78; (b) Yandulov, D. V.; Schrock, R. R., *J. Am. Chem. Soc.* **2002**, *124*, 6252–6253; (c) Schrock, R. R., *Acc. Chem. Res.* **2005**, *38*, 955–962.
4. (a) Brown, S. D.; Betley, T. A.; Peters, J. C., *J. Am. Chem. Soc.* **2003**, *125*, 322–323; (b) Brown, S. D.; Mehn, M. P.; Peters, J. C., *J. Am. Chem. Soc.* **2005**, *127*, 13146–13147; (c) Brown, S. D.; Peters, J. C., *J. Am. Chem. Soc.* **2005**, *127*, 1913–1923; (d) Betley, T. A.; Peters, J. C., *J. Am. Chem. Soc.* **2004**, *126*, 6252–6254; (e) Betley, T. A.; Peters, J. C., *J. Am. Chem. Soc.* **2003**, *125*, 10782–10783; (f) Smith, J. M.; Lachicotte, R. J.; Pittard, K. A.; Cundari, T. R.; Lukat-Rodgers, G.; Rodgers, K. R.; Holland, P. L., *J. Am. Chem. Soc.* **2001**, *123*, 9222–9223; (g) Smith, J. M.; Sadique, A. R.; Cundari, T. R.; Rodgers, K. R.; Lukat-Rodgers, G.; Lachicotte, R. J.; Flaschenriem, C. J.; Vela, J.; Holland, P. L., *J. Am. Chem. Soc.* **2006**, *128*, 756–769; (h) Holland, P. L., *Can. J. Chem.* **2005**, *83*, 296–301; (i) Hendrich, M. P.; Gunderson, W.; Behan, R. K.; Green, M. T.; Mehn, M. P.; Betley, T. A.; Lu, C. C.; Peters, J. C., *Proc. Natl. Acad. Sci. U. S. A.* **2006**, *103*, 17107–17112.
5. Mankad, N. P.; Whited, M. T.; Peters, J. C., *Angew. Chem., Int. Ed.* **2007**, *46*, 5768–5771.
6. Whited, M. T.; Mankad, N. P.; Lee, Y.; Oblad, P. F.; Peters, J. C., *Inorganic Chemistry* **2009**, *48* (6), 2507–2517.
7. (a) Takaoka, A.; Mendiratta, A.; Peters, J. C., *Organometallics* **2009**, *28* (13), 3744–3753; (b) Tsay, C.; Mankad, N. P.; Peters, J. C., *J. Am. Chem. Soc.* **2010**, *132* (40), 13975–13977.

Appendix C
Crystallographic Data

[SiP₃]CoCl

Table 1. Crystal data and structure refinement for [SiP₃]CoCl (PFO01).

Empirical formula	C ₅₂ H ₄₂ ClCoP ₃ Si	
Formula weight	906.26	
Data Collection		
Type of diffractometer	Bruker SMART 1000	
Wavelength	0.71073 Å MoKα	
Data Collection Temperature	100(2) K	
Unit cell dimensions	a = 12.6315(5) Å	α = 90°
	b = 17.4181(6) Å	β = 98.8470(10)°
	c = 19.6713(8) Å	γ = 90°
Volume	4276.5(3) Å ³	
Z	4	
Crystal system	Monoclinic	
Space group	P2 ₁ /c	
Density (calculated)	1.759 Mg/m ³	
F(000)	2345	
Data collection program	Bruker SMART v5.630	
θ range for data collection	1.63 to 39.23°	
Completeness to θ = 39.23°	85.6 %	
Index ranges	-16 ≤ h ≤ 22, -30 ≤ k ≤ 29, -31 ≤ l ≤ 31	
Data reduction program	Bruker SAINT v6.45A	
Reflections collected	72628	
Independent reflections	21620 [R _{int} = 0.0802]	
Absorption coefficient	0.804 mm ⁻¹	
Absorption correction	None	

Table 1 (cont.)

Structure solution and Refinement	
Structure solution program	Bruker XS v6.12
Primary solution method	Direct methods
Secondary solution method	Difference Fourier map
Hydrogen placement	Geometric positions
Structure refinement program	Bruker XL v6.12
Refinement method	Full matrix least-squares on F^2
Data / restraints / parameters	21620 / 0 / 541
Treatment of hydrogen atoms	Riding
Goodness-of-fit on F^2	1.345
Final R indices [$I > 2\sigma(I)$]	$R1 = 0.0489$, $wR2 = 0.0790$
R indices (all data)	$R1 = 0.0917$, $wR2 = 0.0847$
Type of weighting Scheme used	Sigma
Weighting Scheme used	$w=1/\sigma^2(Fo^2)$
Largest diff. peak and hole	1.667 and -0.742 e. \AA^{-3}

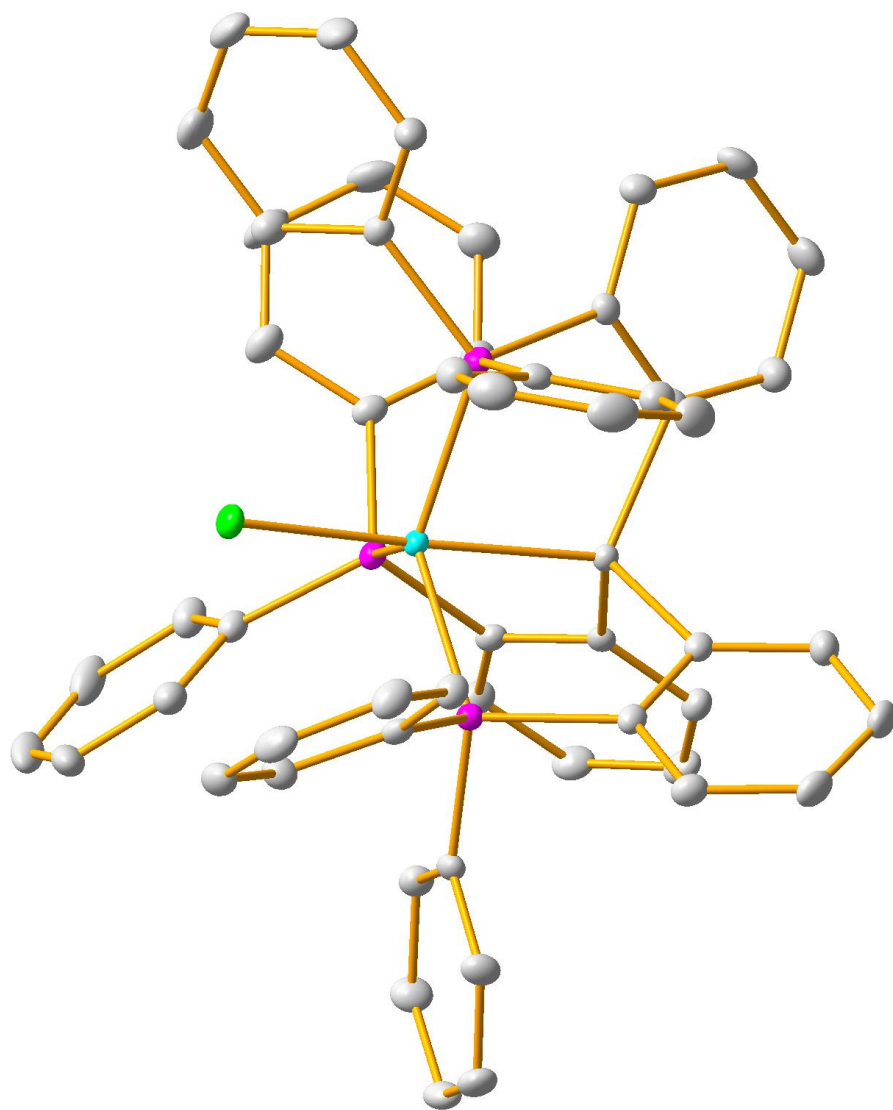


Table 2. Atomic coordinates ($\times 10^4$) and equivalent isotropic displacement parameters ($\text{\AA}^2 \times 10^3$) for [SiP₃]CoCl (PFO01). U_{eq} is defined as the trace of the orthogonalized U^{ij} tensor.

	x	y	z	U_{eq}
Co	2583(1)	6446(1)	7225(1)	9(1)
Cl	2449(1)	7553(1)	7824(1)	15(1)
P(1)	3788(1)	5824(1)	7997(1)	10(1)
P(2)	2908(1)	7031(1)	6278(1)	11(1)
P(3)	908(1)	5998(1)	7105(1)	11(1)
Si	2846(1)	5398(1)	6608(1)	10(1)
C(1)	4216(1)	4991(1)	6902(1)	12(1)
C(2)	4791(1)	4490(1)	6538(1)	17(1)
C(3)	5804(1)	4229(1)	6821(1)	18(1)
C(4)	6271(1)	4484(1)	7469(1)	18(1)
C(5)	5708(1)	4976(1)	7844(1)	16(1)
C(6)	4684(1)	5228(1)	7559(1)	12(1)
C(7)	2677(1)	5639(1)	5662(1)	12(1)
C(8)	2502(1)	5118(1)	5112(1)	17(1)
C(9)	2267(1)	5377(1)	4439(1)	19(1)
C(10)	2212(1)	6163(1)	4299(1)	19(1)
C(11)	2412(1)	6690(1)	4832(1)	16(1)
C(12)	2646(1)	6430(1)	5511(1)	12(1)
C(13)	1810(1)	4662(1)	6763(1)	11(1)
C(14)	1910(1)	3863(1)	6694(1)	15(1)
C(15)	1122(1)	3366(1)	6856(1)	18(1)
C(16)	211(1)	3658(1)	7076(1)	18(1)
C(17)	87(1)	4449(1)	7146(1)	15(1)
C(18)	893(1)	4947(1)	6998(1)	11(1)
C(19)	3463(1)	5136(1)	8642(1)	12(1)
C(20)	4270(1)	4818(1)	9125(1)	17(1)
C(21)	4043(1)	4248(1)	9571(1)	19(1)
C(22)	3302(1)	3991(1)	9552(1)	17(1)
C(23)	2189(1)	4306(1)	9080(1)	18(1)
C(24)	2418(1)	4872(1)	8626(1)	14(1)
C(25)	4665(1)	6509(1)	8514(1)	12(1)
C(26)	5626(1)	6744(1)	8326(1)	16(1)
C(27)	6255(1)	7294(1)	8716(1)	19(1)
C(28)	5913(1)	7621(1)	9286(1)	19(1)
C(29)	4929(1)	7415(1)	9458(1)	18(1)
C(30)	4303(1)	6859(1)	9072(1)	16(1)
C(31)	4365(1)	7184(1)	6412(1)	13(1)
C(32)	5082(1)	6670(1)	6181(1)	17(1)

C(33)	6178(1)	6793(1)	6334(1)	23(1)
C(34)	6576(1)	7433(1)	6712(1)	23(1)
C(35)	5870(1)	7945(1)	6945(1)	22(1)
C(36)	4779(1)	7818(1)	6805(1)	18(1)
C(37)	2414(1)	7990(1)	6009(1)	13(1)
C(38)	2943(1)	8441(1)	5580(1)	17(1)
C(39)	2539(1)	9157(1)	5359(1)	21(1)
C(40)	1618(1)	9430(1)	5575(1)	23(1)
C(41)	1101(1)	8996(1)	6017(1)	23(1)
C(42)	1493(1)	8274(1)	6230(1)	17(1)
C(43)	30(1)	6326(1)	6329(1)	13(1)
C(44)	68(1)	5960(1)	5698(1)	16(1)
C(45)	-473(1)	6267(1)	5089(1)	20(1)
C(46)	-1081(1)	6929(1)	5103(1)	22(1)
C(47)	-1145(1)	7280(1)	5724(1)	24(1)
C(48)	-583(1)	6992(1)	6331(1)	18(1)
C(49)	98(1)	6170(1)	7788(1)	14(1)
C(50)	-1006(1)	6035(1)	7697(1)	18(1)
C(51)	-1575(1)	6115(1)	8242(1)	25(1)
C(52)	-1051(1)	6342(1)	8885(1)	26(1)
C(53)	35(1)	6490(1)	8981(1)	22(1)
C(54)	611(1)	6405(1)	8438(1)	17(1)

[SiP₃]RuCl

Table 1. Crystal data and structure refinement for [SiP₃]RuCl (pfo03) (CCDC)¹.

Empirical formula	C ₅₂ H ₄₂ ClRuP ₃ Si	
Formula weight	1026.50	
Crystallization Solvent	Benzene/ <i>n</i> -pentane	
Crystal Habit	blade	
Crystal size	0.31 x 0.07 x 0.05 mm ³	
Crystal color	orange-brown	
Data Collection		
Type of diffractometer	CCD area detector	
Wavelength	0.71073 Å MoKα	
Data Collection Temperature	100(2) K	
θ range for 6415 reflections used in lattice determination	2.27 to 27.79°	
Unit cell dimensions	a = 9.999(2) Å b = 14.193(3) Å c = 17.379(4) Å	α = 95.13(3)° β = 92.57(3)° γ = 103.18(3)°
Volume	2386.5(8) Å ³	
Z	2	
Crystal system	Triclinic	
Space group	P-1	
Density (calculated)	1.429 Mg/m ³	
F(000)	1056	
Data collection program	Bruker SMART	
θ range for data collection	1.48 to 26.37°	
Completeness to θ = 26.37°	99.7 %	
Index ranges	-12 ≤ h ≤ 12, -17 ≤ k ≤ 17, -21 ≤ l ≤ 21	
Data collection scan type	phi and omega scans	
Data reduction program	Bruker SAINT	
Reflections collected	27993	
Independent reflections	9743 [R _{int} = 0.0921]	
Absorption coefficient	0.551 mm ⁻¹	
Absorption correction	Semi-empirical from equivalents	
Max. and min. transmission	0.9740 and 0.8490	

Table 1 (cont.)

Structure solution and Refinement	
Structure solution program	Bruker SHELXTL
Primary solution method	direct
Secondary solution method	difmap
Hydrogen placement	geom
Structure refinement program	Bruker SHELXTL
Refinement method	Full-matrix least-squares on F ²
Data / restraints / parameters	9743 / 0 / 595
Treatment of hydrogen atoms	constr
Goodness-of-fit on F ²	0.935
Final R indices [I>2σ(I), 6582 reflections]	R1 = 0.0442, wR2 = 0.0960
R indices (all data)	R1 = 0.0773, wR2 = 0.1085
Type of weighting Scheme used	calc
Weighting Scheme used	calc
	$w=1/[\sigma^2(F_o^2)+(0.0464P)^2+0.0000P]$ where $P=(F_o^2+2F_c^2)/3$
Max shift/error	0.001
Average shift/error	0.000
Largest diff. peak and hole	0.994 and -0.544 e.Å ⁻³

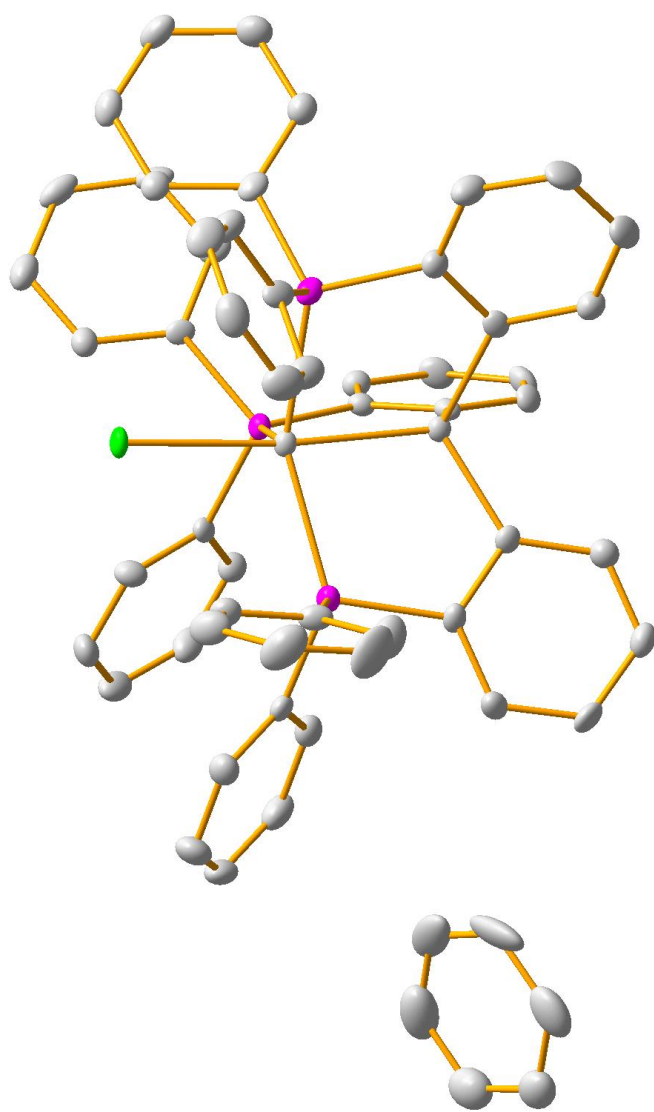


Table 2. Atomic coordinates ($\times 10^4$) and equivalent isotropic displacement parameters ($\text{\AA}^2 \times 10^3$) for $[\text{SiP}_3]\text{RuCl}$ (pfo03). $U(\text{eq})$ is defined as the trace of the orthogonalized U^{ij} tensor.

	x	y	z	U_{eq}
Ru	7070(1)	7223(1)	7358(1)	12(1)
Cl	9626(1)	7461(1)	7283(1)	14(1)
Si	4722(1)	7135(1)	7361(1)	12(1)
P(2)	7060(1)	7937(1)	8536(1)	12(1)
P(3)	6984(1)	8465(1)	6588(1)	16(1)
P(1)	6338(1)	5570(1)	7493(1)	15(1)
C(48)	9200(4)	10007(3)	7032(2)	18(1)
C(26)	5912(4)	4449(3)	6013(2)	31(1)
C(38)	7709(4)	9985(3)	8741(2)	18(1)
C(53)	7985(4)	6779(3)	4791(2)	30(1)
C(18)	5215(4)	8396(3)	6204(2)	18(1)
C(7)	4281(4)	7730(2)	8308(2)	14(1)
C(14)	2796(4)	7739(3)	6272(2)	19(1)
C(12)	5411(4)	8137(2)	8835(2)	14(1)
C(32)	6957(4)	7104(3)	9970(2)	18(1)
C(31)	7634(3)	7256(2)	9292(2)	14(1)
C(2)	2223(4)	5513(3)	7245(2)	20(1)
C(5)	3800(4)	4183(3)	7484(2)	22(1)
C(40)	9962(4)	10986(3)	9112(2)	24(1)
C(30)	8249(4)	5165(3)	6479(2)	19(1)
C(49)	7763(4)	8109(3)	5705(2)	18(1)
C(55)	3891(5)	10425(4)	8076(3)	43(1)
C(6)	4441(4)	5145(3)	7430(2)	15(1)
C(8)	2977(4)	7812(3)	8526(2)	16(1)
C(54)	7423(4)	7125(3)	5439(2)	28(1)
C(3)	1604(4)	4558(3)	7296(2)	21(1)
C(4)	2384(4)	3882(3)	7419(2)	22(1)
C(35)	9258(4)	6352(3)	9729(2)	23(1)
C(1)	3678(4)	5841(2)	7308(2)	16(1)
C(50)	8675(4)	8737(3)	5301(2)	23(1)
C(34)	8587(4)	6218(3)	10411(2)	26(1)
C(9)	2816(4)	8299(3)	9229(2)	19(1)
C(19)	6789(4)	4800(2)	8219(2)	17(1)
C(11)	5249(4)	8657(2)	9536(2)	16(1)
C(28)	7771(5)	4188(3)	5258(3)	40(1)
C(45)	7748(4)	11453(3)	6957(2)	24(1)
C(43)	7786(4)	9753(3)	6806(2)	18(1)
C(37)	8217(4)	9148(2)	8740(2)	13(1)

C(36)	8778(4)	6858(2)	9175(2)	18(1)
C(10)	3963(4)	8729(3)	9730(2)	21(1)
C(25)	6841(4)	5012(2)	6592(2)	17(1)
C(20)	6137(4)	4812(3)	8917(2)	21(1)
C(42)	9623(4)	9253(3)	8896(2)	18(1)
C(47)	9865(4)	10980(3)	7215(2)	21(1)
C(24)	7694(4)	4196(3)	8109(2)	22(1)
C(46)	9138(4)	11691(3)	7173(2)	23(1)
C(29)	8707(5)	4747(3)	5822(2)	29(1)
C(56)	3102(5)	10031(3)	7412(3)	36(1)
C(52)	8899(4)	7410(3)	4409(2)	29(1)
C(51)	9240(4)	8385(3)	4653(2)	28(1)
C(13)	4148(4)	7812(2)	6557(2)	15(1)
C(27)	6394(5)	4042(3)	5360(3)	43(1)
C(44)	7065(4)	10486(3)	6780(2)	21(1)
C(33)	7433(4)	6587(3)	10527(2)	25(1)
C(15)	2521(4)	8197(3)	5638(2)	27(1)
C(39)	8574(4)	10892(3)	8930(2)	20(1)
C(17)	4941(4)	8844(3)	5546(2)	25(1)
C(41)	10491(4)	10164(3)	9075(2)	25(1)
C(59)	4707(5)	11874(4)	7541(5)	64(2)
C(58)	3938(6)	11507(4)	6849(4)	64(2)
C(21)	6399(4)	4243(3)	9480(2)	26(1)
C(23)	7947(4)	3629(3)	8680(2)	29(1)
C(57)	3121(5)	10565(4)	6792(3)	46(1)
C(16)	3589(4)	8732(3)	5260(2)	28(1)
C(22)	7297(4)	3643(3)	9360(3)	30(1)
C(60)	4669(5)	11333(4)	8124(4)	57(2)

[SiP₃]NiCl

Table 1. Crystal data and structure refinement for [SiP₃]NiCl (pfo04) (CCDC 837961).

Empirical formula	C ₅₄ H ₄₂ P ₃ SiClNi
Formula weight	906.04
Crystallization Solvent	Not given
Crystal Habit	Prism
Crystal size	0.44 x 0.24 x 0.16 mm ³
Crystal color	Red

Data Collection

Type of diffractometer	Bruker SMART 1000	
Wavelength	0.71073 Å MoK α	
Data Collection Temperature	100(2) K	
θ range for 7326 reflections used in lattice determination	2.14 to 28.18°	
Unit cell dimensions	a = 12.836(3) Å b = 17.339(3) Å c = 19.481(4) Å	$\alpha = 90^\circ$ $\beta = 98.77(3)^\circ$ $\gamma = 90^\circ$
Volume	4285.2(15) Å ³	
Z	4	
Crystal system	Monoclinic	
Space group	P 2 ₁ /c	
Density (calculated)	1.404 Mg/m ³	
F(000)	1880	
Data collection program	Bruker SMART v5.630	
θ range for data collection	1.58 to 28.33°	
Completeness to $\theta = 28.33^\circ$	93.4 %	
Index ranges	-16 \leq h \leq 17, -22 \leq k \leq 21, -25 \leq l \leq 25	
Data collection scan type	ω scans at 5 settings	
Data reduction program	Bruker SAINT v6.45A	
Reflections collected	51859	
Independent reflections	9966 [R _{int} = 0.0901]	
Absorption coefficient	0.694 mm ⁻¹	
Absorption correction	None	
Max. and min. transmission	0.8971 and 0.7499	

Table 1 (cont.)

Structure solution and Refinement	
Structure solution program	SHELXS-97 (Sheldrick, 2008)
Primary solution method	Direct methods
Secondary solution method	Difference Fourier map
Hydrogen placement	Geometric positions
Structure refinement program	SHELXL-97 (Sheldrick, 2008)
Refinement method	Full matrix least-squares on F^2
Data / restraints / parameters	9966 / 0 / 541
Treatment of hydrogen atoms	Riding
Goodness-of-fit on F^2	1.475
Final R indices [$I > 2\sigma(I)$, 7227 reflections]	$R1 = 0.0421$, $wR2 = 0.0770$
R indices (all data)	$R1 = 0.0629$, $wR2 = 0.0796$
Type of weighting Scheme used	Sigma
Weighting Scheme used	$w=1/\sigma^2(Fo^2)$
Max shift/error	0.001
Average shift/error	0.000
Largest diff. peak and hole	0.842 and -0.467 e. \AA^{-3}

Special Refinement Details

Crystals were mounted on a glass fiber using Paratone oil then placed on the diffractometer under a nitrogen stream at 100K.

Refinement of F^2 against ALL reflections. The weighted R-factor (wR) and goodness of fit (S) are based on F^2 , conventional R-factors (R) are based on F , with F set to zero for negative F^2 . The threshold expression of $F^2 > 2\sigma(F^2)$ is used only for calculating R-factors(gt) etc. and is not relevant to the choice of reflections for refinement. R-factors based on F^2 are statistically about twice as large as those based on F , and R-factors based on ALL data will be even larger.

All esds (except the esd in the dihedral angle between two l.s. planes) are estimated using the full covariance matrix. The cell esds are taken into account individually in the estimation of esds in distances, angles and torsion angles; correlations between esds in cell parameters are only used when they are defined by crystal symmetry. An approximate (isotropic) treatment of cell esds is used for estimating esds involving l.s. planes.

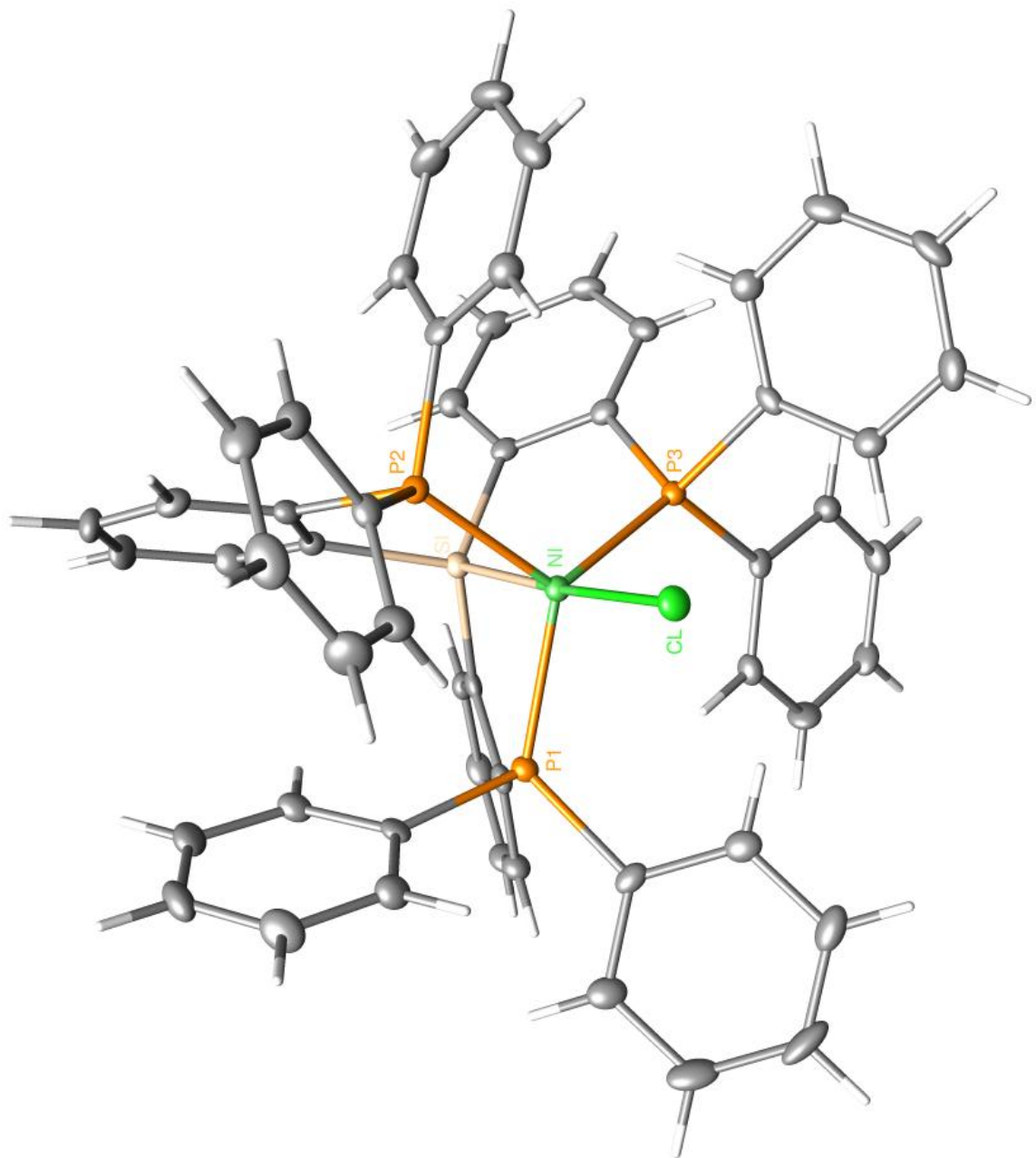


Table 2. Atomic coordinates ($\times 10^4$) and equivalent isotropic displacement parameters ($\text{\AA}^2 \times 10^3$) for $[\text{SiP}_3]\text{NiCl}$ (pfo04) (CCDC 837961). $U(\text{eq})$ is defined as the trace of the orthogonalized U_{ij} tensor.

	x	y	z	U_{eq}
Ni	2556(1)	1389(1)	2229(1)	10(1)
Cl	2404(1)	2488(1)	2856(1)	15(1)
P(1)	883(1)	978(1)	2092(1)	11(1)
P(2)	3062(1)	1982(1)	1323(1)	11(1)
P(3)	3820(1)	846(1)	2979(1)	11(1)
Si	2807(1)	340(1)	1619(1)	11(1)
C(1)	1772(2)	-383(1)	1772(1)	12(1)
C(2)	855(2)	-81(1)	1983(1)	12(1)
C(3)	50(2)	-574(1)	2124(1)	15(1)
C(4)	164(2)	-1366(1)	2067(1)	17(1)
C(5)	1072(2)	-1672(1)	1870(1)	17(1)
C(6)	1863(2)	-1184(1)	1716(1)	15(1)
C(7)	2671(2)	606(1)	667(1)	12(1)
C(8)	2750(2)	1398(1)	536(1)	13(1)
C(9)	2560(2)	1673(2)	-146(1)	17(1)
C(10)	2301(2)	1161(2)	-696(1)	19(1)
C(11)	2253(2)	376(2)	-571(1)	19(1)
C(12)	2444(2)	97(1)	107(1)	17(1)
C(13)	4162(2)	-63(1)	1905(1)	12(1)
C(14)	4671(2)	211(1)	2550(1)	12(1)
C(15)	5687(2)	-42(1)	2815(1)	15(1)
C(16)	6192(2)	-570(1)	2446(1)	17(1)
C(17)	5690(2)	-854(1)	1810(1)	18(1)
C(18)	4692(2)	-597(1)	1546(1)	17(1)
C(19)	61(2)	1148(1)	2772(1)	14(1)
C(20)	545(2)	1364(1)	3436(1)	16(1)
C(21)	-44(2)	1430(1)	3980(1)	22(1)
C(22)	-1109(2)	1284(2)	3861(1)	26(1)
C(23)	-1602(2)	1086(2)	3202(1)	24(1)
C(24)	-1024(2)	1023(1)	2659(1)	18(1)
C(25)	50(2)	1323(1)	1305(1)	12(1)
C(26)	96(2)	965(1)	667(1)	15(1)
C(27)	-406(2)	1282(2)	49(1)	20(1)
C(28)	-982(2)	1957(2)	64(1)	22(1)
C(29)	-1056(2)	2310(2)	691(1)	22(1)
C(30)	-531(2)	1999(1)	1308(1)	17(1)
C(31)	2554(2)	2945(1)	1060(1)	13(1)
C(32)	3066(2)	3421(1)	643(1)	17(1)

C(33)	2635(2)	4123(1)	410(1)	19(1)
C(34)	1686(2)	4359(2)	598(1)	22(1)
C(35)	1182(2)	3899(2)	1023(1)	23(1)
C(36)	1610(2)	3189(2)	1249(1)	19(1)
C(37)	4494(2)	2129(1)	1416(1)	13(1)
C(38)	4932(2)	2772(2)	1787(1)	18(1)
C(39)	6007(2)	2883(2)	1902(1)	22(1)
C(40)	6671(2)	2351(2)	1666(1)	24(1)
C(41)	6246(2)	1706(2)	1310(1)	24(1)
C(42)	5167(2)	1594(1)	1177(1)	17(1)
C(43)	4697(2)	1522(1)	3496(1)	12(1)
C(44)	4372(2)	1872(1)	4075(1)	15(1)
C(45)	5014(2)	2404(1)	4471(1)	18(1)
C(46)	5989(2)	2589(1)	4298(1)	18(1)
C(47)	6302(2)	2261(1)	3711(1)	19(1)
C(48)	5654(2)	1739(1)	3309(1)	15(1)
C(49)	3481(2)	163(1)	3636(1)	11(1)
C(50)	4264(2)	-168(1)	4123(1)	16(1)
C(51)	4018(2)	-741(1)	4567(1)	17(1)
C(52)	2985(2)	-980(1)	4545(1)	17(1)
C(53)	2193(2)	-650(1)	4073(1)	19(1)
C(54)	2448(2)	-82(1)	3621(1)	15(1)

[(diimine)Pt(oxime)][BF₄] (Ar = 3,5-^tBu₂C₆H₃)

Table 1. Crystal data and structure refinement for [(diimine)Pt(oxime)][BF₄] (PFO10) (CCDC 655348)².

Empirical formula	2[C ₄₁ H ₅₈ N ₃ OPt] ⁺ 2[BF ₄] ⁻ • 3(CH ₂ Cl ₂)
Formula weight	2036.39
Crystallization Solvent	Dichloromethane
Crystal Habit	Blade
Crystal size	0.29 x 0.22 x 0.05 mm ³
Crystal color	Orange

Data Collection

Type of diffractometer	Bruker SMART 1000	
Wavelength	0.71073 Å MoKα	
Data Collection Temperature	100(2) K	
θ range for 26963 reflections used in lattice determination	2.30 to 25.00°	
Unit cell dimensions	a = 13.5252(11) Å b = 18.0782(15) Å c = 21.8803(19) Å	α = 69.468(2)° β = 89.940(2)° γ = 71.002(2)°
Volume	4698.4(7) Å ³	
Z	2	
Crystal system	Triclinic	
Space group	P-1	
Density (calculated)	1.439 Mg/m ³	
F(000)	2060	
Data collection program	Bruker SMART v5.630	
θ range for data collection	1.30 to 25.22°	
Completeness to θ = 25.22°	98.9 %	
Index ranges	-16 ≤ h ≤ 16, -21 ≤ k ≤ 21, -26 ≤ l ≤ 26	
Data collection scan type	ω scans at 7 φ settings	
Data reduction program	Bruker SAINT v6.45A	
Reflections collected	73170	
Independent reflections	16800 [R _{int} = 0.1066]	
Absorption coefficient	3.207 mm ⁻¹	
Absorption correction	None	
Max. and min. transmission	0.8561 and 0.4565	

Table 1 (cont.)

Structure solution and Refinement	
Structure solution program	Bruker XS v6.12
Primary solution method	Direct methods
Secondary solution method	Difference Fourier map
Hydrogen placement	Geometric positions
Structure refinement program	Bruker XL v6.12
Refinement method	Full matrix least-squares on F^2
Data / restraints / parameters	16800 / 0 / 1000
Treatment of hydrogen atoms	Riding
Goodness-of-fit on F^2	2.230
Final R indices [$I > 2\sigma(I)$, 11020 reflections]	R1 = 0.0601, wR2 = 0.1224
R indices (all data)	R1 = 0.1218, wR2 = 0.1360
Type of weighting Scheme used	Sigma
Weighting Scheme used	$w=1/\sigma^2(Fo^2)$
Max shift/error	0.001
Average shift/error	0.000
Largest diff. peak and hole	6.960 and -2.486 e.Å ⁻³

Special Refinement Details

All large peaks in the difference map lie neat Pt and presumably arise from absorption.

Refinement of F^2 against ALL reflections. The weighted R-factor (wR) and goodness of fit (S) are based on F^2 , conventional R-factors (R) are based on F , with F set to zero for negative F^2 . The threshold expression of $F^2 > 2\sigma(F^2)$ is used only for calculating R-factors(gt) etc. and is not relevant to the choice of reflections for refinement. R-factors based on F^2 are statistically about twice as large as those based on F , and R-factors based on ALL data will be even larger.

All esds (except the esd in the dihedral angle between two l.s. planes) are estimated using the full covariance matrix. The cell esds are taken into account individually in the estimation of esds in distances, angles and torsion angles; correlations between esds in cell parameters are only used when they are defined by crystal symmetry. An approximate (isotropic) treatment of cell esds is used for estimating esds involving l.s. planes.

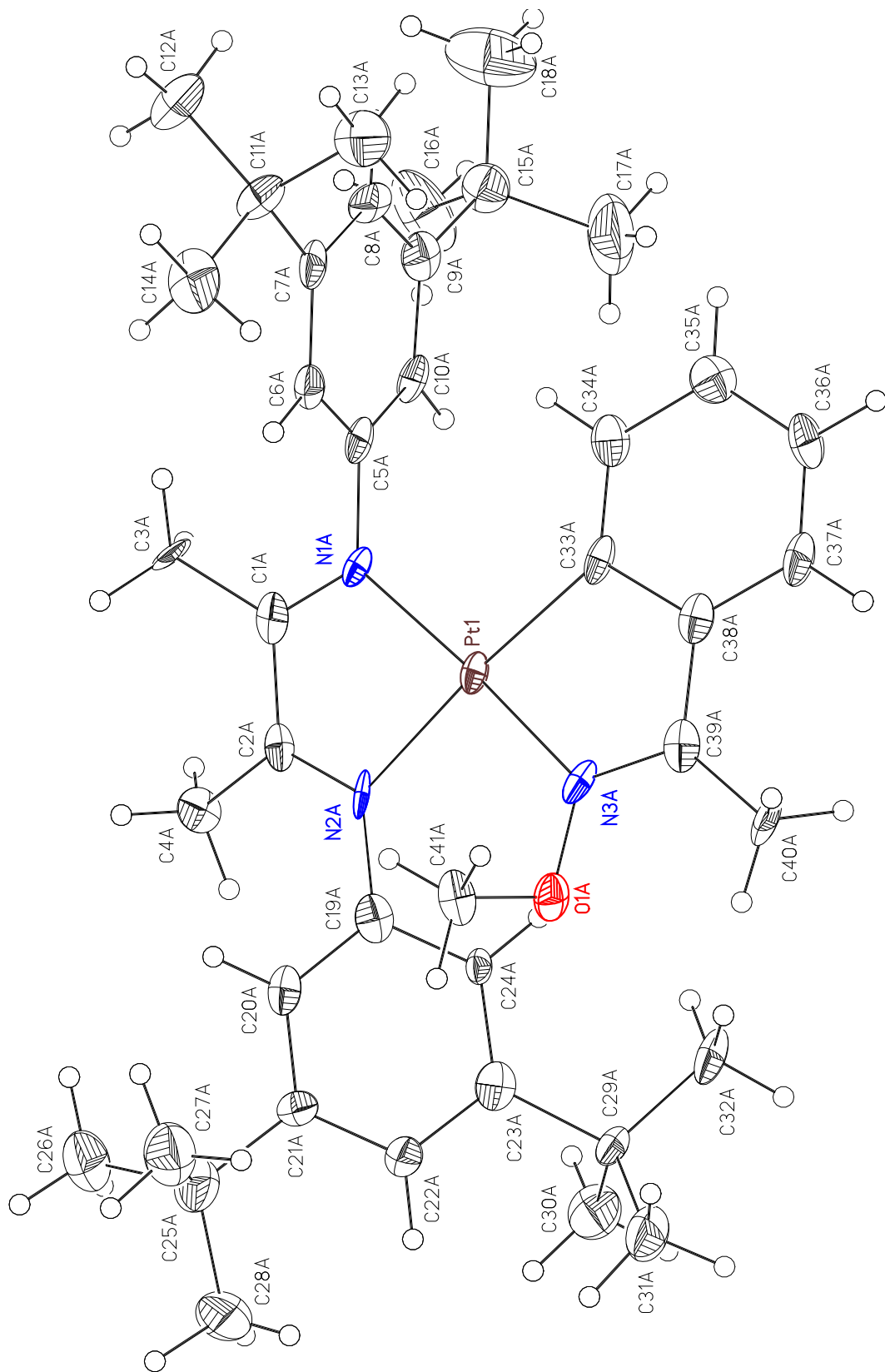


Table 2. Atomic coordinates ($\times 10^4$) and equivalent isotropic displacement parameters ($\text{\AA}^2 \times 10^3$) for [(diimine)Pt(oxime)][BF₄] (PFO10) (CCDC 655348). U(eq) is defined as the trace of the orthogonalized U^{ij} tensor.

	x	y	z	U _{eq}
Pt(1)	1213(1)	410(1)	3899(1)	16(1)
O(1A)	2190(5)	-1082(4)	5150(3)	23(2)
N(1A)	447(6)	993(5)	2962(4)	17(2)
N(2A)	1595(6)	-587(5)	3548(4)	18(2)
N(3A)	1892(6)	-219(5)	4840(4)	19(2)
C(1A)	497(7)	520(7)	2628(5)	20(2)
C(2A)	1219(7)	-366(6)	2936(5)	21(2)
C(3A)	-131(8)	818(6)	1977(5)	26(3)
C(4A)	1482(8)	-898(6)	2533(5)	24(2)
C(5A)	-198(7)	1877(7)	2676(5)	20(2)
C(6A)	-1223(7)	2116(6)	2811(5)	21(2)
C(7A)	-1849(8)	2971(7)	2549(5)	24(2)
C(8A)	-1398(8)	3545(7)	2177(5)	24(2)
C(9A)	-353(8)	3309(7)	2034(5)	25(2)
C(10A)	245(8)	2443(7)	2288(5)	20(2)
C(11A)	-2997(8)	3300(7)	2676(5)	31(3)
C(12A)	-3721(9)	3846(8)	2026(6)	44(3)
C(13A)	-3076(9)	3844(8)	3112(6)	41(3)
C(14A)	-3385(8)	2557(8)	3068(6)	41(3)
C(15A)	151(8)	3943(7)	1637(5)	32(3)
C(16A)	504(12)	3742(9)	1026(6)	61(4)
C(17A)	1126(12)	3837(10)	2056(7)	71(5)
C(18A)	-592(12)	4852(8)	1425(8)	70(5)
C(19A)	2275(8)	-1432(7)	3896(5)	21(2)
C(20A)	1936(8)	-2106(6)	3996(5)	23(2)
C(21A)	2588(8)	-2908(6)	4332(5)	24(2)
C(22A)	3620(8)	-3043(7)	4575(5)	25(2)
C(23A)	3965(8)	-2377(7)	4496(5)	23(2)
C(24A)	3302(7)	-1568(6)	4133(4)	14(2)
C(25A)	2170(9)	-3641(8)	4449(6)	39(3)
C(26A)	1825(10)	-3615(8)	3753(6)	47(3)
C(27A)	1237(10)	-3533(8)	4825(6)	47(3)
C(28A)	3014(11)	-4502(8)	4811(8)	69(5)
C(29A)	5104(8)	-2578(6)	4810(5)	23(2)
C(30A)	5916(8)	-3008(8)	4430(6)	40(3)
C(31A)	5255(9)	-3180(8)	5529(6)	41(3)
C(32A)	5284(8)	-1778(7)	4795(5)	31(3)
C(33A)	1065(7)	1380(7)	4203(5)	19(2)

C(34A)	598(8)	2238(7)	3881(5)	26(3)
C(35A)	710(8)	2823(7)	4142(5)	29(3)
C(36A)	1313(8)	2528(7)	4741(5)	29(3)
C(37A)	1780(8)	1681(7)	5085(5)	28(3)
C(38A)	1660(7)	1111(7)	4816(5)	22(2)
C(39A)	2102(7)	186(7)	5187(5)	23(2)
C(40A)	2652(8)	-218(7)	5850(5)	34(3)
C(41A)	1256(8)	-1288(7)	5238(5)	26(3)
Pt(2)	3449(1)	384(1)	8921(1)	16(1)
O(1B)	3741(5)	-1097(4)	10175(3)	24(2)
N(1B)	3702(6)	967(5)	7984(4)	19(2)
N(2B)	3932(6)	-620(5)	8576(4)	18(2)
N(3B)	3310(6)	-232(5)	9857(4)	19(2)
C(1B)	4075(7)	478(7)	7651(5)	21(2)
C(2B)	4124(8)	-405(6)	7969(5)	22(2)
C(3B)	4430(8)	772(6)	6982(5)	23(2)
C(4B)	4312(8)	-940(7)	7555(5)	26(3)
C(5B)	3580(8)	1843(7)	7689(5)	23(2)
C(6B)	2618(7)	2401(6)	7320(5)	20(2)
C(7B)	2440(8)	3250(7)	7088(5)	24(2)
C(8B)	3287(8)	3519(7)	7198(5)	24(2)
C(9B)	4250(8)	2956(6)	7538(5)	22(2)
C(10B)	4408(7)	2104(7)	7799(5)	24(2)
C(11B)	1369(8)	3878(7)	6708(5)	29(3)
C(12B)	1159(9)	3692(8)	6092(6)	42(3)
C(13B)	1279(9)	4784(8)	6510(7)	49(3)
C(14B)	522(9)	3723(8)	7172(6)	49(3)
C(15B)	5112(8)	3300(7)	7647(6)	31(3)
C(16B)	5277(9)	3881(8)	6977(7)	48(4)
C(17B)	6183(9)	2571(8)	7987(7)	55(4)
C(18B)	4757(9)	3810(8)	8103(6)	45(3)
C(19B)	4009(8)	-1469(6)	8936(5)	18(2)
C(20B)	4939(7)	-2116(6)	9041(5)	24(2)
C(21B)	5015(8)	-2951(7)	9419(5)	27(3)
C(22B)	4102(8)	-3089(7)	9645(5)	29(3)
C(23B)	3152(7)	-2439(6)	9557(5)	20(2)
C(24B)	3096(7)	-1607(6)	9177(5)	21(2)
C(25B)	6068(9)	-3682(8)	9531(7)	50(4)
C(26B)	6372(13)	-3666(13)	8809(10)	114(8)
C(27B)	6012(13)	-4457(11)	9896(18)	260(20)
C(28B)	6914(11)	-3476(9)	9777(9)	82(5)
C(29B)	2190(7)	-2617(6)	9848(5)	20(2)
C(30B)	1752(9)	-3045(8)	9457(6)	41(3)

C(31B)	2518(9)	-3221(7)	10573(5)	40(3)
C(32B)	1301(8)	-1824(7)	9831(5)	32(3)
C(33B)	2742(8)	1374(7)	9209(5)	22(2)
C(34B)	2478(7)	2225(7)	8886(5)	23(2)
C(35B)	1837(8)	2806(7)	9143(5)	31(3)
C(36B)	1458(8)	2525(7)	9729(5)	28(3)
C(37B)	1730(8)	1681(7)	10078(5)	29(3)
C(38B)	2356(7)	1105(7)	9818(5)	22(2)
C(39B)	2720(7)	194(7)	10188(5)	25(2)
C(40B)	2493(9)	-200(7)	10858(5)	32(3)
C(41B)	4868(8)	-1315(7)	10281(5)	30(3)
B(1)	1252(10)	906(9)	7023(7)	31(3)
F(1)	795(5)	511(5)	6729(3)	46(2)
F(2)	2152(5)	988(5)	6739(3)	45(2)
F(3)	1554(6)	435(5)	7694(4)	63(2)
F(4)	566(5)	1677(5)	6963(4)	63(2)
B(2)	2944(9)	929(9)	2014(7)	31(3)
F(8)	1962(5)	1026(5)	1728(3)	48(2)
F(9)	2942(6)	1717(5)	1959(4)	69(2)
F(10)	3748(4)	555(5)	1720(3)	47(2)
F(11)	3063(5)	453(5)	2679(3)	66(2)
Cl(1)	2086(5)	4261(4)	3448(3)	139(2)
Cl(2)	2502(8)	5408(6)	2265(4)	210(4)
C(51)	3190(20)	4452(17)	2856(13)	203(14)
Cl(3)	9664(2)	9486(2)	820(1)	40(1)
Cl(4)	10976(2)	7803(2)	1715(2)	43(1)
C(52)	9682(8)	8518(7)	1389(5)	34(3)
Cl(5)	4074(3)	2209(2)	3268(2)	49(1)
Cl(6)	4203(2)	536(2)	4173(2)	44(1)
C(53)	3379(9)	1528(8)	3603(6)	43(3)



Table 1. Crystal data and structure refinement for [(diimine)Pd(THF)₂][BF₄]₂ (PFO17) (CCDC 679914).

Empirical formula	[C ₄₀ H ₆₄ N ₂ O ₂ Pd] ⁺ 2(BF ₄) ⁻ • 2(C ₄ H ₈ O)
Formula weight	1029.16
Crystallization Solvent	THF/hexanes
Crystal Habit	Fragment
Crystal size	0.14 x 0.12 x 0.10 mm ³
Crystal color	Yellow

Data Collection

Type of diffractometer	Bruker KAPPA APEX II	
Wavelength	0.71073 Å MoKα	
Data Collection Temperature	100(2) K	
θ range for 9299 reflections used in lattice determination	2.16 to 34.18°	
Unit cell dimensions	a = 21.1511(7) Å b = 16.9881(5) Å c = 28.7218(9) Å	β = 95.508(2)°
Volume	10272.6(6) Å ³	
Z	8	
Crystal system	Monoclinic	
Space group	C2/c	
Density (calculated)	1.331 Mg/m ³	
F(000)	4336	
Data collection program	Bruker APEX2 v2.1-0	
θ range for data collection	1.42 to 35.01°	
Completeness to θ = 35.01°	99.7 %	
Index ranges	-34 ≤ h ≤ 34, -27 ≤ k ≤ 27, -46 ≤ l ≤ 42	
Data collection scan type	ω scans; 18 settings	
Data reduction program	Bruker SAINT-Plus v7.34A	
Reflections collected	200912	
Independent reflections	22580 [R _{int} = 0.0862]	
Absorption coefficient	0.433 mm ⁻¹	
Absorption correction	None	
Max. and min. transmission	0.9580 and 0.9419	

Table 1 (cont.)

Structure solution and Refinement	
Structure solution program	SHELXS-97 (Sheldrick, 2008)
Primary solution method	Direct methods
Secondary solution method	Difference Fourier map
Hydrogen placement	Geometric positions
Structure refinement program	SHELXL-97 (Sheldrick, 2008)
Refinement method	Full matrix least-squares on F^2
Data / restraints / parameters	22580 / 25 / 600
Treatment of hydrogen atoms	Riding
Goodness-of-fit on F^2	1.946
Final R indices [$I > 2\sigma(I)$, 13990 reflections]	$R1 = 0.0542$, $wR2 = 0.0768$
R indices (all data)	$R1 = 0.0977$, $wR2 = 0.0786$
Type of weighting Scheme used	Sigma
Weighting Scheme used	$w=1/\sigma^2(Fo^2)$
Max shift/error	0.003
Average shift/error	0.000
Largest diff. peak and hole	1.733 and -1.569 e.Å ⁻³

Special Refinement Details

Crystals were mounted on a glass fiber using Paratone oil then placed on the diffractometer under a nitrogen stream at 100K.

The crystals contain THF as a solvent of crystallization, two per asymmetric unit. Both exhibit signs of disorder, a common trait of THF solvent. One BF_4^- counterion also shows signs of disorder by rotation around one B-F bond, again common. Lastly two of the tertiary butyl group groups on the ligand appear to be disordered. These instances of disorder were not incorporated into the final model as modeling them produced negligible effects.

Refinement of F^2 against ALL reflections. The weighted R-factor (wR) and goodness of fit (S) are based on F^2 , conventional R-factors (R) are based on F , with F set to zero for negative F^2 . The threshold expression of $F^2 > 2\sigma(F^2)$ is used only for calculating R-factors(gt) etc. and is not relevant to the choice of reflections for refinement. R-factors based on F^2 are statistically about twice as large as those based on F , and R-factors based on ALL data will be even larger.

All esds (except the esd in the dihedral angle between two l.s. planes) are estimated using the full covariance matrix. The cell esds are taken into account individually in the estimation of esds in distances, angles and torsion angles; correlations between esds in cell parameters are only used when they are defined by crystal symmetry.

An approximate (isotropic) treatment of cell esds is used for estimating esds involving l.s. planes.

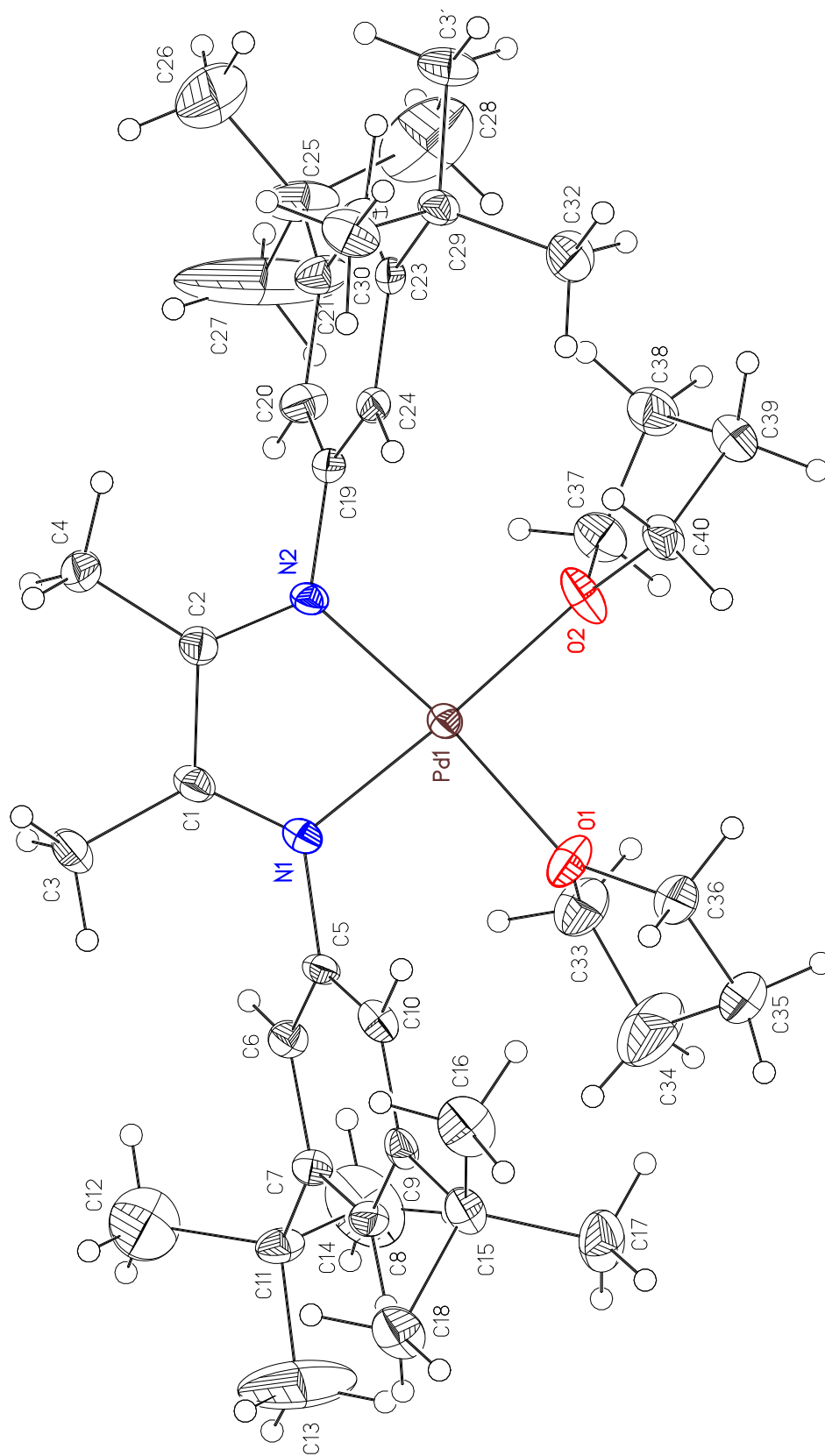


Table 2. Atomic coordinates ($\times 10^4$) and equivalent isotropic displacement parameters ($\text{\AA}^2 \times 10^3$) for [(diimine)Pd(THF)₂][BF₄]₂ (PFO17) (CCDC 679914). U(eq) is defined as the trace of the orthogonalized U^{ij} tensor.

	x	y	z	U _{eq}
Pd(1)	1108(1)	2144(1)	1400(1)	15(1)
O(1)	1223(1)	1346(1)	1939(1)	27(1)
O(2)	1107(1)	3013(1)	1891(1)	27(1)
N(1)	1168(1)	1346(1)	906(1)	16(1)
N(2)	1077(1)	2834(1)	844(1)	15(1)
C(1)	1232(1)	1619(1)	496(1)	19(1)
C(2)	1178(1)	2484(1)	460(1)	19(1)
C(3)	1355(1)	1137(1)	80(1)	31(1)
C(4)	1237(1)	2891(1)	6(1)	27(1)
C(5)	1188(1)	521(1)	1020(1)	15(1)
C(6)	1752(1)	117(1)	1042(1)	17(1)
C(7)	1766(1)	-675(1)	1174(1)	17(1)
C(8)	1201(1)	-1019(1)	1275(1)	18(1)
C(9)	622(1)	-615(1)	1248(1)	18(1)
C(10)	627(1)	173(1)	1124(1)	18(1)
C(11)	2398(1)	-1123(1)	1217(1)	22(1)
C(12)	2729(1)	-1033(2)	772(1)	60(1)
C(13)	2311(1)	-1994(2)	1302(1)	83(1)
C(14)	2821(1)	-785(2)	1625(1)	63(1)
C(15)	16(1)	-1027(1)	1370(1)	23(1)
C(16)	-579(1)	-557(2)	1214(1)	34(1)
C(17)	65(1)	-1135(2)	1907(1)	36(1)
C(18)	-48(1)	-1839(1)	1137(1)	32(1)
C(19)	1036(1)	3678(1)	871(1)	16(1)
C(20)	1592(1)	4110(1)	884(1)	23(1)
C(21)	1567(1)	4924(1)	910(1)	25(1)
C(22)	970(1)	5276(1)	919(1)	20(1)
C(23)	407(1)	4846(1)	908(1)	16(1)
C(24)	453(1)	4026(1)	891(1)	16(1)
C(25)	2170(1)	5433(2)	946(1)	42(1)
C(26)	2120(2)	6040(2)	565(1)	59(1)
C(27)	2760(2)	4963(2)	949(2)	153(2)
C(28)	2214(2)	5897(2)	1416(1)	80(1)
C(29)	-241(1)	5238(1)	925(1)	19(1)
C(30)	-688(1)	4982(1)	497(1)	30(1)
C(31)	-203(1)	6132(1)	927(1)	30(1)
C(32)	-522(1)	4978(2)	1373(1)	34(1)
C(33)	1851(1)	1126(2)	2140(1)	35(1)

C(34)	1711(2)	382(2)	2406(1)	60(1)
C(35)	1109(1)	577(2)	2610(1)	37(1)
C(36)	759(1)	1120(1)	2250(1)	30(1)
C(37)	1670(1)	3446(1)	2065(1)	28(1)
C(38)	1418(1)	4240(1)	2171(1)	30(1)
C(39)	800(1)	4059(1)	2350(1)	30(1)
C(40)	551(1)	3371(1)	2051(1)	24(1)
B(1)	9171(1)	2246(2)	1500(1)	27(1)
F(1)	9233(1)	2920(1)	1238(1)	49(1)
F(2)	8700(1)	1775(1)	1289(1)	44(1)
F(3)	9737(1)	1841(1)	1536(1)	59(1)
F(4)	9026(1)	2465(1)	1936(1)	61(1)
B(2)	2844(1)	2199(2)	1011(1)	34(1)
F(5)	2490(1)	2353(1)	1377(1)	62(1)
F(6)	3395(1)	2591(1)	1050(1)	77(1)
F(7)	2496(1)	2354(1)	601(1)	96(1)
F(8)	2991(1)	1420(1)	1013(1)	101(1)
O(51)	9941(1)	1834(1)	91(1)	54(1)
C(52)	9607(2)	1104(2)	131(2)	114(2)
C(53)	8956(2)	1212(2)	151(1)	62(1)
C(54)	8844(2)	2102(2)	76(1)	74(1)
C(55)	9491(2)	2408(2)	130(1)	97(2)
O(71)	3801(2)	2304(2)	2884(1)	140(1)
C(72)	3407(2)	2425(3)	2464(2)	168(3)
C(73)	3786(3)	1984(5)	2155(2)	233(4)
C(74)	3947(3)	1301(2)	2377(2)	168(3)
C(75)	4178(3)	1634(3)	2840(2)	177(3)

[(diimine)PtBr]₂[BF₄]₂ (Ar = 3,5-^tBu₂C₆H₃)

Table 1. Crystal data and structure refinement for [(diimine)PtBr]₂[BF₄]₂ (PFO25) (CCDC 727546)³.

Empirical formula	[C ₆₄ H ₉₆ N ₄ Br ₂ Pt ₂] ⁺² 2[BF ₄] ⁻ • 2(CH ₂ Cl ₂)
Formula weight	1814.92
Crystallization Solvent	Not given
Crystal Habit	Fragment
Crystal size	0.19 x 0.11 x 0.04 mm ³
Crystal color	Yellow



Data Collection

Type of diffractometer	Bruker KAPPA APEX II
Wavelength	0.71073 Å MoKα
Data Collection Temperature	100(2) K
θ range for 9886 reflections used in lattice determination	2.42 to 29.21°
Unit cell dimensions	a = 31.4961(15) Å b = 12.4942(6) Å c = 19.3944(10) Å β = 92.389(2)°
Volume	7625.4(6) Å ³
Z	4
Crystal system	Monoclinic
Space group	C2/c
Density (calculated)	1.581 Mg/m ³
F(000)	3600
θ range for data collection	1.75 to 29.36°
Completeness to θ = 29.36°	92.3 %
Index ranges	-42 ≤ h ≤ 35, -16 ≤ k ≤ 16, -26 ≤ l ≤ 24
Data collection scan type	ω scans; 16 settings
Reflections collected	92327
Independent reflections	9693 [R _{int} = 0.0886]
Absorption coefficient	4.912 mm ⁻¹
Absorption correction	None
Max. and min. transmission	0.8277 and 0.4555



Table 1 (cont.)

Structure solution and Refinement	
Structure solution program	SHELXS-97 (Sheldrick, 2008)
Primary solution method	Direct methods
Secondary solution method	Difference Fourier map
Hydrogen placement	Geometric positions
Structure refinement program	SHELXL-97 (Sheldrick, 2008)
Refinement method	Full matrix least-squares on F^2
Data / restraints / parameters	9693 / 0 / 488
Treatment of hydrogen atoms	Riding
Goodness-of-fit on F^2	1.371
Final R indices [$I > 2\sigma(I)$, 7524 reflections]	$R1 = 0.0261$, $wR2 = 0.0479$
R indices (all data)	$R1 = 0.0432$, $wR2 = 0.0495$
Type of weighting Scheme used	Sigma
Weighting Scheme used	$w=1/\sigma^2(Fo^2)$
Max shift/error	0.002
Average shift/error	0.000
Largest diff. peak and hole	1.323 and -1.000 e.Å ⁻³

Special Refinement Details

Crystals were mounted on a glass fiber using Paratone oil then placed on the diffractometer under a nitrogen stream at 100K.

The crystal is disordered, two ^tBu groups, the tetrafluoroborate and the dichlormethane all appear to be in two positions. The minor components were modeled isotropically without geometric restraints.

Refinement of F^2 against ALL reflections. The weighted R-factor (wR) and goodness of fit (S) are based on F^2 , conventional R-factors (R) are based on F , with F set to zero for negative F^2 . The threshold expression of $F^2 > 2\sigma(F^2)$ is used only for calculating R-factors(gt) etc. and is not relevant to the choice of reflections for refinement. R-factors based on F^2 are statistically about twice as large as those based on F , and R-factors based on ALL data will be even larger.

All esds (except the esd in the dihedral angle between two l.s. planes) are estimated using the full covariance matrix. The cell esds are taken into account individually in the estimation of esds in distances, angles and torsion angles; correlations between esds in cell parameters are only used when they are defined by crystal symmetry. An approximate (isotropic) treatment of cell esds is used for estimating esds involving l.s. planes.

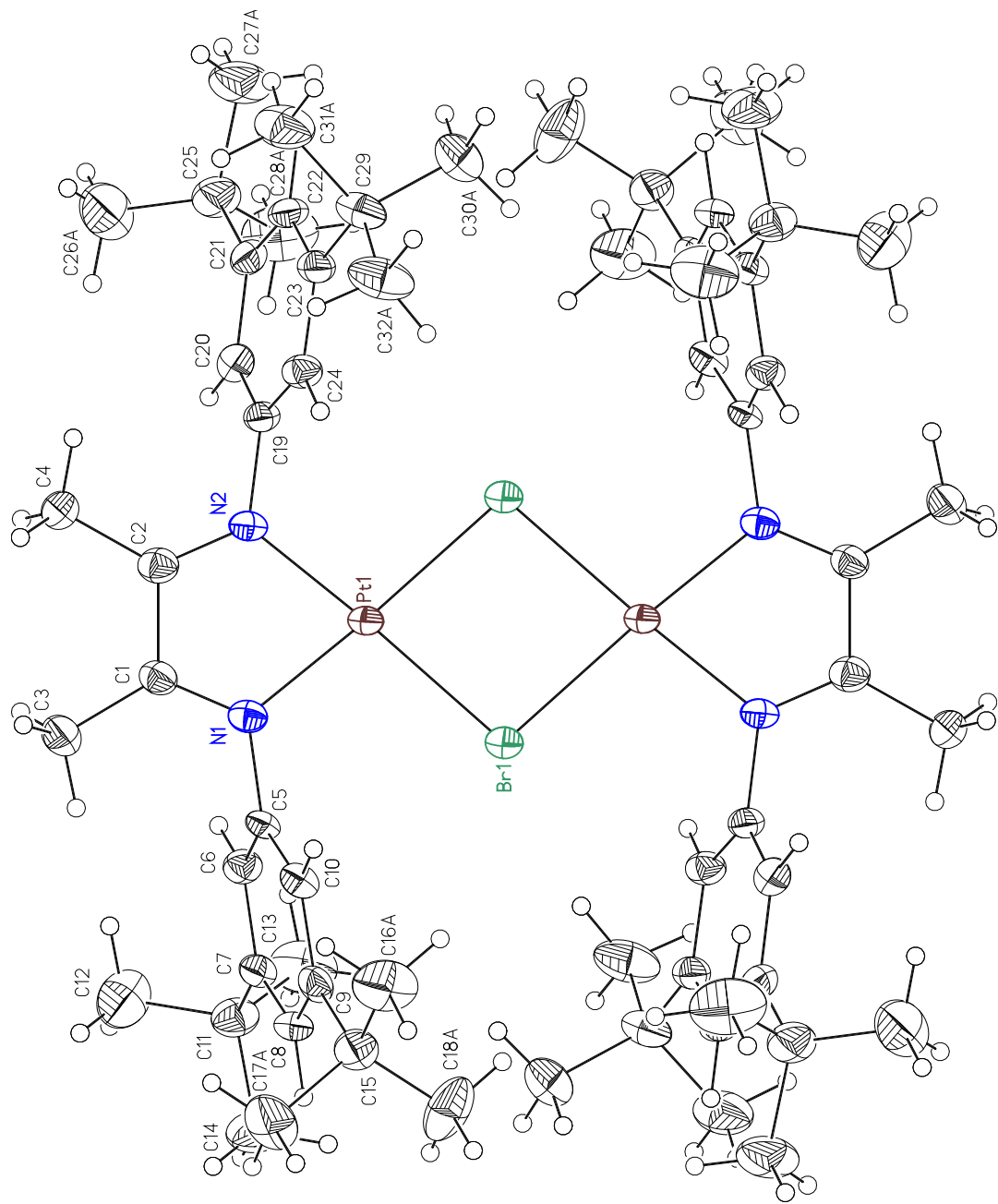


Table 2. Atomic coordinates ($\times 10^4$) and equivalent isotropic displacement parameters ($\text{\AA}^2 \times 10^3$) for [(diimine)PtBr]₂[BF₄]₂ (PFO25) (CCDC 727546). U(eq) is defined as the trace of the orthogonalized U^{ij} tensor.

	x	y	z	U _{eq}	Occ
Pt(1)	2443(1)	3142(1)	4162(1)	22(1)	1
Br(1)	3002(1)	2822(1)	5045(1)	39(1)	1
N(1)	2781(1)	3961(2)	3489(1)	22(1)	1
N(2)	2004(1)	3451(2)	3420(1)	23(1)	1
C(1)	2585(1)	4274(2)	2932(2)	24(1)	1
C(2)	2125(1)	3984(2)	2893(2)	26(1)	1
C(3)	2778(1)	4880(3)	2368(2)	35(1)	1
C(4)	1855(1)	4315(3)	2284(2)	35(1)	1
C(5)	3230(1)	4192(2)	3624(1)	22(1)	1
C(6)	3351(1)	5215(2)	3806(1)	25(1)	1
C(7)	3783(1)	5436(2)	3943(1)	25(1)	1
C(8)	4066(1)	4595(2)	3890(2)	27(1)	1
C(9)	3946(1)	3559(2)	3719(2)	26(1)	1
C(10)	3515(1)	3361(2)	3582(2)	24(1)	1
C(11)	3917(1)	6576(2)	4142(2)	33(1)	1
C(12)	3778(1)	7343(3)	3566(2)	55(1)	1
C(13)	3704(1)	6894(3)	4808(2)	56(1)	1
C(14)	4398(1)	6683(3)	4278(2)	51(1)	1
C(15)	4275(1)	2655(2)	3675(2)	33(1)	1
C(16A)	4066(1)	1555(3)	3544(3)	55(1)	0.860(5)
C(17A)	4553(1)	2875(3)	3057(2)	52(1)	0.860(5)
C(18A)	4546(1)	2600(3)	4333(2)	56(1)	0.860(5)
C(16B)	4257(8)	2260(20)	2983(14)	48(7)	0.140(5)
C(17B)	4749(6)	3182(17)	3895(12)	34(6)	0.140(5)
C(18B)	4173(7)	1940(20)	4225(14)	48(7)	0.140(5)
C(19)	1558(1)	3199(2)	3497(1)	24(1)	1
C(20)	1284(1)	4026(2)	3618(2)	28(1)	1
C(21)	853(1)	3808(2)	3701(2)	28(1)	1
C(22)	726(1)	2753(2)	3659(2)	28(1)	1
C(23)	1002(1)	1897(2)	3543(1)	25(1)	1
C(24)	1428(1)	2141(2)	3461(2)	25(1)	1
C(25)	545(1)	4733(3)	3812(2)	40(1)	1
C(26A)	546(1)	5467(4)	3217(3)	73(2)	0.816(5)
C(27A)	87(1)	4328(3)	3919(3)	56(2)	0.816(5)
C(28A)	681(1)	5329(4)	4492(3)	67(2)	0.816(5)
C(26B)	239(5)	4746(16)	3104(10)	48(5)	0.184(5)
C(27B)	339(6)	4650(16)	4439(11)	53(6)	0.184(5)
C(28B)	774(5)	5900(13)	3728(10)	38(5)	0.184(5)

C(29)	833(1)	750(2)	3516(2)	34(1)	1
C(32A)	1162(1)	-56(3)	3346(2)	49(1)	0.873(4)
C(30A)	642(1)	490(3)	4207(2)	42(1)	0.873(4)
C(31A)	466(1)	690(3)	2954(2)	49(1)	0.873(4)
C(30B)	1221(7)	-40(20)	3990(16)	47(8)	0.127(4)
C(31B)	444(9)	480(30)	3820(17)	57(9)	0.127(4)
C(32B)	897(7)	230(20)	2822(14)	46(8)	0.127(4)
B(1)	2862(3)	2010(5)	1789(4)	49(2)	0.793(6)
F(1)	3126(3)	2689(6)	1509(5)	123(3)	0.793(6)
F(2)	2877(2)	1046(6)	1506(5)	82(2)	0.793(6)
F(3)	2929(2)	1966(3)	2496(2)	103(2)	0.793(6)
F(4)	2454(1)	2393(3)	1691(3)	120(2)	0.793(6)
B(1B)	3054(11)	2050(30)	1760(20)	64(11)	0.207(6)
F(1B)	3133(8)	2800(20)	1355(13)	57(5)	0.207(6)
F(2B)	2696(6)	2254(13)	2188(10)	84(5)	0.207(6)
F(3B)	3352(5)	1717(12)	2247(9)	113(7)	0.207(6)
F(4B)	2889(6)	920(20)	1536(16)	39(5)	0.207(6)
C(41)	2193(2)	6139(5)	5205(4)	56(2)	0.655(3)
Cl(1)	1801(1)	5160(2)	5378(1)	70(1)	0.655(3)
Cl(2)	2682(1)	5573(2)	5258(1)	81(1)	0.655(3)
C(41B)	2054(4)	5722(11)	4947(7)	62(4)	0.345(3)
Cl(1B)	1648(1)	5146(4)	5397(3)	68(2)	0.345(3)
Cl(2B)	2472(1)	6230(4)	5475(2)	88(2)	0.345(3)

[(diimine)Pt(OH₂)₂][BF₄]₂ (Ar = 2,4,6-Me₃C₆H₂)

Table 1. Crystal data and structure refinement for [(diimine)Pt(OH₂)₂][BF₄]₂ (PFO32) (CCDC 837962).

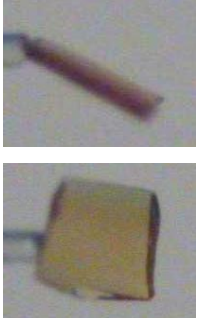
Empirical formula	[C ₂₂ H ₂₈ N ₂ O ₂ Pt] ⁺ 2[BF ₄] ⁻ • 2(H ₂ O)	
Formula weight	757.21	
Crystallization Solvent	Not given	
Crystal Habit	Blade	
Crystal size	0.30 x 0.25 x 0.04 mm ³	
Crystal color	Yellow/orange	
Data Collection		
Type of diffractometer	Bruker KAPPA APEX II	
Wavelength	0.71073 Å MoKα	
Data Collection Temperature	100(2) K	
θ range for 9821 reflections used in lattice determination	2.67 to 34.60°	
Unit cell dimensions	a = 11.1605(7) Å b = 11.5574(7) Å c = 13.5650(8) Å	α = 100.626(3)° β = 95.181(3)° γ = 118.727(3)°
Volume	1475.18(16) Å ³	
Z	2	
Crystal system	Triclinic	
Space group	P-1	
Density (calculated)	1.705 Mg/m ³	
F(000)	740	
Data collection program	Bruker APEX2 v2009.7-0	
θ range for data collection	1.56 to 35.01°	
Completeness to θ = 35.01°	91.5 %	
Index ranges	-17 ≤ h ≤ 17, -18 ≤ k ≤ 18, -21 ≤ l ≤ 21	
Data collection scan type	ω scans; 23 settings	
Data reduction program	Bruker SAINT-Plus v7.66A	
Reflections collected	64310	
Independent reflections	11885 [R _{int} = 0.0342]	
Absorption coefficient	4.836 mm ⁻¹	
Absorption correction	None	
Max. and min. transmission	0.8301 and 0.3248	

Table 1 (cont.)

Structure solution and Refinement	
Structure solution program	SHELXS-97 (Sheldrick, 2008)
Primary solution method	Direct methods
Secondary solution method	Difference Fourier map
Hydrogen placement	Geometric positions
Structure refinement program	SHELXL-97 (Sheldrick, 2008)
Refinement method	Full matrix least-squares on F^2
Data / restraints / parameters	11885 / 0 / 360
Treatment of hydrogen atoms	Riding
Goodness-of-fit on F^2	1.987
Final R indices [$I > 2\sigma(I)$, 11048 reflections]	$R1 = 0.0215$, $wR2 = 0.0490$
R indices (all data)	$R1 = 0.0249$, $wR2 = 0.0494$
Type of weighting Scheme used	Sigma
Weighting Scheme used	$w=1/\sigma^2(Fo^2)$
Max shift/error	0.005
Average shift/error	0.000
Largest diff. peak and hole	2.049 and -1.448 e. \AA^{-3}

Special Refinement Details

Crystals were mounted on a glass fiber using Paratone oil then placed on the diffractometer under a nitrogen stream at 100K.

Refinement of F^2 against ALL reflections. The weighted R-factor (wR) and goodness of fit (S) are based on F^2 , conventional R-factors (R) are based on F , with F set to zero for negative F^2 . The threshold expression of $F^2 > 2\sigma(F^2)$ is used only for calculating R-factors(gt) etc. and is not relevant to the choice of reflections for refinement. R-factors based on F^2 are statistically about twice as large as those based on F , and R-factors based on ALL data will be even larger.

All esds (except the esd in the dihedral angle between two l.s. planes) are estimated using the full covariance matrix. The cell esds are taken into account individually in the estimation of esds in distances, angles and torsion angles; correlations between esds in cell parameters are only used when they are defined by crystal symmetry. An approximate (isotropic) treatment of cell esds is used for estimating esds involving l.s. planes.

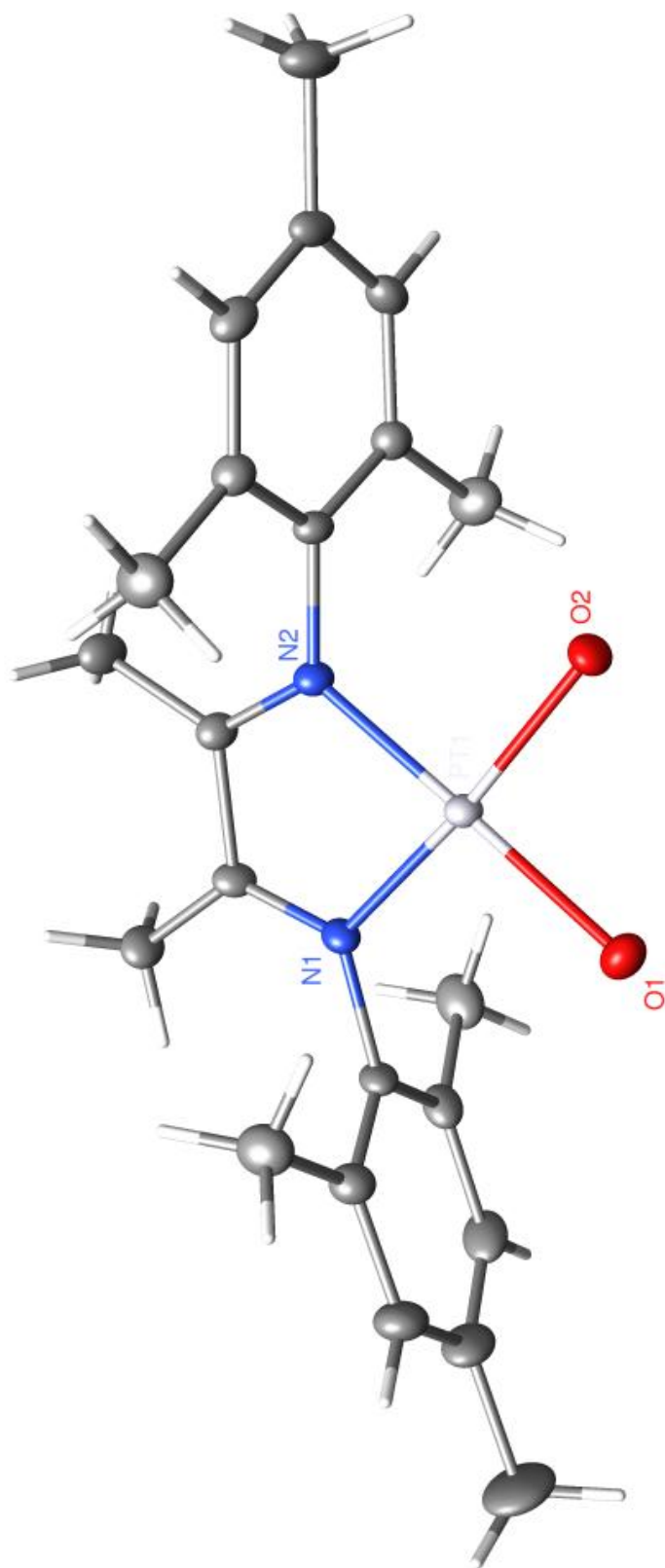


Table 2. Atomic coordinates ($\times 10^4$) and equivalent isotropic displacement parameters ($\text{\AA}^2 \times 10^3$) for [(diimine)Pt(OH₂)₂][BF₄]₂ (PFO32) (CCDC 837962). U(eq) is defined as the trace of the orthogonalized U^{ij} tensor.

	x	y	z	U _{eq}
Pt(1)	8225(1)	7667(1)	7480(1)	14(1)
O(1)	9364(1)	8561(1)	6460(1)	23(1)
O(2)	9747(1)	7216(1)	7834(1)	20(1)
N(1)	6705(2)	8072(2)	7266(1)	15(1)
N(2)	7102(2)	6773(2)	8432(1)	15(1)
C(1)	5753(2)	7618(2)	7802(1)	16(1)
C(2)	5979(2)	6835(2)	8480(1)	17(1)
C(3)	4558(2)	7839(2)	7794(1)	23(1)
C(4)	4985(2)	6201(2)	9137(1)	26(1)
C(5)	6708(2)	8894(2)	6576(1)	18(1)
C(6)	6279(2)	8254(2)	5522(1)	22(1)
C(7)	6400(2)	9081(2)	4864(2)	29(1)
C(8)	6913(2)	10469(2)	5226(2)	32(1)
C(9)	7300(2)	11047(2)	6279(2)	29(1)
C(10)	7208(2)	10276(2)	6976(1)	22(1)
C(11)	5667(2)	6740(2)	5140(1)	27(1)
C(12)	7043(3)	11334(3)	4482(2)	51(1)
C(13)	7611(2)	10913(2)	8119(2)	29(1)
C(14)	7481(2)	6046(2)	9043(1)	16(1)
C(15)	6928(2)	4652(2)	8665(1)	18(1)
C(16)	7304(2)	3985(2)	9273(1)	20(1)
C(17)	8196(2)	4681(2)	10232(1)	21(1)
C(18)	8729(2)	6076(2)	10570(1)	21(1)
C(19)	8418(2)	6803(2)	9987(1)	18(1)
C(20)	5960(2)	3880(2)	7624(1)	27(1)
C(21)	8572(2)	3926(2)	10878(2)	31(1)
C(22)	9086(2)	8328(2)	10322(1)	27(1)
B(1)	8116(3)	5989(3)	3915(2)	31(1)
F(1)	6867(2)	5426(2)	3246(1)	48(1)
F(2)	7966(2)	5300(2)	4668(1)	53(1)
F(3)	9131(2)	5981(2)	3397(1)	55(1)
F(4)	8563(2)	7366(1)	4393(1)	34(1)
B(2)	3384(3)	538(3)	8737(3)	45(1)
F(5)	3254(2)	580(2)	9740(1)	79(1)
F(6)	4604(2)	658(2)	8593(2)	114(1)
F(7)	3270(2)	1601(2)	8452(1)	48(1)

F(8)	2294(2)	-708(2)	8108(1)	61(1)
O(3)	9127(2)	5055(2)	6460(1)	43(1)
O(4)	1000(2)	1099(2)	7064(1)	44(1)

Polypyrazoleborate Pd^I-Pd^I decomposition product

Table 1. Crystal data and structure refinement for Polypyrazoleborate Pd^I-Pd^I decomposition product (PFO37) (CCDC 737900).

Empirical formula	C ₄₅ H ₇₇ BN ₁₀ Pd ₂	
Formula weight	981.78	
Crystallization Solvent	Not given	
Crystal Habit	Fragment	
Crystal size	0.25 x 0.18 x 0.09 mm ³	
Crystal color	Red	
Data Collection		
Type of diffractometer	Bruker KAPPA APEX II	
Wavelength	0.71073 Å MoKα	
Data Collection Temperature	100(2) K	
θ range for 9784 reflections used in lattice determination	2.22 to 34.02°	
Unit cell dimensions	a = 13.0536(5) Å b = 13.6112(5) Å c = 16.5796(6) Å	α = 69.354(2)° β = 78.927(2)° γ = 64.560(2)°
Volume	2486.43(16) Å ³	
Z	2	
Crystal system	Triclinic	
Space group	P-1	
Density (calculated)	1.311 Mg/m ³	
F(000)	1028	
Data collection program	Bruker APEX2 v2.1-0	
θ range for data collection	1.73 to 34.07°	
Completeness to θ = 34.07°	99.3 %	
Index ranges	-16 ≤ h ≤ 20, -21 ≤ k ≤ 21, -26 ≤ l ≤ 26	
Data collection scan type	ω scans; 16 settings	
Data reduction program	Bruker SAINT-Plus v7.34A	
Reflections collected	76738	
Independent reflections	20278 [R _{int} = 0.0625]	
Absorption coefficient	0.763 mm ⁻¹	
Absorption correction	Semi-empirical from equivalents	
Max. and min. transmission	0.7467 and 0.6298	

Table 1 (cont.)

Structure solution and Refinement	
Structure solution program	SHELXS-97 (Sheldrick, 2008)
Primary solution method	Direct methods
Secondary solution method	Difference Fourier map
Hydrogen placement	Geometric positions
Structure refinement program	SHELXL-97 (Sheldrick, 2008)
Refinement method	Full matrix least-squares on F ²
Data / restraints / parameters	20278 / 0 / 543
Treatment of hydrogen atoms	Riding
Goodness-of-fit on F ²	1.612
Final R indices [I>2σ(I), 13738 reflections]	R1 = 0.0437, wR2 = 0.0644
R indices (all data)	R1 = 0.0894, wR2 = 0.0693
Type of weighting Scheme used	Sigma
Weighting Scheme used	w=1/σ ² (Fo ²)
Max shift/error	0.001
Average shift/error	0.000
Largest diff. peak and hole	1.952 and -1.594 e.Å ⁻³

Special Refinement Details

Crystals were mounted on a glass fiber using Paratone oil then placed on the diffractometer under a nitrogen stream at 100K.

Pd(2) appears to be coordinately-unsaturated. Both H(8C) and H(40) lie within 2.4-2.9Å of Pd(2) (see Table 3) which suggests an electrostatic or “anagostic” interaction.⁴

Furthermore, the pyrazole ring containing N(7)-N(8) is protonated at N(8) and is therefore a hydrogen bond donor to N(10). Although there is a possibility that it is N(10) that is protonated the electron density map strongly suggests the major conformation is as modeled (see final figure).

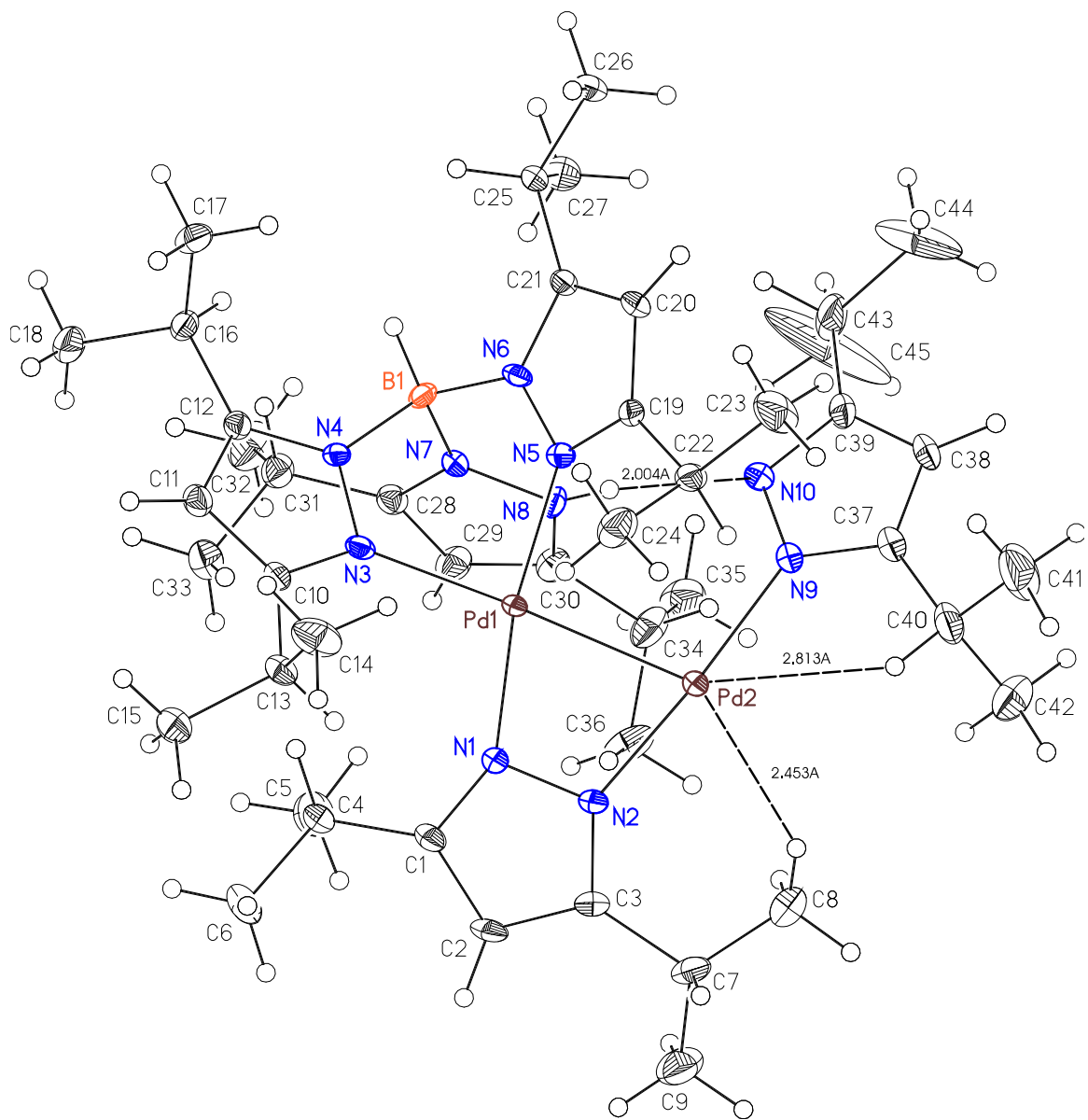


Table 2. Atomic coordinates ($\times 10^4$) and equivalent isotropic displacement parameters ($\text{\AA}^2 \times 10^3$) for Polypyrazoleborate Pd^I-Pd^I decomposition product (PFO37) (CCDC 737900). $U(\text{eq})$ is defined as the trace of the orthogonalized U_{ij} tensor.

	x	y	z	U_{eq}
Pd(1)	3385(1)	1119(1)	3218(1)	12(1)
Pd(2)	4299(1)	2546(1)	2674(1)	14(1)
N(1)	5000(1)	296(1)	2830(1)	13(1)
N(2)	5513(1)	1013(1)	2743(1)	15(1)
N(3)	2685(1)	-114(1)	3598(1)	13(1)
N(4)	1620(1)	209(1)	3341(1)	12(1)
N(5)	1832(1)	2174(1)	3564(1)	13(1)
N(6)	884(1)	2276(1)	3231(1)	12(1)
N(7)	1609(1)	1698(1)	1866(1)	13(1)
N(8)	2077(1)	2491(1)	1610(1)	16(1)
N(9)	2974(2)	4089(2)	2459(1)	17(1)
N(10)	2018(2)	4330(2)	2087(1)	19(1)
B(1)	967(2)	1460(2)	2768(2)	14(1)
C(1)	5755(2)	-590(2)	2559(1)	16(1)
C(2)	6773(2)	-435(2)	2307(2)	20(1)
C(3)	6582(2)	595(2)	2420(1)	17(1)
C(4)	5445(2)	-1477(2)	2462(2)	19(1)
C(5)	5265(2)	-1212(2)	1516(2)	30(1)
C(6)	6365(2)	-2682(2)	2795(2)	30(1)
C(7)	7355(2)	1224(2)	2240(2)	24(1)
C(8)	6702(2)	2510(2)	1947(2)	40(1)
C(9)	8300(2)	850(2)	1585(2)	34(1)
C(10)	3005(2)	-1177(2)	4144(1)	13(1)
C(11)	2133(2)	-1555(2)	4230(1)	17(1)
C(12)	1275(2)	-666(2)	3726(1)	14(1)
C(13)	4093(2)	-1747(2)	4605(1)	17(1)
C(14)	3881(2)	-1533(2)	5473(2)	31(1)
C(15)	4631(2)	-3036(2)	4741(2)	26(1)
C(16)	134(2)	-617(2)	3608(1)	16(1)
C(17)	-703(2)	-336(2)	4361(2)	24(1)
C(18)	242(2)	-1733(2)	3517(2)	27(1)
C(19)	1488(2)	2880(2)	4048(1)	14(1)
C(20)	309(2)	3463(2)	4017(1)	16(1)
C(21)	-53(2)	3073(2)	3508(1)	14(1)
C(22)	2303(2)	2951(2)	4530(2)	18(1)
C(23)	1711(2)	3924(2)	4928(2)	35(1)
C(24)	2886(2)	1822(2)	5218(2)	27(1)

C(25)	-1239(2)	3394(2)	3269(2)	17(1)
C(26)	-2113(2)	4196(2)	3758(2)	23(1)
C(27)	-1400(2)	3963(2)	2303(2)	25(1)
C(28)	1875(2)	1128(2)	1277(1)	16(1)
C(29)	2534(2)	1570(2)	626(2)	21(1)
C(30)	2653(2)	2398(2)	857(1)	19(1)
C(31)	1486(2)	202(2)	1371(2)	20(1)
C(32)	1079(2)	332(2)	526(2)	34(1)
C(33)	2440(2)	-988(2)	1687(2)	30(1)
C(34)	3346(2)	3106(2)	402(2)	26(1)
C(35)	2953(2)	3822(2)	-509(2)	34(1)
C(36)	4611(2)	2335(2)	392(2)	33(1)
C(37)	2916(2)	5065(2)	2522(2)	22(1)
C(38)	1893(2)	5942(2)	2187(2)	34(1)
C(39)	1343(2)	5463(2)	1912(2)	31(1)
C(40)	3866(2)	5088(2)	2873(2)	30(1)
C(41)	3449(3)	5782(2)	3509(2)	46(1)
C(42)	4631(2)	5519(2)	2142(2)	44(1)
C(43)	254(2)	5967(2)	1463(3)	65(1)
C(44)	-502(3)	7104(3)	1583(2)	68(1)
C(45)	440(4)	6073(4)	544(4)	165(3)

Ph₂B(pz)₂PtCl(DMSO)

Table 1. Crystal data and structure refinement for Ph₂B(pz)₂PtCl(DMSO) (PFO39) (738650).

Empirical formula	C ₂₀ H ₂₂ BN ₄ SClPt	
Formula weight	591.83	
Crystallization Solvent	Not given	
Crystal Habit	Block	
Crystal size	0.25 x 0.19 x 0.16 mm ³	
Crystal color	Colorless	
Data Collection		
Type of diffractometer	Bruker KAPPA APEX II	
Wavelength	0.71073 Å MoKα	
Data Collection Temperature	100(2) K	
θ range for 9984 reflections used in lattice determination	2.23 to 50.56°	
Unit cell dimensions	a = 12.9758(4) Å b = 9.5447(3) Å c = 18.0236(6) Å	β = 104.795(2)°
Volume	2158.22(12) Å ³	
Z	4	
Crystal system	Monoclinic	
Space group	P2 ₁ /n	
Density (calculated)	1.821 Mg/m ³	
F(000)	1144	
Data collection program	Bruker APEX2 v2.1-0	
θ range for data collection	1.74 to 50.72°	
Completeness to θ = 50.72°	97.5 %	
Index ranges	-27 ≤ h ≤ 27, -20 ≤ k ≤ 18, -37 ≤ l ≤ 38	
Data collection scan type	ω scans; 18 settings	
Data reduction program	Bruker SAINT-Plus v7.34A	
Reflections collected	135909	
Independent reflections	22757 [R _{int} = 0.0498]	
Absorption coefficient	6.735 mm ⁻¹	
Absorption correction	Semi-empirical from equivalents	
Max. and min. transmission	0.7500 and 0.5014	

Table 1 (cont.)

Structure solution and Refinement	
Structure solution program	SHELXS-97 (Sheldrick, 2008)
Primary solution method	Direct methods
Secondary solution method	Difference Fourier map
Hydrogen placement	Difference Fourier map
Structure refinement program	SHELXL-97 (Sheldrick, 2008)
Refinement method	Full matrix least-squares on F^2
Data / restraints / parameters	22757 / 0 / 341
Treatment of hydrogen atoms	Unrestrained
Goodness-of-fit on F^2	1.517
Final R indices [$I > 2\sigma(I)$, 17750 reflections]	R1 = 0.0317, wR2 = 0.0541
R indices (all data)	R1 = 0.0498, wR2 = 0.0566
Type of weighting Scheme used	Sigma
Weighting Scheme used	$w=1/\sigma^2(Fo^2)$
Max shift/error	0.005
Average shift/error	0.000
Largest diff. peak and hole	7.596 and -2.841 e.Å ⁻³

Special Refinement Details

Crystals were mounted on a glass fiber using Paratone oil then placed on the diffractometer under a nitrogen stream at 100K.

Refinement of F^2 against ALL reflections. The weighted R-factor (wR) and goodness of fit (S) are based on F^2 , conventional R-factors (R) are based on F , with F set to zero for negative F^2 . The threshold expression of $F^2 > 2\sigma(F^2)$ is used only for calculating R-factors(gt) etc. and is not relevant to the choice of reflections for refinement. R-factors based on F^2 are statistically about twice as large as those based on F , and R-factors based on ALL data will be even larger.

All esds (except the esd in the dihedral angle between two l.s. planes) are estimated using the full covariance matrix. The cell esds are taken into account individually in the estimation of esds in distances, angles and torsion angles; correlations between esds in cell parameters are only used when they are defined by crystal symmetry. An approximate (isotropic) treatment of cell esds is used for estimating esds involving l.s. planes.

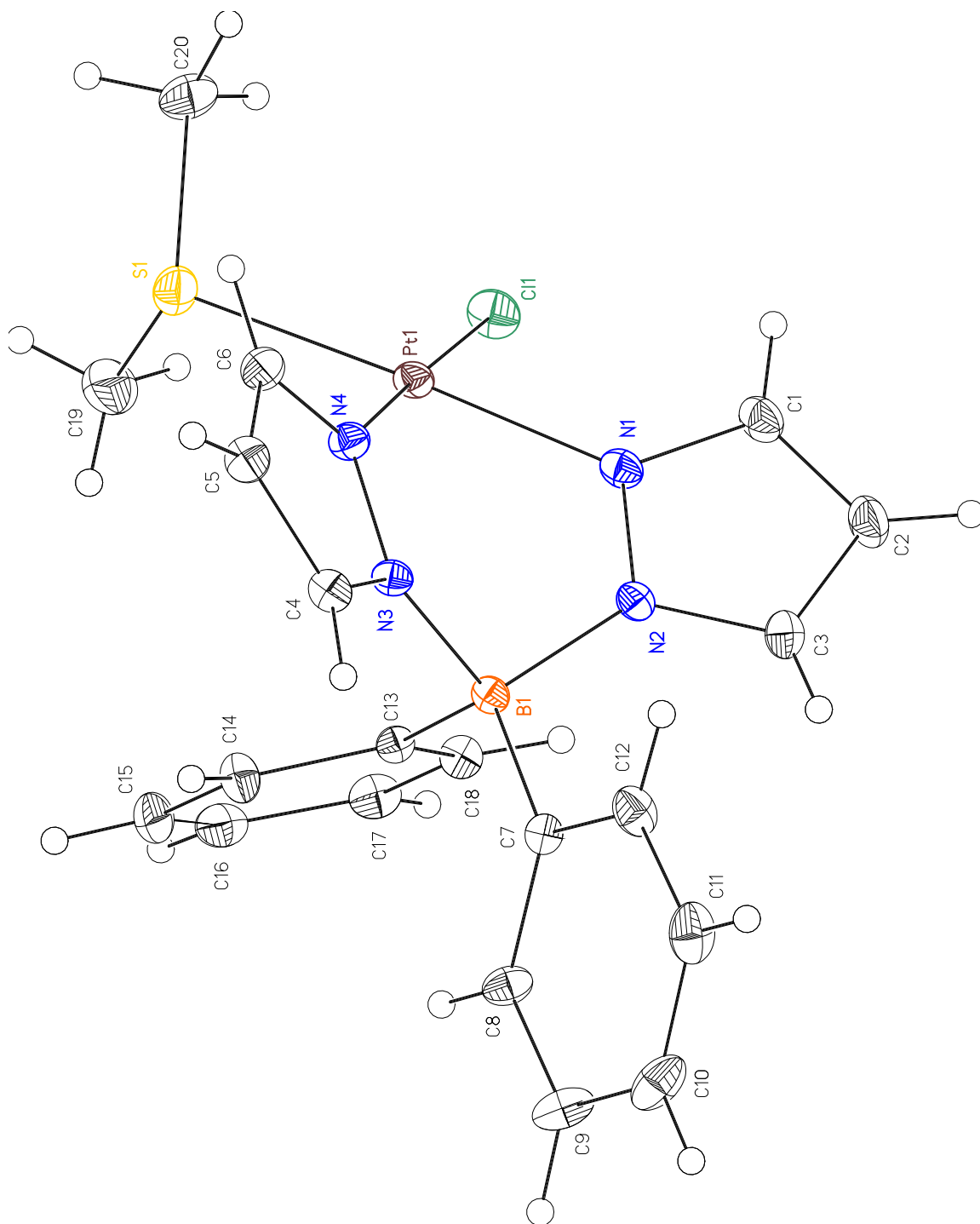


Table 2. Atomic coordinates ($\times 10^4$) and equivalent isotropic displacement parameters ($\text{\AA}^2 \times 10^3$) for $\text{Ph}_2\text{B}(\text{pz})_2\text{PtCl}(\text{DMSO})$ (PFO39) (738650). $U(\text{eq})$ is defined as the trace of the orthogonalized U_{ij} tensor.

	x	y	z	U_{eq}
Pt(1)	4964(1)	6285(1)	1028(1)	12(1)
Cl(1)	6233(1)	7991(1)	1094(1)	19(1)
S(1)	6204(1)	4665(1)	1585(1)	19(1)
N(1)	3806(1)	7685(1)	560(1)	13(1)
N(2)	2870(1)	7697(1)	770(1)	12(1)
N(3)	2891(1)	5163(1)	1136(1)	11(1)
N(4)	3823(1)	4837(1)	962(1)	13(1)
B(1)	2688(1)	6680(1)	1418(1)	11(1)
C(1)	3772(1)	8708(1)	44(1)	17(1)
C(2)	2798(1)	9400(1)	-87(1)	19(1)
C(3)	2262(1)	8740(1)	385(1)	16(1)
C(4)	2290(1)	3999(1)	1065(1)	13(1)
C(5)	2832(1)	2901(1)	829(1)	16(1)
C(6)	3789(1)	3477(1)	771(1)	16(1)
C(7)	1467(1)	6819(1)	1462(1)	12(1)
C(8)	1220(1)	7183(1)	2148(1)	15(1)
C(9)	171(1)	7422(2)	2184(1)	21(1)
C(10)	-658(1)	7313(2)	1526(1)	22(1)
C(11)	-443(1)	6900(2)	842(1)	21(1)
C(12)	604(1)	6653(2)	815(1)	17(1)
C(13)	3571(1)	7001(1)	2208(1)	11(1)
C(14)	3839(1)	5968(1)	2779(1)	17(1)
C(15)	4615(1)	6198(2)	3461(1)	19(1)
C(16)	5144(1)	7475(2)	3590(1)	18(1)
C(17)	4878(1)	8522(1)	3044(1)	16(1)
C(18)	4098(1)	8290(1)	2362(1)	14(1)
C(19)	6941(1)	5426(2)	2478(1)	29(1)
C(20)	7216(1)	4606(2)	1065(1)	22(1)

Tp^{Me}PtCl(DMSO)

Table 1. Crystal data and structure refinement for Tp^{Me}PtCl(DMSO) (PFO40) (CCDC 738919).

Empirical formula	C ₁₇ H ₂₈ BN ₆ ClSPt • CH ₂ Cl ₂	
Formula weight	674.79	
Crystallization Solvent	Dichloromethane	
Crystal Habit	Block	
Crystal size	0.27 x 0.19 x 0.19 mm ³	
Crystal color	Colorless	
Data Collection		
Type of diffractometer	Bruker KAPPA APEX II	
Wavelength	0.71073 Å MoKα	
Data Collection Temperature	100(2) K	
θ range for 9474 reflections used in lattice determination	2.77 to 57.52°	
Unit cell dimensions	a = 9.0798(4) Å b = 11.5455(5) Å c = 13.0920(5) Å	α = 74.129(2)° β = 81.818(3)° γ = 72.377(2)°
Volume	1255.52(9) Å ³	
Z	2	
Crystal system	Triclinic	
Space group	P-1	
Density (calculated)	1.785 Mg/m ³	
F(000)	660	
Data collection program	Bruker APEX2 v2.1-0	
θ range for data collection	1.62 to 57.93°	
Completeness to θ = 57.93°	92.1 %	
Index ranges	-21 ≤ h ≤ 18, -22 ≤ k ≤ 27, -30 ≤ l ≤ 30	
Data collection scan type	ω scans; 25 settings	
Data reduction program	Bruker SAINT-Plus v7.34A	
Reflections collected	125175	
Independent reflections	32865 [R _{int} = 0.0461]	
Absorption coefficient	6.008 mm ⁻¹	
Absorption correction	Semi-empirical from equivalents	
Max. and min. transmission	0.7514 and 0.5006	

Table 1 (cont.)

Structure solution and Refinement	
Structure solution program	SHELXS-97 (Sheldrick, 2008)
Primary solution method	Direct methods
Secondary solution method	Difference Fourier map
Hydrogen placement	Difference Fourier map
Structure refinement program	SHELXL-97 (Sheldrick, 2008)
Refinement method	Full matrix least-squares on F^2
Data / restraints / parameters	32865 / 0 / 391
Treatment of hydrogen atoms	Unrestrained
Goodness-of-fit on F^2	1.220
Final R indices [$I > 2\sigma(I)$, 28230 reflections]	R1 = 0.0283, wR2 = 0.0519
R indices (all data)	R1 = 0.0383, wR2 = 0.0537
Type of weighting Scheme used	Sigma
Weighting Scheme used	$w=1/\sigma^2(Fo^2)$
Max shift/error	0.006
Average shift/error	0.000
Largest diff. peak and hole	6.320 and -3.534 e.Å ⁻³

Special Refinement Details

Crystals were mounted on a glass fiber using Paratone oil then placed on the diffractometer under a nitrogen stream at 100K.

Refinement of F^2 against ALL reflections. The weighted R-factor (wR) and goodness of fit (S) are based on F^2 , conventional R-factors (R) are based on F , with F set to zero for negative F^2 . The threshold expression of $F^2 > 2\sigma(F^2)$ is used only for calculating R-factors(gt) etc. and is not relevant to the choice of reflections for refinement. R-factors based on F^2 are statistically about twice as large as those based on F , and R-factors based on ALL data will be even larger.

All esds (except the esd in the dihedral angle between two l.s. planes) are estimated using the full covariance matrix. The cell esds are taken into account individually in the estimation of esds in distances, angles and torsion angles; correlations between esds in cell parameters are only used when they are defined by crystal symmetry. An approximate (isotropic) treatment of cell esds is used for estimating esds involving l.s. planes.

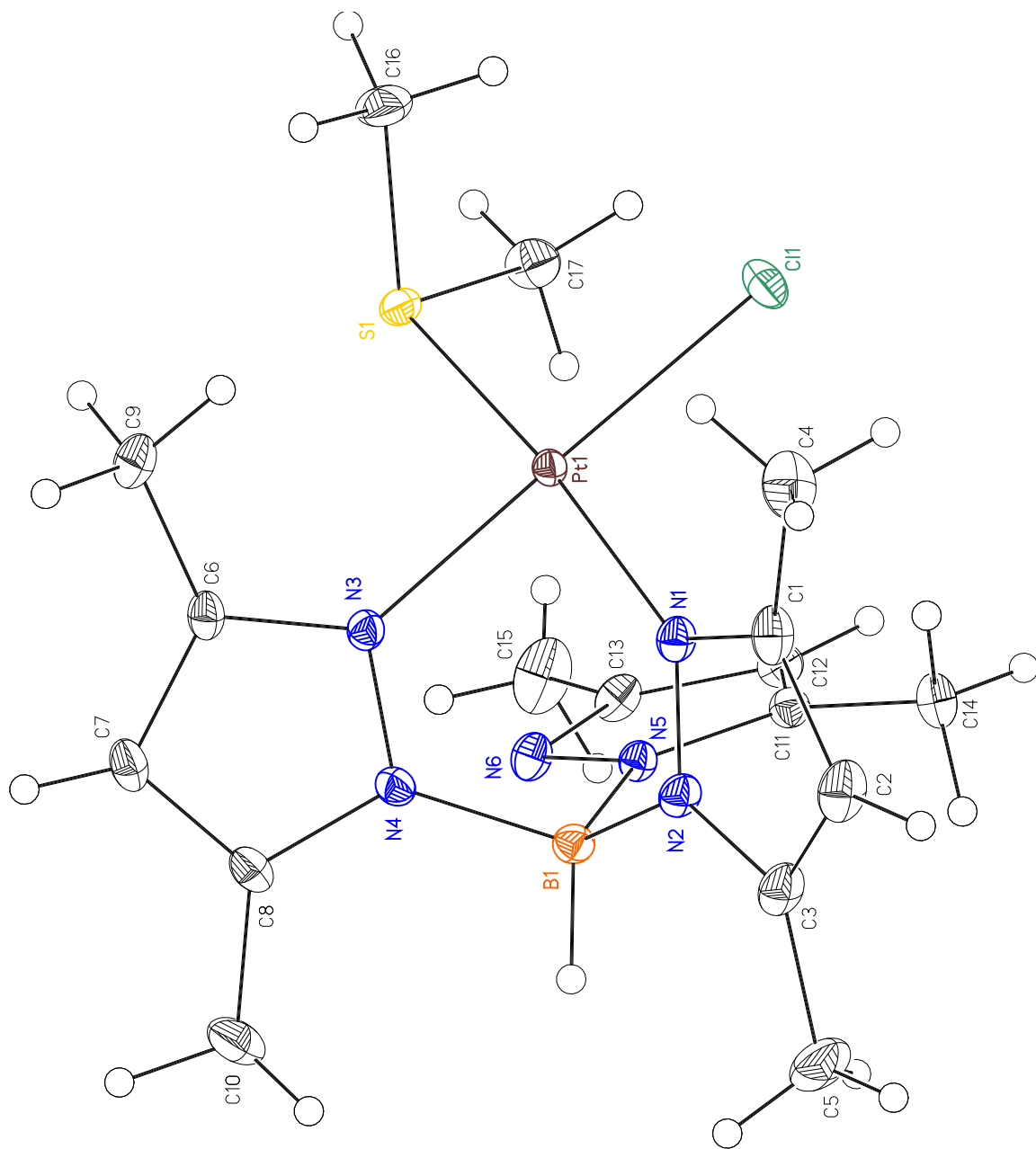


Table 2. Atomic coordinates ($\times 10^4$) and equivalent isotropic displacement parameters ($\text{\AA}^2 \times 10^3$) for $\text{Tp}^{\text{Me}}\text{PtCl}(\text{DMSO})$ (PFO40) (CCDC 738919). $U(\text{eq})$ is defined as the trace of the orthogonalized U_{ij} tensor.

	x	y	z	U_{eq}
Pt(1)	5665(1)	7092(1)	7221(1)	9(1)
S(1)	6291(1)	8741(1)	7485(1)	12(1)
Cl(1)	6679(1)	7420(1)	5483(1)	18(1)
N(1)	4773(1)	5743(1)	7073(1)	12(1)
N(2)	3244(1)	5852(1)	7402(1)	12(1)
N(3)	4769(1)	6779(1)	8724(1)	11(1)
N(4)	3242(1)	6810(1)	8913(1)	11(1)
N(5)	1988(1)	8191(1)	7238(1)	10(1)
N(6)	1549(1)	9180(1)	7711(1)	13(1)
B(1)	2298(1)	6867(1)	7995(1)	12(1)
C(1)	5309(1)	4757(1)	6639(1)	16(1)
C(2)	4104(2)	4223(1)	6672(1)	19(1)
C(3)	2817(1)	4937(1)	7159(1)	17(1)
C(4)	6962(2)	4332(1)	6251(1)	23(1)
C(5)	1214(2)	4799(1)	7362(1)	25(1)
C(6)	5369(1)	6595(1)	9650(1)	13(1)
C(7)	4190(1)	6535(1)	10461(1)	15(1)
C(8)	2868(1)	6679(1)	9969(1)	14(1)
C(9)	7035(1)	6468(1)	9723(1)	17(1)
C(10)	1260(1)	6756(1)	10450(1)	21(1)
C(11)	1867(1)	8609(1)	6167(1)	11(1)
C(12)	1359(1)	9904(1)	5938(1)	14(1)
C(13)	1177(1)	10212(1)	6921(1)	14(1)
C(14)	2204(1)	7795(1)	5402(1)	16(1)
C(15)	633(2)	11487(1)	7133(1)	25(1)
C(16)	8322(1)	8542(1)	7140(1)	20(1)
C(17)	5475(1)	10060(1)	6424(1)	18(1)
C(20)	6830(2)	201(1)	504(1)	24(1)
Cl(3)	6339(1)	-1197(1)	1228(1)	27(1)
Cl(4)	8146(1)	-61(1)	-594(1)	33(1)

Ph₂B(pz)₂PdMe₂K

Table 1. Crystal data and structure refinement for Ph₂B(pz)₂PdMe₂K (PFO41) (CCDC 757089).

Empirical formula	2(C ₂₀ H ₂₂ BN ₄ Pd) ⁻ 2K ⁺ • ¼ (C ₄ H ₁₀ O)	
Formula weight	493.26	
Crystallization Solvent	Diethylether/ <i>n</i> -pentane	
Crystal Habit	Fragment	
Crystal size	0.21 x 0.19 x 0.10 mm ³	
Crystal color	Colorless	
Data Collection		
Type of diffractometer	Bruker KAPPA APEX II	
Wavelength	0.71073 Å MoKα	
Data Collection Temperature	100(2) K	
θ range for 9133 reflections used in lattice determination	2.41 to 35.78°	
Unit cell dimensions	a = 9.8396(4) Å b = 13.2001(6) Å c = 17.4637(8) Å	α = 82.656(2)° β = 87.394(2)° γ = 76.823(2)°
Volume	2190.10(17) Å ³	
Z	4	
Crystal system	Triclinic	
Space group	P-1	
Density (calculated)	1.496 Mg/m ³	
F(000)	1002	
Data collection program	Bruker APEX2 v2009.7-0	
θ range for data collection	1.60 to 39.22°	
Completeness to θ = 39.22°	96.9 %	
Index ranges	-17 ≤ h ≤ 17, -23 ≤ k ≤ 23, -30 ≤ l ≤ 30	
Data collection scan type	ω scans; 27 settings	
Data reduction program	Bruker SAINT-Plus v7.66A	
Reflections collected	168342	
Independent reflections	25047 [R _{int} = 0.0485]	
Absorption coefficient	1.052 mm ⁻¹	
Absorption correction	None	
Max. and min. transmission	0.9021 and 0.8093	



Table 1 (cont.)

Structure solution and Refinement	
Structure solution program	SHELXS-97 (Sheldrick, 2008)
Primary solution method	Direct methods
Secondary solution method	Difference Fourier map
Hydrogen placement	Difference Fourier map
Structure refinement program	SHELXL-97 (Sheldrick, 2008)
Refinement method	Full matrix least-squares on F^2
Data / restraints / parameters	25047 / 0 / 748
Treatment of hydrogen atoms	Unrestrained
Goodness-of-fit on F^2	1.705
Final R indices [$I > 2\sigma(I)$, 18103 reflections]	$R1 = 0.0323$, $wR2 = 0.0467$
R indices (all data)	$R1 = 0.0542$, $wR2 = 0.0476$
Type of weighting Scheme used	Sigma
Weighting Scheme used	$w=1/\sigma^2(Fo^2)$
Max shift/error	0.004
Average shift/error	0.000
Largest diff. peak and hole	1.466 and -1.540 e.Å ⁻³

Special Refinement Details

Crystals were mounted on a glass fiber using Paratone oil then placed on the diffractometer under a nitrogen stream at 100K.

Refinement of F^2 against ALL reflections. The weighted R-factor (wR) and goodness of fit (S) are based on F^2 , conventional R-factors (R) are based on F , with F set to zero for negative F^2 . The threshold expression of $F^2 > 2\sigma(F^2)$ is used only for calculating R-factors(gt) etc. and is not relevant to the choice of reflections for refinement. R-factors based on F^2 are statistically about twice as large as those based on F , and R-factors based on ALL data will be even larger.

All esds (except the esd in the dihedral angle between two l.s. planes) are estimated using the full covariance matrix. The cell esds are taken into account individually in the estimation of esds in distances, angles and torsion angles; correlations between esds in cell parameters are only used when they are defined by crystal symmetry. An approximate (isotropic) treatment of cell esds is used for estimating esds involving l.s. planes.

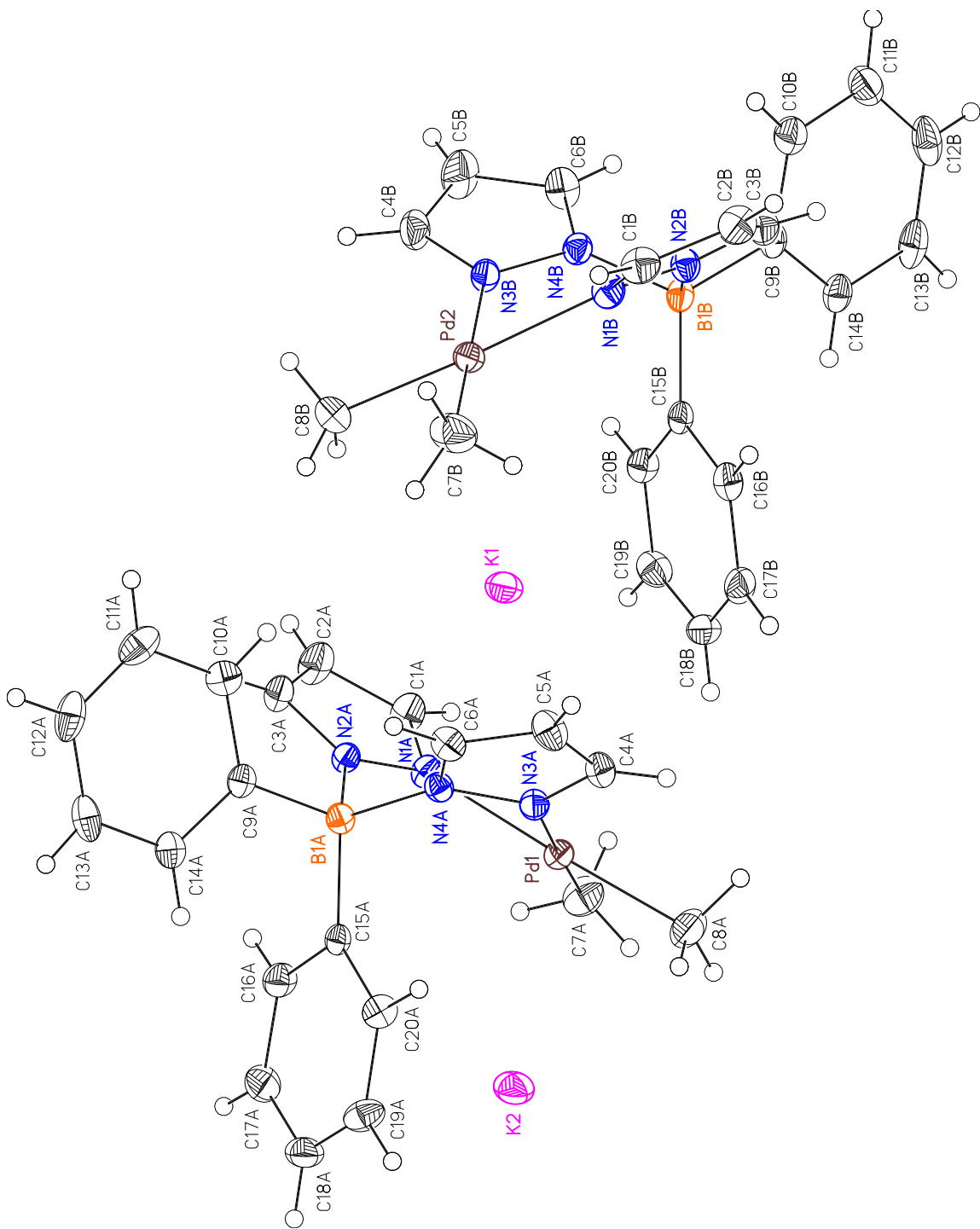


Table 2. Atomic coordinates ($\times 10^4$) and equivalent isotropic displacement parameters ($\text{\AA}^2 \times 10^3$) for $\text{Ph}_2\text{B}(\text{pz})_2\text{PdMe}_2\text{K}$ (PFO41) (CCDC 757089). $U(\text{eq})$ is defined as the trace of the orthogonalized U_{ij} tensor.

	x	y	z	U_{eq}
Pd(1)	8221(1)	5011(1)	2402(1)	16(1)
K(1)	7467(1)	7804(1)	2718(1)	25(1)
N(1A)	6401(1)	6146(1)	2032(1)	17(1)
N(2A)	5299(1)	6469(1)	2516(1)	15(1)
N(3A)	7883(1)	5566(1)	3489(1)	16(1)
N(4A)	6577(1)	5959(1)	3778(1)	15(1)
B(1A)	5222(2)	5875(1)	3356(1)	15(1)
C(1A)	6145(2)	6769(1)	1364(1)	23(1)
C(2A)	4886(2)	7481(1)	1407(1)	26(1)
C(3A)	4379(1)	7265(1)	2133(1)	19(1)
C(4A)	8790(1)	5760(1)	3969(1)	20(1)
C(5A)	8092(2)	6270(1)	4563(1)	24(1)
C(6A)	6705(1)	6370(1)	4431(1)	20(1)
C(7A)	8555(2)	4538(1)	1335(1)	28(1)
C(8A)	9995(2)	3974(1)	2768(1)	29(1)
C(9A)	3869(1)	6478(1)	3814(1)	16(1)
C(10A)	3625(2)	7545(1)	3882(1)	21(1)
C(11A)	2463(2)	8064(1)	4275(1)	26(1)
C(12A)	1518(2)	7516(1)	4618(1)	27(1)
C(13A)	1743(1)	6462(1)	4578(1)	24(1)
C(14A)	2892(1)	5952(1)	4174(1)	18(1)
C(15A)	5187(1)	4673(1)	3309(1)	14(1)
C(16A)	4391(1)	4403(1)	2755(1)	21(1)
C(17A)	4156(2)	3408(1)	2772(1)	25(1)
C(18A)	4730(2)	2624(1)	3353(1)	25(1)
C(19A)	5548(2)	2856(1)	3898(1)	23(1)
C(20A)	5765(1)	3858(1)	3878(1)	19(1)
Pd(2)	6987(1)	10183(1)	2905(1)	20(1)
K(2)	7603(1)	2786(1)	2496(1)	28(1)
N(1B)	8898(1)	10526(1)	3184(1)	20(1)
N(2B)	9955(1)	10601(1)	2661(1)	17(1)
N(3B)	7210(1)	10962(1)	1785(1)	18(1)
N(4B)	8477(1)	11015(1)	1454(1)	17(1)
B(1B)	9885(2)	10316(1)	1816(1)	17(1)
C(1B)	9340(2)	10702(1)	3858(1)	24(1)
C(2B)	10667(2)	10883(1)	3781(1)	25(1)
C(3B)	11022(2)	10805(1)	3024(1)	22(1)

C(4B)	6245(2)	11581(1)	1317(1)	24(1)
C(5B)	6865(2)	12030(1)	684(1)	32(1)
C(6B)	8270(2)	11655(1)	782(1)	24(1)
C(7B)	6777(2)	9462(1)	3987(1)	34(1)
C(8B)	5122(2)	9922(1)	2639(1)	34(1)
C(9B)	11158(1)	10649(1)	1301(1)	17(1)
C(10B)	11395(2)	11654(1)	1255(1)	24(1)
C(11B)	12429(2)	11978(1)	790(1)	28(1)
C(12B)	13267(2)	11288(1)	351(1)	29(1)
C(13B)	13078(2)	10289(1)	382(1)	26(1)
C(14B)	12042(1)	9971(1)	852(1)	20(1)
C(15B)	9887(1)	9093(1)	1844(1)	16(1)
C(16B)	10541(1)	8344(1)	2430(1)	20(1)
C(17B)	10703(1)	7279(1)	2406(1)	24(1)
C(18B)	10206(2)	6921(1)	1791(1)	25(1)
C(19B)	9530(1)	7641(1)	1200(1)	22(1)
C(20B)	9373(1)	8703(1)	1232(1)	19(1)
C(31A)	7001(6)	5378(4)	9208(3)	53(1)
C(32A)	6131(6)	4666(3)	9580(2)	50(1)
O(33A)	4948(5)	5274(2)	9970(2)	48(1)
C(34A)	4158(5)	4613(3)	10454(2)	42(1)
C(35A)	2869(5)	5288(4)	10742(2)	42(1)

[Ph₂Bpz₂Pd(μ-pz)₂]₂**Table 1. Crystal data and structure refinement for [Ph₂Bpz₂Pd(μ-pz)₂]₂ (PFO44) (CCDC 837963).**

Empirical formula	C ₄₂ H ₃₈ B ₂ N ₁₂ Pd ₂	
Formula weight	945.26	
Crystallization Solvent	Not given	
Crystal Habit	Fragment	
Crystal size	0.15 x 0.07 x 0.05 mm ³	
Crystal color	Colorless	
Data Collection		
Type of diffractometer	Bruker KAPPA APEX II	
Wavelength	0.71073 Å MoKα	
Data Collection Temperature	100(2) K	
θ range for 9406 reflections used in lattice determination	2.46 to 23.48°	
Unit cell dimensions	a = 10.292(4) Å b = 25.116(11) Å c = 15.667(7) Å	α = 90° β = 92.493(13)° γ = 90°
Volume	4046(3) Å ³	
Z	4	
Crystal system	Monoclinic	
Space group	P2(1)/n	
Density (calculated)	1.552 Mg/m ³	
F(000)	1904	
Data collection program	Bruker APEX2 v2009.7-0	
θ range for data collection	1.53 to 23.65°	
Completeness to θ = 23.65°	99.8 %	
Index ranges	-11 ≤ h ≤ 11, -28 ≤ k ≤ 28, -17 ≤ l ≤ 17	
Data collection scan type	ω scans; 10 settings	
Data reduction program	Bruker SAINT-Plus v7.68A	
Reflections collected	50932	
Independent reflections	6094 [R _{int} = 0.0958]	
Absorption coefficient	0.937 mm ⁻¹	
Absorption correction	None	
Max. and min. transmission	0.9547 and 0.8723	

Table 1 (cont.)

Structure solution and Refinement	
Structure solution program	SHELXS-97 (Sheldrick, 2008)
Primary solution method	Direct methods
Secondary solution method	Difference Fourier map
Hydrogen placement	Geometric positions
Structure refinement program	SHELXL-97 (Sheldrick, 2008)
Refinement method	Full matrix least-squares on F^2
Data / restraints / parameters	6094 / 0 / 523
Treatment of hydrogen atoms	Riding
Goodness-of-fit on F^2	2.122
Final R indices [$I > 2\sigma(I)$, 4505 reflections]	$R1 = 0.0570$, $wR2 = 0.0829$
R indices (all data)	$R1 = 0.0807$, $wR2 = 0.0887$
Type of weighting Scheme used	Sigma
Weighting Scheme used	$w=1/\sigma^2(Fo^2)$
Max shift/error	0.001
Average shift/error	0.000
Largest diff. peak and hole	2.921 and -0.803 e. \AA^{-3}

Special Refinement Details

Crystals were mounted on a glass fiber using Paratone oil then placed on the diffractometer under a nitrogen stream at 100K.

Refinement of F^2 against ALL reflections. The weighted R-factor (wR) and goodness of fit (S) are based on F^2 , conventional R-factors (R) are based on F , with F set to zero for negative F^2 . The threshold expression of $F^2 > 2\sigma(F^2)$ is used only for calculating R-factors(gt) etc. and is not relevant to the choice of reflections for refinement. R-factors based on F^2 are statistically about twice as large as those based on F , and R-factors based on ALL data will be even larger.

All esds (except the esd in the dihedral angle between two l.s. planes) are estimated using the full covariance matrix. The cell esds are taken into account individually in the estimation of esds in distances, angles and torsion angles; correlations between esds in cell parameters are only used when they are defined by crystal symmetry. An approximate (isotropic) treatment of cell esds is used for estimating esds involving l.s. planes.

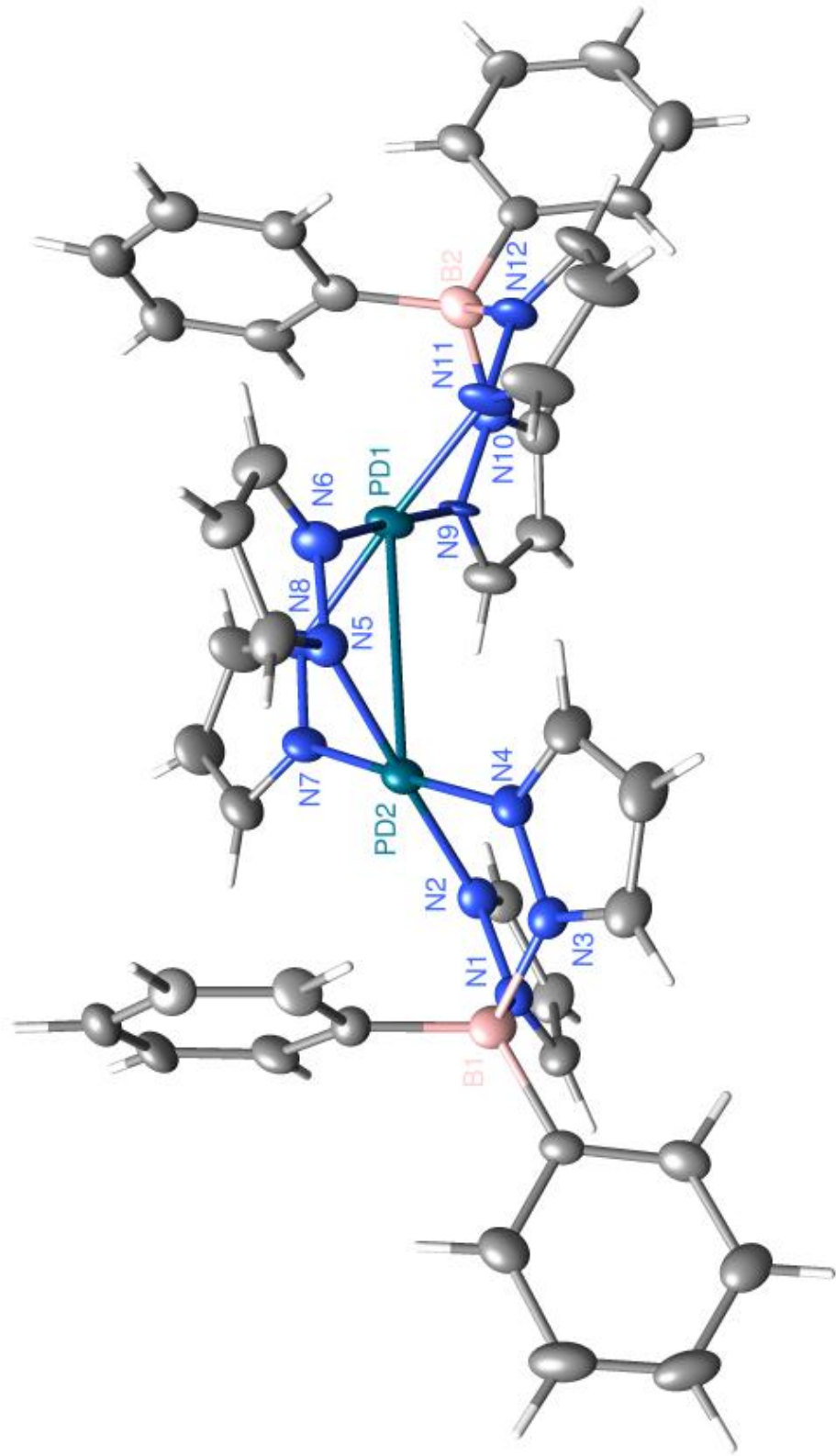


Table 2. Atomic coordinates ($\times 10^4$) and equivalent isotropic displacement parameters ($\text{\AA}^2 \times 10^3$) for $[\text{Ph}_2\text{Bpz}_2\text{Pd}(\mu\text{-pz})_2]_2$ (PFO44) (CCDC 837963). $U(\text{eq})$ is defined as the trace of the orthogonalized U_{ij} tensor.

	x	y	z	U_{eq}
Pd(1)	9981(1)	2070(1)	7819(1)	26(1)
Pd(2)	9899(1)	750(1)	7547(1)	23(1)
N(1)	8681(5)	-79(2)	6445(3)	24(1)
N(2)	8541(5)	421(2)	6757(3)	24(1)
N(3)	11121(5)	-87(2)	6540(3)	23(1)
N(4)	11267(5)	408(2)	6872(3)	25(2)
N(5)	11270(5)	1091(2)	8322(3)	25(2)
N(6)	11280(6)	1616(2)	8464(3)	30(2)
N(7)	8527(5)	1114(2)	8197(3)	26(2)
N(8)	8545(6)	1646(2)	8301(3)	29(2)
N(9)	8713(6)	2495(2)	7149(3)	28(2)
N(10)	8920(5)	3020(2)	6971(3)	26(1)
N(11)	11432(6)	2467(2)	7298(3)	31(2)
N(12)	11352(6)	2990(2)	7122(3)	29(2)
B(1)	9903(8)	-441(3)	6739(5)	26(2)
B(2)	10137(8)	3310(3)	7410(5)	26(2)
C(3)	7943(7)	3193(3)	6459(4)	34(2)
C(4)	7077(7)	2796(3)	6273(4)	37(2)
C(5)	7580(7)	2375(3)	6732(4)	33(2)
C(8)	12466(7)	3129(3)	6763(4)	34(2)
C(9)	13262(8)	2705(3)	6710(5)	47(2)
C(10)	12576(8)	2298(3)	7052(5)	43(2)
C(13)	12278(7)	1738(3)	9009(4)	31(2)
C(14)	12919(7)	1274(3)	9228(4)	33(2)
C(15)	12266(7)	881(3)	8783(4)	31(2)
C(18)	7504(8)	1793(3)	8735(4)	41(2)
C(19)	6798(7)	1348(3)	8908(4)	40(2)
C(20)	7463(7)	935(3)	8560(4)	34(2)
C(23)	12199(7)	-200(3)	6126(4)	29(2)
C(24)	13023(7)	220(3)	6180(4)	37(2)
C(25)	12418(7)	593(3)	6653(4)	33(2)
C(28)	7420(6)	617(3)	6431(4)	25(2)
C(29)	6823(7)	240(3)	5902(4)	30(2)
C(30)	7642(7)	-188(3)	5928(4)	29(2)
C(31)	9979(7)	-1438(3)	4821(4)	33(2)
C(32)	9996(7)	-1931(3)	5221(5)	37(2)
C(33)	9906(7)	-1476(3)	6552(4)	30(2)
C(34)	9955(7)	-1951(3)	6097(5)	38(2)

C(35)	9939(7)	-973(3)	5290(4)	28(2)
C(36)	9913(6)	-974(3)	6183(4)	20(2)
C(37)	9877(7)	-516(3)	7768(4)	23(2)
C(38)	11031(6)	-567(3)	8272(4)	24(2)
C(39)	11017(7)	-635(3)	9142(4)	25(2)
C(40)	9862(8)	-649(3)	9551(4)	30(2)
C(41)	8738(7)	-519(3)	8205(4)	27(2)
C(42)	8731(7)	-576(3)	9074(4)	29(2)
C(43)	10078(7)	3303(3)	8426(4)	27(2)
C(44)	11199(7)	3323(3)	8954(4)	28(2)
C(45)	11153(8)	3349(3)	9827(5)	34(2)
C(46)	8882(7)	3310(3)	8836(5)	30(2)
C(47)	8826(8)	3332(3)	9711(4)	34(2)
C(48)	9958(9)	3366(3)	10216(5)	39(2)
C(49)	9947(7)	4351(3)	7504(4)	30(2)
C(50)	10180(7)	3906(3)	7007(4)	24(2)
C(51)	10413(7)	4000(3)	6160(4)	31(2)
C(52)	9928(7)	4864(3)	7182(5)	31(2)
C(53)	10174(7)	4939(3)	6338(5)	40(2)
C(54)	10434(8)	4506(3)	5825(5)	42(2)

(Ph₂Bpz₂)₂Pd

Table 1. Crystal data and structure refinement for (Ph₂Bpz₂)₂Pd (PFO46) (CCDC 838482).

Empirical formula	C ₃₆ H ₃₂ B ₂ N ₈ Pd
Formula weight	704.72
Crystallization Solvent	Not given
Crystal Habit	Fragment
Crystal size	0.18 x 0.07 x 0.06 mm ³
Crystal color	Colorless



Data Collection

Type of diffractometer	Bruker KAPPA APEX II	
Wavelength	0.71073 Å MoKα	
Data Collection Temperature	100(2) K	
θ range for 9911 reflections used in lattice determination	2.28 to 32.25°	
Unit cell dimensions	a = 18.2023(17) Å b = 10.3621(11) Å c = 8.6844(8) Å	α = 90° β = 105.395(3)° γ = 90°
Volume	1579.2(3) Å ³	
Z	2	
Crystal system	Monoclinic	
Space group	C 2/m	
Density (calculated)	1.482 Mg/m ³	
F(000)	720	
Data collection program	Bruker APEX2 v2009.7-0	
θ range for data collection	2.28 to 35.06°	
Completeness to θ = 35.06°	99.8 %	
Index ranges	-29 ≤ h ≤ 29, -16 ≤ k ≤ 16, -14 ≤ l ≤ 13	
Data collection scan type	ω scans; 11 settings	
Data reduction program	Bruker SAINT-Plus v7.68A	
Reflections collected	26366	
Independent reflections	3647 [R _{int} = 0.0454]	
Absorption coefficient	0.629 mm ⁻¹	
Absorption correction	None	
Max. and min. transmission	0.9633 and 0.8952	

Table 1 (cont.)

Structure solution and Refinement	
Structure solution program	SHELXS-97 (Sheldrick, 2008)
Primary solution method	Direct methods
Secondary solution method	Difference Fourier map
Hydrogen placement	Geometric positions
Structure refinement program	SHELXL-97 (Sheldrick, 2008)
Refinement method	Full matrix least-squares on F^2
Data / restraints / parameters	3647 / 0 / 122
Treatment of hydrogen atoms	Riding
Goodness-of-fit on F^2	3.502
Final R indices [$I > 2\sigma(I)$, 3490 reflections]	R1 = 0.0467, wR2 = 0.0835
R indices (all data)	R1 = 0.0497, wR2 = 0.0837
Type of weighting Scheme used	Sigma
Weighting Scheme used	$w=1/\sigma^2(Fo^2)$
Max shift/error	0.000
Average shift/error	0.000
Largest diff. peak and hole	1.990 and -1.084 e.Å ⁻³

Special Refinement Details

Crystals were mounted on a glass fiber using Paratone oil then placed on the diffractometer under a nitrogen stream at 100K.

Refinement of F^2 against ALL reflections. The weighted R-factor (wR) and goodness of fit (S) are based on F^2 , conventional R-factors (R) are based on F , with F set to zero for negative F^2 . The threshold expression of $F^2 > 2\sigma(F^2)$ is used only for calculating R-factors(gt) etc. and is not relevant to the choice of reflections for refinement. R-factors based on F^2 are statistically about twice as large as those based on F , and R-factors based on ALL data will be even larger.

All esds (except the esd in the dihedral angle between two l.s. planes) are estimated using the full covariance matrix. The cell esds are taken into account individually in the estimation of esds in distances, angles and torsion angles; correlations between esds in cell parameters are only used when they are defined by crystal symmetry. An approximate (isotropic) treatment of cell esds is used for estimating esds involving l.s. planes.

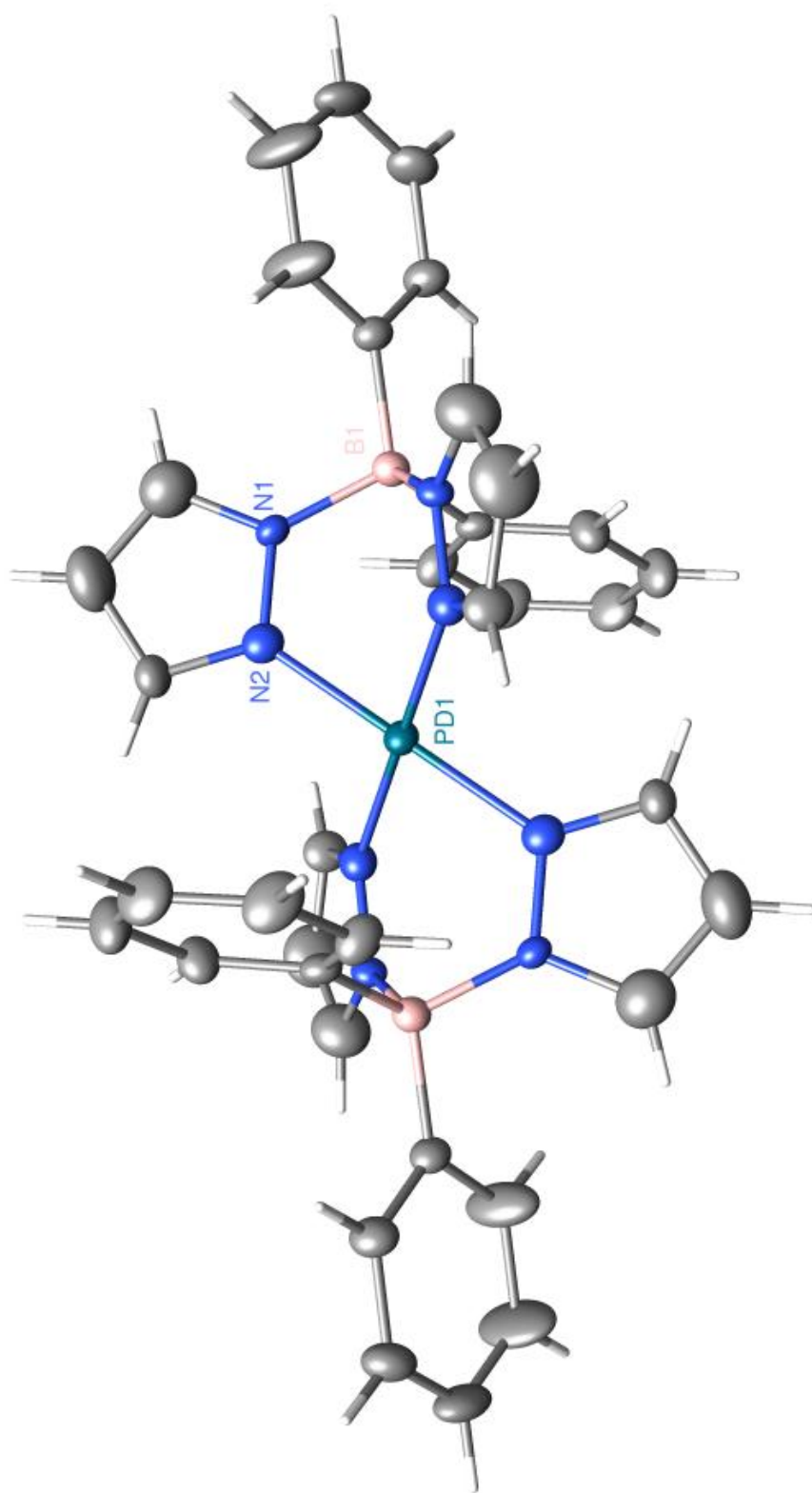


Table 2. Atomic coordinates ($\times 10^4$) and equivalent isotropic displacement parameters ($\text{\AA}^2 \times 10^3$) for $(\text{Ph}_2\text{Bpz}_2)_2\text{Pd}$ (PFO46) (CCDC 838482). $U(\text{eq})$ is defined as the trace of the orthogonalized U_{ij} tensor.

	x	y	z	U_{eq}
Pd(1)	0	0	5000	18(1)
N(1)	1482(1)	1194(2)	6471(2)	17(1)
N(2)	729(1)	1349(2)	6220(2)	24(1)
C(1)	1842(2)	2207(3)	7390(3)	51(1)
C(2)	1284(2)	3012(3)	7715(4)	55(1)
C(3)	579(1)	2434(2)	6961(2)	28(1)
C(4)	1504(2)	0	3857(3)	21(1)
C(5)	1382(1)	-1143(2)	2984(2)	29(1)
C(6)	1155(1)	-1150(2)	1320(3)	38(1)
C(7)	1048(2)	0	494(4)	38(1)
C(8)	2728(2)	0	6433(3)	23(1)
C(9)	3094(2)	0	8073(4)	56(1)
C(10)	3882(2)	0	8618(5)	63(1)
C(11)	4323(2)	0	7572(5)	40(1)
C(12)	3988(2)	0	5978(4)	35(1)
C(13)	3202(2)	0	5439(4)	29(1)
B(1)	1815(2)	0	5770(4)	21(1)

Ph₂B(pz)₂PdMe₄(DMSO)

Table 1. Crystal data and structure refinement for Ph₂B(pz)₂PdMe₄(DMSO) (PFO50) (CCDC 837964).

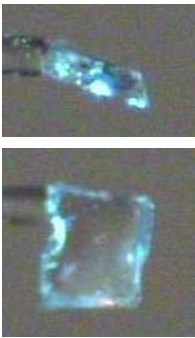
Empirical formula	C ₂₁ H ₂₅ BN ₄ OSPd	
Formula weight	498.72	
Crystallization Solvent	Not given	
Crystal Habit	Blade	
Crystal size	0.19 x 0.18 x 0.05 mm ³	
Crystal color	Colorless	
Data Collection		
Type of diffractometer	Bruker KAPPA APEX II	
Wavelength	0.71073 Å MoKα	
Data Collection Temperature	100(2) K	
θ range for 9989 reflections used in lattice determination	2.19 to 36.34°	
Unit cell dimensions	a = 8.3067(3) Å b = 10.0948(4) Å c = 13.8871(5) Å	α = 93.370(2)° β = 95.543(2)° γ = 112.410(2)°
Volume	1065.72(7) Å ³	
Z	2	
Crystal system	Triclinic	
Space group	P-1	
Density (calculated)	1.554 Mg/m ³	
F(000)	508	
Data collection program	Bruker APEX2 v2009.7-0	
θ range for data collection	2.19 to 36.61°	
Completeness to θ = 36.61°	99.8 %	
Index ranges	-13 ≤ h ≤ 13, -16 ≤ k ≤ 16, -23 ≤ l ≤ 23	
Data collection scan type	ω scans; 22 settings	
Data reduction program	Bruker SAINT-Plus v7.66A	
Reflections collected	76300	
Independent reflections	10506 [R _{int} = 0.0432]	
Absorption coefficient	0.988 mm ⁻¹	
Absorption correction	None	
Max. and min. transmission	0.9522 and 0.8344	

Table 1 (cont.)

Structure solution and Refinement	
Structure solution program	SHELXS-97 (Sheldrick, 2008)
Primary solution method	Direct methods
Secondary solution method	Difference Fourier map
Hydrogen placement	Geometric positions
Structure refinement program	SHELXL-97 (Sheldrick, 2008)
Refinement method	Full matrix least-squares on F^2
Data / restraints / parameters	10506 / 0 / 265
Treatment of hydrogen atoms	Riding
Goodness-of-fit on F^2	3.601
Final R indices [$I > 2\sigma(I)$, 8967 reflections]	$R1 = 0.0577$, $wR2 = 0.0885$
R indices (all data)	$R1 = 0.0668$, $wR2 = 0.0890$
Type of weighting Scheme used	Sigma
Weighting Scheme used	$w=1/\sigma^2(Fo^2)$
Max shift/error	0.001
Average shift/error	0.000
Largest diff. peak and hole	5.318 and -4.240 e. \AA^{-3}

Special Refinement Details

Crystals were mounted on a glass fiber using Paratone oil then placed on the diffractometer under a nitrogen stream at 100K.

Refinement of F^2 against ALL reflections. The weighted R-factor (wR) and goodness of fit (S) are based on F^2 , conventional R-factors (R) are based on F , with F set to zero for negative F^2 . The threshold expression of $F^2 > 2\sigma(F^2)$ is used only for calculating R-factors(gt) etc. and is not relevant to the choice of reflections for refinement. R-factors based on F^2 are statistically about twice as large as those based on F , and R-factors based on ALL data will be even larger.

All esds (except the esd in the dihedral angle between two l.s. planes) are estimated using the full covariance matrix. The cell esds are taken into account individually in the estimation of esds in distances, angles and torsion angles; correlations between esds in cell parameters are only used when they are defined by crystal symmetry. An approximate (isotropic) treatment of cell esds is used for estimating esds involving l.s. planes.

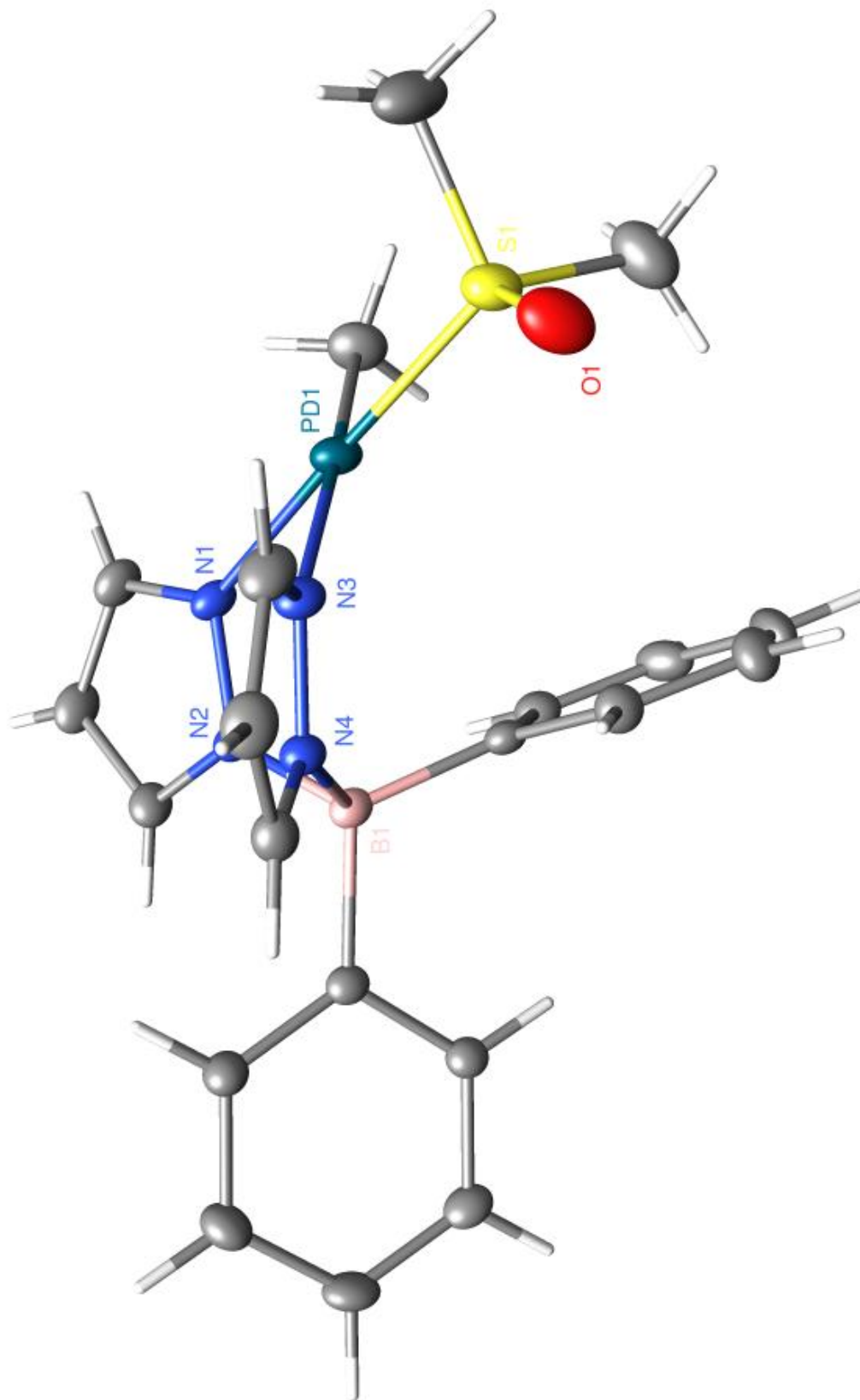


Table 2. Atomic coordinates ($\times 10^4$) and equivalent isotropic displacement parameters ($\text{\AA}^2 \times 10^3$) for $\text{Ph}_2\text{B}(\text{pz})_2\text{PdMe}(\text{DMSO})$ (PFO50) (CCDC 837964). $U(\text{eq})$ is defined as the trace of the orthogonalized U^{ij} tensor.

	x	y	z	U_{eq}
Pd(1)	5871(1)	6418(1)	6497(1)	20(1)
S(1)	5645(1)	8212(1)	5702(1)	25(1)
O(1)	3862(2)	8064(2)	5325(1)	35(1)
N(1)	6160(2)	4864(2)	7309(1)	17(1)
N(2)	4918(2)	4185(2)	7877(1)	16(1)
N(3)	3200(2)	4984(2)	6120(1)	18(1)
N(4)	2312(2)	4223(2)	6816(1)	16(1)
B(1)	3231(3)	4565(3)	7902(2)	16(1)
C(1)	7404(3)	4335(3)	7433(2)	23(1)
C(2)	6987(3)	3307(3)	8091(2)	23(1)
C(3)	5411(3)	3256(3)	8355(2)	20(1)
C(4)	2086(3)	4606(3)	5301(2)	24(1)
C(5)	462(3)	3601(3)	5452(2)	24(1)
C(6)	658(3)	3394(2)	6422(2)	20(1)
C(7)	3839(3)	6261(2)	8212(2)	16(1)
C(8)	5278(3)	7010(2)	8914(2)	19(1)
C(9)	5750(3)	8459(3)	9220(2)	25(1)
C(10)	4791(4)	9206(3)	8829(2)	28(1)
C(11)	3351(3)	8496(3)	8142(2)	26(1)
C(12)	2890(3)	7048(3)	7842(2)	21(1)
C(13)	1950(3)	3551(2)	8601(2)	15(1)
C(14)	1137(3)	2052(3)	8411(2)	20(1)
C(15)	10(3)	1204(3)	9008(2)	23(1)
C(16)	-310(3)	1854(3)	9842(2)	23(1)
C(17)	487(3)	3319(3)	10064(2)	20(1)
C(18)	1594(3)	4157(2)	9448(2)	17(1)
C(19)	6640(4)	9892(3)	6415(2)	39(1)
C(20)	6869(4)	8528(4)	4699(2)	48(1)
C(21)	8476(3)	7668(3)	6940(2)	29(1)

[(diimine)PtCl]₂[BF₄]₂**Table 1. Crystal data and structure refinement for [(diimine)PtCl]₂[BF₄]₂ (PFO56) (CCDC 838234).**

Empirical formula	[C ₆₄ H ₉₆ N ₄ Cl ₂ Pt ₂] ⁺² 2[BF ₄] ⁻ • 2(CH ₂ Cl ₂)
Formula weight	863.00
Crystallization Solvent	Dichloromethane
Crystal Habit	Column
Crystal size	0.27 x 0.14 x 0.11 mm ³
Crystal color	Yellow

**Data Collection**

Type of diffractometer	Bruker KAPPA APEX II
Wavelength	0.71073 Å MoK α
Data Collection Temperature	150(2) K
θ range for 9835 reflections used in lattice determination	2.43 to 30.12°
Unit cell dimensions	a = 31.6298(19) Å α = 90° b = 12.4471(7) Å β = 92.7270(10)° c = 19.2607(10) Å γ = 90°
Volume	7574.3(7) Å ³
Z	8
Crystal system	Monoclinic
Space group	C 2/c
Density (calculated)	1.514 Mg/m ³
F(000)	3456
Data collection program	Bruker APEX2 v2009.7-0
θ range for data collection	2.04 to 35.59°
Completeness to θ = 35.59°	99.9 %
Index ranges	-51 \leq h \leq 51, -20 \leq k \leq 20, -31 \leq l \leq 31
Data collection scan type	ω scans; 11 settings
Data reduction program	Bruker SAINT-Plus v7.68A
Reflections collected	138832
Independent reflections	17402 [R _{int} = 0.0937]
Absorption coefficient	3.960 mm ⁻¹
Absorption correction	None
Max. and min. transmission	0.6698 and 0.4144

Table 1 (cont.)

Structure solution and Refinement	
Structure solution program	SHELXS-97 (Sheldrick, 2008)
Primary solution method	Direct methods
Secondary solution method	Difference Fourier map
Hydrogen placement	Geometric positions
Structure refinement program	SHELXL-97 (Sheldrick, 2008)
Refinement method	Full matrix least-squares on F^2
Data / restraints / parameters	17402 / 0 / 411
Treatment of hydrogen atoms	Riding
Goodness-of-fit on F^2	1.138
Final R indices [$I > 2\sigma(I)$, 12128 reflections]	$R1 = 0.0306$, $wR2 = 0.0556$
R indices (all data)	$R1 = 0.0543$, $wR2 = 0.0580$
Type of weighting Scheme used	Sigma
Weighting Scheme used	$w=1/\sigma^2(Fo^2)$
Max shift/error	0.002
Average shift/error	0.000
Largest diff. peak and hole	1.456 and -1.941 e.Å ⁻³

Special Refinement Details

Crystals were mounted on a glass fiber using Paratone oil then placed on the diffractometer under a nitrogen stream at 100K.

Refinement of F^2 against ALL reflections. The weighted R-factor (wR) and goodness of fit (S) are based on F^2 , conventional R-factors (R) are based on F , with F set to zero for negative F^2 . The threshold expression of $F^2 > 2\sigma(F^2)$ is used only for calculating R-factors(gt) etc. and is not relevant to the choice of reflections for refinement. R-factors based on F^2 are statistically about twice as large as those based on F , and R-factors based on ALL data will be even larger.

All esds (except the esd in the dihedral angle between two l.s. planes) are estimated using the full covariance matrix. The cell esds are taken into account individually in the estimation of esds in distances, angles and torsion angles; correlations between esds in cell parameters are only used when they are defined by crystal symmetry. An approximate (isotropic) treatment of cell esds is used for estimating esds involving l.s. planes.

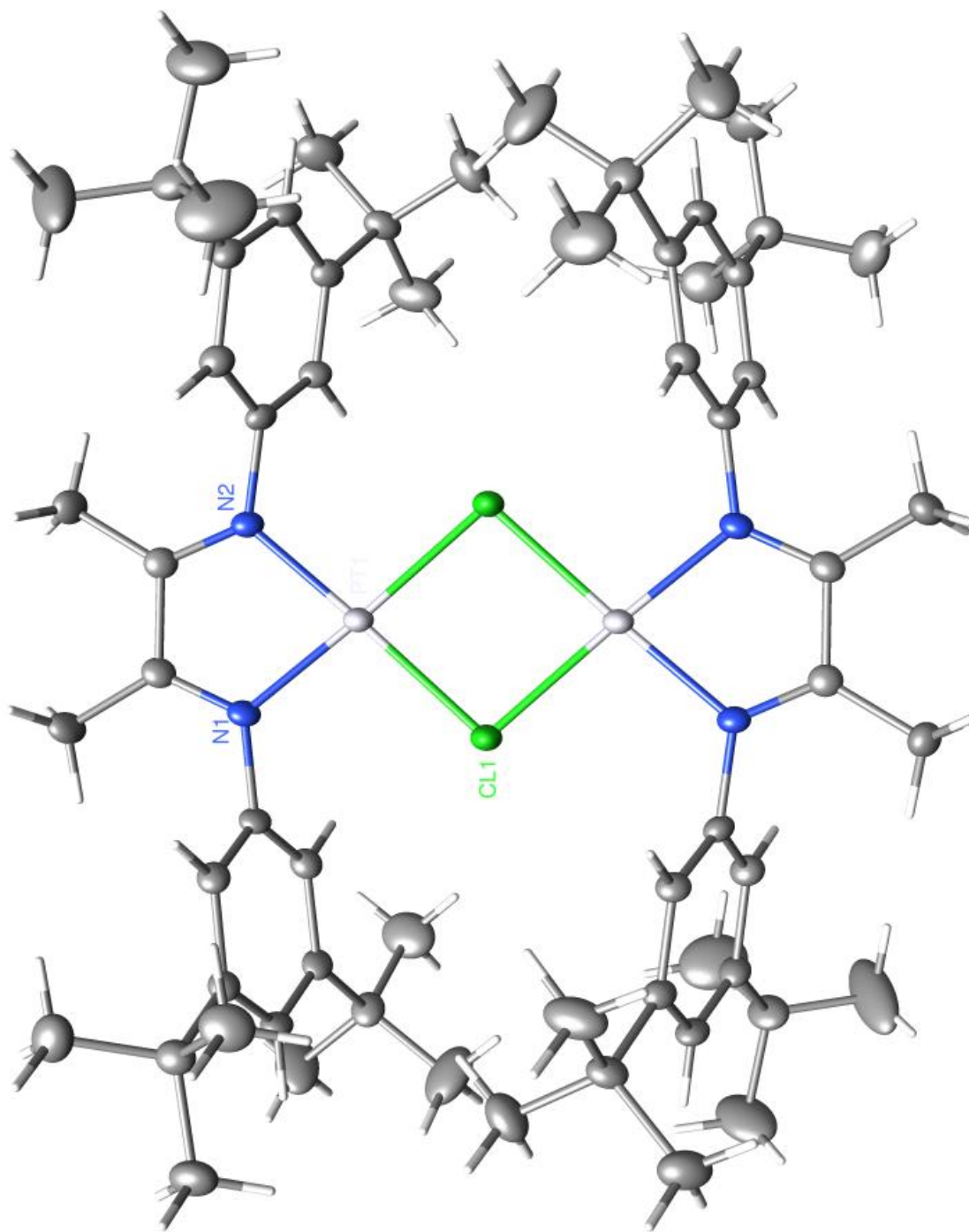


Table 2. Atomic coordinates ($\times 10^4$) and equivalent isotropic displacement parameters ($\text{\AA}^2 \times 10^3$) for [(diimine)PtCl₂][BF₄]₂ (PFO56) (CCDC 838234). $U(\text{eq})$ is defined as the trace of the orthogonalized U_{ij} tensor.

	x	y	z	U_{eq}
Pt(1)	2558(1)	6870(1)	807(1)	19(1)
Cl(1)	2023(1)	7227(1)	-34(1)	32(1)
N(1)	2221(1)	6059(1)	1482(1)	18(1)
N(2)	3001(1)	6543(1)	1544(1)	18(1)
C(1)	2425(1)	5732(2)	2046(1)	20(1)
C(2)	2880(1)	6005(2)	2075(1)	20(1)
C(3)	2233(1)	5134(2)	2616(1)	29(1)
C(4)	3156(1)	5665(2)	2680(1)	26(1)
C(5)	1777(1)	5834(2)	1353(1)	18(1)
C(6)	1649(1)	4806(2)	1188(1)	20(1)
C(7)	1217(1)	4587(2)	1069(1)	19(1)
C(8)	936(1)	5438(2)	1123(1)	21(1)
C(9)	1064(1)	6486(2)	1280(1)	20(1)
C(10)	1494(1)	6678(2)	1395(1)	21(1)
C(11)	1077(1)	3445(2)	879(1)	26(1)
C(12)	1229(1)	2673(2)	1464(1)	39(1)
C(13)	595(1)	3337(2)	772(2)	36(1)
C(14)	1280(1)	3106(2)	205(1)	38(1)
C(15)	739(1)	7390(2)	1336(1)	24(1)
C(16)	465(1)	7173(2)	1957(2)	49(1)
C(17)	947(1)	8494(2)	1460(2)	50(1)
C(18)	457(1)	7451(2)	672(2)	51(1)
C(19)	3442(1)	6805(2)	1467(1)	19(1)
C(20)	3717(1)	5975(2)	1347(1)	22(1)
C(21)	4145(1)	6194(2)	1274(1)	22(1)
C(22)	4273(1)	7257(2)	1320(1)	22(1)
C(23)	3994(1)	8111(2)	1435(1)	20(1)
C(24)	3570(1)	7865(2)	1504(1)	19(1)
C(25)	4455(1)	5274(2)	1168(1)	30(1)
C(26)	4448(1)	4521(3)	1774(2)	87(2)
C(27)	4906(1)	5660(2)	1068(2)	59(1)
C(28)	4324(1)	4674(3)	487(2)	70(1)
C(29)	4165(1)	9261(2)	1474(1)	24(1)
C(30)	4518(1)	9339(2)	2042(1)	39(1)
C(31)	4357(1)	9544(2)	775(1)	37(1)
C(32)	3827(1)	10081(2)	1631(2)	41(1)
B(1)	2154(1)	7957(3)	3237(2)	45(1)

F(1)	2123(1)	8972(1)	3517(1)	59(1)
F(2)	2563(1)	7594(2)	3362(1)	99(1)
F(3)	2089(1)	8008(2)	2538(1)	90(1)
F(4)	1885(1)	7266(2)	3542(2)	100(1)
C(41)	2795(1)	6126(3)	4767(2)	67(1)
Cl(2)	3221(1)	5186(1)	4611(1)	65(1)
Cl(3)	2318(1)	5527(1)	4744(1)	86(1)

References

1. Takaoka, A.; Mendiratta, A.; Peters, J. C., *Organometallics* **2009**, 28 (13), 3744–3753.
2. Williams, T. J.; Caffyn, A. J.; Hazari, N.; Oblad, P. F.; Labinger, J. A.; Bercaw, J. E., *J. Am. Chem. Soc.* **2008**, 130 (8), 2418–2419.
3. Oblad, P. F.; Bercaw, J. E.; Hazari, N.; Labinger, J. A., *Organometallics* **2010**, 29 (4), 789–794.
4. Brookhart, M.; Green, M. L. H., *Journal of Organometallic Chemistry* **1983**, 250 (1), 395–408.